FCS SLAG FOR CONTINUOUS COPPER CONVERTING

A thesis submitted in fulfilment of the requirements for the degree of Doctor of Philosophy (PhD)

Rajneet Kaur

B.Eng (Chemical Engineering, Hons.)

School of Civil, Environmental & Chemical Engineering

Science, Engineering & Technology (SET) Portfolio

RMIT University

July 2007

Declaration

I, Rajneet Kaur, certify that the work presented in this thesis comprises only my original work. The experiments were carried out by me in the laboratories at the School of Civil, Environmental and Chemical Engineering, RMIT University. This research has not been previously submitted to any other university or institute for a degree or an award. Due acknowledgements have been made throughout this thesis to all materials used.

Rajneet Kaur

July 2007

Acknowledgements

I wish to thank my supervisors, A/Prof Doug Swinbourne (Head of the School of Civil, Environmental & Chemical Engineering, RMIT University) and Dr. Colin Nexhip (Rio Tinto Technology and Innovation) for their constant supervision and guidance during the course of this research project and for their thoroughness in editing this thesis. I would like to thank the Department of Civil and Chemical Engineering, RMIT University as well as Rio Tinto Technology and Innovation for the provision of their laboratories and other facilities needed to carry out the experimental work. My appreciation is extended to the Mineralogy team at Rio Tinto Technology and Innovation for their help in sample preparation, in using the QEM SEM and for their assistance in data analysis.

This work was financially supported by an Australian Government APAI scholarship and by Rio Tinto Technology and Innovation.

TABLE OF CONTENTS

LIST OF FIGURES

LIST OF TABLES

ABSTRACT

The Peirce-Smith converter has served the copper industry well for over a century, but increasingly stringent environmental regulations and burgeoning energy costs have set the trend towards continuous copper matte converting. A major technical issue with continuous converting is the choice of slag. Iron silicate slags, as used in the Pierce-Smith converter, have many favourable properties including limited wear of the magnesia-chrome refractories and high ability to absorb elements with basic oxides such as lead oxide. Unfortunately, at the high oxygen partial pressures used during copper-making, they have too low a solubility for magnetite and this results in semi-solid viscous slag. Mitsubishi introduced calcium ferrite slag for their continuous converting process because it has high magnetite solubility and high ability to remove elements with acidic oxides such as antimony and arsenic, but it attacks magnesia-chrome refractories severely. Ferrous calcium silicate (FCS) slag has been proposed as a third slag for copper converting. It has been predicted that FCS slag should not be aggressive towards refractories and would have a low copper oxide solubility and suitable solubility for magnetite and both acidic and basic impurity metal oxides. Little is known about the properties of FCS slag, in particular its affect on the wear of magnesia-chrome refractories and the distribution ratio of minor elements between it and copper.

The purpose of this research was to test the potential of FCS slag for application in continuous copper converting. Firstly, refractory wear was investigated and compared to the wear caused by calcium ferrite slag. Secondly, distribution of antimony, lead and nickel between FCS slag and copper was determined. It was found that FCS slag attacks the refractories far less than calcium ferrite slag. The slag/metal distribution ratios for nickel, lead and antimony were determined to be 0.98, 0.93, and 0.54 respectively. These compare very favorably to those for calcium ferrite slag. It was concluded that FCS slag has potential for continuous copper converting and warrants further consideration by industry.

1.0 INTRODUCTION

During copper converting the slag is required to have a relatively low viscosity so that it can be tapped easily, and a low rate of attack on the refractory bricks lining the furnace (Biswas and Davenport, 1980). A high solubility for magnetite, Fe_3O_4, is essential. It is also required to have a large Cu_2O activity coefficient to minimize copper loss and a small activity coefficient for minor element oxides to maximise their absorption into the slag and therefore the purity of the copper product (Rosenqvist, 1974). Two slag systems, iron silicate slag (FeO-Fe_2O_3-SiO_2) and calcium ferrite slag (CaO-FeO-Fe_2O_3), are being used for copper converting, however each slag has its drawbacks. Iron silicate slag has the advantage of high immiscibility with copper and the ability to remove impurities with basic oxides, such as lead. Iron silicate slag is a well established slag for batch converting, however in the case of continuous copper converting where the oxygen partial pressure at which the process operates is much higher, it has some important disadvantages. These include a small composition range within which the slag is fully molten, a low magnetite solubility and a poor ability to remove elements with acidic oxides such as arsenic and antimony. Although some magnetite is desirable as a deposit on the converter walls to protect the refractories, an excessive amount leads to viscous slags, which increases the entrained copper losses to the slag and makes tapping difficult. Mitsubishi Cooperation introduced calcium ferrite slag to overcome the drawbacks of iron silicate slag. The removal of acidic oxides from copper is about of ten times better with calcium ferrite slag than iron silicate slag (Vartianinen *et al.*, 2002). Calcium ferrite also has a much higher magnetite solubility than iron silicate slag. However, due the high basicity and low viscosity of calcium ferrite slag, significant wear to the magnesia-chrome refractories results. Calcium ferrite slag also has limited solubility for silica and a poorer ability to absorb basic oxides, such as that of lead.

Given satisfactory magnetite solubility, the two major issues involving the suitability of a slag for converting are the severity and rate of refractory attack and its ability to absorb minor elements from blister copper. The presence of minor elements such as antimony, arsenic, bismuth, lead and zinc, among others, has a detrimental effect on the physical properties of copper. Arsenic and antimony in copper result in a loss of electrical conductivity whilst the workability of copper is reduced by lead and bismuth. Refractory wear is a major economic and environmental concern. The cost of maintaining and finally replacing refractory bricks as a consequence of slag attack is a significant cost component in copper production. Contact with highly aggressive slags such as calcium ferrite, mechanical stresses and increasingly higher operating temperatures all combine to destroy the refractory bricks lining

the furnace. The most common wear mechanisms include corrosion, erosion and various forms of spalling including mechanical, structural and thermal spalling.

A compromise between calcium ferrite and iron silicate slags offers a possibility to remove both acidic and basic oxides with one slag type whilst retaining a long refractory life. Known as ferrous calcium silicate (FCS) slag, it is located in the FeO_x-CaO-SiO_2 system. It was first recognized by Yazawa *et al.* (1999) as having the potential to become the third copper converting slag, with the ability to solve the difficulties associated with both iron silicate and calcium ferrite slags whilst retaining their merits. It also presents the additional advantage of lower dissolution loss of oxidic copper during the continuous converting process.

The effects of FCS slag on the wear of magnesia-chrome refractories remains unknown, however it could be expected that the ferrous calcium silicate slag would be mild towards refractory bricks (Takeda, 2001). Yazawa *et al.* (1999) believe that FCS slag should have an optimum viscosity, high enough to limit refractory wear by slag penetration but low enough to reduce entrained copper losses. However any slag used for copper converting must have favorable minor element distribution characteristics, otherwise it will not be used. Whilst calcium ferrite slag is superior in the removal of acidic oxides and iron silicate slag in the removal of basic oxides, FCS slag is expected to perform well in the removal of both acidic and basic oxides. Yazawa *et al.* (1999) first predicted that for the removal of acidic oxides such as that of antimony, FCS slag will perform similarly to calcium ferrite slag and, whilst the removal of lead from copper is most efficient using acidic iron silicate slag, FCS slag is expected to be two to three times better than calcium ferrite slag. Neutral oxides, such as Cu_2O and NiO, are expected to distribute slightly less to FCS slag than both iron silicate and calcium ferrite slags. While predictions have been made, experimental data is very limited and has been measured under conditions rather different to that applying to continuous copper converting.

This research will provide the first rigorous investigation of the wear mechanisms of magnesia-chrome refractories employed in converting furnaces by FCS slag. It will also provide the first experimentally determined distribution data for a neutral, an acidic and a basic oxide between FCS slag and copper at typical copper converting conditions viz. a temperature of 1300^{o}C and an oxygen partial pressure of 10^{-6} atm. This information will allow a soundly based assessment of the suitability or otherwise of FCS slag for continuous copper converting.

2.0 LITERATURE REVIEW

This chapter is a detailed review of the literature relevant to this research. Pertinent background information regarding copper smelting and converting practices as well as the thermodynamics of smelting and converting are highlighted in the initial sections of this chapter. This is followed by a review on the phase equilibria of iron silicate and calcium ferrite slags, used currently in copper converting operations. Due to the importance of understanding magnesia-chrome refractories, which line the converters and the wear caused by iron silicate and calcium ferrite slags to such bricks, the preceding chapters discuss the refractories and refractory wear caused by the current converting slags. The present practices used to alleviate refractory wear are also discussed in this chapter. Following the discussion on refractory wear, this chapter reviews minor element distribution thermodynamics in a slag/metal system as well as reviewing the data available on the distribution of an acidic ($SbO_{1.5}$), basic (PbO) and neutral (NiO) oxide between iron silicate slag and copper as well as calcium ferrite slag and copper. This review on refractory wear and minor element distribution is vital to the current research as it allows comparison of the data available on the current two converting slags with the experimental results on FCS slag and be able discuss the benefits of FCS slag, if any, in regards to these two issues. Finally the body of knowledge available at present on the phase equilibria of FCS slag and minor element distribution between FCS slag and copper at converting conditions is discussed. At present there is no information in the literature on refractory wear by FCS slag, so a discussion on refractory wear by FCS slag, using published data, cannot be made.

2.1 COPPER SMELTING & CONVERTING

2.1.1 Introduction

Copper is mainly available for extraction as sulphide mineral ores such as chalcopyrite ($CuFeS_2$). The extraction processes for the recovery of copper metal from these ores are largely by pyrometallurgical techniques. Initially the copper minerals in the ore are concentrated into high-grade concentrates through physical means of froth flotation, by which copper minerals selectively attach to air bubbles by use of reagents, which render the copper minerals hydrophobic whilst the gangue minerals remain hydrophilic. The high-grade concentrate then undergoes optional roasting, which consists of partially oxidising the sulphides of flotation concentrates and eliminating sulphur as sulphur dioxide. Roasting is accomplished with air at temperatures between 500-700^{o}C, in hearth or fluid bed roasters. The roasting operation is used in smelters, which employ reverberatory or electric furnaces for smelting, where its principal purpose is to dry and heat the furnace charge, using the exothermic heat from the roasting reactions. Roasting also increases the copper concentration of the Cu_2S-FeS matte produced during smelting by oxidising some of the FeS to FeO. The copper concentrate product from roasting undergoes successive stages of smelting, converting and refining, to produce pure copper metal. The process of smelting involves melting and partially oxidising the copper concentrate with air/oxygen to remove most of the FeS as FeO, producing a silicate slag and a Cu_2S-rich matte. Converting is the formation of 'blister' copper (99% copper) and slag via the oxidation of iron and sulphur in the copper matte at 1250-1300^{o}C. Figure 2.1.1 illustrates the simplified flow sheet for the typical stages of processing sulphide mineral ores via pyrometallurgical practices to produce copper metal.

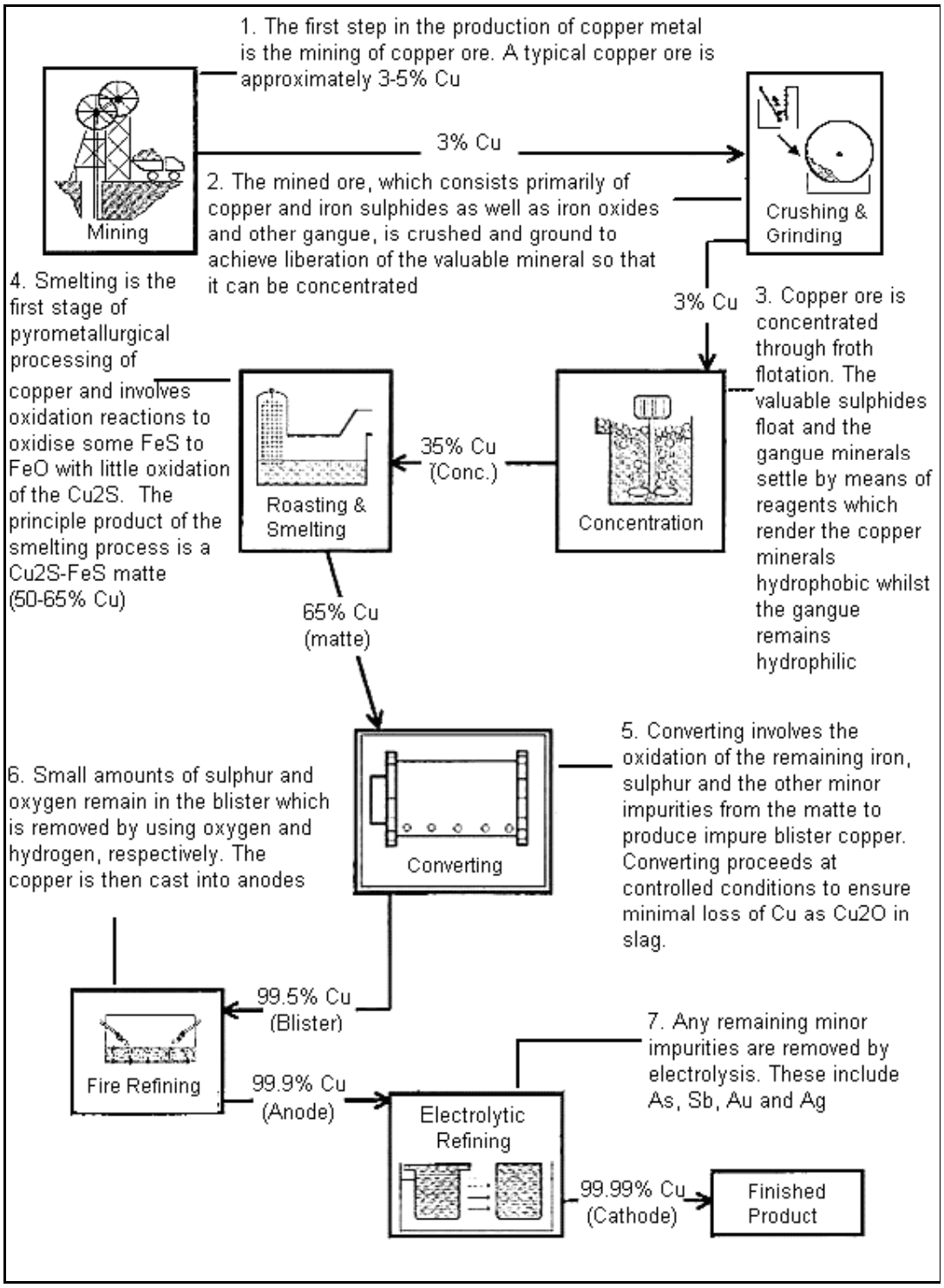

Figure 2.1.1: Flow sheet of the typical processing of copper ore via pyrometallurgical operations (Fahey, 2002)

2.1.2 Copper Smelting

The objective of smelting is to form a molten sulphide matte phase, Cu_2S-FeS, which contains 55-75% copper and a discard slag phase with the lowest possible copper content. Smelting is accomplished by melting the copper concentrates or partially roasted concentrates at approximately 1150-1250^{o}C. Silica flux is added to the furnace to separate the copper rich sulphide matte and oxide slag phases as silica addition forms an iron silicate slag with low solubility in the sulphide matte. The effects of silica on matte and slag immiscibility are discussed in Section 2.2.1.

Smelting operations are carried out in bath (blast, reverberatory, electric, Mitsubishi, Ausmelt and Noranda furnaces) and flash furnaces (Outokumpu). The earliest large-scale method of producing copper matte was by blast furnace, which could efficiently treat high-grade (5-20% Cu) sulphide ores to produce matte and slag. As ore grades declined, however, it became too expensive to treat ore directly, and concentration by froth flotation became common (Rosenqvist, 1974). The impossibility of using the blast furnace for directly treating fine flotation concentrates led to hearth or reverberatory furnace smelting. Recent developments have led to developments in flash smelting and bath smelting including the electric furnace, Mitsubishi S-furnace as well as the Ausmelt and Noranda furnaces. An in-depth discussion on the smelting furnaces is not offered in this section as the current study addresses only the copper converting processes, in particular, continuous copper converting. The following section gives a detailed review on the current batch and continuous converting practices and the motives behind the growing transitions from batch to continuous converting practices at smelters around the world.

2.1.3 Copper Converting

Molten matte from smelting contains copper, iron and sulphur as its major components. In addition, it contains minor amounts of impurity metals (e.g. As, Bi, Ni, Pb, Sb, Zn and precious metals), present in the original concentrate and not removed during smelting. This matte is charged to a converter for converting to 'blister copper'. Essentially, converting removes iron, sulphur and other impurities from the matte, thereby producing liquid copper in a crude (98.5-99.5% Cu) form, low in both sulphur and oxygen (0.02-0.1% S and 0.5-0.8% O). Converting proceeds by oxidation reactions at high temperatures of 1250-

1300^{o}C where the oxidant is air, oxygen-enriched air or pure oxygen, depending on the technology being implemented. The converting reactions are exothermic and the process is autogenous. The physical chemistry of the converting process as well as the thermodynamics of the process is given in greater detail in Section 2.2.1. The production of blister copper is conducted in two main process types:

- Batch converting, embodied by the traditional PS converters, and
- Continuous converting, including bath converting (Mitsubishi C-furnace and the Noranda converter) and Flash converting.

While batch converting, especially the Peirce-Smith converter, has served the copper industry for over a century, increasingly stringent environmental regulations, rapidly increasing energy costs and a trend towards continuous processing have set the stage for major improvements in this area of copper production.

2.1.4 Batch Converting

A) Peirce-Smith Converter

Industrial Peirce-Smith (PS) converters (Figure 2.1.2) are typically 4m in diameter and 9m in length (Biswas and Davenport, 1980) and lined with magnesia or chrome-magnesia refractory brick. A smelter normally has three to six converters depending upon its smelting furnace capacity. Air is blown into the converters through a single line of tuyeres, with there being 40-50 tuyeres per converter. Air passes through the matte to achieve oxidation reactions. The converter is provided with a rotating mechanism, which permits it to be positioned for charging, blowing and pouring (Figure 2.1.3).

The Peirce-Smith converter uses a two stage blowing process. In the first step, enriched air blown through tuyeres in the side of the vessel reacts with iron sulphide dissolved in the matte to produce sulphur dioxide gas and FeO. Silica flux is added through the top of the converter and the reaction of FeO with the silica generates an immiscible iron silicate slag phase similar to that produced in the matte smelter. The iron silicate slag is batch removed by skimming from the converter to leave an almost pure Cu_2S, 'white metal' with less than 2% iron. The skimmed slag contains a considerable amount of copper oxide at the end of the first

blowing stage and is thus recycled back to the smelting furnace to recover the copper from the slag.

The second blow in the PS batch process oxidises the remaining sulphur in the white metal generating blister copper analysing about 0.2% sulphur. No slag is produced at this stage, as very little iron remains to generate an iron silicate slag.

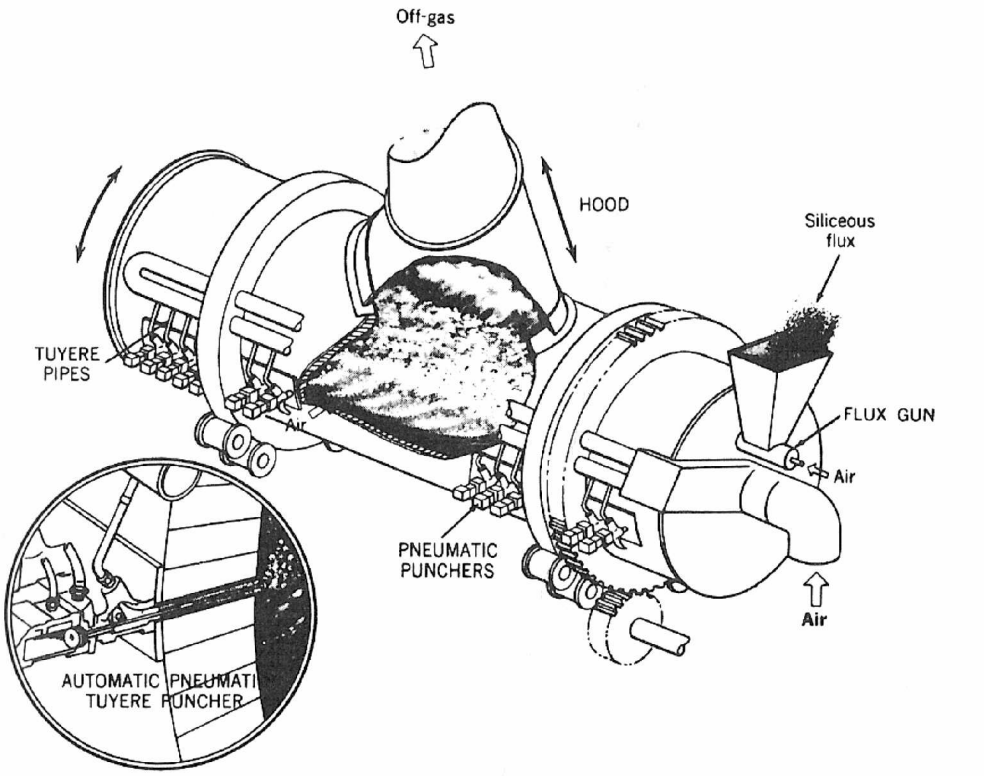

Figure 2.1.2: Peirce-Smith Converter (Boldt and Queneau, 1967)

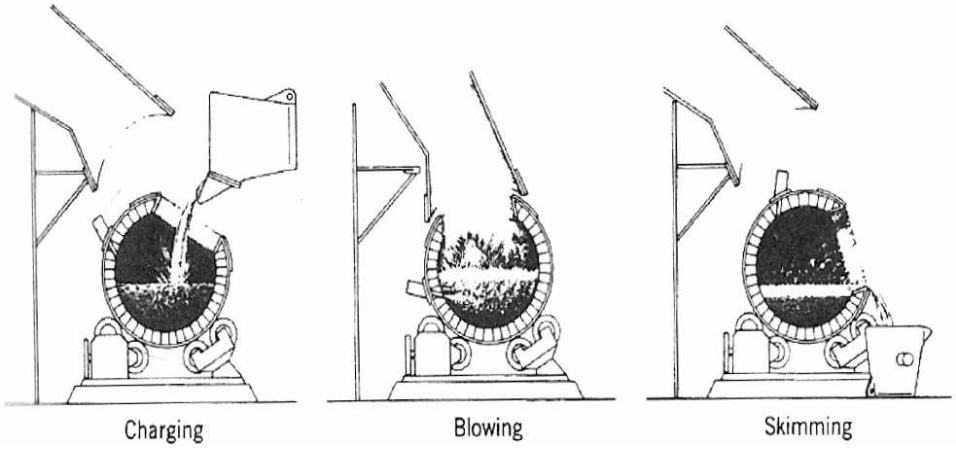

Figure 2.1.3: Charging, Blowing and Skimming action of the PS converter (Boldt and Queneau, 1967)

2.1.5 Pressures on Batch Converting Practices

The main copper smelting processes in the world today are Outokumpu flash smelting and the Pierce-Smith converting processes. Presently it is estimated that about 50% of the worldwide copper matte production is undertaken by Flash Smelting and 80% of blister copper production is by the PS converting process (Ojima, 2003). Despite its batch operation, the Pierce-Smith converting process has been widely used in many smelters for more than 100 years due to its operational flexibility (Ojima, 2003). Batch treatment of molten copper mattes in rotary Peirce-Smith furnaces has allowed the copper industry to meet increased demands for the metal, brought about by world industrialisation. However, increased awareness of environmental issues and the need to reduce capital and production costs in an increasingly competitive market are forcing the industry to re-examine the Peirce-Smith converting process and evaluate new alternatives to overcome current process limitations.

Over 90% of the world's primary copper originates in sulphide minerals so that sulphur in some form is a by-product of most copper processing (Biswas and Davenport, 1980). Furthermore, most of the sulphur is emitted as SO_2 gas, which is harmful to fauna and flora if present in the air to even a limited extent. Putting the problem into perspective, a $CuFeS_2$ concentrate produces nearly 1 tonne of sulphur (2 tonnes of SO_2) per tonne of copper extracted (Goto and Hayashi, 2003). The sulphur problem is the most controversial aspect of copper extraction and is forcing smelters to employ more environmentally friendly processes.

Copper smelters are faced with two major problems in association with the sulphur dioxide product stream, how to capture most of the SO_2 gas and how to fix the sulphur in a useful or stable form (e.g. elemental sulphur, liquid SO_2 or sulphuric acid). The most common method of fixing sulphur from SO_2 gases is the production of sulphuric acid.

The Peirce-Smith converter was developed at a time when its SO_2-bearing gases could be legally vented directly to the atmosphere. However, due to the increasing concerns over air pollution, it has become desirable, to collect all of the converter gases and to prevent their dilution with air. In order to conform to strict environmental regulations, inclusion of sulphuric acid plants to capture SO_2 in many smelters has resulted and whilst tight-fitting, water-cooled hoods have solved the problem of SO_2 capture to some extent, the gases can still escape from the P-S furnace during the charging and pouring sequences. The greatest pitfall of the P-S converter is the large amounts of fugitive gases given off during the cyclic

operation of the converter and variation in the draft of its gas handling system. Fugitive emissions are generated during charging and discharging of furnaces and during the batch transfer of molten materials into ladles. Huge volumes of air have to be collected along with the fugitive emissions and thus, a very large volume of gas with extremely low SO_2 content has to be treated. The cost of collection, handling and treating a gaseous stream with SO_2 content is proportional to its volume or inversely proportional to its SO_2 concentration. Thus emissions of fugitive gases limit the effective operation of sulphur fixation plants due to the varying concentrations of input gas, temperature and gas flow-rates. In light of complying with environmental standards the Peirce-Smith converter has required an ever-increasing number of 'add-on' modifications in many plants, adding to the cost of operating the smelter. Another restriction of the Peirce-Smith converter is the limited automation and computer control allowed by the batch process, leading to higher operating costs as a result of the labour required to operate the technology. Conversely, the high cost of gas collection and sulphur fixation equipment has become a major limitation along with increases in energy and labour costs for the P-S technology. Having served the copper industry for many years, the P-S converter is struggling to maintain the environmental, hygiene and efficiency standards of today.

Recently several newly constructed or modernised smelters have applied continuous converting processes in replacement of the P-S converting technology to alleviate the problems associated with batch converting. Continuous copper converting has been commercially available for over 25 years and now produces 15% of copper smelter production (Ojima, 2003). However, the only two commercially proven continuous converting processes with a large production capacity are the Mitsubishi C-furnace and the Kennecott-Outokumpu Flash converter. The continuous converting technology has been in operation in the Mitsubishi C-furnace since 1974 and the flash converter started operation in Kennecott Utah Copper USA in 1995. Although the continuous converting processes have been increasingly used in smelters they still occupy a small portion of the world's copper production and in spite of the many well-known problems inherent in P-S converting, it remains the dominant copper converting process.

2.1.6 Moving towards Continuous Converting Practices

Since the continuous converting process is carried out in a stationary and sealed vessel allowing tight connections to gas handling equipment and eliminating the need for charging, skimming and pouring, fugitive gas emissions are significantly reduced due to minimised air infiltration. The stationary nature of the furnace also means that the furnace can be sealed more effectively against the outside atmosphere, hence reducing the dilution of SO_2 with air.

Continuous converters use high levels of oxygen enrichment, producing concentrated SO_2 waste gas at constant flow-rate and temperature and permitting excellent sulphur capture. Production of highly concentrated off-gases by utilising oxygen enrichment avoids the dilution of furnace off-gases with nitrogen in the air, which results in the production of lower volumes of waste gas. The low volume, concentrated SO_2 off-gases, reduces both gas cleaning and acid plant requirements and thus lowers capital costs. The constant temperature of the gas treated in the acid plant also results in reduced corrosion caused by temperature cycling.

As matte transport in ladles is eliminated and replaced by launders in the process of continuous technology, the corresponding fugitive emissions in the working space are avoided and there is also a reduction in the difficulties of materials handling.

The continuous technology is also better suited for a greater degree of automation and computer control, thereby reducing the labour costs associated with batch converting and increasing production rate of the copper product.

Currently there are a number of continuous and semi-continuous converting processes employed in the copper industry, including the Mitsubishi process, the Noranda process, the Ausmelt technology and the Kennecott/Outokumpu flash converting process. However the following section will only address the Mitsubishi and Kennecott/Outokumpu processes as their converting process is a slag-metal system, which is the interest of this study. The Mitsubishi process is the only successful continuous smelting, converting and refining operation that has been implemented on a commercial scale. In addition to the Mitsubishi process, the Kennecott/Outokumpu process, which is a continuous converting process with the capability of being retrofitted with any smelting technology, for reasons explained later,

has been successfully tested and used industrially. The main advantage of the Mitsubishi and Kennecott technologies is the continuous and uniform production of effluent gas high in SO_2 concentration, which permits efficient collection of the gas for SO_2 removal.

2.1.7 Mitsubishi Process

Beginning in the late 1960's Mitsubishi began development of a multi-furnace continuous smelting, converting and slag cleaning process. The process involves the continuous and coordinated operation of three furnaces arranged in a cascading orientation to allow gravity transfer of molten materials in heated launders.

The Mitsubishi process (Figure 2.1.4) is comprised of three interconnected furnaces, the Smelting furnace (S-furnace), Slag Cleaning furnace (CL-furnace) and Converting furnace (C-furnace), which can produce blister copper continuously from concentrates. In the circular S-furnace, feed materials of copper concentrate, flux and in-plant reverts, are charged through multiple top blowing consumable lances, together with oxygen-enriched air, into the matte phase inside the furnace.

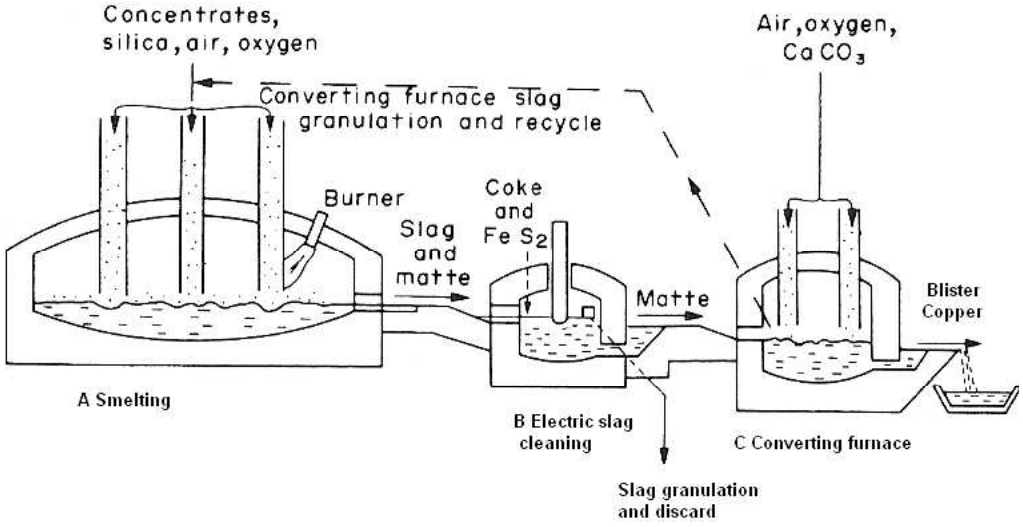

Figure 2.1.4: Mitsubishi Process (Shibasaki and Kanamori, 1989)

The high-grade (60-65% Cu) matte and slag produced are transferred through a launder to an electric slag-cleaning furnace, where the matte settles and the discard slag (0.5% Cu) overflows to a granulation system. The matte from the slag-cleaning furnace is siphoned

out of the unit for transfer through another launder to the converting furnace. The circular converting furnace continuously oxidises the matte to produce blister copper, by-product slag and SO_2 gas. Consumable lances installed through the roof of the converting unit introduce oxygen-enriched air (35-40% O_2) and limestone flux to the matte for conversion to blister.

The C-slag that overflows from the C-furnace contains about 10-15% copper and is water granulated, dried and recycled to the S-furnace to recover its copper content. At the same time, the blister copper produced contains about 0.6-0.7% sulphur and is continuously siphoned from the C-furnace and forwarded to one of several anode furnaces using switching launders that divert the flow of blister to any anode furnace at will. The off-gas is withdrawn through a flue where it is treated prior to release.

In the Mitsubishi process, the matte flow-rate to the converting furnace is constant because the bath levels in the smelting and converting furnaces are fixed by overflow weirs and the matte production is governed by the concentrate feed rate.

The oxidant in the smelting and converting furnaces is oxygen-enriched air (26% O_2 and 35-40% O_2, respectively) and is blown onto the slag surface by 8-10 vertical non-submerged lances (George, 2002).

One important pioneering aspect of the Mitsubishi process is the use of limestone flux, producing a basic calcium ferrite slag in the converting furnace. The major advantage of using calcium ferrite slag compared to iron silicate slag is the higher holding capacity of magnetite in the ferrite slag, which otherwise precipitates from iron silicate slag at continuous converting oxygen partial pressure. Precipitation of magnetite results in solid particle suspension in the slag which once settled out on the converter walls causes loss of furnace volume, increase in slag viscosity and entrained copper loss. A detailed discussion of magnetite behaviour in both iron silicate and calcium ferrite slag is given in Section 2.2.2. The adoption of limestone as flux was one of the major reasons that Mitsubishi succeeded in the development of continuous production method of copper. This slag also avoids foaming problems associated with iron silicate slag operating at the high partial pressure of oxygen necessary for the production of copper when using gas injection through lances. Unfortunately, the slag is highly corrosive to all commercial refractory bricks. This corrosion is exacerbated by the high degree of bath agitation induced by the multiple top-blowing lances. The fundamental problem with the highly agitated bath is the difficulty in maintaining

refractory protection on the water-cooled slag line. The low melting point and corrosive slag prevents formation of a suitable magnetite protection lining on the cooling elements.

Currently the Mitsubishi process is employed at the Kidd Creek Smelter, Naoshima Smelter, LG Metals in Korea (Onsan Smelter) and in Gresik, Indonesia (Gresik Smelter).

2.1.8 Kennecott/Outokumpu Oy Flash Converting Process

In contrast to a growing number of approaches for continuous converting using molten copper mattes, Kennecott developed a process for treating solidified matte. Kennecott Corporation's primary motivation for the development and implementation of the Flash converting technology was to be able to abide by the rigid new sulphur dioxide gas emission laws in the state of Utah, USA, which the existing P-S converter at the smelter was failing to meet due to fugitive gas emissions and SO_2 gas capture problems.

In 1979, Kennecott began development of a new concept for continuous copper converting known as Solid Matte Oxygen Converting or SMOC. The concept involves the deliberate solidification of copper matte followed by its conversion to copper metal by oxidation in a flash furnace.

In 1984 Kennecott and Outokumpu entered into a technology development and marketing agreement for SMOC and in 1991 Kennecott began the final phase of testing at Outokumpu to confirm the design of its new Utah Smelter using the technology. The first converting process at full industrial scale was put into operation in Kennecott Corporation's Salt Lake City Plant in June 1995 and consisted of the Kennecott Flash Smelting and the Kennecott-Outokumpu Flash Converting technology (Figure 2.1.5).

Solid matte oxygen converting eliminates transfer of molten matte between furnaces and allows tight control of emissions, minimising fugitive gases and thus producing high-strength SO_2 off-gases, which subsequently reduce off-gas handling requirements. Hot metal cranes and ladles are also eliminated and independent operation of the smelting and converting furnace is possible, i.e. allows decoupling the smelting and converting processes as a result of being able to stockpile the solidified matte between the two furnaces.

Furthermore, since the furnaces can be operated independent of one another, the whole line does not have to be shut down when one furnace stops.

The molten high grade matte produced in the flash smelting furnace is led by means of covered launders to be solidified by cooling in ladles or pits or directly by granulation, where the matte is dispersed by means of high pressure water jets. The matte granules are ground by conventional techniques into a grain size of 80% less than 100 mesh, which is sufficient for complete reactions in the flash converting furnace (Hanniala *et al.*, 1993). Once the matte feed is granulated, dried and ground it can be stockpiled or continuously charged to the flash converter.

The fine-grained matte and limestone flux are fed to a single burner on the reaction shaft of the flash converter where matte is oxidised to blister copper and calcium ferrite slag using pure oxygen or up to 70% oxygen enriched air. The slag composition is controlled to 18% Cu and 16% CaO (Hanniala *et al.*, 1998). The copper content of the slag produced in the flash converting furnace is high but because of the small slag amount it can be fed back into the primary flash smelting furnace directly in the molten state or in granulated form. The slag can also be treated separately for copper recovery. Blister copper, containing 0.1-0.5% sulphur is laundered to the anode furnace for refining prior to casting (Newman *et al.*, 1998). The converting furnaces also produce gas rich in SO_2 and small gas volume due to the high oxygen enrichment, making the process the cleanest in the world in terms of gas emission (George, 2002). The gas is continuously cooled and cleaned through gas scrubbers before passing to the sulphur recovery plant.

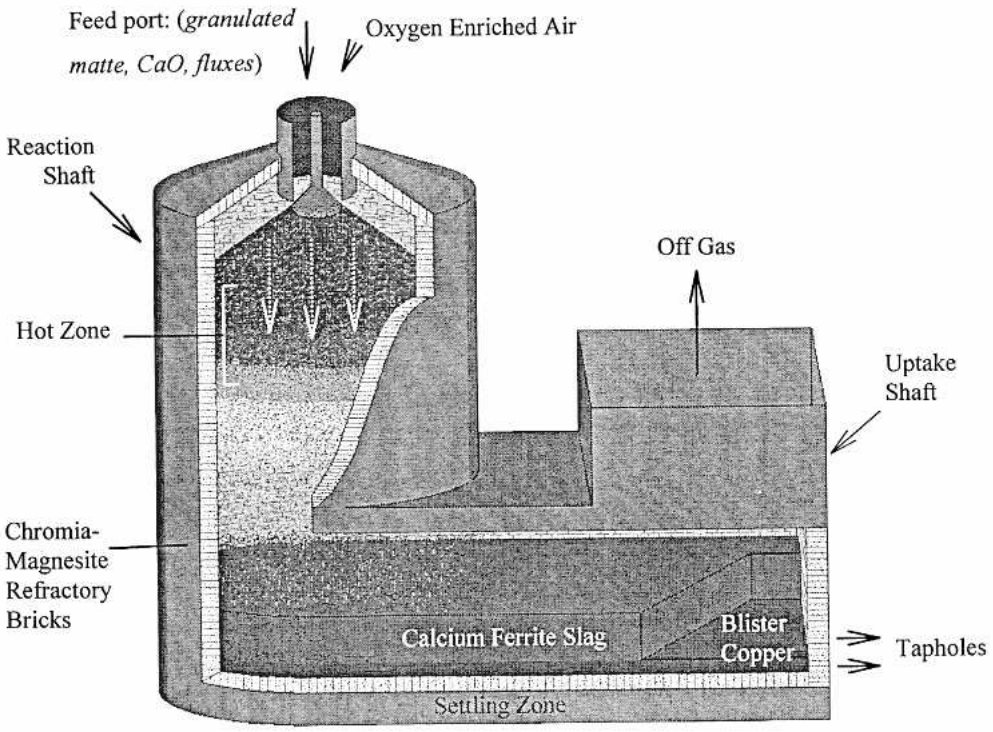

Figure 2.1.5: Kennecott-Outokumpu Flash Converting technology (Fahey, 2002)

2.2 THERMODYNAMIC DESCRIPTION

2.2.1 Physical Chemistry and Thermodynamics

The copper concentrate in the form of chalcopyrite, $CuFeS_2$, contains approximately 36% copper, 25% iron and 27% sulphur with other minor metal impurities. Copper is extracted from the sulphide ore via three steps of matte smelting, converting to blister copper and anode refining. The following section briefly discusses the physical chemistry of matte smelting and then discusses in more detail the chemistry and thermodynamics of copper converting.

A) Physical Chemistry of Smelting

The charge entering the smelting furnace can be represented as a Cu_2S-FeS concentrate. Matte smelting involves the oxidation of FeS in the charge to FeO at 1150-1250^oC with little oxidation of Cu_2S. The smelting process produces two liquid phases of slag (mostly oxides) and matte (mostly sulphides) which is much richer in copper (55-75% Cu).

The matte contains approximately. Even though the complete separation of copper and iron is the eventual aim, some iron in the form of FeS remains in the matte to ensure that any Cu_2O, which forms or is present from the recycled converting slag, is converted back to Cu_2S. Copper oxide reacts with iron sulphide to revert to Cu_2S due to the thermodynamic higher stability of FeO compared to FeS and Cu_2O, acting as the driving force for equilibrium reaction 2.2.1.

$$FeS_{(matte)} + Cu_2O_{(slag)} \rightarrow FeO_{(slag)} + Cu_2S_{(matte)}$$

$$K = \frac{a_{FeO}.a_{Cu_2S}}{a_{FeS}.a_{Cu_2O}}$$

$$a_{Cu_2O} = \frac{a_{FeO}.a_{Cu_2S}}{a_{FeS}} K^{-1} \qquad \textbf{Equation 2.2.1}$$

$$\Delta G^{o}_{1300^{o}C} = -119.93\,\text{kJ/mol}$$

$$\mathrm{K}_{1300^{o}C} = 9.60\times10^{3}$$

For equilibrium between an iron-copper matte and slag, the Cu_2O activity is defined by Equation 2.2.1. Assuming that the matte is an ideal solution, such that $N_{Cu2S} + N_{FeS} = 1$, and $a_{Cu2S} = N_{Cu2S}$ and $a_{Fe2S} = N_{Fe2S}$, for a slag with constant FeO activity, which is a reasonable assumption because the slag is typically close to silica saturation, it is expected that the activity of Cu_2O and consequently the amount of copper dissolved in slag will increase with increasing matte grade, first slowly and then rapidly as the FeS activity approaches zero. The activity of copper oxide (a_{Cu2O}) is inversely proportional to the activity of FeS (a_{FeS}). Thus whilst the activity of FeS in matte is high, copper oxide cannot form in any appreciable form, ensuring that dissolved copper loss to slag is low. Reaction 2.2.1 can also be used to advantage for recovering oxidised copper from converter slags. The large equilibrium constant K for reaction 2.2.1 indicates that the reaction strongly favours the product side and that copper oxide is almost completely sulphurised by FeS at smelting temperatures.

Initially the iron oxide formed in smelting is dissolved in matte. In order to separate the oxide from the matte phase silica is added to the furnace, which interacts strongly with FeO, forming a slag phase with low solubility in matte. Figure 2.2.1 shows the effect of silica upon matte/slag separations. Liquid FeO and FeS are completely miscible so the sulphide-oxide system is a single phase, but the presence of SiO_2 causes the molten oxysulphide phase to separate into two immiscible liquid phases, the sulphide rich liquid and the oxide rich

liquid, the compositions of which are given by the tie lines a, b, c and d on the curve ACB. The arrow shows the increase in silica content of the system. The greater the silica concentration the more marked is the differentiation between the two phases with maximum separation at silica saturation. The compositions of the two phases at silica saturation are given by points A (slag) and B (matte).

The structures of matte and slag, and the effects of silica upon them, explains the observed matte-slag immiscibility behaviour. As explained by Biswas and Davenport, 1980, when silica is absent, the oxides and sulphides combine into one covalently bonded, semi-conducting Cu-Fe-O-S phase. When silica is present, however, it combines with the oxides to form strongly bonded silicate polymer anions, one such anion being, $Si_3O_8^{4-}$, which group together to form an iron silicate slag phase, $2FeO.SiO_2$. The sulphides show no tendency to form these anion complexes and hence they remain as a distinct covalent matte phase, dissimilar to the silicate slag, creating two immiscible phases.

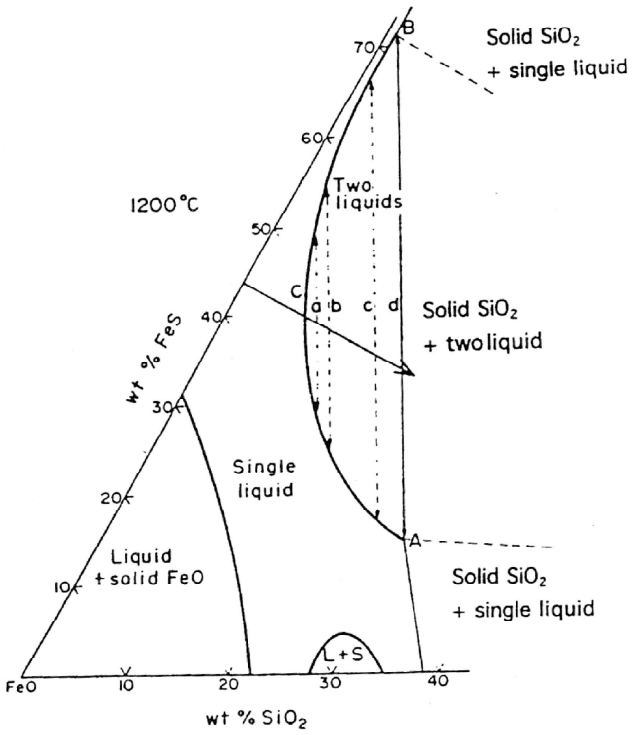

Figure 2.2.1: Effect of silica upon matte/slag separations (Biswas and Davenport, 1980)

B) Physical Chemistry & Thermodynamics of Converting

The purpose of converting is to remove iron, sulphur and the other minor impurities from the matte, producing blister copper (99% Cu) and a converting slag.

In batch converting, two sequential stages of slag blow and copper blow take place, with the converter slag removed at the completion of slag-blow. In continuous converting, however, both the 'slag-blow' and 'copper-blow' stages occur simultaneously in contact with the slag phase. The converting reactions are exothermic and the process is autogenous. The first stage, the slag-blow stage, is the oxidation of iron sulphide, which is done by blowing oxygen (pure or as air) into molten Cu_2S-FeS matte producing FeO and SO_2, according to Equation 2.2.2.

$$FeS + 1.5O_2 = FeO + SO_2$$
$$\Delta G^{o}_{1300^{o}C} = -342.17 \text{ kJ/mol} \qquad \textbf{Equation 2.2.2}$$
$$\mathrm{K}_{1300^{o}C} = 2.304 \times 10^{11}$$

The blowing of oxygen into the matte results in the preferential oxidation of FeS to FeO over the oxidation of Cu_2S, according to the Gibbs free energy minimization rule, which states that all reactions proceed to lower their Gibbs free energy and is illustrated on the Ellingham diagram at standard conditions (Figure 2.2.2). The Gibbs free energy of formation primarily determines the sequence of oxidation of the matte components, and hence components with the lowest free energy should be oxidized first.

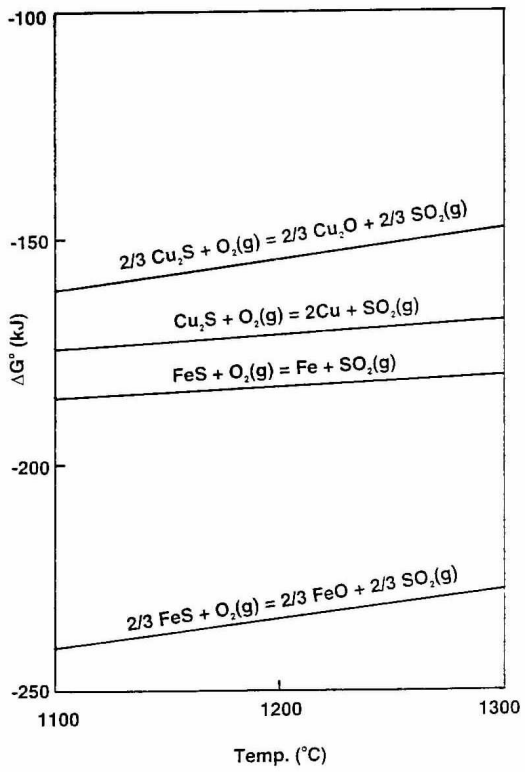

Figure 2.2.2: Ellingham Diagram at Standard Conditions (Swinbourne, 2003)

Moving down the Ellingham diagram, towards the bottom of the diagram, the reactions become progressively more negative in Gibbs free energy, and their products more stable. As can be seen from Figure 2.2.2, at a particular temperature, iron sulphide in the Cu_2S-FeS matte, will oxidise to iron oxide much more readily than the copper sulphide to copper oxide or even Cu_2S to copper. The process of smelting and converting is based on the fact that FeO is more stable and the standard Gibbs free energy of formation of FeO per mole of oxygen is more negative than that of copper oxide and copper. Since FeS is much less stable than FeO, it is readily oxidised. The formation of FeO is the driving force for the oxidation reactions in smelting. The oxidation of Cu_2S will not occur until the system is devoid of FeS, thus explaining the initial oxidation of iron sulphide in matte smelting and the slag blow stage of copper converting. As in copper smelting, any copper oxide that forms is re-sulphurised to Cu_2S according to Reaction 2.2.1.

Once iron sulphide is removed from the matte as FeO, white metal, which is essentially pure Cu_2S with less than 2-wt% iron, remains. The copper blow stage, involves the oxidation of the remaining sulphur in copper sulphide to produce blister copper. There are three steps in the copper making stage as indicated by Cu-S phase diagram in Figure 2.2.3. When oxygen (as air or pure oxygen) is first blown through Cu_2S, sulphur is removed as SO_2

to give a sulphur-deficient white metal and no metallic copper, with the melt remaining as a single phase. As further sulphur is oxidised, the melt composition enters a "miscibility gap" where two immiscible liquids coexist in equilibrium. Subsequent blowing of oxygen causes a second liquid phase, blister copper, to appear at point c, and the average composition of the liquids is now in the liquid-liquid immiscibility region. Further blowing of oxygen into the white metal results in additional sulphur being removed and the amount of blister copper increases at the expense of white metal. Whilst the composition of both phases remains constant, the proportions of the phases change. Once the melt composition leaves the miscibility gap, only the blister copper remains. The overall reaction for this step, given by Equation 2.2.3, takes place until the sulphur is lowered to point d.

$$Cu_2S + O_2 = 2Cu + SO_2$$
$$\Delta G^{o}_{1300^{o}C} = -169\ \text{kJ/mol} \qquad \textbf{Equation 2.2.3}$$
$$\mathrm{K}_{1300^{o}C} = 4.11\times10^{5}$$

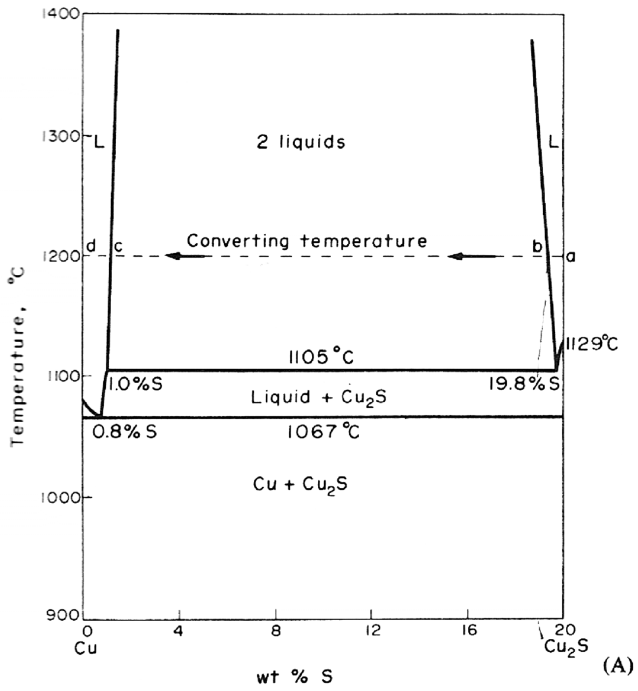

Figure 2.2.3: Cu-S phase diagram (Biswas and Davenport, 1980)

The Ellingham diagram also explains the tendency of copper sulphide to oxidise to copper metal more readily than to copper oxide. This is primarily due to the more negative Gibbs free energy of formation of copper per mole of oxygen gas reacted with copper sulphide than the Gibbs free energy of formation of copper oxide at temperatures in the order

of 1200-1300°C. As indicated by Reaction 2.2.1, late in the slag-forming stage, when the converting system is devoid of FeS, its activity decreases, and there is an increase in Cu_2O activity (and concentration) in the slag produced. However, some of the copper oxide formed reacts with the copper sulphide to produce copper and sulphur dioxide in the copper blow stage of the converting process. Once again the large K indicates that the reaction strongly favours the product side.

$$Cu_2S + 2Cu_2O = 6Cu + SO_2$$
$$\Delta G^o_{1300^oC} = -62.64 \text{ kJ/mol} \qquad \textbf{Equation 2.2.4}$$
$$\mathrm{K}_{1300^oC} = 1.202 \times 10^2$$

However, as the Gibbs free energy of formation for copper is not much higher than that of copper oxide, Cu_2O formation is inevitable. The stability of Cu_2S is not much different to Cu_2O, thus depending on the technology implemented, it is possible to obtain a high recovery of Cu metal at the expense of copper loss to slag as copper oxide or a lower direct recovery of copper and higher sulphur content in blister copper.

When the converter contains only impure blister copper, two competing reactions (competing for the reactant oxygen) predominate, Equation 2.2.5;

$$S + 2O = SO_2(g) \qquad \textbf{Equation 2.2.5}$$

Where the sulphur and oxygen are both dissolved in copper, and Equation 2.2.6;

$$4Cu + O_2 = 4Cu_2O$$
$$\Delta G^o_{1300^oC} = -106.4 \text{ kJ/mol} \qquad \textbf{Equation 2.2.6}$$
$$\mathrm{K}_{1300^oC} = 3.42 \times 10^3$$

where the dissolved oxygen reacts instead with copper to form copper oxide. When there is still an abundance of sulphur remaining in the converter, the first reaction dominates and copper is not appreciably oxidised to copper oxide until the melt is almost devoid of sulphur. Although removing sulphur is the aim, it is not all removed in the converter, to avoid excessive amounts of copper oxide forming. The final sulphur is removed by fire refining in the anode furnace and great care is taken to ensure that copper is not over-oxidised to

excessive amounts of copper oxide. The final product of copper converting is approximately 0.02-0.1% S and 0.5-0.8% O as copper sulphide and copper oxide, respectively and 99% Cu.

2.2.2 Yazawa Chemical Potential Diagram

In Section 2.2.1, the chemistry and thermodynamic interactions taking place in smelting and converting operations were described. In order to correlate the inter-relations between the main reactions of copper smelting and converting, the Sulphur-Oxygen Chemical Potential diagram for the Cu-Fe-S-O-SiO_2 system at 1300°C, originated by Yazawa (1980), can be utilised. The chemical potential diagram was constructed for an silica-saturated iron silicate slag system and demonstrates the conventional smelting process as outlined by path 'pqrcstp' for smelting and path 'cd' for converting in Figure 2.2.4. In tracing this path, the Yazawa diagram integrates the smelting and converting thermodynamics described in Section 2.2.1 and identifies the constraints to overcome in order to achieve a continuous converting process.

A) Smelting

As illustrated in Figure 2.2.4, the part enclosed by 'pqrcstp' represents smelting where the two liquid phases of matte and iron silicate slag coexist with the gas phase at 1300°C under ambient pressure conditions.

Current smelting operations worldwide implement oxygen-enriched air as the oxidising gas for the conversion of copper concentrates to matte. At smelting conditions, the reaction of oxygen with the sulphide concentrate results in the reaction of oxygen and sulphur to produce sulphur dioxide as per reaction 2.2.7.

$$\frac{1}{2}S_2 + O_2 = SO_2$$

$$\mathrm{K}_{1300^oC} = 1.61\times10^8 \qquad \textbf{Equation 2.2.7}$$

$$\log p_{O_2} = -8.21 - \frac{1}{2}\log p_{S_2} + \log p_{SO_2}$$

The large equilibrium constant (K) shows that the reaction heavily favours the product side. The molar ratio between the oxygen reactant and the sulphur dioxide product is very

close to 1:1, so at equilibrium the input partial pressure of oxygen will be approximately equal to the partial pressure of sulphur dioxide. The oxygen partial pressure in equilibrium with sulphur dioxide is typically of the order of 10^{-8} atm. in industrial smelting furnaces.

For pure oxygen $p_{O_2} \approx p_{SO_2} \approx 1$ atm. and Equation 2.2.7 equates to:

$$\log p_{O_2} = -8.21 - \frac{1}{2}\log p_{S_2} \qquad \textbf{Equation 2.2.8}$$

Equation 2.2.8 is represented on the chemical potential diagram as line 'tp', corresponding to $p_{SO_2} \approx 1$ atm. The gas phase composition will be on this line. If air is used as the oxidant gas, then the gas phase composition lies a little above the line for $p_{SO_2} \approx 0.1$ atm. line. Modern smelters use air with 40% oxygen enrichment, where the typical oxygen partial pressure of the input gas is 0.4 atm., and smelting proceeds along the line of $p_{SO_2} = 0.31$ atm. Although, the two liquid phases of matte and slag can coexist over the region of 'pqrcst', smelting operations proceed on the isobars between $p_{SO_2} = 0.1$ atm. (air) to $p_{SO_2} = 1$ atm. (pure oxygen), depending on the level of oxygen enrichment.

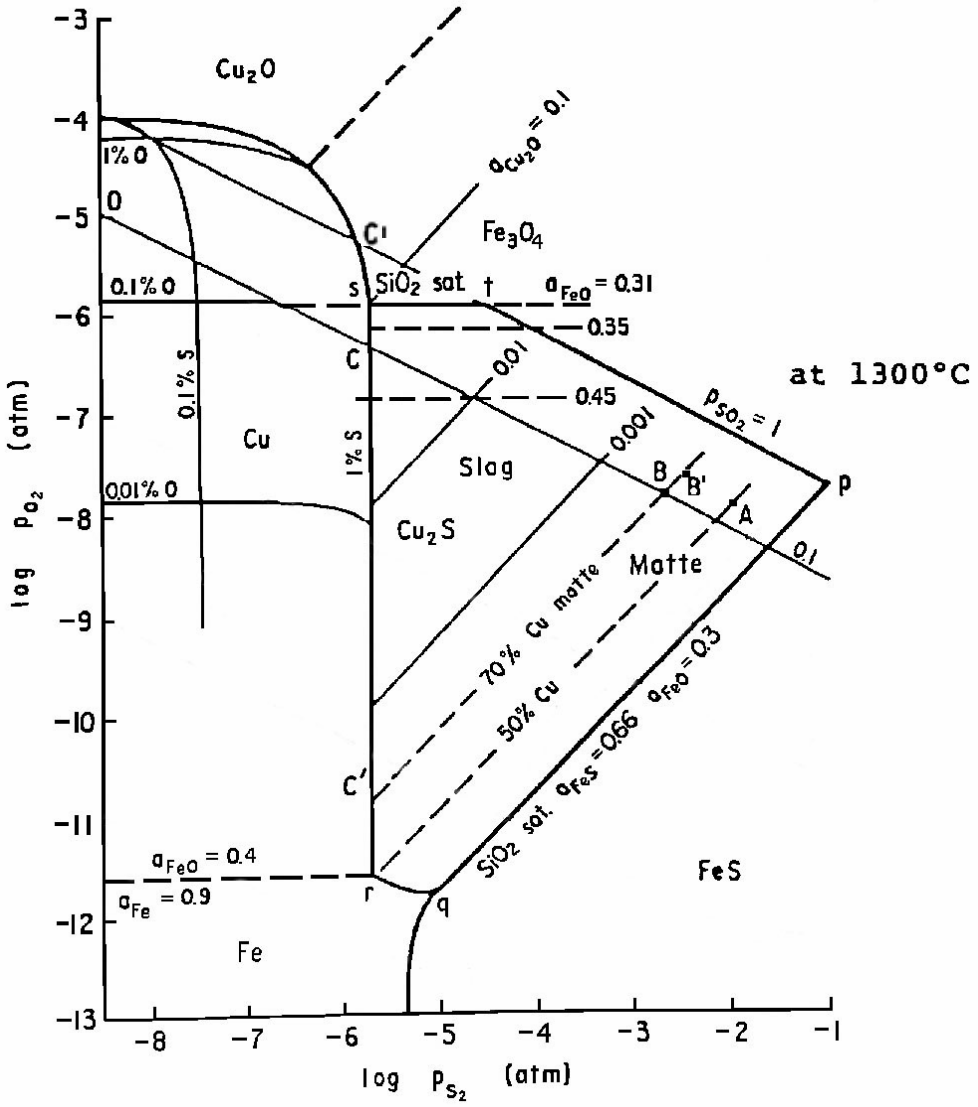

Figure 2.2.4: Yazawa Chemical Potential Diagram (Yazawa, 1980)

The line 'pq' in Figure 2.2.4 represents the beginning of smelting and the oxidation of FeS (Equation 2.2.9). On this line copper free matte coexists with silica saturated iron silicate slag.

$$FeS_{(l)} + \frac{1}{2}O_{2(g)} = \frac{1}{2}S_{2(g)} + FeO_{(l)}$$

$$\log p_{O_2} = [-2\log K + 2\log a_{FeO}] - 2\log a_{FeS} + \log p_{S_2}$$

Equation 2.2.9

The activity of FeS is a function of matte composition whilst the activity of FeO depends on the silica content in the slag. The higher the silica content, the lower the a_{FeO}. In commercial operations the silica content of the slag is kept close to silica saturation as

maximum separation of matte and silicate slag occurs at slag composition corresponding to silica saturation (Figure 2.2.1). Under these conditions, by experiment at 1300°C, the activity of FeO in the silica-saturated slag is constant at approximately 0.3. According to experimental data as illustrated in Figure 2.2.5, at this FeO activity, the maximum a_{FeS} is 0.66 where the matte contains no copper.

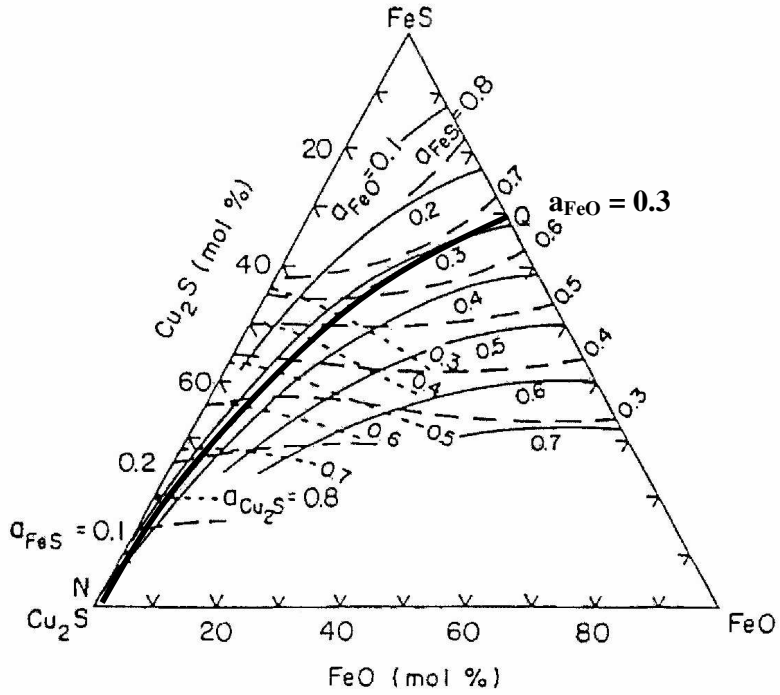

Figure 2.2.5: FeS-FeO-Cu2S System (Swinbourne, 2003)

The dotted lines parallel to 'pq' represent the increase of matte grade, under the assumption that the iron silicate slag is silica-saturated and thus a_{FeO} is fixed at 0.3. As FeS is oxidised from the matte, the weight percent of copper in matte increases and the line 'pq' shift to the left.

The typical concentrate entering the smelter contains approximately 35wt% copper and is represented on the Yazawa Diagram by point A, where p_{SO_2} = 0.31 atm. (for 40% oxygen enriched air). Smelting starts at point A and the matte making step stops at point B' along the p_{SO_2} = 0.31 atm. line. At this point the concentration of copper in the matte is approximately 65-68wt% Cu. Between point A and B', there is little variation in the partial pressures of O_2 and S_2 despite the large matte grade changes. Activities of Cu_2O in the melt are shown by lines parallel to matte grade lines representing Equation 2.2.10. The activity of

copper oxide at point B' is very low, below 0.001, so the amount of copper dissolved in slag is small. Thus, it is possible to discard the smelting slag without losing an unacceptably high amount of dissolved copper.

$$2Cu_2S_{(l)} + O_{2(g)} = S_{2(g)} + 2Cu_2O_{(l)}$$
$$\log p_{O_2} = [-\log K - 2\log a_{Cu_2S} + 2\log a_{Cu_2O}] + \log p_{S_2}$$

Equation 2.2.10

The line 'rq' corresponds to the boundary where solid iron precipitates under extremely low SO_2 and O_2 pressure, a condition not normally experienced in commercial matte smelting processes. Matte, (which contains no iron sulphide) and silicate slag coexist with liquid copper on the straight-line 'rcs'.

B) Effects of Magnetite on Converting

At high oxygen partial pressures, as experienced in copper converting, Fe^{2+} tends to partially oxidise to Fe^{3+}, such that both Fe^{2+} and Fe^{3+} are present in the slag. Under such conditions, a very stable iron oxide, magnetite (Fe_3O_4), which contains both Fe^{2+} and Fe^{3+} ions, can also form and precipitate from the slag. Although some magnetite deposits are desirable as a protection layer on the converter walls to protect the refractories, an excessive amount leads to viscous slags. The highly viscous behaviour of the resulting slag increases the entrained copper losses to the slag and makes slag tapping from the furnace difficult.

As shown in Equation 2.2.11, the oxygen partial pressure at which magnetite precipitates from slag is inversely proportional to a_{FeO}. Given that the activity of FeO is approximately fixed and lowest in a SiO_2 saturated iron silicate slag, the equilibrium partial pressure of oxygen for magnetite saturation is calculated as approximately 10^{-6} atm. at 1300°C, according to Equation 2.2.11.

$$6FeO + O_{2(g)} = 2Fe_3O_4$$

$$K_{1300^oC} = 1.29 \times 10^9$$

$$a_{FeO} = 0.31$$

$$a_{Fe_3O_4} = 1$$

$$p_{O_2} = \frac{(a_{Fe_3O_4})}{(K)(a_{FeO})} \qquad \textbf{Equation 2.2.11}$$

$$\log p_{O_2} = -\log K - 2\log a_{Fe_3O_4} - 6\log a_{FeO}$$

$$\log p_{O_2} = -\log(1.29 \times 10^9) - 2\log(1) - 6\log(0.31)$$

$$p_{O_2} = \sim 10^{-6}\, atm$$

When the equilibrium oxygen partial pressure rises above 10^{-6} atmospheres, solid magnetite will precipitate from iron silicate slag. The solid line 'st' on the Yazawa diagram represents magnetite precipitation $\log p_{O_2}$. Since the equilibrium oxygen partial pressure for magnetite saturation is inversely proportional to a_{FeO}, if a_{FeO} becomes higher (i.e. the slag is not silica saturated), the $\log p_{O_2}$ at which solid magnetite precipitates becomes lower. For example, if the activity of FeO is 0.45, then magnetite will precipitate from the silicate slag at approximately 10^{-7} atm so magnetite will precipitate from the slag before the end of the slag-blow stage of converting. Thus it is vital to keep the slag saturated with silica during smelting.

Temperature control is also vital to eliminate the possibility of magnetite precipitation as it affects the equilibrium constant, K, for Reaction 2.2.11. If the temperature in the reactor is reduced, K is increased and the oxygen partial pressure at which magnetite saturates decreases. As per Equation 2.2.11, if the smelting temperature is reduced to 1200°C, $K_{1200^oC} = 3.12 \times 10^{10}$ and assuming $a_{FeO} = 0.31$, magnetite precipitates at p_{O_2} = ~10^{-8} atm. Thus Fe_3O_4 crystals form before the slag blow stage of converting is complete.

C) Batch Converting

The detailed discussion in Section 2.2.1 on the reactions involved in copper converting can be traced on the Yazawa diagram from point B to D. Traditional batch converting is conducted with the use of air, thus p_{SO_2} drops from 0.31 atm. to 0.15 atm., that is, from point B' to B. The slag blow stage, starts at point B and finishes at point C, with an increase in matte grade from around 68% to 80wt% copper as copper sulphide. According to Reaction 2.2.1, as the activity of copper sulphide increases (i.e. increase in matte grade), the activity of

FeS in matte decreases, approaching zero. Whilst the activity of FeS in matte is high (closer to point B), copper oxide does not form in any appreciable amount, however the activity of copper oxide rises considerable as point C is approached and matte grade increases. Increasing copper oxide activity results in higher dissolution loss of copper to slag. Converter slag is normally recycled to the smelting furnace since it contains enough copper to make it economical to reprocess. Between points B and C, the partial pressures of both O_2 and S_2 increase severely. Another revelation from the Yazawa diagram is that as point C is approached, the activity of magnetite rises sharply, however, provided the slag is silica saturated and air is used as the oxidising gas (p_{SO_2} = 0.1 atm.), magnetite will remain dissolved in slag and the slag-blow stage will terminate before the slag is saturated with magnetite (i.e. point C is reached before the vertical $a_{FeO} = 0.31$ line where $a_{Fe3O4} = 1$).

The copper-blow stage begins at point C and ends at point D. At point C, sulphur in white metal is oxidised to produce blister copper and the two phases exist in equilibrium with the gas phase. The gas composition remains constant at point C. The blister copper contains 1.0% sulphur, 0.1% oxygen at this point. The copper in equilibrium with Cu_2S remains at this composition until eventually the system becomes so sulphur deficient that the sulphide phase disappears and only the blister copper remains. The gas composition then moves along the p_{SO2} line and two competing reactions (Reactions 2.2.5 and 2.2.6) predominate whilst approaching point D, such that the oxygen in blister copper increases and the sulphur decreases. The copper blow stage stops at point D and copper has around 0.5wt% oxygen and 0.05wt% sulphur that is removed through anode refining. In the copper region of Figure 2.2.4, vertical and horizontal lines represent dissolved sulphur and oxygen in the copper respectively.

D) Continuous Converting

Continuous converting processes operate either with pure oxygen or oxygen enriched air in order to reduce waste gas volume and maintain heat balance without excessive supplementary heat input. Consequently these reactions proceed along the isobar close to $p_{SO_2} \approx 1\,\text{atm.}$, whilst in contact with slag. As can be observed on the Yazawa diagram, the use of pure oxygen creates no problems in the smelting process; however, in the later stages of the slag blow (i.e. as C' is approached), the activity of copper oxide is very high, an order of magnitude higher than in batch converting (i.e. at point C). Although the amount of slag

formed is not very large, it must be recycled to recover any copper loss. Another significant metallurgical consequence of the use of oxygen enriched air is that the oxygen partial pressure at which magnetite precipitation is reached occurs prior to the completion of the slag blow stage in copper converting. Thus with magnetite present in the slag, the slag becomes viscous and the entrained copper losses to the slag increase drastically if the slag is iron silicate. Continuous converting of white metal to metallic copper in coexistence with iron silicate slag without magnetite precipitation is only possible if a_{FeO} remains constant at 0.31 (i.e. slag is saturated with silica) and air is implemented (i.e. $p_{SO_2} \approx 0.1\,\text{atm.}$) as experienced in conventional converting. However, as pure oxygen or oxygen enriched air is utilised in continuous operations, even a silica saturated slag is not sufficient to prevent magnetite precipitation. As a result of these factors, the use of conventional iron silicate slag in continuous converting processes is unattractive. In the Mitsubishi and the Kennecott Flash converter, the molten 68% Cu matte is fed into the furnace melt, where calcium ferrite slag and blister copper coexist at constant p_{O_2} and p_{S_2}. The use of CaO as a flux eliminates the process difficulties associated with magnetite precipitation, as magnetite is very soluble in lime. The behaviour of magnetite in calcium ferrite slag is discussed in Section 2.3.1.

2.3 COPPER SMELTING SLAGS

In the process of copper converting, two slags, iron silicate and calcium ferrite, are currently being used commercially. Iron silicate slag is used in the first stage of batch converting whilst calcium ferrite slag is used in continuous copper converting. The reasoning behind the different applications of the two slags has been discussed in Section 2.2.2. The following section will review the phase equilibria of calcium ferrite and iron silicate slags as well as their Fe^{3+}/Fe^{2+} ratio. A comparison of the phase equilibria of calcium ferrite and iron silicate slags with FCS slag is provided in Section 2.9. At present there is no information in the literature on the Fe^{3+}/Fe^{2+} ratio in FCS slag, so a comparison of FCS slag with iron silicate and calcium ferrite slags for this ratio, using published data, cannot be made.

2.3.1 Phase Equilibria

A) The FeO-Fe_2O_3-SiO_2 and FeO-Fe_2O_3-CaO systems

The iron silicate and calcium ferrite slag compositions can be described as being within the FeO-Fe_2O_3-SiO_2 and FeO-Fe_2O_3-CaO systems, respectively. Whilst iron silicate slag has long been the most widely used in copper smelting, the inherent problems associated with it for continuous converting (Section 2.2.2), led to the development of calcium ferrite slag. Calcium ferrite slag was proposed over two decades ago for copper smelting by Mitsubishi Materials Corporation and has been proven to be especially successful for continuous copper converting. The liquid region of the silicate and ferrite slags is compared in Figure 2.3.1 at 1300°C, together with the iso-equilibrium oxygen partial pressure lines.

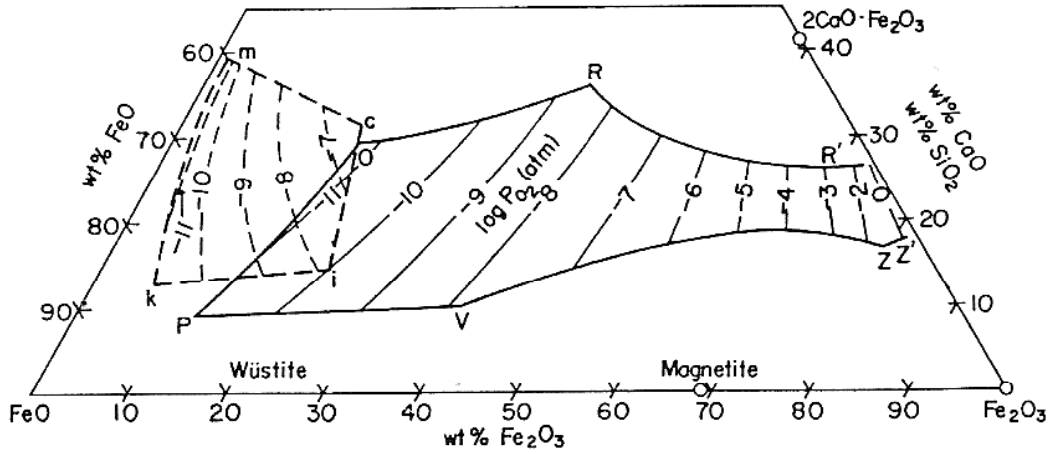

Figure 2.3.1: Liquidus region and iso-equilibrium oxygen potential lines at 1300°C for the systems of FeO-Fe_2O_3-CaO (solid lines) and FeO-Fe_2O_3-SiO_2 (dashed lines) (Yazawa, Takeda and Waseda, 1981)

In Figure 2.3.1, the homogeneous melt region of calcium ferrite slag at 1300°C is limited by the isotherms OP, PV, VZ, OR and RR' which illustrate that the melt can be in equilibrium with solid iron, wustite, magnetite, lime and dicalcium ferrite, respectively. Within this liquid region the equilibrium oxygen partial pressure isobars range from 10^{-11} to 1 atm. The liquid region of the iron silicate slag is represented by icmk at 1300°C. The liquids on the isotherms of mk, ki, ic and cm correspond to slag in equilibrium with solid iron, wustite, magnetite and silica, respectively. Comparison of the homogeneous melt regions clearly indicates that the compositional coverage of calcium ferrite slag is far greater than iron

silicate slag at copper converting temperatures (1300°C). At 1300°C, provided that the lime is kept above approximately 18wt% in calcium ferrite slag, the slag will remain liquid at oxygen partial pressures ranging from 10^{-11} to 1 atm. without magnetite precipitation. However at the same temperature, the liquid region of iron silicate slag is comparatively small and restricted near the SiO_2-FeO join (isotherm ic) where oxygen partial pressure is 10^{-6} atm., above which solid magnetite precipitation occurs. Most continuous converting processes operate at oxygen partial pressures of 10^{-6} to 10^{-5} atm. However at 1300°C and oxygen partial pressure of 10^{-6} atm., iron silicate slag is saturated with magnetite, which results in a highly viscous slag, causing inherent process difficulties, such as increased copper entrainment losses to slag and difficulties in tapping the slag from the furnace. Such problems are not experienced in calcium ferrite slag as calcium ferrite slag does not precipitate magnetite at the operating oxygen partial pressures.

B) The Effects of Copper on the Liquid Region of both Iron Silicate & Calcium Ferrite Slags

Copper metal in equilibrium with slag will inevitably result in the dissolution of some copper as copper oxide into the slag. The effects of copper oxide on the liquid region of iron silicate and calcium ferrite slags were demonstrated by Kongoli *et al.* (2006) and Kongoli *et al.* (2003), respectively, through the use of the FLOGEN model. The FLOGEN software is a thermo-physicochemical model of multicomponent slag systems and produces multicomponent phase and liquidus surface diagrams. The model predictions have been validated with existing experimental data under known conditions at several temperatures and oxygen partial pressures (Section 2.9). The FLOGEN model was used to demonstrate the effects of copper oxide on the liquid region of iron silicate slag at an oxygen partial pressure of 10^{-6} atm. and 1300°C and the resulting phase diagram is shown in Figure 2.3.2, where 'F' represents iron silicate slag. Figure 2.3.3 illustrates the phase diagram under the same conditions for calcium ferrite slag. The presence of copper oxide in either slag results in an increase in the slag liquid region, the maximum increase being for slag in equilibrium with copper (approximately 15-17 wt% Cu_2O). The increase in the liquid region is most significant at the magnetite saturation boundary, especially in the case of iron silicate slag. Copper oxide in iron silicate slag decreases the activity coefficient of magnetite in the slag as a result of the strong interactions between Cu_2O and Fe_3O_4 to form ferrites (Kongoli *et al.*, 2006). Consequently copper oxide in the silicate slag increases the solubility of magnetite in slag and

reduces the risk of magnetite precipitation during converting, ensuring a homogeneous liquid slag.

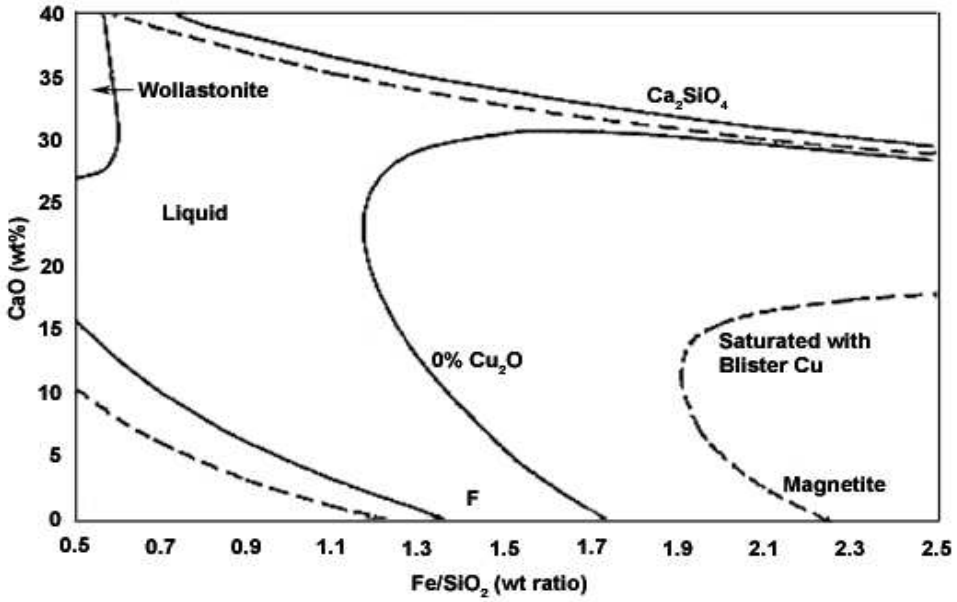

Figure 2.3.2: Effects of Cu_2O on the liquid region of FeO-Fe2O3-SiO2 at 1300°C and an oxygen partial pressure of 10^{-6} atm. (Kongoli, McBow and Yazawa, 2006)

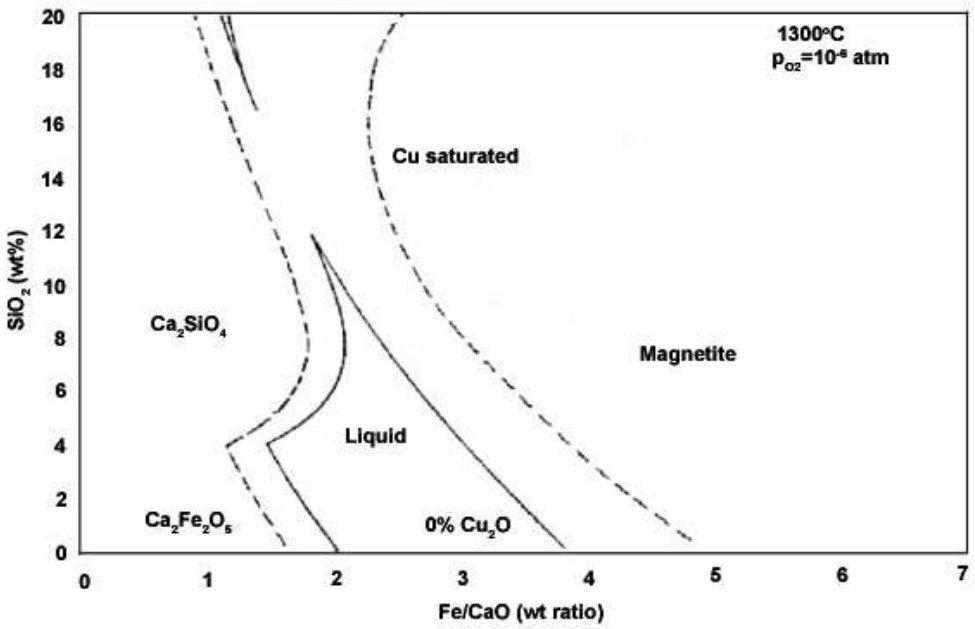

Figure 2.3.3: Liquid region of calcium ferrite slag at 1300°C and an oxygen partial pressure of 10^{-6} atm. (Kongoli, McBow and Yazawa, 2003).

Dashed Lines: Copper Saturated; Solid Lines: Copper-free slag

C) The Fe^{3+}/Fe^{2+} ratio of Iron Silicate and Calcium Ferrite Slags

As seen in Figure 2.3.1, at any given oxygen partial pressure, the Fe^{3+}/Fe^{2+} ratio of calcium ferrite slag is much higher than that of iron silicate slag. A review of the Fe^{3+}/Fe^{2+} ratio in both iron silicate and calcium ferrite slags it important to this research as this ratio affects the wear of magnesia-chrome refractories. As explained in detail in Section 2.5, iron silicate slag tends to preferentially attack the periclase phase of magnesia-chrome refractories due to high Fe^{2+} content of the silicate slag which reacts with Mg^{2+} in the periclase to form magnesiowustite and magnesioferrite, resulting in spalling. Calcium ferrite slag however attacks the chromite spinel phase of the brick due to the high Fe^{3+} content of the slag which interdiffuses with Cr^{3+} in the chromite phase resulting in the degradation of the chromite spinel bonding phase. Thus it is vital to understand the Fe^{3+}/Fe^{2+} ratio of both slags in order to discuss the rate and mechanism of magnesia-chrome refractory wear. The Fe^{3+}/Fe^{2+} ratio of both iron silicate and calcium ferrite slags has been investigated in detail by various authors and is discussed in the following section.

1) IRON SILICATE SLAG

The Fe^{3+}/Fe^{2+} ratio in iron silicate slag containing copper oxide and copper-free iron silicate slag at 1300°C and various oxygen partial pressures was studied by Oishi *et al.* (1983). They found that the Fe^{3+}/Fe^{2+} ratio increases with an increase in the oxygen partial pressure and a decrease in the silica content of iron silicate slag. They also established that the presence of copper in slag has no measurable effect of the ratio. Whilst interactions between $CuO_{0.5}$ and either FeO and $FeO_{1.5}$ do result in copper ferrites, such compounds are not very stable at high temperatures (above 1000°C) as was determined by Kenfack and Langbein (2004) in their study on the phase formation in the system Cu – Fe – O. This is why copper oxide has little affect, if at any, on the Fe^{3+}/Fe^{2+} ratio. The state of oxidation of an element changes with oxygen partial pressure, such that the higher the oxygen partial pressure the higher the oxidation state of iron, that is, Fe^{3+}. As calculated from Equation 2.3.1 at oxygen partial pressure of approximately 10^{-7} atm. at 1300°C, the activities of FeO and $FeO_{1.5}$ are equal. Below this oxygen partial pressure Fe^{2+} is the dominating species of iron in slag and above 10^{-7} atm., Fe^{3+} becomes dominant. The increase in the slag Fe^{3+}/Fe^{2+} ratio with increasing oxygen partial pressure was also noticed by Michal *et al.* (1952), Elliot *et al.* (1984) and Ruddle *et al.* (1966).

$$FeO + \frac{1}{4}O_2 = FeO_{1.5}$$ **Equation 2.3.1**

$$K = \frac{(a_{FeO_{1.5}})}{(a_{FeO}).p_{O_2}^{1/4}}$$

assume $a_{FeO} = a_{FeO_{1.5}}$

$$K = \frac{1}{p_{O_2}^{1/4}} \quad \Rightarrow \quad p_{O_2} = \left(\frac{1}{K}\right)^4$$

$$K_{1300^oC} = 39.99$$
$$K_{1200^oC} = 81.96$$
$$p_{O_2} = 3.94 \times 10^{-7}\, atm \text{ at } 1300^{\circ}\text{C}$$

Silica strongly interacts with ferrous iron as is evidenced by the formation of fayalite and increasing the silica content of iron silicate slag favours greater interactions between FeO and SiO_2. The reduction in the activity coefficient of FeO in slag as the SiO_2 content increases causes the mole fraction of FeO in slag to also increase hence resulting in a drop in the Fe^{3+}/Fe^{2+} ratio. Thus the conclusions formed by Oishi *et al.* (1983) on the effects of slag silica and copper content and the oxygen partial pressure agree with expectations.

Figure 2.3.4 makes a comparison between the Fe^{3+}/Fe^{2+} ratios in iron silicate as determined by various authors under similar conditions and slag compositions. The highest oxygen partial pressure at which Fe^{3+}/Fe^{2+} data is available is limited to 10^{-6} atm., due to magnetite precipitation. Taking into account experimental uncertainties, the data in Figure 2.3.4 is in good agreement.

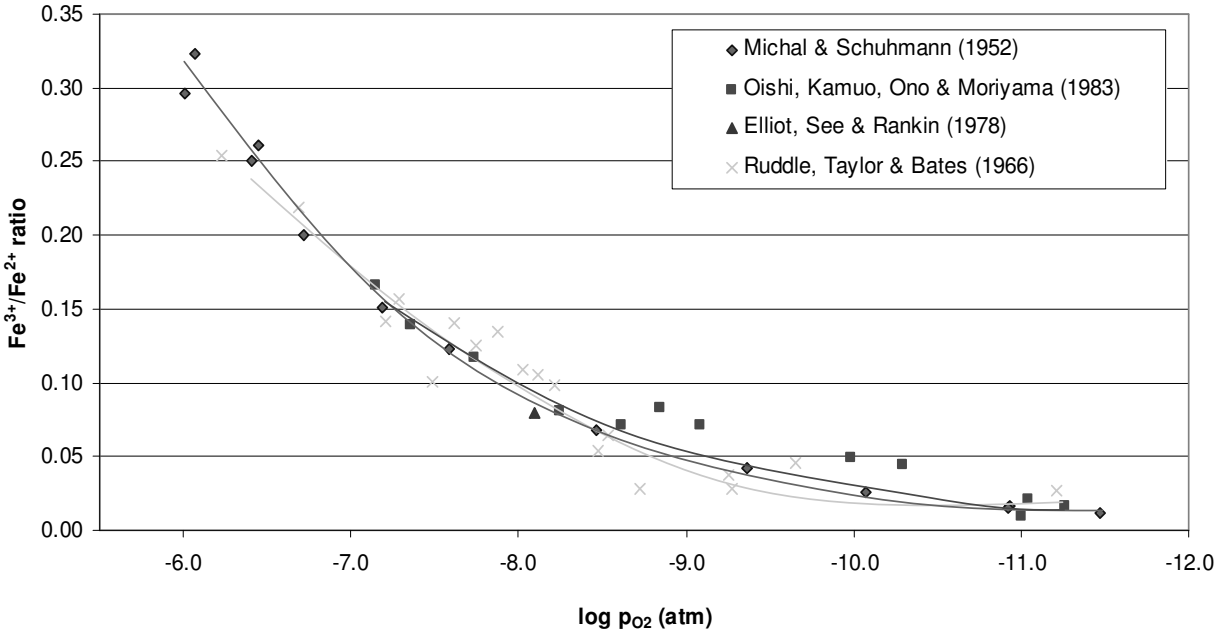

Figure 2.3.4: Fe^{3+}/Fe^{2+} ratio in iron silicate slag at 1300°C and various oxygen potentials

2) CALCIUM FERRITE SLAG

Takeda *et al.* (1980) found that for calcium ferrite slag, the equilibrium oxygen partial pressure, lime content of the slag, Fe^{3+}/Fe^{2+} (wt%) ratio of the slag and temperature are related by the Equation 2.3.2 in the oxygen partial pressure range of 10^{-10} to 10^{-4} atm.

$$\log(Fe^{3+}/Fe^{2+}) = 0.170\log(p_{O2}) + 0.018(wt\%CaO) + 5500/T - 2.52 \qquad \textbf{Equation 2.3.2}$$

They determined that Fe^{3+}/Fe^{2+} ratio increases with increasing slag CaO content and oxygen partial pressure and decreasing temperature. Increasing the CaO content of the slag causes greater interactions between CaO and $FeO_{1.5}$, as these two components form compounds (i.e. calcium ferrites), resulting in a higher Fe^{3+}/Fe^{2+} ratio in slag. Increase in oxygen partial pressure favours the higher oxidation state of iron, Fe^{3+}, therefore resulting in an higher Fe^{3+}/Fe^{2+} ratio. An increase in temperature results in the decrease of equilibrium constant K for Reaction 2.3.1, as shown at 1200°C and 1300°C. The decrease in K-value indicates that as temperature rises, the formation of FeO is more favoured than the formation of $FeO_{1.5}$, resulting in a decrease in the slag Fe^{3+}/Fe^{2+} ratio. Thus, the findings made by Takeda *et al.* (1980) are in accord with expectations.

Yazawa and Takeda (1982) also studied the effects of oxygen partial pressure, slag compositions and temperature on the Fe^{3+}/Fe^{2+} ratio of calcium ferrite slag containing copper oxide. The results from the latter study were very similar to those for the copper-free slag, suggesting that the effects of $CuO_{0.5}$ on the Fe^{3+}/Fe^{2+} ratio are relatively small and Equation 2.3.2 is applicable also to the slag equilibrated with liquid copper. As previously explained, although interactions between $CuO_{0.5}$ and either FeO and $FeO_{1.5}$ do result in copper ferrites, they are not stable compounds and therefore have little affect on the Fe^{3+}/Fe^{2+} ratio.

A comparison of the Fe^{3+}/Fe^{2+} ratio in calcium ferrite slag at similar conditions and slag compositions as determined by Somerville *et al.* (1995) and Yazawa and Takeda (1982) is shown in Figure 2.3.5. The two sets of data are in excellent agreement, taking into account experimental uncertainty.

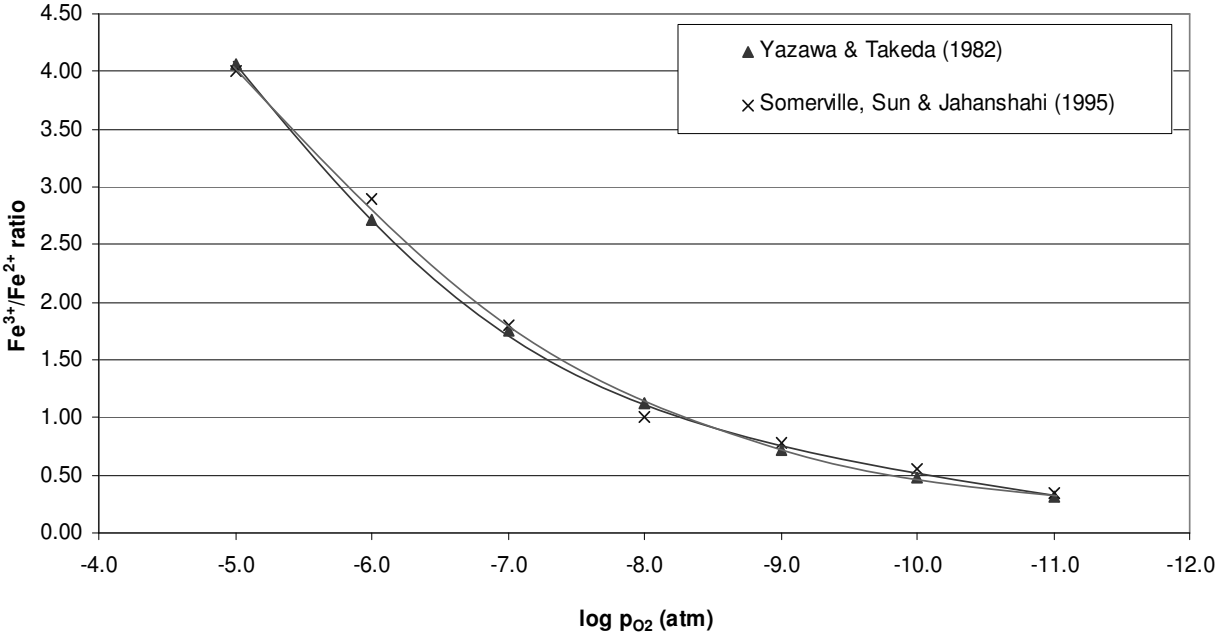

Figure 2.3.5: Fe^{3+}/Fe^{2+} ratio in calcium ferrite slag at 1300°C and various oxygen potentials

3) COMPARISON OF CALCIUM FERRITE AND IRON SILICATE SLAGS

When comparing the data in Figures 2.3.4 and 2.3.5, it can be seen that regardless of the converting slag used, the Fe^{3+}/Fe^{2+} ratio increases exponentially with increasing oxygen potential. However at any given oxygen partial pressure, the Fe^{3+}/Fe^{2+} ratios for ferrite slag are around 10 times higher than those for iron silicate slag. The activity coefficients of FeO and Fe_2O_3 affect the Fe^{3+}/Fe^{2+} ratio in slag as the activity coefficients of both species are affected by their interactions with oxides in the slag. The Fe^{3+}/Fe^{2+} ratio in calcium ferrite slag is higher than that of iron silicate slag due to the strong interactions between Fe_2O_3 and CaO to form compounds, such as calcium ferrites whilst the interactions between CaO and ferrous iron are weak. The strong interaction between ferric iron and lime means that an increase in the CaO content of the ferrite slag decreases the activity coefficient of Fe_2O_3, thus increasing the mole fraction of Fe_2O_3 in the slag (i.e. the solubility of Fe_2O_3 in slag) for a given activity of Fe_2O_3, which is set by the process conditions. On the contrary, silica strongly interacts with ferrous iron as illustrated by the formation of fayalite and has weak interactions with ferric iron and increasing the slag silica contents results in the reduction in the activity coefficient of FeO in the silicate slag, thus increasing the solubility of FeO in the slag and hence the Fe^{3+}/Fe^{2+} ratio decreases.

2.4 FURNACE REFRACTORIES

The converting of copper matte to blister copper takes place in furnaces lined with refractories manufactured from magnesia and chrome ores. The furnace which poses the greatest refractories challenge is the converter. Highly aggressive slags, mechanical stresses and increasingly higher operating temperatures all combine to destroy most refractory materials. The cost of maintaining and eventually replacing refractory bricks as a result of slag attack is a significant cost component in the copper industry. The most common wear mechanisms (discussed in greater detail in Section 2.5) include the dissolution of refractory components into the slag phase, the formation of weakly bonded new phases within the brick and various forms of spalling including mechanical, structural and thermal. According to copper producers, the properties to improve in order to increase refractory life in the converter are:

- Resistance to thermal shock and spalling,
- Physical strength at operating temperatures and
- Resistance to penetration and corrosion by copper slags (Renkey *et al.*, 1981).

Initially, copper smelters used silica bricks in the primary melting and refining furnaces, however due to the slag conditions and increased production demands from the equipment, silica bricks were replaced by basic bricks. Basic bricks, known better as magnesia-chrome refractory, were first used some fifty years ago and were manufactured from two major raw materials, magnesia and chrome ore.

Bricks with both magnesia and chrome have higher hot strengths, better volume stability and better resistance to thermal shock than silica bricks. Furthermore, magnesia and chrome refractories have a higher corrosion resistance to slags than those used previously. Since the 1960's, refractories used for nearly all copper smelting, converting and fire-refining furnaces have featured compositions from the magnesia-chrome system for linings in contact with molten matte, slag or metal. No other common refractory system features the combination of high-temperature corrosion resistance to converter slags, high hot strength and thermal stability that magnesia-chrome refractories exhibit. Magnesia-chrome refractories became dominant in the 1950's and 1960's and changes in refractory practice that have taken place since then have largely been in refractory composition and manufacturing techniques.

Refractory grade dead-burned magnesia is known by several different names within the refractories industry. Magnesium oxide and MgO are chemical terms, periclase and magnesite are mineral names and magnesia is the term often used by the refractory technologist. All terms have been used interchangeably in literature to describe this refractory oxide, which melts above 2700^{o}C. Magnesia is sourced either from seawater (or other brines) or from natural magnesite ore. Magnesia is produced by calcining and sintering magnesium hydroxide in the case of seawater and magnesium carbonate in the case of magnesite ore. Magnesia produced from natural magnesite has a large range of purity, with the most common grades varying from 80% to 95% MgO. The main impurities found in magnesia are Fe_2O_3, Al_2O_3, CaO and SiO_2.

Chromite ores are primarily obtained from South Africa, Brazil, the Philippines, Greece and Turkey. Chrome ore is a complex material having one major refractory phase and minor associated gangue minerals, chiefly silicates. The major phase is an extensive magnesium and ferrous spinel solid solution. In addition to Cr_2O_3 and MgO, chromite ore also contains significant amounts of Al_2O_3, Fe_2O_3, CaO and SiO_2. The amount of silica associated with chrome ores is usually much higher than the amount of silica associated with magnesia.

There have been four types of basic brick used in smelting, converting and refining furnaces;

1. Silicate bonded periclase chrome brick (burnt)
2. Improved silicate bonded periclase chrome brick showing minor amounts of direct bonding (chemically bonded)
3. Direct bonded magnesia-chrome brick
4. 'Fused-cast' direct bonded magnesia-chrome brick

At present the most commonly used magnesia-chrome bricks in the copper industry, in particular in the Kennecott Flash converter and Mitsubishi C-furnace are direct bonded and to a lesser extent fused-cast magnesia-chrome refractories. The following discussion therefore concentrates largely on these two brick types.

2.4.1 Silicate-Bonded Magnesia-Chrome Refractory Bricks

When crushed chrome ore is fired at low temperatures (< 1550^{o}C), the resulting microstructure features grains of a spinel-based structure [$(Mg,Fe)O.(Al,Fe,Cr)_2O_3$] surrounded by a rim consisting largely of forsterite ($MgO.SiO_2$), monticellite ($CaMgSiO_4$), merwinite ($Ca_3Mg(SiO_4)_2$) and similar silicates (Schlesinger, 1996). Such silicates are a bonding agent between magnesia and chrome and result from the reaction between chrome ore gangue and magnesia during sintering. These silicate-bonded bricks were the first magnesia-chrome refractories produced.

The presence of silicate phases was a serious limitation of silicate-bonded bricks as these phases have a low melting point (about 1200°C) and the silicate bond tended soften at copper converting temperatures, making this bond weak and readily prone to attack by typical copper slags (Staut, 1972).

The refractory industry worked on improving the stability of the silicate bond by firing the same brick composition to a higher temperature (1600-1800^{o}C). This method of improvement established an important fact that by 'hard' firing it was possible to partially diffuse chrome ore and magnesia at the boundary between the two species and produce high quality magnesia spinel bonds. The firing treatment resulted in the direct bonding of the chromite grains to adjacent magnesia grains. The findings from such experiments led to direct bonded bricks, which focused on the periclase chrome system but also took into consideration the impurity level, particularly those of silica and lime.

2.4.2 Direct-Bonded Magnesia-Chrome Refractory Bricks

Introduced in the late 1950's and early 1960's, the direct bonded magnesia-chrome refractories were produced as a result of the lack of quality and performance of silicate-bonded bricks. A typical direct-bonded magnesia-chrome brick contains large amounts of magnesia and chromite grains with a low quantity of silicates. The refractories, produced from dense sintered magnesia grain and beneficiated low silica chrome ore, became popular due to their superior high-temperature properties, including improved hot strength, lower porosity and better resistance to spalling. The high firing temperatures of direct-bonded brick demands materials with low silica content, thus lower amounts of residual silicate phases are present in the fired brick. Low-silica chrome ores are produced by the beneficiation of lump ore to remove the associated silicate gangue. Low-silica magnesia is produced by the precipitation and chemical treatment of the hydrate from seawater or underground wells rather than from the mineral magnesite. The resulting concentrates are used in direct-bonded magnesia-chrome brick. The silicate bonds are replaced by the direct bonding of magnesia and chrome grains. The preferred bonding phase for the formation of direct bonds between the periclase and chromite grains is picrochromite spinel ($MgO.Cr_2O_3$), where Cr_2O_3 can be replaced by Fe_2O_3 and Al_2O_3. Periclase-periclase and chromite-chromite bonds are also formed. The degree of direct bonding is highest in the case of low silica content brick and proportionally decreases with the increase of silica content of refractories (Chaudhuri *et al.*, 2001).

A) Phases present in Direct-Bonded Magnesia-Chrome Refractory Bricks

The major components of an unused direct-bonded brick are MgO and Cr_2O_3 with minor amounts of Fe_2O_3, Al_2O_3, SiO_2 and CaO impurities. Such bricks contain greater than 50% magnesia, around 15-30% chrome and the remainder being the impurity constituents, most of which is Fe_2O_3. The Cr_2O_3-Fe_2O_3-MgO phase diagram at 1300°C is given in Figure 2.4.1. As can be observed on the phase diagram, at an MgO composition of greater than 20wt%, there exists two phases of impure periclase solid solution and a chromite spinel solid solution. Although the composition of both these phases is dependant on the Fe_2O_3/Cr_2O_3 ratio in Figure 2.4.1, the effects of the Fe_2O_3/Cr_2O_3 ratio are most evident for changes in the spinel composition, the periclase phase in magnesia-chrome bricks is very close to pure MgO with very minor inclusions of Cr_2O_3 and Fe_2O_3. In Figure 2.4.1, the solubility of Cr_2O_3 in periclase is approximately 2.5wt% and that of Fe_2O_3 is approximately 9wt%.

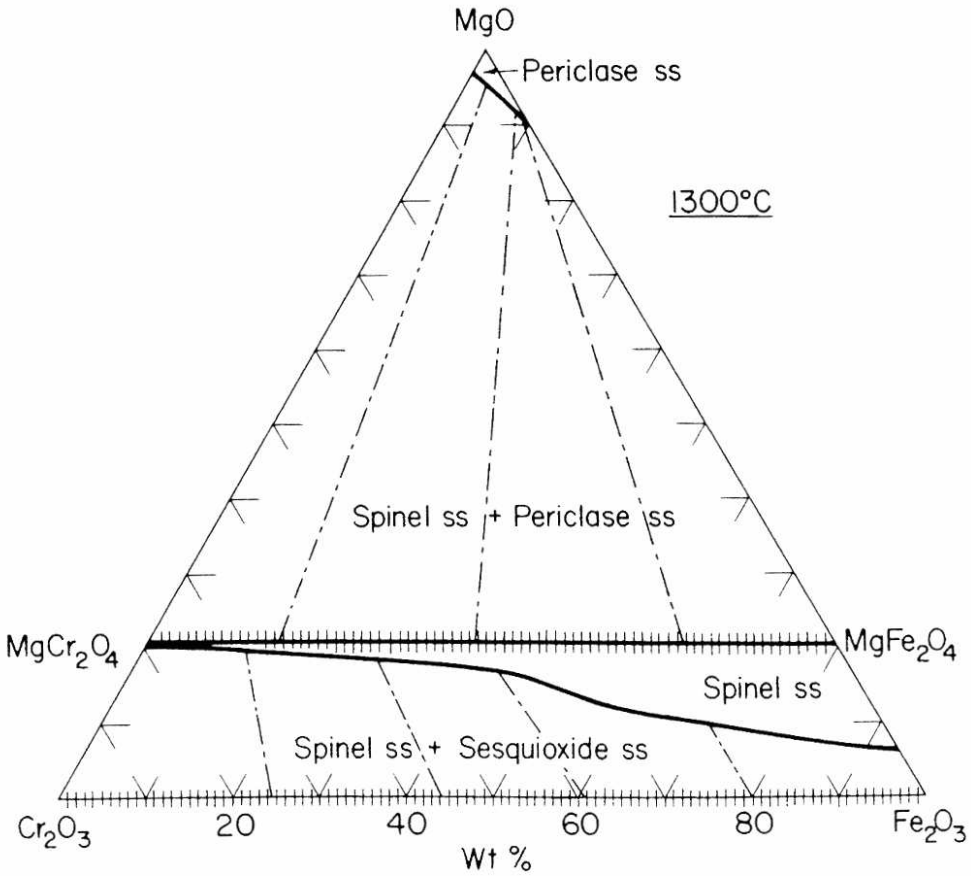

Figure 2.4.1: Phase Diagram of the System MgO-Cr_2O_3-Fe_2O_3 at 1300°C (Levin and McMurdie, 1975)

The presence of chromite spinel and periclase phases in the direct-bonded magnesia-chrome refractory are supported by Fahey (2002) and Renkey *et al.* (1981) who studied the microstructure of such brick using the SEM (Scanning Electron Microscope). The microstructure revealed by Fahey (2002) is illustrated in Figure 2.4.2.

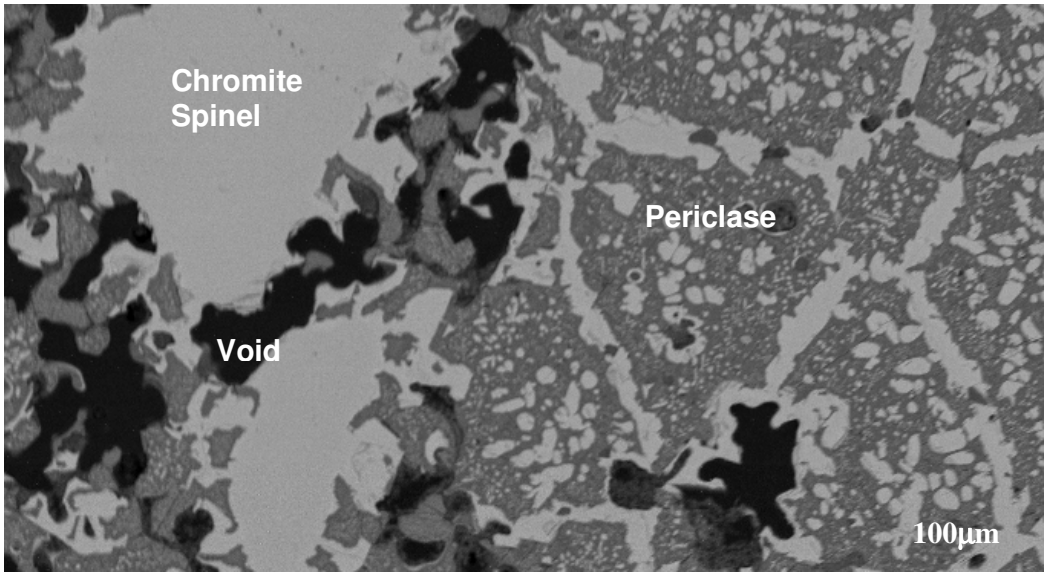

Figure 2.4.2: SEM backscattered electron image showing periclase phase existing in a commercial magnesia-chromia refractory brick at ambient temperature (Fahey, 2002).

Both Fahey (2002) and Renkey *et al.* (1981) observed the presence of three types of chromite spinel grains within the brick microstructure:

- Primary phase (large grains)
- Secondary phase (medium-sized grains)
- Exsolved chromite spinel phase within the periclase phase (small grains which have precipitated from the periclase phase).

A detailed discussion of each phase is given below. The microstructure of the direct-bonded brick also revealed bond formation at the grain boundaries of both primary and secondary chromite spinel with the periclase grains as well as direct bonding between periclase-periclase grains. However, there exists a greater degree of bonding between the chromite and periclase phases in comparison to the bonding between periclase-periclase bonding, indicating that chromite and periclase diffuse and bond more readily than periclase and periclase.

1) PERICLASE

Periclase appears as a dark grey phase under the scanning electron microscope (Figure 2.4.2). The periclase grains are essentially a solid solution of magnesia, iron oxide, Cr_2O_3 and Al_2O_3. Within the periclase crystal, there appears a light grey phase distributed evenly, which is exsolved chromite spinel. During manufacturing the brick is slowly cooled from about 1600-1800^oC to ambient temperature. At high temperatures some chromite spinel dissolves into the periclase. With the temperature drop the solubility of the chromite spinel in the periclase drops and the spinel precipitates along the crystallographic planes in the MgO to give a "Widmanstatten" cross-hatched morphology (Fahey, 2002). The periclase grains are either in direct contact with one another or are bound by primary and secondary chromite spinel phases. On average the size of the periclase grains is between 50 and 150 μm in diameter.

2) CHROMITE SPINEL

Appearing as light grey, the chromite spinel phase of magnesia-chrome brick has three distinct forms, that is, primary, secondary and exsolved (Figure 2.4.3). The primary spinel grains are large (~200-500 μm) in diameter whilst the secondary spinel grains are medium sized (~20-100 μm). Both secondary and exsolved spinel are dissolved in periclase during high temperature firing and precipitate upon cooling. The favoured site for precipitation is a periclase grain boundary, such that secondary chromite spinel is the dominating form over exsolved spinel. The amount and size of the secondary chromite spinel phases increases with a decrease in cooling rate, such that, slow cooling accelerates the formation of secondary spinel grains. However if the cooling rate is rapid, spinel diffusion to a grain boundary cannot occur and exsolved spinel results. Secondary spinel grains exist around periclase grains, acting as a bonding phase. Both Renkey *et al.* (1981) and Fahey (2002) determined the secondary spinel to be the most prevalent physical form in terms of volume fraction and found no appreciable difference in the chemical compositions of the three forms of chromite spinel (i.e. primary, secondary or exsolution), representing the chromite spinel phase as a solid solution of magnesium-, aluminium-, and iron-oxides in chromia.

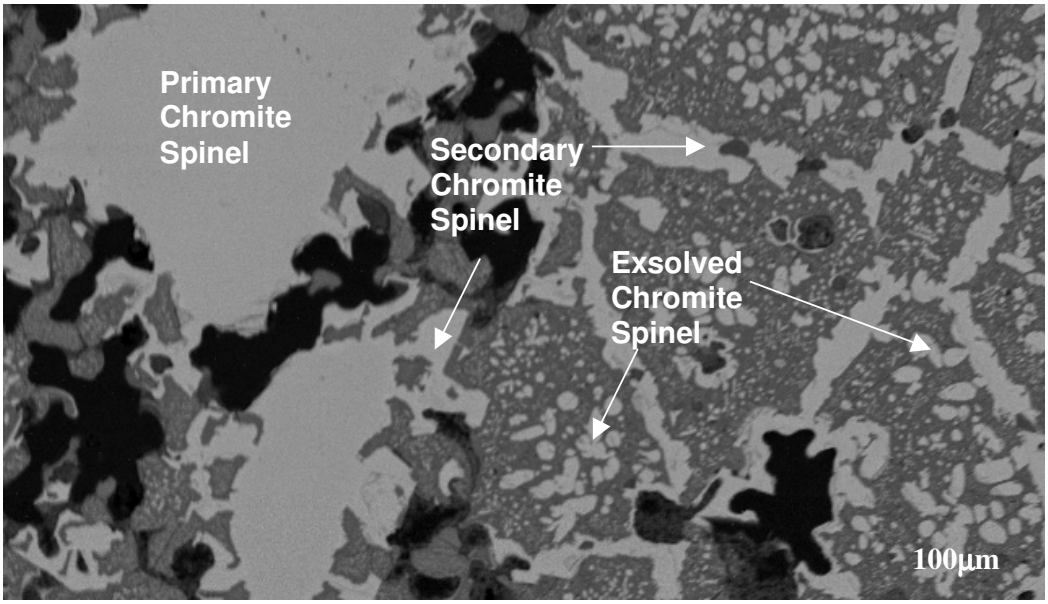

Figure 2.4.3: SEM backscattered electron image showing spinel phase existing in a commercial magnesia-chromia brick at ambient temperature (Fahey, 2002).

3) VOIDAGE

The direct bonded commercial refractory has an apparent porosity of 16-18%. Figure 2.4.4 indicates that the pore structure within the brick is open and interconnected rather than being closed. An open pore structure is detrimental to the life of the refractory brick as it makes the brick more prone to slag penetration.

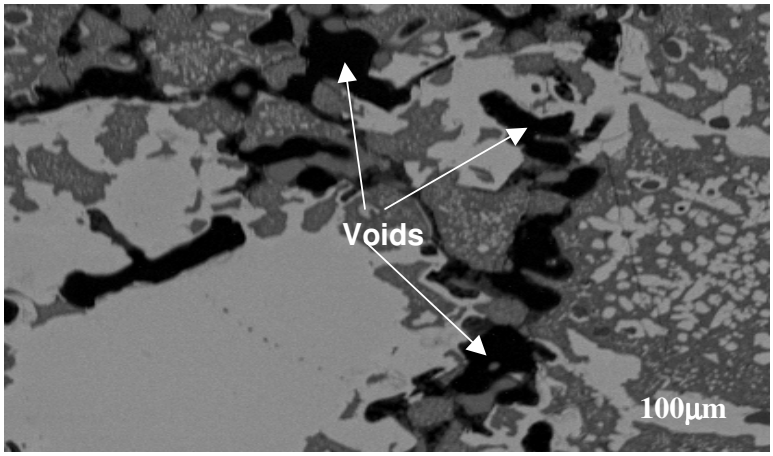

Figure 2.4.4: SEM backscattered electron image showing voidage in a commercial magnesia-chromia refractory brick microstructure at ambient temperature (Fahey, 2002).

B) Properties of Direct-Bonded Magnesia-Chrome Refractory Bricks

The major improvements for direct-bonded brick over silicate-bonded brick are their superior high temperature properties of improved hot strength, high thermal shock resistance, lower apparent porosity and permeability, better spalling resistance and lower amounts of densification as well as improved resistance to slag attack and penetration and volume stability. Densification is caused by the accumulation of oxides, primarily lime and silica, a short distance behind the hot face as a result of slag penetration. Such oxides from the slag do not react with the brick phases and reside in the brick pores. Densification of the hot face of the brick by impurities and subsequent temperature cycling results in the peeling of the brick (i.e. spalling). The average apparent porosity of direct-bonded magnesia chrome refractories ranges from 16-18%. The porosity of direct-bonded brick is lower than si1icate-bonded brick. The lower porosity reduces the amount of slag infiltration and thereby reduces the possibility of densification and leads to improved spall resistance.

During the manufacture of direct-bonded bricks, the open porosity of the refractory increases as the amount of primary chromite spinel grains increases. This increase in open porosity results due to thermal expansion of the brick at high temperatures which leads to the formation of gaps in the microstructure during the cooling process resulting from the 'mismatch' of grain boundaries between the chromite and the periclase grains. The precipitation of secondary chromite also results in an increase in porosity; however it is of a 'closed' nature. Whilst open porosity is detrimental to the life of the brick resulting from slag penetration, it has been found that the presence of the closed pores in the direct-bonded bricks results in high thermal shock resistance as the gaps within the matrix act as a barrier to crack growth, thus improving both the hot modulus of rupture and the cold crushing strength (Yazdi *et al.*, 2001) of the refractory.

The high temperature firing treatment of direct-bonded bricks results in high hot strength and improves volume stability at converting temperatures. High hot strength at elevated temperatures is one of the most important properties of direct-bonded bricks and is achieved due to the formation of bonds between magnesia and chromite spinel. Since the firing temperature is much higher than the operating temperature of the furnace in which the product bricks are used, the seconding chromite spinel phase, acting as a bonding agent between periclase grains remains intact during converting, unlike the silicate bonds which soften and disintegrate (Davies and McCollum, 1988).

As previously determined, iron oxide is the main impurity present in direct-bonded refractory and is present both in chromite and periclase grains. As suggested by Yazdi *et al.* (2001), iron oxide addition increases the amount of secondary spinel phases at grain boundaries and within the magnesia grains, resulting in an increase in the direct bonding between chromite and periclase grains. The decrease in the percentage of primary chromite particles and the increase in the secondary chromite spinel improve both the resistance to slag attack and the high-temperature properties of the brick due to a decrease in open porosity in the brick and increase in the closed pore network. Yadzi *et al.* (2001) also found that the presence of iron oxide up to 4% increases resistance to slag penetration as well as improving cold crushing strength and the hot modulus rupture.

2.4.3 Fused-Cast Magnesia-Chrome Refractory Bricks

Open porosity in the direct bonded brick is a major drawback. To further improve the properties of the direct-bonded brick, especially porosity and spalling, the raw materials are sometimes melted and fused together at 2450^{o}C in an electric arc furnace and cast into appropriate shapes. Such bricks are known as 'fused-cast' or 'fused-grain' direct-bonded bricks and are characterised by the presence of large isolated closed pores and the absence of a fine open pore network. The major advantage of the 'fused-grain' brick is that it is impervious to the melt inside the furnace.

Fused grain bricks are made from prereacted magnesia-chrome grains manufactured by sintering a mixture of high purity magnesia and low silica chrome ore concentrates at high temperatures. The refractory grains are blended and intimately mixed with a lignosulphonate binder. This binder provides for green strength and is completely burned away during firing in the high temperature kiln. The fused grain bricks contain limited primary chromite spinel and have the maximum amount of secondary and exsolved chromite spinel. Essentially, the brick is a periclase solid solution with chromite spinel exsolution distinctly disseminated as fine precipitates within the periclase crystals and secondary chromite spinel acting as a bonding phase between periclase grains. The periclase accounts for approximately 40 to 70% of the brick microstructure whilst the secondary spinel accounts for 10 to 30%, the remainder being primary and exsolved chromite spinel. Some silicate phases, mostly forsterite and monticellite, are still present in fused-grain materials, but appear only as minor discrete intergranular films rather than the continuous phase seen in silicate-bonded brick. In comparison with secondary chromite spinel, exsolved spinel contains more magnesium and

iron, but less chrome and aluminium. Secondary spinel is mainly composed of magnesium aluminate ($MgAl_2O_4$) and picrochromite ($MgO.Cr_2O_3$) as solid solution. The higher percentage of secondary spinel grains throughout the fused-grain bricks account for the high spall resistance of this product.

The fused-grain brick has a much lower silica content and apparent porosity (by 2-3%) than the direct-bonded product. Because the grain is sintered at temperatures higher than those used in direct bonding and due to the lower silica content, bricks containing pre-reacted grain have increased hot strength compared to direct-bonded magnesia chrome brick and outstanding slag corrosion-erosion resistance.

With direct bonded magnesia-chrome brick, preferential attack of either the magnesia or the chrome often occurs in service. For instance, a high-lime slag will attack the chromite grains whilst a high silica slag will attack the MgO phase. So even though one phase resists attack, the brick is susceptible to corrosion. Chaudhuri *et al.* (2001) found that prereacted grain reduces this problem by providing a virtually continuous periclase solid solution, which is resistant to both high lime and high-silica slags. The authors failed to mention why this would be the case as a silica slag has been proven to attack periclase. Fused magnesia will continue to gain interest during the next several years however, with high production costs and selling prices, the future of fused grain magnesia-chrome refractories is limited.

2.5 REFRACTORY WEAR BY SLAG

Refractory wear by slag is categorised as either chemical or physical wear (Allen *et al.*, 1995). The most important wear mechanism of refractory bricks lining the converter is slag attack (Ainsworth and Starzacher, 1988). The cost of replacing and the maintenance of refractory bricks as a result of slag attack is one of the significant cost components in the copper industry.

Chemical wear can either result from chemical reactions between the slag and refractory components at the slag/brick interface or with penetrated slag within the refractory pores. Nikoo *et al.* (2001) found that reactions between the slag and brick components resulted in either the dissolution of refractory components into the slag phase or the formation of new phases within the brick, leading to weak bonding.

Physical wear occurs due to the erosion of refractory particles caused by spalling (Donald and Toguri, 1997). Spalling is the 'flaking' of the refractory and results from the build-up of stresses within the brick's structure. As explained by Donald and co-author (1997) and Mikami and Sidler (1963), there exists various forms of spalling, which leads to physical wear, including structural, thermal expansion, thermal cycling and mechanical spalling, all of which results in crack propagation and hence mechanical abrasion of the refractory caused from the swirling action of the slag.

1. Structural spall is caused by localised volumetric expansion of the refractory, following the formation of new compounds within the brick
2. Thermal expansion spall is caused by the difference in the thermal expansion coefficient of the slag penetrated region of the refractory and the underlying region of the refractory.
3. Thermal cycle spall, that is, thermal shock caused by expansion and contraction of the refractory brick, results from cyclic temperature changes.
4. Mechanical spall is a result of operational damage such as tuyere punching during P-S converting.

All current converting processes use magnesia-chrome refractories as they have the greatest resistance to slag attack in terms of all forms of degradation of any refractories now available. The main components of a magnesia-chrome refractory brick are MgO and Cr_2O_3. The properties and structure of magnesia-chrome refractory bricks are discussed in detail in Section 2.4.

The following section discusses refractory wear by iron silicate and calcium ferrite slag as well as comparing the severity and mechanism of the wear caused by the two converter slags. It should be noted that the following discussion on refractory wear by iron silicate slag applies only to batch converting and not to continuous converting, where iron silicate slag cannot be used as explained in Section 2.2.2. In batch converting, oxygen partial pressure steadily increases throughout the converting stage whilst with continuous converting the oxygen partial pressure is constant. As explained in detail later in this section, refractory wear caused by iron silicate slag is mainly a result of the reactions between iron oxide (FeO) in slag and magnesia in the brick. Thus the intensity of slag attack is driven by the oxygen partial pressure as it affects the FeO content of the slag (Section 2.3) and thus refractory wear. Studies conducted on refractory wear caused by calcium ferrite slag and discussed in this section have been carried out at fixed oxygen partial pressure as is the case in continuous converting operations.

2.5.1 Refractory Wear by Iron Silicate Slag

The wear of direct-bonded magnesia-chrome refractories by iron silicate slag at converting conditions has been studied in great depth by various authors, who all have come to similar conclusions. Studies of refractory wear caused by the silicate slag were mainly through analysis of used Peirce-Smith converter bricks from various smelters as well as some laboratory experiments. The main component of the magnesia-chrome brick which was attacked by the slag was the periclase phase (i.e. magnesia grains). The periclase phase was found to react with both iron oxide and silica in the slag whilst the chromite phase resisted iron silicate slag well. Such findings were reported by Nikoo *et al.* (2001), Ainsworth and Starzacher (1988), Cherif *et al.* (1997), Correia and White (1988), Makipaa and Taskinen (1992), Rigby (1962) and Mikami and Sidler (1963). Cherif and co-authors (1997) found that the periclase phases in direct contact with one another were more prone to slag attack in comparison to the periclase phases surrounded by the secondary chromite spinel phases. The

chromite spinel grains were responsible for increasing the resistance against slag attack. Mikami and Sidler also made such observations.

Cherif *et al.* (1997) and Nikoo *et al.* (2001) used both EDX and XRD analysis to determine the reaction products that formed from the slag/brick interactions. Elemental analysis was performed using the EDX technique and when the amount of phase present was more than 5wt%, phase analysis was performed using XRD. The results from the analysis indicated the presence of magnetite (Fe_3O_4), magnesiowustite (MgO.FeO), magnesioferrite ($MgO.Fe_2O_3$), forsterite ($2MgO.SiO_2$), olivine ($2MgO.2FeO.SiO_2$) and pyroxine ($MgO.FeO.SiO_2$) in addition to the main periclase and chromite spinel phases present in the original brick. The possibility of the formation of such phases, depending on composition changes, when FeO, Fe_2O_3, MgO and SiO_2 are in contact with one another is shown in the three-dimensional model of the $FeO\text{-}Fe_2O_3\text{-}MgO\text{-}SiO_2$ system as compiled by Muan and Osborn and shown in Figure 2.5.1.

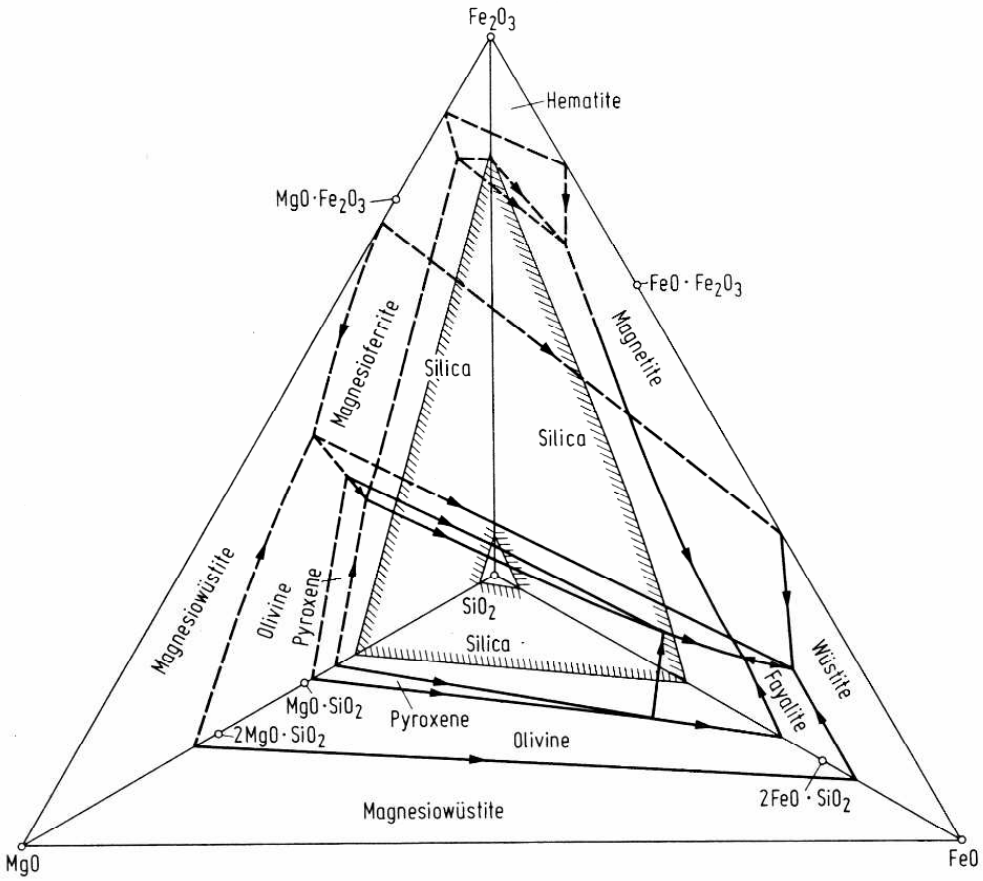

Figure 2.5.1: The three-dimensional model of the $FeO\text{-}Fe_2O_3\text{-}MgO\text{-}SiO_2$ system as compiled by Muan and Osborn (Slag Atlas, 1995)

Nikoo *et al.*'s (2001) explanation of the formation of the new phases observed in the used Peirce-Smith converter bricks was also supported by Rigby (1962). At converting conditions, both FeO and Fe_2O_3 are present in the silicate slag as discussed in Section 2.3. The ratio of FeO to Fe_2O_3 in the slag is controlled by oxygen partial pressure. During Peirce-Smith batch converting, the oxygen partial pressure is set by the reactions involving copper matte oxidation and increases with blowing time as the proportion of FeS in the matte decreases. Thus as oxygen partial pressure increases, more FeO in slag oxidises to Fe_2O_3. Rigby and Nikoo *et al.* (2001) explain that during the initial stages of batch converting, FeO in iron silicate slag reacts with magnesia in the brick to form magnesiowustite and the silica reacts with the magnesia to form forsterite. As the oxygen partial pressure increases however, the MgO.FeO solid solution oxidises to magnesioferrite ($MgO.Fe_2O_3$). As reactions progress, magnesia at the interface disappear. When no free magnesia remains a further series of reactions occur in which iron oxides from the slag react with MgO in forsterite to form more magnesiowustite and magnesioferrite. When this occurs, the forsterite silicate phase is degraded to olivine ($2MgO.2FeO.SiO_2$) and pyroxene ($MgO.FeO.SiO_2$) phases, which soften at converting temperatures. The explanation provided by Rigby (1962) and Nikoo *et al.* (2001) on the primary reactions proceeding at the slag/brick interface indicates that the main reactants are the magnesia from the refractory and the iron oxides from the slag.

The formation of magnesiowustite and magnesioferrite as explained by Rigby (1962) and Nikoo *et al.* (2001) can be confirmed by application of Figure 2.5.2, the phase diagram of the $FeO-Fe_2O_3-MgO$ system at 1300^oC and various oxygen partial pressures. As illustrated by the Yazawa chemical potential diagram in Figure 2.2.4, in Section 2.2.2, the conditions for the first stage of batch converting are 1300^oC and an oxygen partial pressure of 10^{-8} atm. In Figure 2.5.2, this point is along the FeO/Fe_2O_3 side, where FeO is the dominating iron oxide. When in contact with MgO the system composition will move along a line heading towards the MgO apex, such that the magnesiowustite phase forms and is the dominating reaction product. However, the oxygen partial pressure in the converter is rising as FeS is oxidised from matte and the line swings across towards the 'magnesiowustite+magnesioferrite' field and magnesioferrite becomes the dominating phase as the oxygen partial pressure becomes more oxidising and magnesiowustite is oxidised to magnesioferrite.

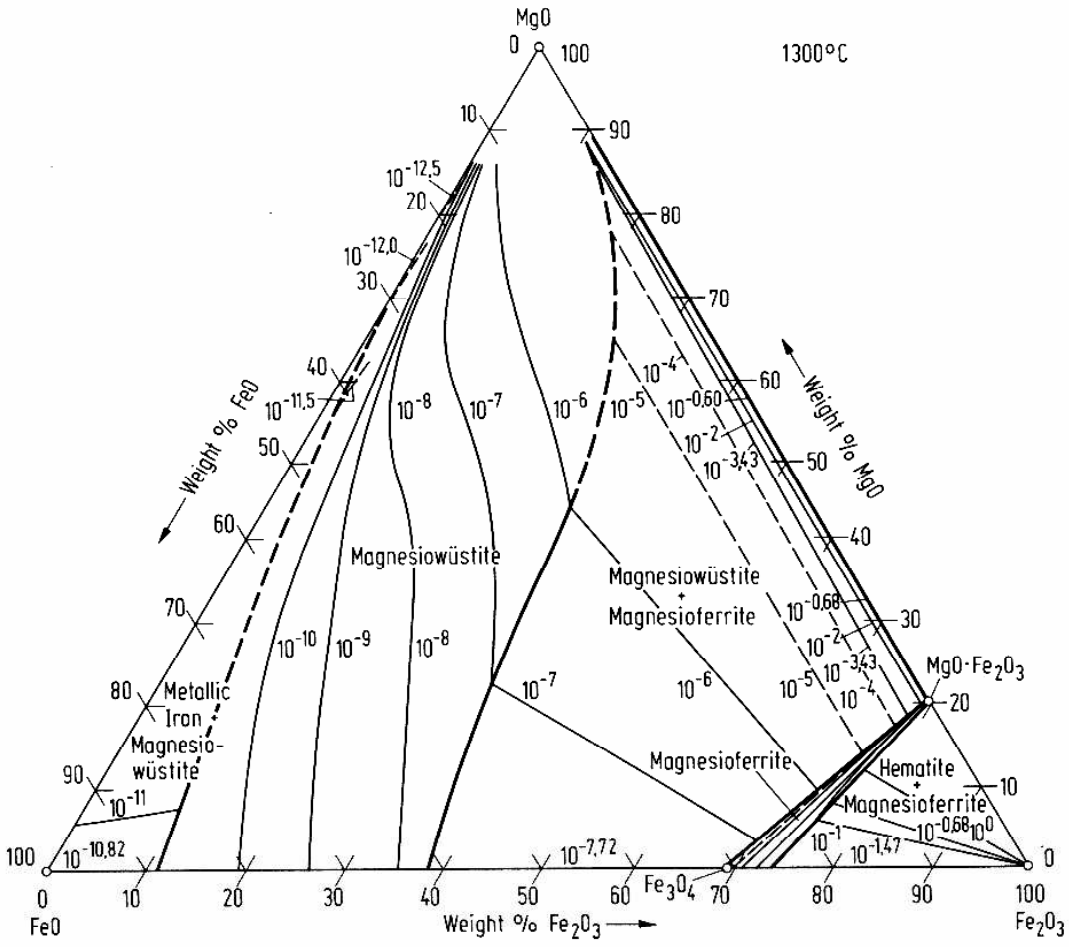

Figure 2.5.2: Phase diagram of the FeO-Fe_2O_3-MgO system at 1300°C and various oxygen partial pressures (Levin and McMurdie, 1975)

A discussion of the formation of forsterite, olivine and pyroxene at converting conditions requires the phase diagram for the FeO_x-MgO-SiO_2 system at the prevailing oxygen partial pressure, but this is not available. The FeO_x-MgO-SiO_2 system phase diagrams in equilibrium with air (Figure 2.5.3) and at 1 atm. (Figure 2.5.4) are available. The isotherms on the diagrams show the temperature at which the first crystals of solid will form in the FeO_x-MgO-SiO_2 system upon cooling i.e. they are liquidus curves. According to Figure 2.5.3, the temperatures at which the silicates form are much higher than those experienced at converting conditions. However from Figure 2.5.4, it can been seen that as the oxygen partial pressure decreases, the temperatures at which forsterite, olivine and pyroxene form also decreases. Whilst this phenomenon is not very noticeable, as can be seen in the centre of Figure 2.5.3, the liquidus temperature for both olivine and pyroxene has decreased and both phases are seen to form at 1400°C which is not the case in Figure 2.5.4 where the oxygen

partial pressure is 1 atm. Thus according to this trend, it is likely that as the oxygen partial pressure decreases further, the liquidus temperature at which the olivine and pyroxene phases form will also decrease and the phases will be present in the FeO_x-MgO-SiO_2 system at an oxygen partial pressure of 10^{-6} atm. and 1300°C.

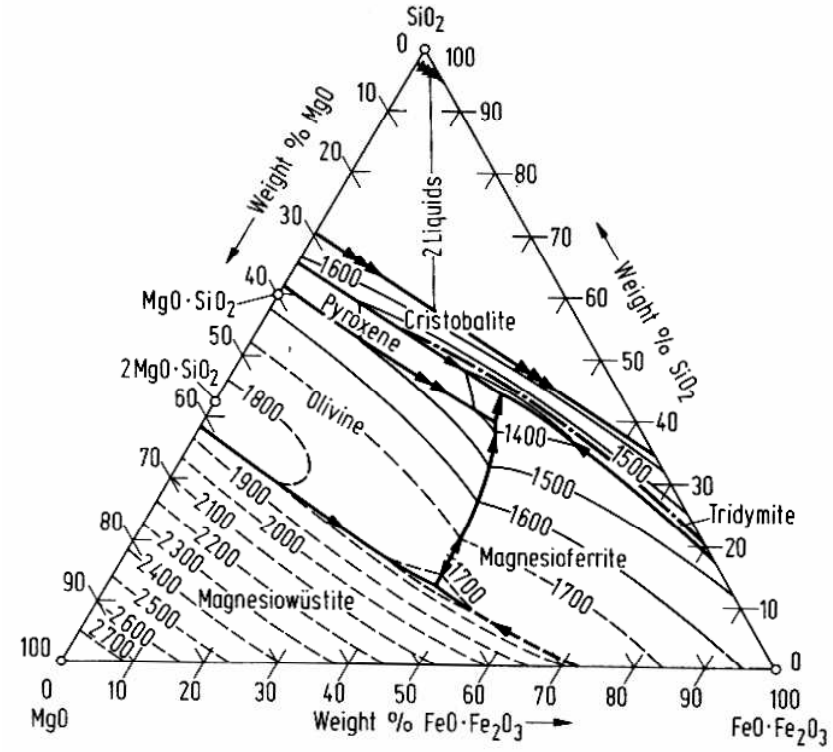

Figure 2.5.3: Phase diagram of the FeO_x-MgO-SiO_2 system in air (Slag Atlas, 1995)

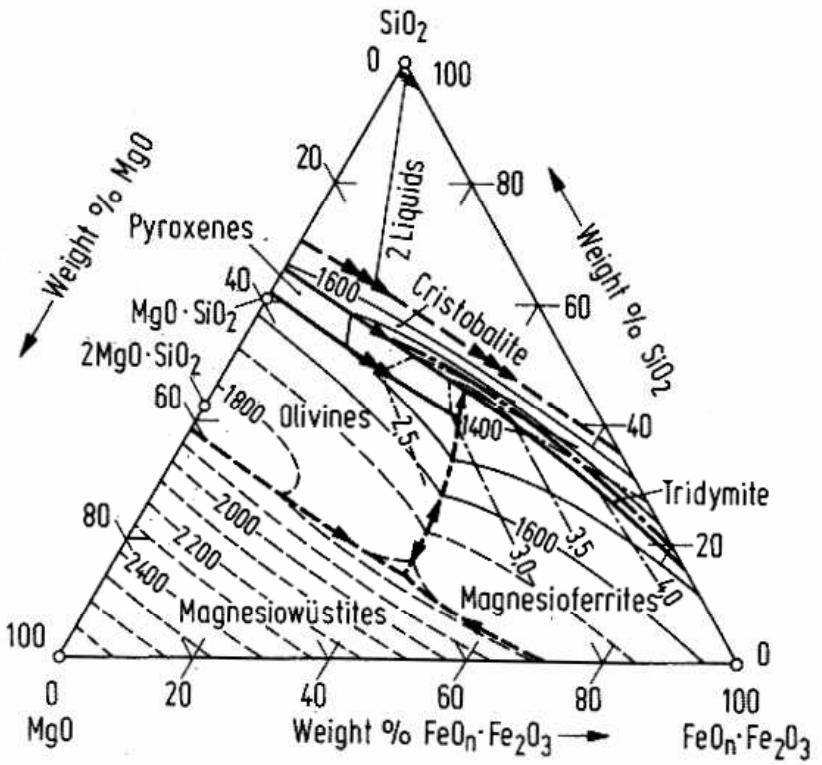

Figure 2.5.4: Phase diagram of the FeO_x-MgO-SiO_2 system at 1 atm (Slag Atlas, 1995)

Nikoo *et al.* (2001) and Rigby (1962) found that the chromite spinel grains in magnesia-chrome refractories remain unattacked and are mechanically detached from the interface by being washed away in the fluid slag with the weakening of bonds between phases. Such findings are further supported by Makipaa *et al.* (1993) and Mikami and Sidler (1963) who noticed detached chromite spinel grains, with no signs of new phase formation on their surfaces, in the slag.

Makipaa *et al.* (1993), Ainsworth and Starzacher (1988) and Mikami and Sidler (1963) observed that the slag infiltrated the open porosity of the refractory brick, as evidenced by the presence of copper oxide in the brick network. However due to the high viscosity of the silicate slag, approximately 0.25 Pa.s at 1300^{o}C (Vartiainen, 1998), slag penetration was not severe and the wear rate of the refractory is mainly determined by the chemical attack on the magnesia at the interface by the formation of forsterite and magnesioferrite. They found that the reactions between the slag and brick components in the pores were similar to the reactions at the interface but decreased in intensity with depth of penetration into the brick. The authors attributed this to the change in slag composition, that is, the depletion of iron oxides resulting from reaction with the magnesia in the brick, as slag penetrates further into the refractory. Such reactions raised the slag liquidus and led to freezing. However as the slag

penetrates further into the brick, the temperature is also decreasing through the brick towards the outer surface and thus slag freezing is inevitable regardless of the changes in the slag liquidus temperature. The penetration of slag did not result in severe chemical wear of the brick but rather the formation of cracks due to thermal shock damage and therefore led to spalling. The penetration of the highly viscous iron silicate slag densified the brick's structure, making it more prone to thermal shock damage.

In summary, research indicates that the reaction of MgO in the periclase phase with iron oxides in iron silicate slag is the main cause of refractory wear. The surface reactions that result at the interface transform the periclase phase into reaction products magnesiowustite, magnesioferrite, forsterite, olivines and pyroxenes. The formation of compounds such as forsterite, olivines and pyroxenes results in a microstructure with modified direct bonding which is prone to slag attack. The presence of such silicates is a serious limitation to the refractory as these phases have a low melting point and soften at copper converting temperatures, making the brick weak and readily prone to attack by the slag. Continual washing and abrasion by the slag removes weakly bonded brick particles from the surface layer and the reaction zone progresses further into the brick. In addition, the difference in the physical properties between the original brick phases and the newly formed phases, results in crack propagation and spalling caused by local volume expansion as well as the build up of thermal and mechanical stresses. Thermal and structural expansion leading to spalling which results from slag penetration is also believed to contribute to brick degradation to a much lesser extent. The chromite spinel phase of the refractories remains almost unattacked by the silicate slag but rather was present in the slag phase as detached particles resulting from weakening of bonds between the periclase and the spinel phases.

2.5.2 Refractory Wear by Calcium Ferrite Slag

One of the major drawbacks of calcium ferrite slag in copper converting is its aggressiveness towards magnesia-chrome refractories. However, despite the importance of understanding the nature of slag attack caused by the ferrite slag, there exists limited literature on the subject, especially at copper converting conditions. Furthermore, although chromia is a vital component of magnesia-chrome refractories, studies on its role in refractory wear are very scarce, with most literature concentrating on the interactions between magnesia bricks and calcium ferrite slag. However as Fahey *et al.* (2004) discovered, there is a significant solubility of Cr_2O_3 in calcium ferrite slag, which results in the dissolution of the chromite

spinel bonding phase of the brick and thus contributes to the degradation of the refractory. They also found that when calcium ferrite slag is in contact with magnesia-chrome refractories, the ferrite slag easily penetrates through the pores in the refractory making it difficult to contain the slag, irrespective of whether or not the brick components are being attacked. The reported work on the refractory was at a uniform high temperature (1300^{o}C) whilst in reality there exists a temperature gradient through the brick. Slag penetration is limited to a point in the refractory brick where the temperature equals the slag liquidus, thus slowing down further penetration, before eventually stopping as a result of freezing the slag.

According to Allen *et al.* (1995), Yamaguchi *et al.* (1994) and Sato *et al.* (1999) who studied reactions between pure MgO and calcium ferrite slag over a temperature range of 1300-1500^{o}C in air, when magnesia refractories are brought into contact with calcium ferrite slag, reaction between iron oxide in slag and the magnesia brick results in the formation of a dense magnesioferrite spinel reaction product and behind this layer, closer to the brick, is a region of magnesiowustite solid solution and periclase. Donald and Toguri (1997), who studied the interactions between calcium ferrite slag and MgO-refractories at an oxygen partial pressure of 10^{-6} atm. and 1300^{o}C, also found that at this oxygen partial pressure, magnesioferrite and magnesiowustite formed from the reaction between magnesia in the refractory and iron oxides from the ferrite slag. Both Sato *et al.* (1999) and Donald and Toguri (1997) agree that the proportions of magnesioferrite and magnesiowustite formed vary according to the change in Fe^{3+}/Fe^{2+} ratio in slag, which is affected by the oxygen partial pressure. Magnesiowustite is the dominating reaction product under reducing conditions (below 10^{-8} atm.) whilst magnesioferrite is dominant under oxidising conditions. Sato *et al.* and Donald and Toguri's (1997) findings are supported by Figure 2.5.2 which illustrates the phase diagram of the FeO-Fe_2O_3-MgO system at 1300^{o}C and various oxygen partial pressures. As can be seen in the figure, as the oxygen partial pressure increases, Fe_3O_2 becomes the dominant iron oxide and magnesioferrite the dominant reaction product.

An SEM scan by Allen *et al.* (1995), revealed the presence of cracks at the interface of the magnesioferrite spinel and magnesiowustite phases. Such observations were also reported by Yamaguchi *et al.* (1994) and Sato *et al.* (1999). The authors proposed that at the boundary of each region, the difference in physical properties results in cracks and spalling caused by local volume expansion as well as the build up of thermal and mechanical stresses. Following the region of magnesioferrite and magnesiowustite solid solution at the slag/brick interface, Allen *et al.* (1995), Yamaguchi *et al.* (1994) and Sato *et al.* (1999) also noticed a brick

structure penetrated by slag rich in copper oxide and CaO. The authors hypothesised that due to the low viscosity of calcium ferrite slag and low interfacial tension between the ferrite slag and the refractory, the slag easily penetrated into refractory pores. As slag penetrated further into the brick, the concentration of iron oxides in slag decreased, as it preferentially reacted with MgO, leaving behind a slag rich in copper oxide and CaO. From their findings, Sato and co-authors (1999) suggested that the wear of magnesia-chrome refractories in copper converters by calcium ferrite slag is dominated by the internal structural damage and spalling caused by slag penetration and the formation of new phases on the periphery of the periclase grains. However, Sato *et al.* (1999) only studied MgO-bricks, without having studied the behaviour of calcium ferrite slag towards Cr_2O_3; the conclusions drawn by the authors therefore are not directly relevant to the wear mechanism of magnesia-chrome refractories, which contain greater than 20wt% Cr_2O_3.

In both the case of iron silicate and calcium ferrite slag interactions between magnesia and iron oxides in the slags have resulted in similar reaction products. However, interdiffusion of iron into MgO is only possible if they have the same ionic charge and a similar ionic radius, such that Mg^{2+} will only interdiffusion with Fe^{2+} and not Fe^{3+} in the slag. As previously determined (Section 2.3), FeO is the dominating iron oxide in iron silicate slag. In batch converting, where the silicate slag is employed, the oxygen partial pressure is increasing and during the initial stages, interactions between MgO in the brick and FeO in the slag result in magnesiowustite. The magnesiowustite is oxidised to magnesioferrite as converting progresses and the oxygen partial pressure increases. On the contrary, the oxygen partial pressure is fixed in the continuous converter, where calcium ferrite slag is used, between 10^{-6} to 10^{-5} atm. The Fe^{3+}/Fe^{2+} ratio is therefore also fixed. As detailed in Section 2.3, at such oxidising conditions, the Fe^{3+}/Fe^{2+} ratio in the ferrite slag is very high. Thus, with little FeO present in the ferrite slag to interact with MgO in the brick, magnesioferrite is most likely not the main reaction product formed in the wear of magnesia-chrome refractories by calcium ferrite slag.

Fahey *et al.* (2000) were the only authors to investigate the wear of commercial magnesia-chrome refractories by calcium ferrite slag. They conducted their study under a CO_2 atmosphere (oxygen partial pressure of 3.7×10^{-4} atm.) and at 1300°C, using a magnesia-chrome refractory crucible to contain the slag. Fahey *et al.* (2000) observed that after melting the crucible was completely emptied of slag, indicating that calcium ferrite slag easily penetrates the microstructure of the magnesia-chrome refractory. Similar to Yamaguchi *et al.*

(1994) and Sato *et al.* (1999), slag penetration was confirmed by Fahey *et al.* (2000) through analysis of the brick's microstructure using the SEM, noticing the presence of calcium and copper within the microstructure. From SEM analysis, the authors found that the concentration of copper and calcium in the brick phases did not change from the pre-reacted brick, concluding that neither CaO nor Cu_2O in the penetrated slag chemically reacted with the phases in the brick. Whilst also observing the formation of the magnesioferrite product layer on the periphery of the magnesia grains in contact with the slag at the interface, Fahey *et al.* (2000) noticed three distinct zones in the chromite spinel grains, a magnesioferrite spinel product layer adjacent to the slag, an interdiffusion zone where chromium content is decreasing whilst the iron content is increasing and a chromite spinel phase with approximately the same composition as in the initial brick. The authors found that the magnesioferrite layer on both brick phases formed due to interdiffusion between iron in the slag and the magnesium from the periclase as well as between iron in slag and the chromium and aluminium from the chromite spinel phase. They did not observe the presence of magnesiowustite in their sample. Fahey *et al.* (2000) found that the reaction between the periclase grains and the ferrite slag was not as severe as the reaction between the chromite spinel grains and calcium ferrite slag; such that, an SEM analysis of the contact brick and slag revealed the presence of periclase grains detached from the refractory surface within the slag and iron impregnation of the chromite spinel grains (Figure 2.5.5). Fahey *et al.* (2000) concluded that calcium ferrite slag causes degeneration of the chromite spinel bonding phase, possibly by dissolution or interdiffusion between Fe^{3+} in slag and Cr^{3+} and Al^{3+} in the chromite grains. As a consequence of this degeneration, periclase grains detach from the surface of the brick and appear in the slag phase.

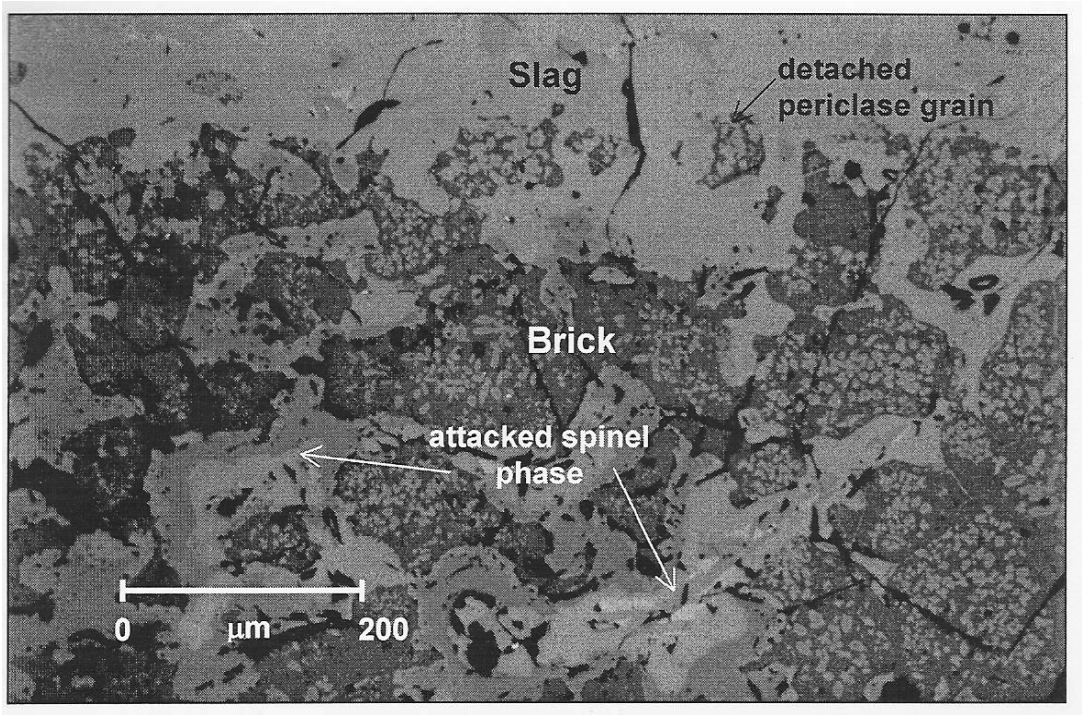

Figure 2.5.5: Magnesia-chrome refractory wear caused by calcium ferrite slag at 1300°C and 3.7 x 10^{-4} atm (Fahey, 2002)

Yan and co-authors (2001) investigated the reactions between synthetic $MgCr_2O_4$ crucibles and copper-containing calcium ferrite slags under controlled CO-CO_2 atmospheres at 1300°C. They measured the dissolution rate of Cr_2O_3 and MgO in calcium ferrite slag at an oxygen partial pressure of 10^{-6} atm and 1300°C and came to similar conclusions. They found that the dissolution rate of Cr_2O_3 (2.3 x 10^{-6} $g.cm^{-2}.s^{-1}$) in calcium ferrite slag is higher than the dissolution rate of MgO (1.1 x 10^{-6} $g.cm^{-2}.s^{-1}$). Such findings are in agreement with the comments made by Fahey *et al.* (2000) on the severity of the reactions between the periclase and chromite spinel grains and calcium ferrite slag.

In a later study, Fahey *et al.* (2004) investigated the solubility of Cr_2O_3 in calcium ferrite slag by use of drop quench experiments at 1300°C and under a CO_2 atmosphere. By observations of quenched calcium ferrite slag samples containing between 5 to 15 wt% Cr_2O_3 under the SEM, Fahey and co-authors (2004) found a liquid slag in equilibrium with 3 solid phases which resulted from the dissolution of Cr_2O_3 in the ferrite slag. Not all samples contained three solid phases and the number of solid phases in equilibrium with the slag depended on the system composition. The three solids which formed were:

- Chromia-magnetite solid solution, composed of $FeO.Fe_2O_3$, $CuO.Cr_2O_3$ and $CaO.Cr_2O_3$,
- Calcium ferrite solid solution composed of $CaO.Fe_2O_3$ and $CaO.Cr_2O_3$
- Dicalcium ferrite solid solution consisting of $2CaO.Fe_2O_3$ and $2CaO.Cr_2O_3$.

The dicalcium ferrite phase as well as the chromia-magnetite solid solution were also observed by Yan *et al.* (2001). Fahey *et al.* (2004) found that due to the low viscosity of calcium ferrite slag, reported as approximately 0.030 Pa.s at 1300°C (Sumita *et al.*, 1980), it readily penetrated the magnesia-chrome refractory and iron (Fe^{3+}) from the penetrated slag preferentially interdiffused with chromium (Cr^{3+}) in the spinel phase, which then dissolved into the ferrite slag. This dissolved chromium reacts with the penetrated slag to form new phases such as chromia-magnetite spinel solid solution, calcium ferrite and dicalcium ferrite solid solutions.

A similar investigation on Cr_2O_3 solubility in the ferrite slag was also conducted by Yan *et al.* (2001) as is illustrated in Figure 2.5.6. They found the solubility of Cr_2O_3 increased from 0.29 to 0.78 wt% as the Cu_2O content of the slag increased from 0 to 8wt%. On the contrary, at similar conditions, Fahey *et al.* (2004) found Cr_2O_3 solubility to be independent of the Cu_2O content of the slag, measuring a constant value of 2.0wt%, below 75wt% FeO_x in the ferrite slag and predicted that it may decrease at higher FeO_x contents. The slag composition studied by Yan and co-authors (2001) typically contained 80 wt% FeO_x. The proposition made by Fahey *et al.* (2004) suggests that with an increase in FeO_x in slag from 75wt% to 80 wt% FeO_x, there is a rapid decrease in Cr_2O_3 solubility in the ferrite slag.

When comparing the solubility of Cr_2O_3 and MgO in calcium ferrite slag at similar conditions, it is clearly evident from Figure 2.5.6, that the solubility of Cr_2O_3 is higher than the solubility of MgO. This further supports Fahey *et al.*'s (2004) findings that the main phase attacked by calcium ferrite slag is the chromite spinel.

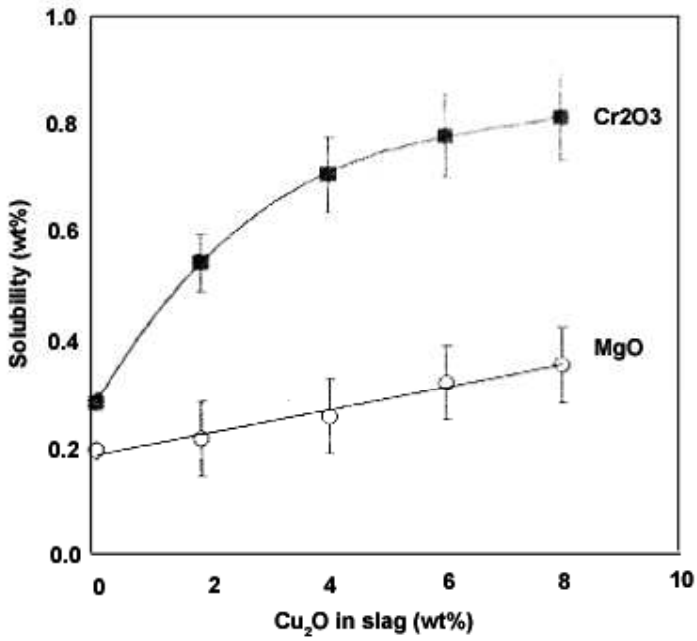

Figure 2.5.6: The solubilities of MgO and Cr_2O_3 (from synthetic $MgCr_2O_4$ bricks) in calcium ferrite slag for various copper oxide contents in slag at 1300°C and 3.7 x 10^{-4} atm (Yan, Sun and Jahanshahi, 2001)

Comparing Yan *et al.*'s (2001) work on the solubility of MgO in calcium ferrite slag from pure magnesia bricks and synthetic $MgCr_2O_4$ bricks indicates that the solubility of MgO in slag is higher when in contact with pure MgO. The solubility of MgO in calcium ferrite slag is 2.4wt% when in contact with pure MgO and 0.32wt% when in contact with $MgCr_2O_4$. The activity of MgO in a pure MgO brick is unity however in $MgCr_2O_4$ it is much less than unity. The activity of MgO in slag equals the activity of MgO in the solid equilibrating phase. Thus the lower the activity of MgO in the solid, the lower the activity of MgO in the slag, i.e. the lower the concentration of MgO in the slag. The solubility of Cr_2O_3 was only measured when the ferrite slag was in contact with $MgCr_2O_4$, being approximately 0.8wt%.

In summary, most literature on refractory wear caused by calcium ferrite slag has concentrated on the slag's interactions with magnesia, with limited studies focussing on the effects of calcium ferrite slag on the wear of magnesia-chrome refractories and in particular the chromite spinel phase. However as is clearly evident from the above discussion, reaction and dissolution of the Cr_2O_3 in slag plays a vital role in the wear mechanism of magnesia-chrome refractories. Although the solubilities of MgO and Cr_2O_3 in calcium ferrite slag are not very different, as chromite spinel is the main bonding phase within the magnesia-chrome bricks, the dissolution of the chromite phase is damaging to the integrity of the brick. The

wear mechanism proposed by Fahey *et al.* (2004) and Yan *et al.* (2001), suggests that the main cause of refractory wear by calcium ferrite slag are the reactions between the penetrated slag and the chromite spinel phase. As Fahey *et al.* (2000) proposed, due to the low viscosity and low interfacial tension between calcium ferrite slag and magnesia-chrome refractories, the slag readily penetrates into the refractory via the voids within the structure of the brick. Calcium ferrite slag acts a source of iron, preferentially interdiffusing with chromium and aluminium in the spinel phase and causing degeneration of the chromite spinel bonding phase by dissolution or interdiffusion. As a consequence, the periclase grains detach from the surface of the brick and appear in the slag phase. Thus the 2 wt% solubility of Cr_2O_3 in the ferrite slag as measured by Fahey *et al.* (2004) is quite significant in terms of dissolution of chromite spinel binding phase in magnesia-chrome refractories. Furthermore, whilst work conducted on pure MgO-bricks suggests that the periclase phase in magnesia-chrome refractories is relatively resistant to dissolution in the ferrite slag; this phase is susceptible to reaction with iron oxides in the slag, resulting in the formation of new phases such as magnesioferrite and magnesiowustite. The formation of such new products on both the periclase and chromite spinel grains contributes to brick degradation due to local volume expansion, which causes stress and leads to interfacial cracking.

2.5.3 Refractory Wear by Calcium Ferrite Slag vs. Iron Silicate Slag

Iron silicate slag is used only for batch converting where the oxygen partial pressure changes with blowing time whilst calcium ferrite slag is used only for continuous converting operations where the oxygen partial pressure remains fixed. The main cause of refractory wear by iron silicate slag is physical wear resulting from crack propagation and spalling. Reactions between MgO in the periclase phase with iron oxides in the silicate slag at the interface result in the formation of new phases such as magnesiowustite, magnesioferrite, forsterite, olivines and pyroxenes. The formation of forsterite, olivines and pyroxenes results in a microstructure with weak direct bonding which is prone to slag attack. The difference in the physical properties between the original brick phases and the newly formed phases, results in crack propagation, local volume expansion and the build up of thermal and mechanical stresses, leading to spalling. Contrasting to the behaviour of periclase, the chromite spinel phase of the refractories remained almost unattacked by the silicate slag and slag penetration is limited due to the high viscosity of iron silicate slag. Refractory wear caused by calcium

ferrite slag is far more severe and a major reason for this is the ease with which calcium ferrite slag infiltrates the voids within the brick, as a result of the low viscosity of calcium ferrite slag and the low interfacial tension between the ferrite slag and brick. Calcium ferrite slag penetrates deep into the refractory and attacks the chromite spinel bonding phase, causing internal damage by altering the physical, chemical and mechanical properties that initially made the brick useful and resulting in the collapse of the brick's structure. The penetrated slag initiates crack propagation within the brick due to thermal shock, the dissolution of the chromite spinel bonding phase and volume expansion.

2.6 REFRACTORY WEAR ALLEVIATION

The Kennecott/Outokumpu Flash Converter, which uses calcium ferrite slag, has reported a number of problems in containing the slag within the magnesia-chrome refractory lined furnace. During the furnace relining operation, Newman *et al.* (1998) reported that the wear of the refractory lining inside the converter was most severe at the sidewall area beneath the reaction shaft. The refractories in this area were in direct contact with the highly corrosive calcium ferrite slag. The containment of the ferrite slag is also a major issue in the Mitsubishi converter. As reported by Ajima *et al.* (1993), calcium ferrite slag is far more aggressive towards the magnesia-chrome refractories than iron silicate slag. Campaign lives of less than one year were experienced in the early development stages of the Mitsubishi converting process. Lee *et al.* (1999) documented that after 13 months of operation; the Mitsubishi converter at the Onsan Smelter required refractory relining. Similar to the Kennecott flash converter, inspection of the Mitsubishi C-furnace during programmed shutdown revealed that brick damage was most severe at the furnace sidewalls in contact with the slag as well as the slag outlet port. MacRae *et al.* (1998) and Tanaka *et al.* (1999) further reported that in addition to the refractory damage caused by slag penetration at the slag/brick interface, the attack was aggravated by the melt splash and waves generated by the lance blowing O_2/air. MacRae *et al.* (1998) found that the aggressive refractory corrosion within the slag zone and the outlet port is further exacerbated by the presence of copper oxide in the penetrated slag, which causes structural stresses and crack propagation in the brick. The nominal copper oxide content of the slag is 16-19%. Whilst the campaign lives of the refractory linings in the Mitsubishi and Kennecott Flash converters have been extend by various means, including moving to fused-cast magnesia-chrome refractories, water cooling jackets and the magnetite

protective layer, refractory wear caused by the calcium ferrite slag is still a major issue in smelter operations around the world.

Copper smelters around the world have implemented a number of strategies to reduce the rate of wear of refractory lining in the converter. The Mitsubishi Corporation initially implemented the replacement of direct bonded bricks with fused-cast magnesia-chrome refractories in the high wear region at the slag line to deal with the slag containment problem. Fused-cast bricks have a closed pore network, which consequently reduces slag infiltration. Whilst application of fused-grain refractories proved partially successful in limiting slag penetration, the bricks are considerably more expensive than the magnesia-chrome refractories as they are processed at temperature above 2000^{o}C (Cherif *et al.*, 1997).

Mitsubishi also installed water cooled copper jackets in the side walls of the C-furnace to further reduce refractory wear caused by calcium ferrite slag. The copper bars inserted into the brickwork extract heat by water-cooling the ends of the bars which project from the furnace. The water-cooling elements were specifically designed to handle the high heat flux developed by the converting process. The sidewall brick and jacket arrangement designed by Mitsubishi is shown in Figure 2.6.1. The design of the converting furnace's copper cooling jacket arrangement consisted of placing the jackets directly behind and between the fused-cast bricks at the slag line. The extraction of heat by the cooling jacket arrangement from the brick lining lowers slag corrosion by increasing the temperature gradient within the brick, containing and limiting the slag penetration region of the brickwork close to the slag/brick interface. Water-cooling the furnace lining has lowered refractory consumption at the slag line.

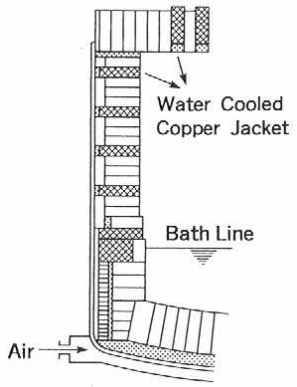

Figure 2.6.1: Arrangement of refractory brick and cooling jackets in the C-furnace (Ajima, Hayashi, Nishiyama and Shimizu, 1993)

This strategy proved to be effective, with the life of the sidewalls doubling from approximately two years to four years (Ajima *et al.*, 1993). The implementation of the improved cooling system, although relatively successful, comes at a significant cost, since the heat removed as a result of the cooling system must be replaced to maintain smelting temperature. Thus in order in achieve this, increased fossil fuel usage and process air enrichment is necessary.

Whilst Kennecott Copper also has employed a sidewall cooling system, they also control slag composition in order to precipitate a protective layer of magnetite on the sidewall bricks (Newman *et al.*, 1998). This is done by controlling the lime and copper levels in the slag. Any reduction in the thickness of the magnetite protective layer on the surface of the bricks can be readily detected by monitoring the heat losses in the settler sidewall cooling system. Whilst magnetite coating prolongs furnace campaign lives by protecting the bricks and jackets inside the furnace, if the magnetite content in the slag is too high, troubles such as accretion build-up and taphole blockages and increase in slag viscosity results.

The cost of maintaining and replacing refractory bricks as a result of slag attack is one of the significant cost components in the copper industry. All current converting processes use magnesia-chrome refractories in contact with slag because they have the best properties available at present. With the application of all the techniques mentioned to reduce refractory wear caused by calcium ferrite slag, the bricks are still only adequate in containing the ferrite slag. The alternative FCS slag for copper converting proposed by Yazawa *et al.* (1999) has been predicted to have the potential to avoid the refractory wear problems encountered by use of calcium ferrite slag in the converting furnace (Takeda, 2001). However experimental data to support such predictions is yet to be published.

2.7 MINOR ELEMENT DISTRIBUTION

The matte entering the converter consists of significant amounts of minor impurities such as antimony, arsenic, bismuth, lead and zinc, which need to be removed, in order to produce market grade copper metal. It is important to eliminate such deleterious minor elements as they affect the electrical conductivity and hot workability of copper. During smelting the minor elements are only partially removed by oxidation from the melt, either to slag or gas. The converting process further removes minor elements from the metal, producing blister copper and a Cu-rich converter slag, which is recycled to the smelter for copper recovery (discussed in Section 2.2). To produce market grade copper, it is essential to understand the distribution and thermodynamic properties of minor elements between the slag and copper phases.

The properties of the converter slag play a vital role in maximising the removal of minor elements to the slag phase. Oxides present in slag are classified as behaving in either an acidic or basic manner, with the earliest slag models, which are based on the aqueous chemistry analogy, suggesting that acidic oxides will attract basic oxides in slag whilst acidic oxides will repel acidic oxides and basic oxides will repel basic oxides (Section 2.7.3). In the case of the slag theory, the terms “repel” and “attract” indicate the affect one oxide has on the activity coefficient of another. The removal of a minor element, whose oxide is basic in nature, will be enhanced by use of an acidic slag, where the impurity oxide will have a low activity coefficient. In order to give the slag the required composition for successful removal of impurities, addition of fluxes is required. The most common fluxes in copper converting are acidic silica and basic lime.

Whilst the basicity of the slag plays an important role in the elimination of minor elements into the slag phase, so do process conditions such as oxygen partial pressure and temperature. The oxidation of impurities to the slag is limited during smelting due to the low oxygen partial pressure. In continuous converting however, the oxygen partial pressure is high, resulting in very oxidising conditions which strongly favour the oxidation of impurities to the slag. Copper is also oxidised to the slag and its recovery is lower in continuous converters. The following chapter discusses distribution thermodynamics in continuous copper converting in terms of oxygen partial pressure and the ‘acid/base’ properties of

converter slags. As the focus of this research is the converting stage of the Kennecott/Outokumpu process, only slag/metal equilibrium will be considered.

2.7.1 Distribution Thermodynamics

The distribution of minor element M having the valence of 2ν in a slag-metal system at equilibrium may be represented by Reaction 2.7.1 and evaluated by use of equilibrium constant, K, which is expressed by the terms of activity and oxygen partial pressure and derived from the free energy data (Yazawa *et al.*, 1983).

$$M + \frac{\nu}{2} O_2 = MO_\nu \qquad \textbf{Equation 2.7.1}$$

$$K_1 = \frac{a_{MO\nu}}{(a_M . p_{O2}^{\nu/2})}$$

Where:

$$a_{MO} = \gamma_{MO} N_{MO} = \gamma_{MO} \frac{n_M}{n_T} = \gamma_{MO} \frac{\%M}{M_M n_T} = \frac{\gamma_{MO} \%M}{M_M n_T}$$

and

$$a_M = \gamma_M N_M = \gamma_M \frac{n_M}{n_T} = \gamma_M \frac{\%M}{M_M n_T} = \frac{\gamma_M \%M}{M_M n_T}$$

Thus

$$K_1 = \frac{[n_T](\gamma_{MO\nu})(\%M)}{(n_T)[\gamma_M][\%M] p_{O2}^{\nu/2}}$$

Where:

M_M: molar mass of element M,

N_M: molar amount of element M in 100g slag (this is only the case if the oxide is expressed in monocation form as is implicit in Reaction Equation 2.7.1)

Reaction 2.7.1 shows that element M is present in slag in oxide form and the distribution ratio of M between slag and liquid copper is described as follows:

$$L_M^{s/m} = \frac{(\%M)}{[\%M]} = \frac{K_1 (n_T)[\gamma^o{}_M] p_{O2}^{\nu/2}}{[n_T](\gamma_{MO\nu})} \qquad \textbf{Equation 2.7.2}$$

where ( ) and [ ] denote the values in slag and metal phases, respectively and n_T is the total mole number of constituents in 100g of each phase, which is calculated from chemical analysis data.

Though oxides exist in the form of ions in molten slags, it is impossible to define the activities of these ions because a standard state for ions cannot be defined. Thus oxides are expressed in their molecular form and molecular expressions are used for the activities and activities coefficients of such oxides. It has been shown by Yazawa *et al.* (1983) that, when species are described in their monocation form, then the activity coefficients remain very close to constant over a large composition range. This is shown in Figure 2.7.1, which represents the relationship between the mole fractions and the activity coefficients of the dissolved oxides of Ag, Cu, As, Sb and Bi in calcium ferrite slag, based on the distribution ratios of the species between slag and liquid copper.

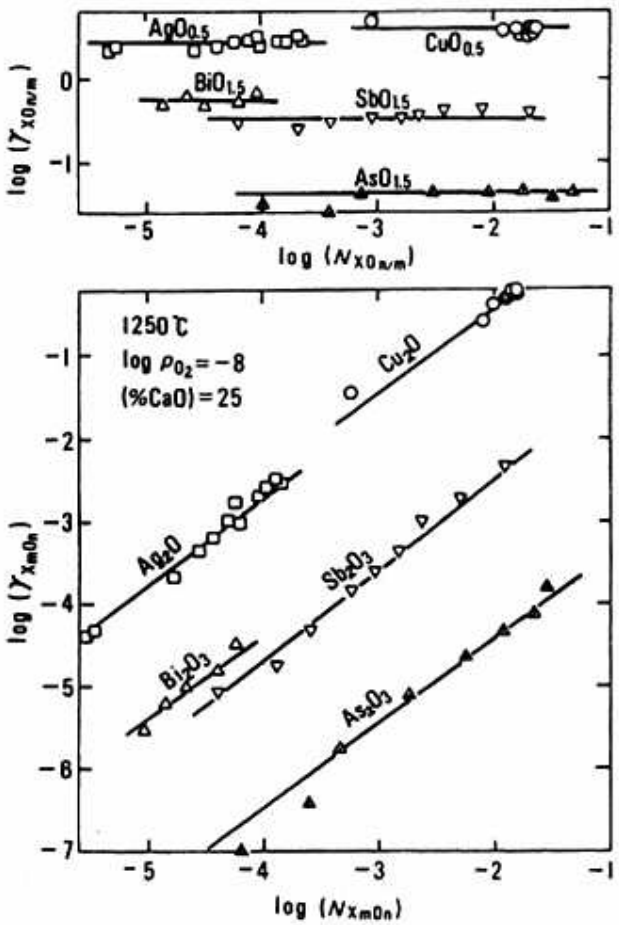

Figure 2.7.1: Relationship between the activity coefficients of oxides and the mole fraction of oxides in calcium ferrite slag at 1250°C (Yazawa, Nakazawa and Takeda, 1983)

Top Figure: Components represented in monocation form

Bottom Figure: Components represented in molecular expression

The total number of moles of species in slag is also closely similar in value for all industrial slag when species are described in their monocation form, which is evident in Figure 2.7.2. The total moles for 100 g of slag corresponds to 1.45 and 1.48 in the ferrite or the silicate slag, respectively and 1.57 for the metal phase.

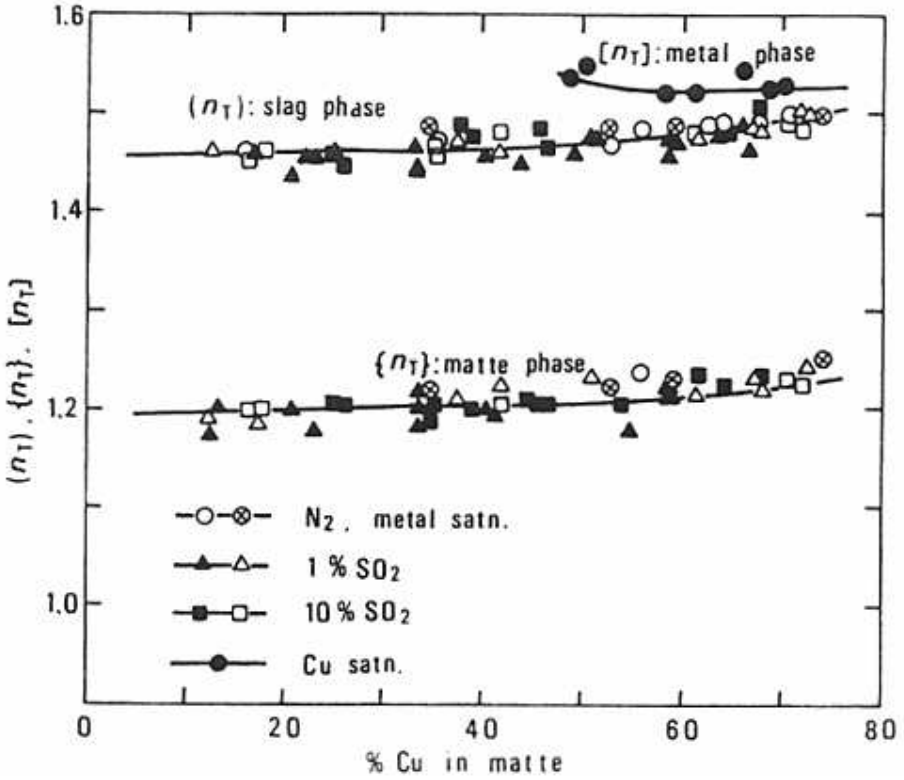

Figure 2.7.2: Total moles of constituents in 100g of calcium ferrite slag and copper phases (Yazawa, Nakazawa and Takeda, 1983)

The distribution ratio $L_M^{s/m}$ is affected by the equilibrium constant K (which is a function of temperature), the activity coefficients of γ_M and γ_{MOv} in both the metal and slag, respectively and the oxygen partial pressure p_{O2}:

- The equilibrium constant, K, is a function of the stability of the metal oxide since the equilibrium constant is calculated from the Gibbs free energy change for the oxide forming reaction.
- The activity coefficient of the oxide in the slag is a function of the interactions occurring between species in the slag and is strongly affected by the slag composition.
- The activity coefficient of the impurity in the copper phase (i.e. the metal phase) is a function of the interactions between the impurity and the copper.

Provided that the composition of the metal and slag do not change significantly, the activity coefficients M and MO_v can be assumed to be constant and the plot of log $L_M^{s/m}$ against log p_{O2} should give a linear relationship with a slope of v/2, which indicates the state of oxidation of the dissolved species distributed in the slag. When the impurities are present in small amounts γ_M will be constant and will be the limiting activity coefficient γ^o_M. The activity coefficients of M in liquid copper [γ^o_M], in particular in binary alloys, are much more widely available in literature than the activity coefficient of oxides in slags (γ_{MOv}).

2.7.2 Distribution Behaviour of Typical Minor Elements between Slag and Liquid Copper

Distribution equilibria of various elements between liquid copper and iron silicate or calcium ferrite slag were extensively compiled and reported by Yazawa (1994). In Figure 2.7.3 and 2.7.4, distribution ratios are illustrated as a function of oxygen potential.

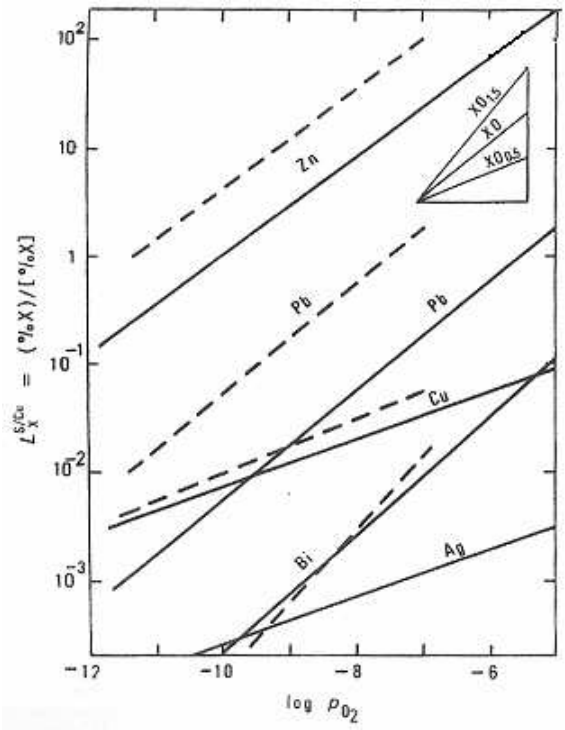

Figure 2.7.3: Distribution ratios of Zn, Pb, Cu, Bi and Ag between slag and liquid copper in sulphur free systems at 1250°C (Yazawa, 1984)

Solid Lines- Calcium ferrite slag

Dashed Lines- Iron Silicate slag

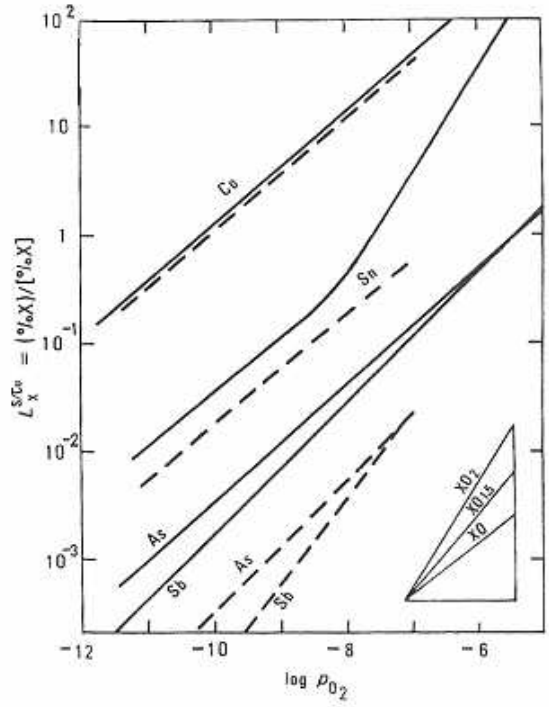

Figure 2.7.4: Distribution ratios of Co, Sn, Sb and As between slag and liquid copper in sulphur free systems at 1250°C (Yazawa, 1984)
Solid Lines- Calcium ferrite slag
Dashed Lines- Iron Silicate slag

It can be seen that the oxides with the most negative Gibbs free energy of formation appear at the top of the diagrams, that is, the oxide strongly distributes to the slag phase and those with the least negative Gibbs free energy of formation at the bottom. Since K varies over many orders of magnitude, it dominates distribution behaviour. Whilst the distribution ratio of an element is also a function of the activity coefficient of M in metal and MO_v in slag, Figures 2.7.3 and 2.7.4 assume constant activity coefficient values of M and MO_v for the studied oxygen partial pressure range. The relationship between Gibbs free energy of formation and distribution ratios of elements between copper and both iron silicate and calcium ferrite slags is illustrated in Table 2.7.1 which also gives the values of K for the oxide forming reactions of species shown in Figures 2.7.3 and 2.7.4. It is interesting to note in Table 2.7.1 that whilst for most elements distribution to the slag phase decreases as the Gibbs free energy of formation becomes less negative, this is not the case for cobalt. Distribution of cobalt to the slag phase is the highest of all elements in Table 2.7.1 however its Gibbs free energy of formation is not the most negative. The behaviour of cobalt in both iron silicate and calcium ferrite slag is an anomaly. The thermodynamic data in Table 2.7.1 was compiled from HSC Chemistry 5.0 for Windows database.

Table 2.7.1: Gibbs free energy and K-values for oxide forming reactions at 1250°C and the distribution ratios of elements between copper and iron silicate and calcium ferrite slags at an oxygen partial pressure of 10^{-7} atm. and 1250°C. *(Source: HSC Chemistry 5.0 for Windows database)*

Reaction	Gibbs Free Energy (kJ)	K-values	$L_M^{s/m}$	
			Iron Silicate slag	Calcium Ferrite Slag
$2Zn + O_2 = 2ZnO$	-383.102	$1.38 \times 10^{+13}$	100	37.5
$2Sn + O_2 = 2SnO$	-269.069	$1.69 \times 10^{+9}$	-	-
$Sn + O_2 = SnO_2$	-260.401	$8.53 \times 10^{+8}$	0.75	5.31
$2Co + O_2 = 2CoO$	-253.871	$5.09 \times 10^{+8}$	56.25	62.5
$1.33As + O_2 = 1.33AsO_{1.5}$	-204.863	$1.06 \times 10^{+7}$	0.0375	0.156
$1.33Sb + O_2 = 1.33SbO_{1.5}$	-197.914	$6.14 \times 10^{+6}$	0.0375	0.131
$2Pb + O_2 = 2PbO$	-154.684	$2.02 \times 10^{+5}$	2.5	0.25
$1.33Bi + O_2 = 1.33BiO_{1.5}$	-118.123	$1.13 \times 10^{+4}$	0.0156	0.0094
$4Cu + O_2 = 4CuO_{0.5}$	-111.387	$6.61 \times 10^{+3}$	0.075	0.056
$4Ag + O_2 = 4AgO_{0.5}$	115.646	1.08×10^{-4}	-	0.0011

Provided that the lime in the ferrite slag is kept at a suitable level, the ferrite slag will remain liquid at oxygen partial pressures ranging from 10^{-12} to 1 atm. without magnetite precipitation. On the contrary however, at 1250°C, solid magnetite precipitates from iron silicate slag once oxygen partial pressure reaches approximately 10^{-7} atm. as shown in Equation 2.7.3. For this reason, the distribution data for iron silicate slag in Figures 2.7.3 and 2.7.4 are limited to an oxygen partial pressure of 10^{-7} atm. The phase equilibria and homogenous melt region of iron silicate and calcium ferrite slag is discussed in detail in Section 2.3.

$$6FeO + O_{2(g)} = 2Fe_3O_4 \qquad \textbf{Equation 2.7.3}$$

$$K = \frac{(a_{Fe3O4})^2}{(a_{FeO})^6 . p_{O_2}}$$

Assume:

$K_{1250^oC} = 5.749 \times 10^9$

$a_{FeO} = 0.31$ When iron silicate slag is saturated with silica

$a_{Fe3O4} = 1$ at magnetite precipitation

$$p_{O_2} = \frac{(a_{Fe3O4})^2}{(a_{FeO})^6.K} = \frac{1^2}{(0.31^6)(5.749\times10^9)} = 1.95\times10^{-7}\,atm$$

In the bottom right hand corner of Figures 2.7.3 and 2.7.4 are the slopes expected for the different valencies of element M, for example, if:

- the slope of the log $L_M^{s/Cu}$ versus log p_{O2} plot of element M is 1, the oxidation state of MO_v is 2 and the valency of element M is 4+
- the slope is 0.75 then the valency of element M is 3+
- the slope is 0.5 then the valency of element M is 2+
- the slope of the log $L_M^{s/Cu}$ versus log p_{O2} plot of element M is 0.25, the oxidation state of MO_v is 0.5 the valency of element M is 1+.

By observation of the results for the distribution ratios between slag and liquid copper, the slopes for Co, Zn, Sn and Pb suggest that these elements dissolve in slag as the divalent oxides, CoO, ZnO, SnO and PbO. Arsenic, antimony and bismuth, however, dissolve in the slag as trivalent oxides, $AsO_{1.5}$, $SbO_{1.5}$ and $BiO_{1.5.}$ Silver dissolves in slag as $AgO_{0.5}$ and whilst copper is not a minor element; it also exists as monovalent oxide, $CuO_{0.5}$. The slope for Sn changes at an oxygen partial pressure of approximately $10^{-8.5}$ atm. in calcium ferrite slag, indicating that the valency of tin when dissolved in the ferrite slag changes at an oxygen partial pressure of $10^{-8.5}$ atm. Tin has two oxides, SnO and SnO_2, that is, the oxidation state for tin is 2+ and 4+. The presence of both Sn^{2+} and Sn^{4+} in the ferrite slag at approximately $10^{-8.5}$ atm. as determined experimentally is supported by thermodynamic calculations for the oxidation reaction of SnO/SnO_2 in Equation 2.7.4. In agreement with experimental findings, Equation 2.7.4 demonstrates that above approximately $10^{-8.5}$ atm., both Sn^{2+} and Sn^{4+} are present in slag whilst below this oxygen partial pressure tin exists in slag only as SnO. Above $10^{-8.5}$ atm., as oxygen partial pressure increases, the Sn^{4+}/Sn^{2+} activity ratio increases.

$$2SnO + O_2 = 2SnO_2 \qquad \textbf{Equation 2.7.4}$$

$$K = \frac{(a_{SnO_2})^2}{(a_{SnO})^2.p_{O_2}}$$

assume $a_{SnO} = a_{SnO_2}$

$$K = \frac{1}{p_{O_2}} \quad \Rightarrow \quad p_{O_2} = \frac{1}{K}$$

$$K_{1250^oC} = 4.17 \times 10^{8}$$
$$p_{O_2} = 2.39 \times 10^{-9}\, atm = 10^{-8.62}\, atm$$

In both Figures 2.7.3 and 2.7.4, it can be seen that the use of the silicate slag rather than ferrite slag or vice versa makes a significant difference to the distribution ratios of some elements, whilst for other elements their distribution ratio are similar in both slags, for example:

- The distribution ratio of lead is an order of magnitude higher in iron silicate slag than in calcium ferrite slag. This is also true for zinc. The silicate slag is more effective in the removal of lead from copper than the ferrite slag.
- Contrary to the behaviour of lead, the distribution ratios of tin, antimony and arsenic are high in calcium ferrite slag than iron silicate slag, indicating that the dissolution of these elements in the ferrite slag is higher than in the silicate slag, especially in the case of antimony and arsenic.
- For minor elements such as iron, bismuth and cobalt, the use of calcium ferrite slag or iron silicate slag makes very little difference to their distribution ratio.

The difference in the behaviour of such impurities in the two slag types can be explained by the basicity of the slag (i.e. the measure of the activity of oxide ions in the slag).

2.7.3 Regular Solutions Model and its Application to Ternary FeO_x-SiO_2-CaO Slag System

According to the earliest slag theories, which are based on the aqueous chemistry analogy, metal oxides in slags are referred to as acidic, basic and neutral. Based on this theory, acidic oxides are those which have a strong tendency to accept oxide ions into their structure much more than its tendency to lose oxides ions whilst basic oxides are reverse and have a strong tendency to donate oxide ions. Neutral oxides both donate and accept oxide ions. The underlying assumption made on the interactions of oxides in solution together is that acidic oxides will interact with basic oxides whilst acids will repel acids and bases will repel bases. The acid-base properties of molten oxides and metallurgical slags are discussed in greater depth by Duffy and Ingram (1978) and Masson (1984). Knowing whether the oxides

in the slag are acidic, basic or neutral helps quantify the degree of interaction expected between pairs of oxides. The strength of the interactions between species in the slag indicates the value of the activity coefficients and the stronger the interactions between species, the smaller the activity coefficient.

The regular solution model can be used to describe deviations of any solution from ideal behaviour by taking into account the interactions between the components in the solution. The α-function for regular solution expressed with activity coefficient γ and mole fraction N, ($RT \ln \gamma_i = \alpha(1 - N_i)^2$), is a parameter which represents the degree of deviation of activity, a, from ideality in a regular solution model for slag activity behaviour. The more negative the α-values, the more negative the deviation of activity from ideality, the smaller is the activity coefficient of the species and the greater the degree of interaction between species in slag. The model gives a good representation of binary regular solutions, however, it is not a very good representation of the activities in real slags, but it is adequate for a general description of the behaviour of many different oxides in slags. The model approximates the activity coefficients and hence the activities of any component for any composition within the ternary system using thermodynamic data.

The activity behaviour for a typical ternary system in copper smelting operations was demonstrated by Yazawa (1994) as shown in Figures 2.7.5 and 2.7.6. Both ternary diagrams in Figures 2.7.5 and 2.7.6 are a compilation of data from binary AO-BO, AO-MO and BO-MO systems, where AO is the strong acidic oxide SiO_2, BO is the strong basic oxide CaO and MO is a typical metal oxide. In Figure 2.7.5 MO represents neutral metal oxide FeO and in Figure 2.7.6 MO is the basic metal oxide PbO. In both Figures 2.7.5 and 2.7.6, the α-values, a parameter of the regular solutions model, indicate the degree of interactions between the binary AO-BO, AO-MO and BO-MO systems. The activity and activity coefficients data for MO in the ternary system is illustrated by the solid and dashed concaved lines, respectively. The activity and activity coefficient values in both Figures 2.7.5 and 2.7.6 are based on the assumption that all three binary sub-systems and the ternary system are regular solutions and that the assigned α-values are applicable. In order to discuss the effects of slag basicity on the distribution of MO in slag, two points A and B are selected on Figures 2.7.5 and 2.7.6. Points A and B represent iron silicate and calcium ferrite slags, respectively.

As seen in Figure 2.7.5, the activity coefficient of the neutral metal oxide in both slags A and B is similar, indicating that the distribution of a neutral metal oxide is unaffected by the solvent slag. Such predictions are in accord with the experimental distribution data for neutral oxides in Figures 2.7.3 and 2.7.4 for the silicate and ferrite slags. However, the addition of CaO to iron silicate slag and the addition of SiO_2 to calcium ferrite slag results in an increase in (γ_{MO}), and a decreases in the activity of the metal oxide in the slag. The increase in (γ_{MO}) suggests a decrease in the distribution ratio of the neutral oxide in the ternary slag. As previously explained in Section 2.7.1, the distribution ratio $L_M^{s/m}$ is thus a function of the equilibrium constant K, which depends on temperature, the activity coefficients of γ^o_M and γ_{MOv} in metal and slag, respectively and the oxygen partial pressure. Assuming infinite-dilution, γ^o_M, is a constant. At a given temperature and oxygen partial pressure, the slag system used determines the value of γ_{MOv} and therefore controls the distribution of the impurity between the slag and the copper, such that, the distribution ratio of an element in a slag/metal system is inversely proportional to γ_{MOv} in slag, according to Equation 2.7.5.

$$L_M^{s/m} = \frac{1}{(\gamma_{MOv})} \qquad \textbf{Equation 2.7.5}$$

It should be noticed in Figure 2.7.5 that for all compositions within the ternary system, the activity of MO exceeds the mole fraction of MO and the activity coefficient of FeO is greater than one. Such behaviour suggests that there exists strong repulsive forces between FeO, CaO and SiO_2 and the interactions between the species are weak. The interactions between FeO, CaO and SiO_2 are particularly weak on the tie-lines between FeO and $xCaO.SiO_2$, which is demonstrated by the strongly concave nature of the activity and activity coefficient isobars of MO on the tie line between MO and xBO.AO, where x represents the BO/AO (CaO/SiO_2) ratio ranging from 1-2. When strong acids and bases such as SiO_2 and CaO are in solution together they are strongly associating. The addition of a constituent to the solution, such as a neutral metal oxide, FeO, which does not have strong interactions with either CaO or SiO_2 results in weak interactions between FeO and the $xCaO.SiO_2$ compound within the solution, which is caused by the repulsive forces between stable solution of $xCaO.SiO_2$ and neutral metal oxide FeO. The larger negative α-value for the $CaO\text{-}SiO_2$ system in comparison to the α-values for both the $FeO\text{-}SiO_2$ and FeO-CaO binary systems further provides evidence for the strong interactions between CaO and SiO_2. Such behaviour of FeO in slag is similar also for other neutral metal oxides such as $CuO_{0.5}$, NiO, CoO and

SnO and the distribution of not only FeO but also other neutral metal oxides in slag will be low in a slag containing both CaO and SiO_2, with distribution expected to be lowest in a slag whose CaO and SiO_2 compositional ratio is similar to that of intermediate compound, xBO.AO, where x is between 1-2.

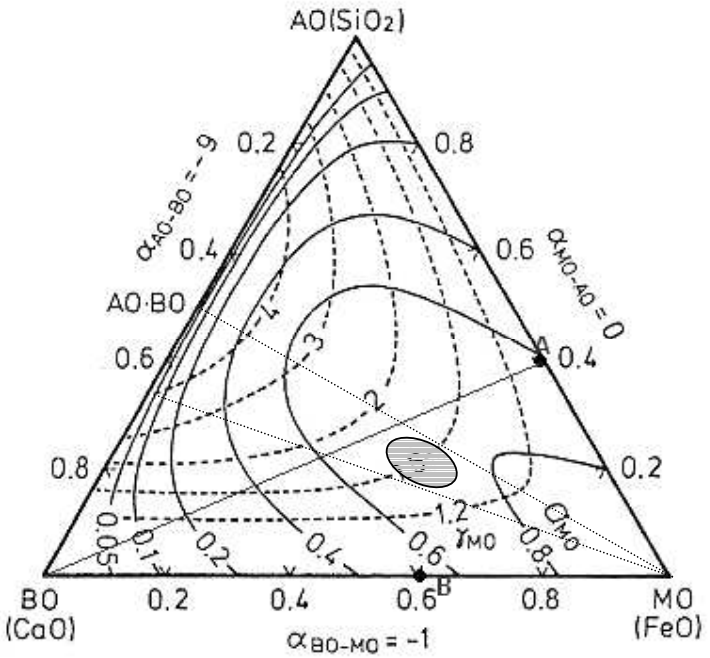

Figure 2.7.5: Isobars of activity and activity coefficients of neutral oxides in AO-BO-MO ternary derived from α values of –9, 0 and –1 for each binary (Yazawa, 1994)

As evident in Figures 2.7.3 and 2.7.4, in general, the solubility of minor elements in calcium ferrite slag is comparably higher than in iron silicate slag with the exception of PbO. To explain the behaviour of lead oxide in both slags, thermodynamic model of system MO-BO-AO, where MO represents a basic metal oxide such as PbO is demonstrated in Figure 2.7.6.

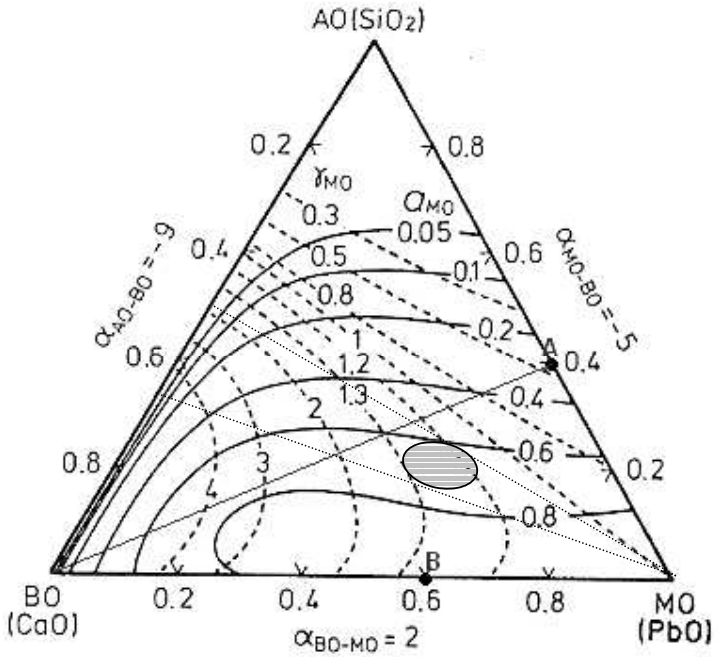

Figure 2.7.6: Isobars of activity and activity coefficients of basic oxides in AO-BO-MO ternary derived from α -values of –9, 2 and –5 for each binary (Yazawa, 1994)

When the metal oxide is considerably basic, the activity behaviour of MO strongly deviates from ideal behaviour and as can be observed in Figure 2.7.6 the isobars of a_{MO} and γ_{MO}, are considerably deformed in comparison to the neutral metal oxide behaviour. It is clearly evident that the activity coefficient of MO, when MO is a basic metal oxide PbO, is much larger in slag B in comparison to slag A. However, when silica is added to the basic FeO_x-CaO slag, the activity coefficient of lead oxide in slag decreases, suggesting higher solubility of lead oxide. Inversely when basic CaO is added to acidic iron silicate slag, activity coefficient of PbO increases and the distribution of lead in slag is reduced. As PbO is a basic metal oxide, it is strongly associating with acidic silica when in solution together, as is indicative by the relatively large negative α-value for the MO_{basic}-BO binary system. However with the addition of basic lime, iron silicate slag becomes less acidic and more neutralised, such that the activity coefficient of PbO in the silicate slag increases. The degree of interactions between PbO and SiO_2 in slag are reduced by the addition of CaO because CaO interacts much more strongly with SiO_2 than PbO. Calcium ferrite slag (slag B) is a basic slag, with weak interactions present between CaO and PbO, thus explaining the low solubility of basic oxides in calcium ferrite slag.

Similarly to the case of lead oxide, the effects of slag composition are also considerable for acidic oxides, such as $SbO_{1.5}$ and $AsO_{1.5}$, but differing from PbO, the high dissolution of antimony is expected in slag B due to their acidic character. If MO is an acidic oxide such as $AsO_{1.5}$ or $SbO_{1.5}$, the isobars in Figure 2.7.6 are valid if AO and BO are exchanged in the figure and thus activity coefficients become a minimum for the MO-BO system, and a maximum for the MO-AO slag system. When the metal oxide is acidic, the basic slag will attract the acidic oxide to it whilst the acidic slag will repel it. Hence, $SbO_{1.5}$ will absorb into the basic CaO-FeO slag, with strong interactions between the species in the slag whilst SiO_2-FeO slag will repel $SbO_{1.5}$.

Arsenic and antimony strongly interact with copper (i.e. have small activity coefficients) and the removal of these elements is generally difficult, however through use of the strong acidic character of their oxides, oxidative removal of such V group elements into a basic slag is possible. The effects of CaO content in the ferrite slag on the distribution ratios can be confirmed further by Figure 2.7.7. The distribution ratio of As and Sb into the slag phase increases with increasing CaO content, while decreases for Pb.

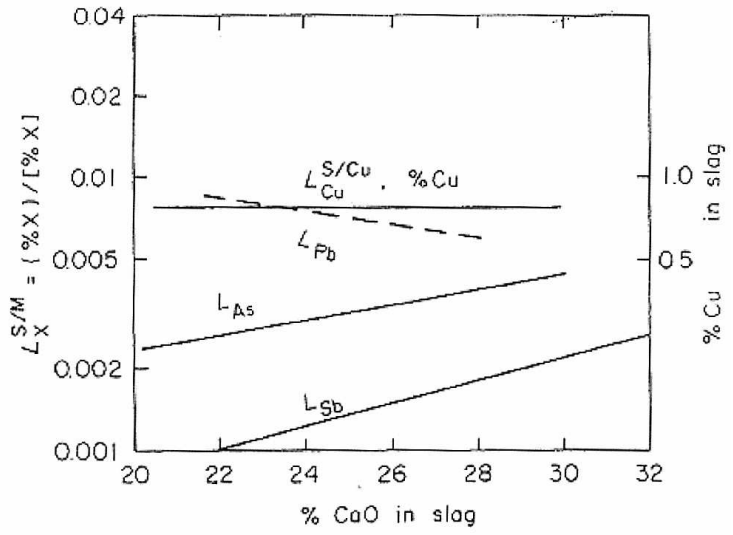

Figure 2.7.7: Effects of CaO contents in slag on distribution ratio between calcium ferrite slag and liquid copper (Yazawa, 1984)

2.7.4 Predicted Distribution Behaviour of Minor Elements in FCS Slag

Whilst calcium ferrite slag is superior for the removal of acidic oxides and iron silicate for the removal of basic oxides, Yazawa *et al.* (1999) predicted, that FCS slag, having both strong basic and acidic oxides, CaO and SiO_2, in its slag structure, will perform similar to calcium ferrite slag in the removal of acidic oxides and is expected to be 2 to 3 times better than calcium ferrite slag in the removal of basic oxides from copper metal. Thus from thermodynamic predictions, ferrous calcium silicate slag has the potential to improve both acidic and basic impurity removal from copper during converting. Neutral oxides are expected to distribute more to the silicate and ferrite slags than to FCS slag. Both Figures 2.7.5 and 2.7.6 can be used to explain the predictions made by Yazawa *et al.* (1999) on the distribution of minor elements in FCS slag. The composition of ferrous calcium silicate slag is located near the dicalcium silicate crystalline surface in the region of high FeO_x content. An approximation of the location of FCS slag in the ternary system is provided by the shaded oval in Figures 2.7.5 and 2.7.6.

The activity coefficient of a neutral oxide in both the silicate and ferrite slags, as predicted by the model in Figure 2.7.5, is approximately similar (i.e. $\gamma_{MO} < 1$). The predicted activity coefficient value of a neutral oxide in FCS slag as indicated in Figure 2.7.5 is between 1.2-1.5. Here (γ_{MO}) is slightly higher in comparison to both the ferrite and silicate slags. The observation of Figure 2.7.5, thus gives the initial indication that γ_{MO} is larger in FCS slag than both iron silicate and calcium ferrite slag and thus a lower $L_M^{s/m}$ for a neutral metal oxide, such as NiO and CoO, in FCS slag can be expected. Although copper is not a minor element, lower dissolution loss of copper, as copper oxide, to FCS slag is also expected as Cu_2O is considered a neutral oxide. The copper loss to slag is a function of the activity coefficient of Cu_2O in the slag which is a function of the slag composition because the extent of interactions between species is dependant on the composition of the species in the slag. The activity of Cu_2O is a function of temperature and oxygen partial pressure only. Thus, the mole fraction of Cu_2O in slag (or wt%Cu_2O) is an inverse function of the activity coefficient.

In Figure 2.7.6, the activity coefficient of lead oxide for iron silicate slag A (γ_{PbO} ~ 0.5) is lower than in calcium ferrite slag B (γ_{PbO} ~ 1.3), suggesting higher removability of lead from copper by the silicate slag. At the composition of FCS slag, it is observed that γ_{PbO} is lower (γ_{PbO} ~ 1 to 1.2) than in calcium ferrite slag but higher than in iron silicate slag. This observation coincides with the predictions made by Yazawa *et al.* (1999), that whilst the removal of lead from copper is most efficient in the acidic silicate slag, FCS slag is expected perform better than calcium ferrite slag. Whilst a thermodynamic model is not presented for the AO-BO-MO_{acidic} system, it is expected that the behaviour of acidic oxides such as arsenic and antimony in FCS slag will be similar to calcium ferrite slag.

2.8 MINOR ELEMENT DISTRIBUTION- A REVIEW OF EXPERIMENTAL DATA

The thermodynamics of minor element distribution in a slag-metal system have been discussed in detail in Section 2.7. The following section addresses the distribution of lead oxide (PbO), nickel oxide (NiO) and antimony oxide ($SbO_{1.5}$) between iron silicate and calcium ferrite slags and copper metal. The three oxides, PbO, NiO and $SbO_{1.5}$, were selected for study as they are a basic, neutral and acidic oxide, respectively (Yazawa, 1994). Given that this study concerns the distribution behaviour of minor elements at converting conditions, the following section deals with distribution data in both slags at an oxygen partial pressure of 10^{-6} atm. and 1300^{o}C. The minor element distribution data on iron silicate and calcium ferrite slags compiled from literature and evaluated in this chapter will be compared with the experimentally determined values of distribution of lead, nickel and antimony between FCS slag and copper metal at similar conditions. This will test Yazawa *et al.* (1999) predictions on the expected distribution of an acidic, basic and neutral oxide between FCS slag and copper.

2.8.1 Distribution of Lead between Slag and Copper Metal

The distribution of lead between iron silicate slag and copper metal has been studied by various authors, including Kim and Sohn (1998), Kashima *et al.* (1978), Yazawa (1980), Takeda *et al.* (1984) and Kudo *et al.* (2000), all of whom agree that lead dissolves in iron silicate slag as PbO in the oxygen partial pressure range of 10^{-12} to 10^{-7} atm. and temperatures

between 1200-1300°C, according to the equilibrium Reaction 2.8.1. The thermodynamic data for Reaction 2.8.1 was taken from HSC Chemistry for Windows database.

$$Pb_{(l)} + \frac{1}{2}O_{2(g)} \rightarrow PbO_{(l)}$$
$$\Delta G^{o}_{1300oC} = -73.863kJ \qquad \textbf{Equation 2.8.1}$$
$$K_{1300oC} = 2.836 \times 10^{2}$$

Studies on the distribution of lead between calcium ferrite slag and copper metal also agree that within the oxygen partial pressure range of 10^{-12} to 10^{-6} atm. and at temperatures between 1200-1300°C, lead dissolves in the ferrite slag as PbO, as per Reaction 2.8.1. Such findings were made by Yazawa *et al.* (1983), Takeda *et al.* (1984), Acuna and Yawaza (1987), Kudo *et al.* (2000), as well as Eerola *et al.* (1984).

Whilst most distribution data for both the silicate and ferrite slags has been reported at 1300°C, some distribution data is at 1250°C. In the case of lead distribution between calcium ferrite slag and copper, data has been reported at an oxygen partial pressure of 10^{-6} atm., however, literature data available on lead distribution between iron silicate slag and copper is at an oxygen partial pressure of 10^{-7} atm. due to the problems encountered with magnetite precipitation in the silicate slag. In order to compare minor element distribution data for iron silicate slag with that of calcium ferrite and FCS slag, the data needs to be at similar conditions, that is at 1300°C and an oxygen partial pressure of 10^{-6} atm. The distribution data can be extrapolated from literature data at 1300°C and an oxygen partial pressure of 10^{-6} atm., using Equation 2.8.2, as derived from Section 2.7.1.

$$L_M^{s/m} = \frac{(\%M)}{[\%M]} = \frac{K(n_T)[\gamma^{o}{}_M]p_{O2}^{v/2}}{[n_T](\gamma_{MOv})} \qquad \textbf{Equation 2.8.2}$$

If all species are expressed in the monocation form, the total number of moles of species in the silicate and ferrite slags are constant at 1.48 and 1.45, respectively and 1.57 for the copper metal (Yazawa *et al.*, 1983). It is assumed that these total numbers of moles are correct for the slags used in the literature studies reviewed. However Yazawa *et al.* (1983) have verified these values against many typical slags and found them to be very good approximations as detailed in Section 2.7.1. Thus at 1300°C and an oxygen partial pressure of 10^{-6} atm., Equation 2.8.2 is simplified to Equation 2.8.3 for distribution ratio of lead between

iron silicate slag and copper and Equation 2.8.4 for distribution ratio of lead between calcium ferrite slag and copper. Equations 2.8.3 and 2.8.4 correct for both the oxygen partial pressure and temperature differences in distribution data extracted from literature.

$$L_{Pb}^{s/m} = \frac{0.267[\gamma^{o}_{Pb}]}{(\gamma_{PbO})} \quad \textbf{…. Iron Silicate Slag} \qquad \textbf{Equation 2.8.3}$$

$$L_{Pb}^{s/m} = \frac{0.262[\gamma^{o}_{Pb}]}{(\gamma_{PbO})} \quad \textbf{… Calcium Ferrite Slag} \qquad \textbf{Equation 2.8.4}$$

If the effects of oxygen partial pressure and temperature on $[\gamma^{o}_{Pb}]$ and (γ_{PbO}) are small and negligible, the activity coefficient data from literature can be used to calculate the distribution ratio of lead at an oxygen partial pressure of 10^{-6} atm. and 1300°C using Equations 2.8.3 and 2.8.4 for the respective slags. The effects of oxygen partial pressure and temperature on the activity coefficients will be examined below.

The original activity coefficient data extracted from literature for both iron silicate and calcium ferrite slags is shown in Tables 2.8.1 and 2.8.2, respectively, along with the experimental conditions and the standard states used for Pb and PbO.

Table 2.8.1: Activity coefficients of lead in copper and lead oxide in iron silicate slag extracted from literature at various conditions

Reference	Temperature (°C)	Oxygen Partial Pressure (atm.)	Standard State of Pb/PbO	Activity Coefficient $[\gamma^{o}_{Pb}]$	Activity Coefficient (γ_{PbO})
Takeda, Ishiwata & Yazawa (1984)	1250	10^{-7}	Liquid /Liquid	4.8	0.4 ± 0.04
Kashima, Eguchi & Yazawa (1978)	1300	10^{-7}	Liquid /Liquid	4.8	0.25
Yazawa (1980)	1300	10^{-7}	Liquid /Liquid	4.8	0.3
Takeda, Ishiwata & Yazawa (1983)	1250	10^{-7}	Liquid /Liquid	4.8	0.4
Kim & Sohn (1998)	1250	10^{-7}	Liquid /Liquid	4.8	0.21 ± 0.06
Kudo, Jak, Hayes, Yamaguchi and Takeda (2000)	1300	10^{-7}	Liquid /Liquid	4.8	0.4 ± 0.2

Table 2.8.2: Activity coefficients of lead in copper and lead oxide in calcium ferrite slag extracted from literature at various conditions

Reference	Temperature (^oC)	Oxygen Partial Pressure (atm.)	Standard State of Pb/PbO	Activity Coefficient [γ^o_{Pb}]	Activity Coefficient (γ_{PbO})
Takeda, Ishiwata & Yazawa (1984)	1250	10^{-6}	Liquid /Liquid	4.8	3.0 ± 0.02
Eerola, Jylha & Taskinen (1984)	1250	10^{-6}	Liquid /Liquid	4.7	1.7 ± 0.6
Takeda, Ishiwata & Yazawa (1983)	1250	10^{-6}	Liquid /Liquid	4.8	3.2
Acuna & Yawaza (1987)	1300	10^{-6}	Liquid /Liquid	4.8	2.94
Kim & Sohn (1991)	1250	10^{-6}	Liquid /Liquid	4.8	3.2
Kudo, Jak, Hayes, Yamaguchi and Takeda (2000)	1300	10^{-11}	Liquid /Liquid	4.8	1.7 ± 0.3

Both Takeda *et al.* (1984) and Kim and Sohn (1998) studied the effects of oxygen partial pressure on the activity coefficient of lead oxide in iron silicate slag. They found that over the oxygen partial pressure range of $10^{-11} – 10^{-7}$ atm., the activity coefficient of PbO(l) in the silicate slag was independent of oxygen partial pressure, as shown in Figure 2.8.1 for Takeda *et al.*'s (1984) findings. Takeda *et al.* (1984) calculated $\gamma_{PbO(l)}$ in iron silicate slag to be a constant value of 0.4±0.04 whilst Kim and Sohn (1998) found $\gamma_{PbO(l)}$ to be a constant value of 0.21±0.06. The difference in the activity coefficient values determined by Takeda *et al.* (1984) and Kim and Sohn (1998) can be accounted for by possible errors in experimental and analytical techniques. The errors encountered during experiments and analysis affect the accuracy of the distribution and activity coefficient data. Possible sources of error during experiments include accurate measuring of temperature and oxygen partial pressure, possible cross contamination of the slag and metal samples during phase separation for analysis as well as the error in the analytical technique used for chemical analysis. As evident in Equation 2.8.2, the activity coefficient of MO_v is a function of K (i.e. temperature), oxygen partial pressure and the distribution ratio. The error in the temperature and oxygen partial pressure measurements, affects the accuracy of the distribution ratio. Distribution equilibrium of an element in a slag-metal system varies according to the conditions at which the experiments are conducted. Thus in order to ensure equilibrium is attained at the correct conditions, it is vital to accurately measure the temperature and oxygen partial pressure during experiments. Poor phase separation can result in cross contamination of the copper with slag or vice versa

which could only be avoided using EDAX analysis rather than chemical analysis, which was used by the present sets of authors. The error the temperature measurements also impact the accuracy of the equilibrium constant, used in activity coefficient calculations, indicating that not only are calculations sensitivity to experimental data, they are also highly sensitive to the choice of thermodynamic data. However both sets of authors fail to mention any potential causes for the uncertainties in their data.

Takeda *et al.* (1984) also studied the effects of oxygen partial pressure over the range of 10^{-11}-10^{-6} atm. on the activity coefficient of PbO(l) in calcium ferrite slag and found $\gamma_{PbO(l)}$ to be a constant value of 3.0±0.02, as also shown in Figure 2.8.1. Takeda and co-authors (1984) were the only investigators to study the relationship between $\gamma_{PbO(l)}$ and oxygen partial pressure for calcium ferrite slag.

Many authors including, Yazawa *et al.* (1983), Acuna and Yazawa (1987), Kudo *et al.* (2000), Eerola *et al.* (1984), Kim and Sohn (1991) and Kashima *et al.* (1978), have assumed [$\gamma^{o}_{Pb(l)}$] and ($\gamma_{PbO(l)}$) to be constant when studying the relationship between log $L_M^{s/m}$ and log p_{O2} for lead for both the silicate and ferrite slags. This assumption has been validated by Takeda *et al.* (1984) and Kim and Sohn (1998).

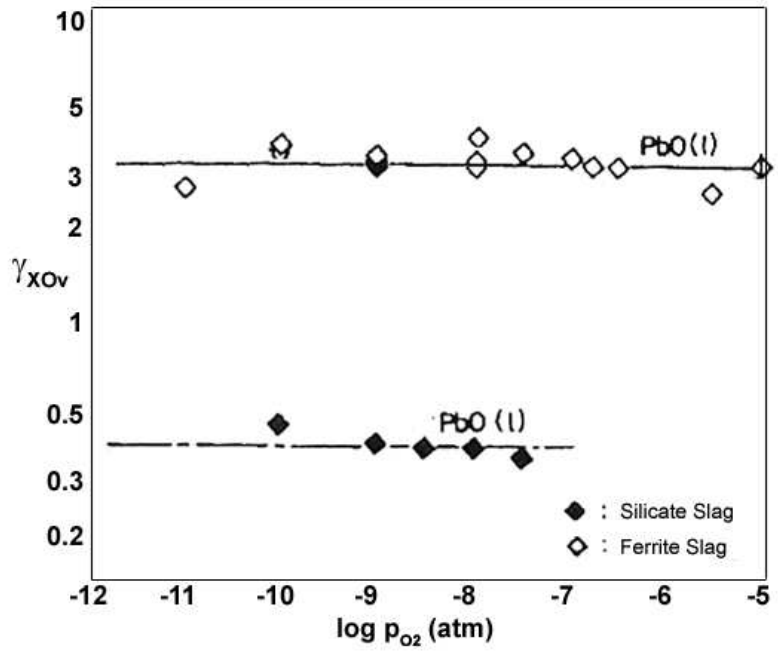

Figure 2.8.1: Relationship between oxygen partial pressure and the activity coefficient of PbO in both iron silicate and calcium ferrite slags and copper at 1250°C (Takeda, Ishiwata and Yazawa, 1984)

The effects of temperature in the range of 1200-1300°C on the activity coefficient of PbO(l) in iron silicate slag has been studied by Kudo *et al.* (2000) at iron saturation (i.e. at very low oxygen partial pressures). The authors found that temperature did not significantly affect the activity coefficient values of PbO(l) and found $\gamma_{PbO(l)}$ to be 0.4±0.2. Kudo *et al.*'s (2000) findings are in agreement with Takeda *et al.* (1984) who also determined that temperature in the range of 1200-1300°C does not significantly effect $\gamma_{PbO(l)}$ in iron silicate slag. The relationship between $\gamma_{PbO(l)}$ in iron silicate slag and temperature as derived from Takeda *et al.*'s (1984) data is given by Equation 2.8.5. Takeda and co-authors (1984) found $\gamma_{PbO(l)}$ to be 0.4±0.02 in the silicate slag within the same temperature range. The values calculated by both sets of authors are in excellent agreement.

$$\gamma_{PbO} = e^{-1392/T(K)} \quad \textbf{… Iron Silicate Slag} \qquad \textbf{Equation 2.8.5}$$

Both Kudo *et al.* (2000) and Takeda *et al.* (1984) also studied the effects of temperature on the activity coefficient of PbO(l) in calcium ferrite slag. The relationship between $\gamma_{PbO(l)}$ and temperature as derived from Takeda *et al.*'s (1984) data is given by Equation 2.8.6 for calcium ferrite slag. Once again, both sets of authors agree that temperature in the range of 1200-1300°C does not significantly affect the activity coefficient values of PbO(l) in the ferrite slag. Kudo and co-authors (2000) calculated $\gamma_{PbO(l)}$ to be 1.7±0.3 in calcium ferrite slag whilst Takeda *et al.* (1984) found $\gamma_{PbO(l)}$ to be 3.0±0.1 within the temperature range of 1200-1300°C. The difference in the activity coefficient values determined by the authors can be attributed to possible experimental and analytical errors as mentioned previously.

$$\gamma_{PbO} = e^{1771.48/T(K)} \quad \textbf{… Calcium Ferrite Slag} \qquad \textbf{Equation 2.8.6}$$

Takeda *et al.* (1984) and Eerola *et al.* (1984) investigated the effects of temperature on the activity coefficient of Pb(l) in a copper-lead system. The authors found that changes in temperature do not have a significant impact on the activity coefficient of lead in copper. Takeda and co-authors (1984) found $\gamma^{o}_{Pb(l)}$ to be a 4.8 at 1250°C and 4.4 at 1300°C. Eerola and co-authors (1984) found $\gamma^{o}_{Pb(l)}$ to be 4.9 at 1250°C and 4.7 at 1300°C. The activity coefficient values of lead in copper determined by both sets of authors are in good agreement and within experimental error.

It has been seen that the effects of temperature and oxygen partial pressure on the activity coefficients of lead in copper and lead oxide in both the silicate and ferrite slags are small. The activity coefficient data extracted from literature can therefore be used to estimate the distribution of lead between iron silicate slag and copper metal using Equation 2.8.3 and between calcium ferrite slag and copper using Equation 2.8.4. Listed in Table 2.8.3 are the distribution ratios of lead between the silicate slag and copper at 1300°C and an oxygen partial pressure of 10^{-6} atm. calculated using the activity coefficient data in Table 2.8.1. The distribution ratios of lead between calcium ferrite slag and copper were calculated using the activity coefficient data in Table 2.8.2 and are also shown in Table 2.8.3.

Table 2.8.3: Calculated distribution ratios of lead between iron silicate slag and copper metal as well as calcium ferrite slag and copper metal at 1300°C and an oxygen partial pressure of 10^{-6} atm.

Reference	Distribution Coefficient ($L_{Pb}^{s/m}$)	
	Calcium Ferrite Slag	**Iron Silicate Slag**
Takeda, Ishiwata & Yazawa (1984)	0.42 ± 0.003	3.2 ± 0.3
Takeda, Ishiwata & Yazawa (1983)	0.39	3.2
Kudo, Jak, Hayes, Yamaguchi and Takeda (2000)	0.76 ± 0.14	3.9 ± 2.2
Kashima, Eguchi & Yazawa (1978)	-	5.2
Kim & Sohn (1998)	-	6.5 ± 1.9
Yazawa (1980)	-	4.3
Eerola, Jylha & Taskinen (1984)	0.8 ± 0.3	-
Acuna & Yawaza (1987)	0.43	-
Kim & Sohn (1991)	0.39	-

In the case of iron silicate slag in Table 2.8.3, there is a significant variation in the distribution data between most literature shown. The distribution ratio of lead between iron silicate slag and copper varies between 3.2 and 6.5, suggesting that between 76-87% of lead distributes to the slag phase, which is a large range of lead distribution. The distribution ratio of lead between the silicate slag and copper is taken as being 4.4 ± 1.3 as this is best compromise between all data reported. Similarly, the values of $\gamma^{o}_{Pb(l)}$ and $\gamma_{PbO(l)}$ were taken as

4.8 ± 0.02 and 0.3 ± 0.1, respectively, as these values best agree with most of the data in Table 2.8.1, within the quoted error. Of the six studies on the distribution ratio of lead in calcium ferrite slag, four studies, with the exception of Kudo *et al.* (2000) and Eerola *et al.* (1984), agree that the distribution ratio of lead between the ferrite slag and copper is close to 0.4 ± 0.02 and $\gamma^{o}_{Pb(l)}$ and $\gamma_{PbO(l)}$ are 4.8 ± 0.02 and 3.1 ± 0.8, respectively. The discrepancy in the distribution and activity coefficient data could be a result of errors encountered during experiments and chemical analysis, as mentioned previously. When comparing the distribution ratio of lead and $\gamma_{PbO(l)}$ in the silicate and ferrite slags, the ratio in iron silicate slag is an order of magnitude greater than that in calcium ferrite slag and $\gamma_{PbO(l)}$ is an order of magnitude smaller. The distribution of lead between slag and copper highly favours the slag phase when iron silicate slag is used whilst favouring the metal phase in case of calcium ferrite slag. This behaviour is in accord with the acid-base theory of slags, discussed in detail in Section 2.7, which states that the distribution of basic oxides such as lead oxide will be higher in the acidic silicate slag than in the basic ferrite slag.

2.8.2 Distribution of Antimony between Slag and Copper Metal

According to Yazawa (1980), Jimbo *et al.* (1984), Takeda *et al.* (1984) and Kashima *et al.* (1978), at low oxygen partial pressures antimony dissolves in the silicate slag in both the metallic (Sb^{o}) and oxidic states ($SbO_{1.5}$), however, at high oxygen partial pressures, antimony oxide as $SbO_{1.5}$, is the predominating form. The distribution of antimony between copper and iron silicate slag as a function of oxygen partial pressure as extracted from Yazawa's (1980) literature is shown in Figure 2.8.2, where at lower oxygen partial pressures (below 10^{-10} atm.), the distribution ratio of antimony between copper and the silicate slag is independent of oxygen partial pressure (slope of zero), suggesting metallic dissolution, whilst above about 10^{-9} atm. the slope of the line is approximately 0.75, indicating that antimony dissolves in slag as $SbO_{1.5}$. Between 10^{-10} and 10^{-9} atm. both metallic and oxidic antimony exists in the slag.

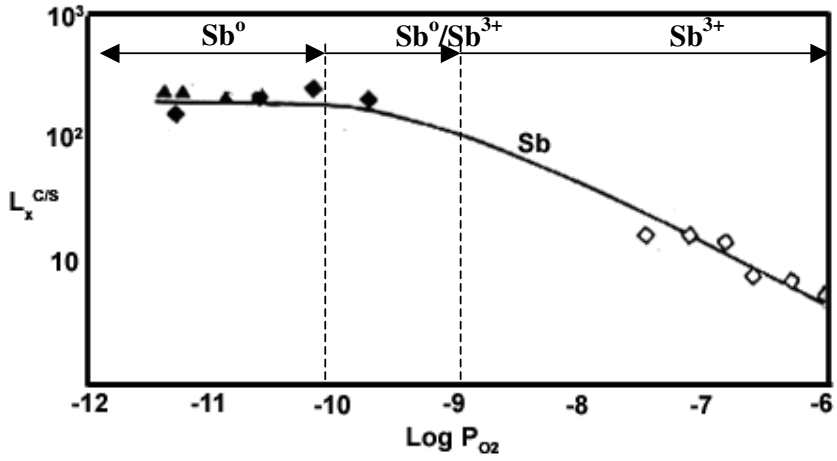

Figure 2.8.2: Distribution of antimony between copper and iron silicate slag as a function of oxygen partial pressure at 1250°C (Yazawa, 1980).

Kim and Sohn (1998) also studied the distribution of antimony between copper and iron silicate slag, and found that in the oxygen partial pressure range of 10^{-12} to 10^{-7} atm. and at 1250°C, the distribution of antimony between copper and iron silicate slag was independent of oxygen partial pressure over the entire oxygen partial pressure range, supporting metallic dissolution of antimony in slag. When observing their data as presented in Figure 2.8.3, it is apparent that it is so scattered that to make any deduction from the data is impossible. The scatter may be due to cross-contamination of the copper with slag and/or vice versa possibly as a result of poor phase separation between copper and slag.

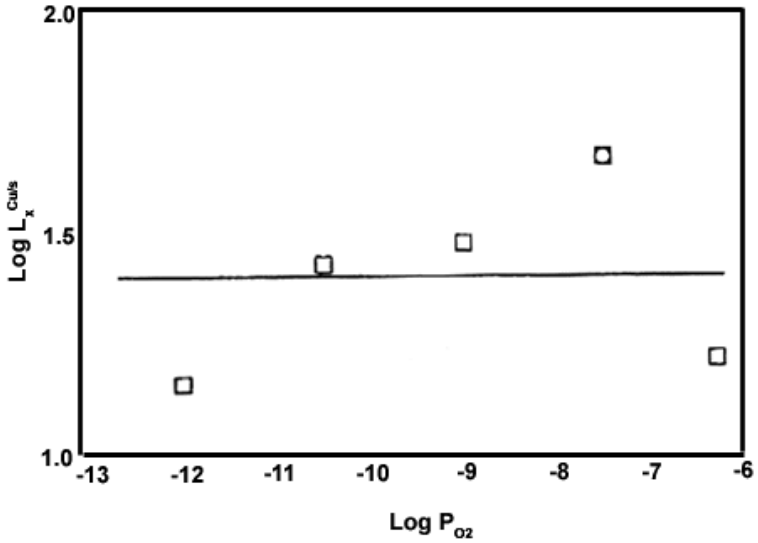

Figure 2.8.3: Distribution of antimony in copper and iron silicate slag as a function of oxygen partial pressure at 1250°C (Kim and Sohn, 1998).

Thus as determined by most literature, at converting conditions, antimony dissolves in iron silicate slag as $SbO_{1.5}$, according to the equilibrium Reaction 2.8.7. The thermodynamic data for Reaction 2.8.7 was taken from the HSC Chemistry for Windows database.

$$Sb_{(l)} + \frac{3}{4}O_{2(g)} \rightarrow SbO_{1.5(l)}$$
$$\Delta G^{o}_{1300oC} = -168.863kJ \qquad \textbf{Equation 2.8.7}$$
$$K_{1300oC} = 4.049 \times 10^{5}$$

Takeda *et al.* (1984), Acuna *et al.* (1987), Eerola *et al.* (1984) and Yazawa *et al.* (1983) studied the distribution of antimony between calcium ferrite slag and copper metal at 1250°C and oxygen partial pressure ranging between 10^{-11} and 10^{-6} atm. and found that antimony dissolves in calcium ferrite slag as $SbO_{1.5}$, according to Reaction 2.8.7 for the entire oxygen partial pressure range as is evident in Figure 2.8.4, where a linear relationship between log $L_{Sb}^{s/m}$ and log p_{O2} exists with a slope of 0.75. Calcium ferrite slag, which has a high activity of basic CaO, has strong interactions with the acidic $SbO_{1.5}$, such that in calcium ferrite slag the activity coefficient of $SbO_{1.5}$ is relatively small and the ferrite slag is able to stabilise the antimony oxide at low oxygen partial pressures.

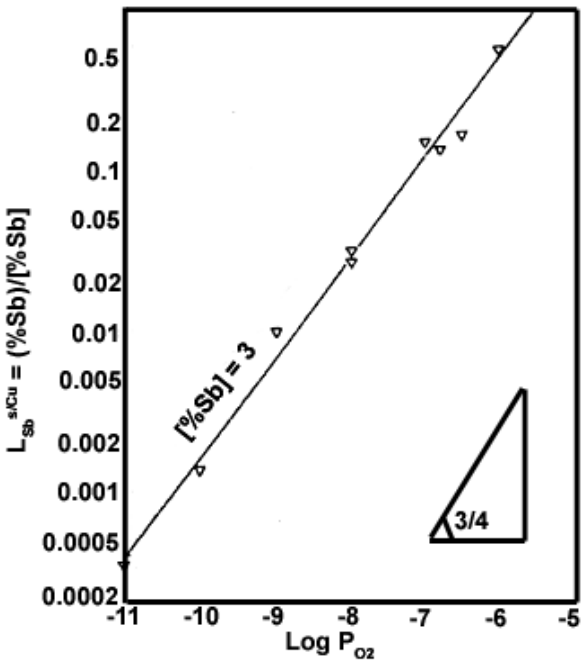

Figure 2.8.4: Distribution of antimony in calcium ferrite slag and copper as a function of oxygen partial pressure at 1250°C (Takeda, Ishiwata and Yazawa, 1984).

Similar to the case of lead distribution, literature on the distribution of antimony between the silicate slag and copper and between calcium ferrite slag and copper is not at the conditions required for comparison (1300°C and oxygen partial pressure of 10^{-6} atm.). Using the assumptions made to simplify Equation 2.8.2, antimony distribution between iron silicate slag and copper can be calculated using Equation 2.8.8 and antimony distribution between calcium ferrite slag and copper can be calculated using Equation 2.8.9.

$$L_{Sb}^{s/m} = \frac{12.07[\gamma^{o}_{Sb}]}{(\gamma_{SbO1.5})} \quad \textbf{… Iron Silicate Slag} \qquad \textbf{Equation 2.8.8}$$

$$L_{Sb}^{s/m} = \frac{11.83[\gamma^{o}_{Sb}]}{(\gamma_{SbO1.5})} \quad \textbf{… Calcium Ferrite Slag} \qquad \textbf{Equation 2.8.9}$$

Once again, Equations 2.8.8 and 2.8.9 assume that the activity coefficient of antimony and antimony oxide is not a function of oxygen partial pressure and temperature. The original activity coefficient data extracted from literature for both iron silicate and calcium ferrite slags is shown in Tables 2.8.4 and 2.8.5, respectively, along with the experimental conditions and the standard states used for Sb and $SbO_{1.5}$.

Table 2.8.4: Activity coefficients of antimony in copper and antimony oxide in iron silicate slag extracted from literature at various conditions

Reference	Temperature (°C)	Oxygen Partial Pressure (atm.)	Standard State of $Sb/SbO_{1.5}$	Activity Coefficient $[\gamma^{o}_{Sb}]$	Activity Coefficient $(\gamma_{SbO1.5})$
Takeda, Ishiwata & Yazawa (1984)	1250	10^{-7}	Liquid /Liquid	0.03	3
Kashima, Eguchi & Yazawa (1978)	1300	10^{-7}	Liquid /Liquid	0.02	0.4
Takeda, Ishiwata & Yazawa (1983)	1250	10^{-7}	Liquid /Liquid	0.03	2.0 ± 0.5
Kim & Sohn (1991)	1250	10^{-7}	Liquid /Liquid	0.02	1.2
Jimbo, Goto & Ogawa (1984)	1250	10^{-7}	Liquid /Liquid	0.03	3.3

Table 2.8.5: Activity coefficients of antimony in copper and antimony oxide in calcium ferrite slag extracted from literature at various conditions

Reference	Temperature (^oC)	Oxygen Partial Pressure (atm.)	Standard State of $Sb/SbO_{1.5}$	Activity Coefficient $[\gamma^o_{Sb}]$	Activity Coefficient ($\gamma_{SbO1.5}$)
Takeda, Ishiwata & Yazawa (1984)	1250	10^{-6}	Liquid /Liquid	0.03	0.58
Eerola, Jylha & Taskinen (1984)	1250	10^{-6}	Liquid /Liquid	0.02	0.17 ± 0.05
Takeda, Ishiwata & Yazawa (1983)	1250	10^{-6}	Liquid /Liquid	0.03	0.6 ± 0.03
Acuna & Yawaza (1987)	1300	10^{-6}	Liquid /Liquid	0.03	0.57
Kim & Sohn (1991)	1250	10^{-6}	Liquid /Liquid	0.03	0.6

The effects of oxygen partial pressure on the activity coefficient of antimony oxide in the silicate slag have not been studied by many authors, however Kashima *et al.* (1978), Yazawa *et al.* (1983) and Jimbo *et al.* (1984), assumed $[\gamma^o_{Sb(l)}]$ and $(\gamma_{SbO1.5(l)})$ to be constant when studying the relationship between log $L_M^{s/m}$ and log p_{O2} for antimony. This assumption has been justified by Takeda *et al.* (1984) who found that in the oxygen partial pressure range of 10^{-11} to 10^{-7} atm., the activity coefficient of $SbO_{1.5}$(l) in the silicate slag remains constant at 2.0±0.5. Takeda *et al.* (1984) have also studied the effects of oxygen partial pressure on the activity coefficient of antimony oxide in calcium ferrite slag; however the authors found that the activity coefficient of antimony oxide in calcium ferrite slag was dependant on the oxygen partial pressure, as shown in Figure 2.8.5. Figure 2.8.5 assumes that antimony is present in slag as Sb^{3+} over the oxygen partial pressure range of 10^{-11} to 10^{-6} atm.

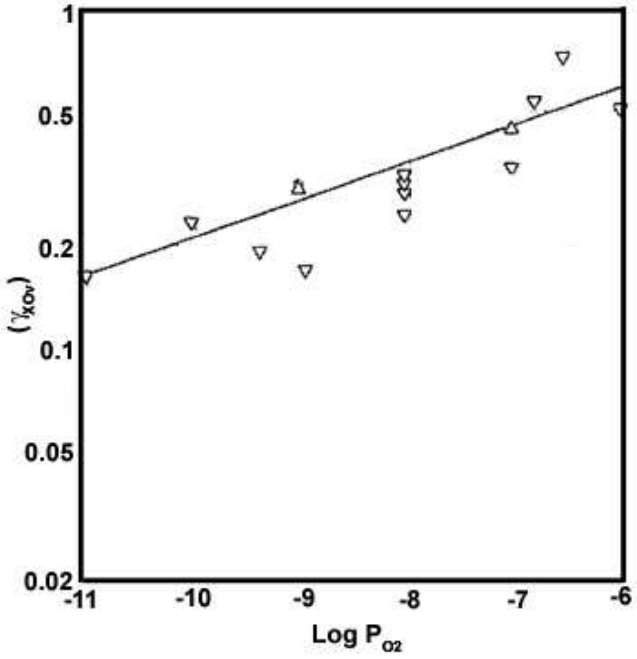

Figure 2.8.5: Activity coefficient of antimony oxide in calcium ferrite slag as a function of oxygen partial pressure at 1250°C (Takeda, Ishiwata and Yazawa, 1984).

Observations of Figure 2.8.5 clearly indicate that there is large scatter in the data. The activity coefficient data in Figure 2.8.5 was calculated using the distribution data in Figure 2.8.4 and Equation 2.8.2. Thus its accuracy is largely a function of the accuracy in the distribution data, the equilibrium constant, K, the measured oxygen partial pressure and the activity coefficient of antimony in metal. Accordingly it is possible that the relationship observed in Figure 2.8.5 is a result of experimental errors and uncertainties. Takeda and co-authors (1984) agree that the relationship predicted from Figure 2.8.5 is contrary to expectations and likely to be invalid. However, if there exists interactions between Fe^{2+} and/or Fe^{3+} and $SbO_{1.5}$ in the slag, then the $\gamma_{SbO1.5(l)}$ in the ferrite slag could be a function of oxygen partial pressure. As discussed in Section 2.7.3, FeO is considered a neutral oxide and thus its interactions with acidic $SbO_{1.5}$ are highly unlikely. Nonetheless it is still possible that there are interactions between $SbO_{1.5}$ and $FeO_{1.5}$, which is the dominating iron oxide in the ferrite slag (Section 2.3). As shown in Figure 2.3.1, over the oxygen partial pressure range of 10^{-11} to 10^{-6} atm., the change in Fe^{3+}/Fe^{2+} ratio in the calcium ferrite slag is quite significant and if $SbO_{1.5}$ interacts with Fe^{3+} in the ferrite slag, a relationship between oxygen partial pressure and $\gamma_{SbO1.5(l)}$ would be expected. Due to the lack of literature available on the FeO-$FeO_{1.5}$-$SbO_{1.5}$ system this possibility cannot be validated.

Contrary to Takeda and co-author's (1984) findings, Eerola *et al.* (1984) found that the activity coefficient of $SbO_{1.5}(l)$ in the ferrite slag was independent of oxygen partial pressure and calculated a constant value of 0.17±0.05 between oxygen partial pressures of 10^{-8} to 10^{-6} atm.

Shown in Figure 2.8.6 is the distribution data calculated by Eerola *et al.* (1984) along with the data from Takeda *et al.* (1984).

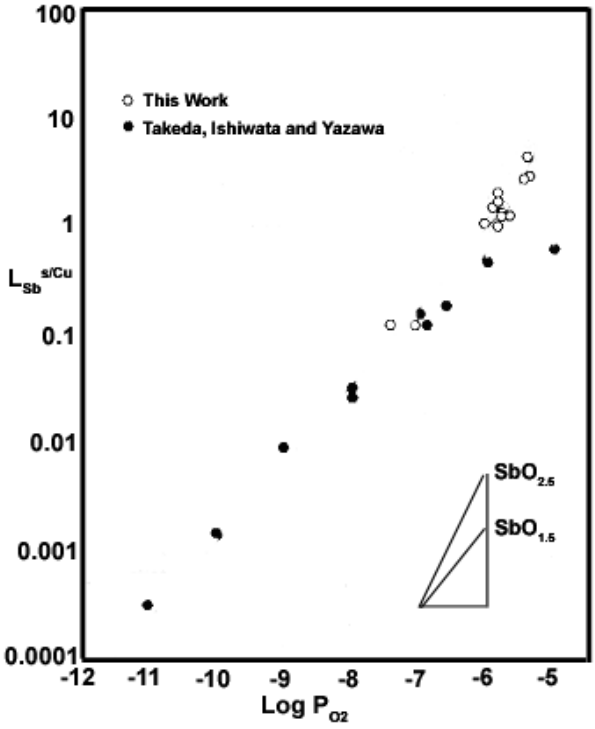

Figure 2.8.6: Distribution of antimony in calcium ferrite slag and copper as a function of oxygen partial pressure at 1250°C (Eerola, Jylha and Taskinen, 1984).

The distribution ratios measured by both authors are very similar at similar conditions, such that, at an oxygen partial pressure of 10^{-7} atm. and 1250°C, Takeda *et al.* (1984) found the distribution ratio of antimony between slag and metal to be 0.13 and Eerola *et al.* (1984) found it to be 0.12. However, Takeda and co-authors (1984) calculated the activity coefficient of antimony oxide in slag to be 0.40 whilst Eerola *et al.* (1984) calculated a value of 0.21. Such a difference in values is largely a result of the different thermodynamic data (i.e. ΔG^o and K) the authors used to calculated ($\gamma_{SbO1.5}$), which is shown in Table 2.8.6. Both authors calculated $\gamma_{SbO1.5}$ using Equation 2.8.2.

Table 2.8.6: Comparison of the thermodynamic and experiment data used by Eerola *et al.* (1984) and Takeda *et al.* (1984) to calculate the activity coefficient of antimony oxide in calcium ferrite slag.

	Eerola *et al.* (1984)	**Takeda *et al.* (1984)**
Standard State	Sb(l) & $SbO_{1.5}$(l)	Sb(l) & $SbO_{1.5}$(l)
ΔG^o	-347 746 + 125.2T(K)	-334 820 + 114.23T(K)
K	2.44×10^5	3.29×10^5
$[\gamma^o_{Sb}]$	0.02	0.03
$L_{Sb}^{s/m}$	0.12	0.13
p_{O2}	10^{-7} atm.	10^{-7} atm.
Temperature	1250°C	1250°C

If however the same thermodynamic data is used to calculate ($\gamma_{SbO1.5}$), keeping all other conditions and data constant, then ($\gamma_{SbO1.5}$) calculated from Eerola and co-author's (1984) distribution data is 0.21 (K = 2.44×10^5) and 0.28 (K = 3.29×10^5) and by Takeda *et al.* (1984) is 0.29 (K = 2.44×10^5) and 0.40 (K = 3.29×10^5). Taking into account the errors experienced during experimentation, these activity coefficient values are in very good agreement. It is clearly evident from these calculations, that besides having the sensitivity to experimental data, the antimony oxide activity coefficient calculations are highly sensitive to the choice of thermodynamic data.

The effect of temperature on the activity coefficient of antimony oxide in both iron silicate and calcium ferrite slags has only been studied by Takeda *et al.* (1984). They found that temperature has little effect on the on the activity coefficient of $SbO_{1.5}$(l) in both slags. The authors determined that $\gamma_{SbO1.5(l)}$ is 2.0±0.06 for iron silicate slag and 0.6±0.03 for calcium ferrite slag within the temperature range of 1200-1300°C.

The relationships between temperature and the activity coefficient of antimony in copper are given in Table 2.8.7 from various sources. Azakami and Yazawa (1967) found the activity coefficient of Sb(l) in copper to be 0.02±0.006 over the temperature range 1200-1300°C. Eerola and co-authors (1984) found $\gamma^o_{Sb(l)}$ to be 0.02±0.003 within the same temperature range. Both Eerola *et al.* (1984) and Azakami and Yazawa (1967) established that the effects of temperature on the activity coefficient of antimony in copper are minor.

Table 2.8.7: Correlations between activity coefficient of antimony and temperature

Reference	Activity Coefficient Relationship [γ^{o}_{Sb}]
Azakami and Yazawa (1967)	$10^{(-4560/T(K))+1.24}$
Eerola, Jylha & Taskinen (1984)	$e^{-6390/T(K)}$

From the above discussion it is concluded that temperature and oxygen partial pressure have no significant effects on the activity coefficients of antimony oxide in both iron silicate and calcium ferrite slags, nor on the activity coefficient of antimony in copper. Thus using literature activity coefficient data in Table 2.8.4 and Equation 2.8.8, distribution ratios of antimony between iron silicate slag and copper, as shown in Table 2.8.8, have been calculated at the standardised conditions of 1300°C and an oxygen partial pressure of 10^{-6} atm. In the case of calcium ferrite slag, distribution ratios of antimony between the ferrite slag and copper were calculated using the activity coefficient data in Table 2.8.5 and Equation 2.8.9 and the results are also illustrated in Table 2.8.8.

Of the seven studies conducted on the distribution of antimony between the silicate slag and copper, with the exception of Kashima *et al.* (1978), all other studies agree that the distribution ratio is 0.15 ± 0.04 and $\gamma^{o}_{Sb(l)}$ and $\gamma_{SbO1.5(l)}$ are 0.03 ± 0.01 and 2.4 ± 0.9, respectively. Similarly, for calcium ferrite slag, all sets of authors, with the exception of Eerola *et al.* (1984), agree that the distribution ratio of antimony between calcium ferrite slag and copper is 0.61 ± 0.03 and $\gamma^{o}_{Sb(l)}$ and $\gamma_{SbO1.5(l)}$ are 0.03 ± 0.01 and 0.5 ± 0.2, respectively. The discrepancy in the distribution data by Kashima *et al.* (1978) and Eerola *et al.* (1984) could be a result of errors encountered during experiments and chemical analysis. One such factor which could cause errors in the data is the poor separation of the metal and slag phases for analysis following experiments, as discussed previously, which could be avoided using EDAX analysis, rather than chemical analysis, which was used by the present sets of authors. The distribution of antimony to the slag phase is higher when calcium ferrite slag is used rather than iron silicate slag. Such behaviour is in accord with the predicted behaviour of acidic oxides detailed in Section 2.7 and illustrates that antimony removal is superior when using basic ferrite slag in comparison to the acidic silicate slag.

Table 2.8.8: Calculated distribution ratios of antimony between iron silicate slag and copper metal and between calcium ferrite slag and copper at 1300°C and oxygen partial pressure of 10^{-6} atm.

Reference	Distribution Coefficient ($L_{Sb}^{s/m}$)	
	Calcium Ferrite Slag	**Iron Silicate Slag**
Takeda, Ishiwata & Yazawa (1984)	0.61	0.12
Yazawa, Nakazawa & Takeda (1983)	0.65	0.16
Takeda, Ishiwata & Yazawa (1983)	0.59 ± 0.03	0.19 ± 0.05
Kim & Sohn (1991)	0.59	0.2
Jimbo, Goto & Ogawa (1984)	-	0.11
Kashima, Eguchi & Yazawa (1978)	-	0.60
Yazawa (1980)	-	0.14
Eerola, Jylha & Taskinen (1984)	1.48 ± 0.5	-
Acuna & Yawaza (1987)	0.62	-

2.8.3 Distribution of Nickel between Slag and Copper Metal

Takeda *et al.* (1984), Yazawa (1980), Wang *et al.* (1973), Kashima *et al.* (1978), and Grimsey and Biswas (1976) have all found that nickel dissolves in iron silicate slag as NiO above an oxygen partial pressure of approximately 10^{-9} atm. as per Reaction 2.8.10. The thermodynamic data for Equation 2.8.10 was taken from HSC Chemistry for Windows database.

$$Ni_{(l)} + \frac{1}{2}O_2(g) \rightarrow NiO_{(l)}$$
$$\Delta G^o_{1300oC} = -99.370kJ \qquad \textbf{Equation 2.8.10}$$
$$K_{1300oC} = 1.994 \times 10^3$$

Below an oxygen partial pressure of 10^{-9} atm., Yazawa (1980) and Grimsey and Biswas (1976) suggested that nickel is present in slag as both Ni^o and Ni^{2+} and as the oxygen

partial pressure increases, the concentration of nickel oxide in slag also increases with the oxide being the only species at converting conditions. This behaviour is shown in Figure 2.8.7 from which Yazawa (1980) predicted that below the oxygen partial pressure of $10^{-11.5}$ atm., the slope of log $L_x^{c/s}$ vs. log p_{O2} is approximately horizontal, inferring metallic dissolution and above 10^{-9} atm., the slope of the line is 0.5. However when observing Figure 2.8.7, a large scatter is evident below an oxygen partial pressure of 10^{-11} atm., with only two data points suggesting a horizontal relationship between log p_{O2} and log $L_x^{c/s}$ and thus the presence of nickel metal in slag. If the two 'horizontal data points' are ignored, the remaining data fits on the straight line which suggests nickel in slag is present as Ni^{2+}. Hence, it is possible that this indication of the existence of Ni^o in slag is a result of errors in the measurements and experimental uncertainties.

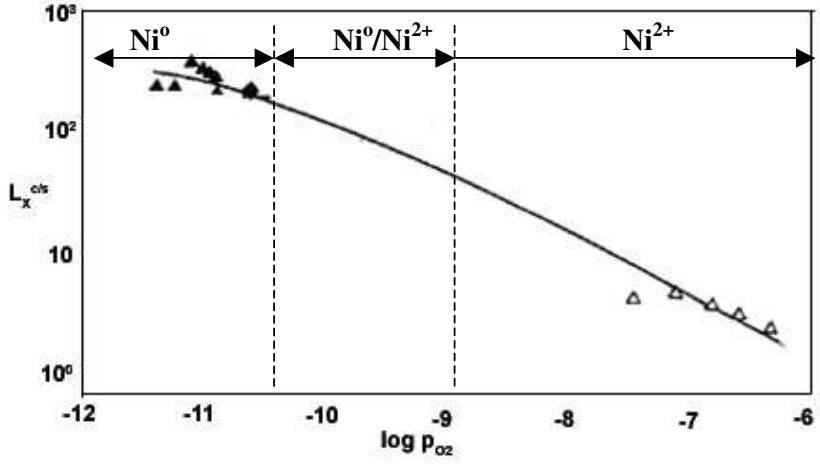

Figure 2.8.7: Distribution of nickel between iron silicate slag and copper as a function of oxygen partial pressure at 1250°C (Yazawa, 1980).

Grimsey and Biswas (1976) discussed the presence of nickel metal in slag at low oxygen partial pressures (below 10^{-9} atm.) based on the relationship shown in Figure 2.8.8. The equilibrium constant K, for reaction 2.8.10 is given as per below (Equation 2.8.11).

$$K = \frac{a_{NiO(l)}}{a_{Ni(l)} p_{O2}^{1/2}} = \frac{\gamma_{NiO} N_{NiO}}{a_{Ni(l)} p_{O2}^{1/2}}$$

Equation 2.8.11

Since $2CO + O_2 = 2CO_2$, p_{O2} is proportional to $(p_{CO}/p_{CO2})^2$

Assuming wt% Ni in slag is approximately proportional to N_{NiO} in slag and that Henry's law is obeyed over the entire N_{NiO} range studied, then Equation 2.8.11 is simplified to Equation 2.8.12.

$$K.\frac{p_{CO2}}{p_{CO}} = \frac{(Ni\ wt\%)}{a_{Ni(l)}} \qquad \textbf{Equation 2.8.12}$$

According to Equation 2.8.12, if all nickel is present in slag as NiO, then its solubility is a function of the oxygen partial pressure (i.e. p_{CO2}/p_{CO} ratio) and when $p_{CO2}/p_{CO} = 0$, then the solubility of nickel is slag should also be zero. Thus the plot of (Ni wt%)/$a_{Ni(l)}$ versus p_{CO2}/p_{CO} (Figure 2.8.8) should pass through the ordinate. If there is a positive intercept on the ordinate, then the presence of nickel metal in slag is indicated. The dashed line in Figure 2.8.8, which has a positive intercept on the ordinate, is the relationship established by Grimsey and Biswas (1976). However, as is evidenced from the comparison of the solid line, which passes through the origin and thus concludes nickel in slag is present only as nickel oxide, line through the origin fits the data points just as well as the line drawn by Grimsey and Biswas (1976). Thus, given the errors on the slope of the straight line as a result of scatter in the data, especially at high p_{CO2}/p_{CO}, the presence of Ni^o in slag is not proven conclusively.

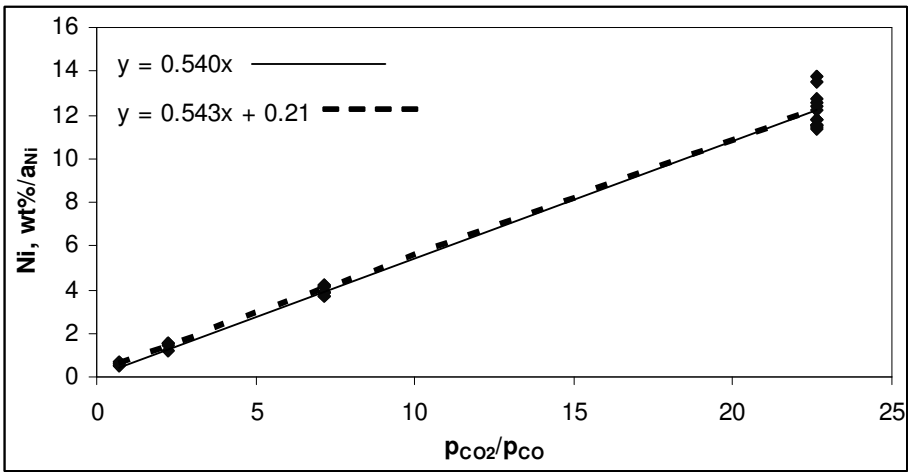

Figure 2.8.8: Relationship between (Ni wt%)/$a_{Ni(l)}$ and p_{CO2}/p_{CO} ratio (Grimsey and Biswas, 1976)

There exist very few studies on the distribution of nickel between calcium ferrite slag and copper metal. Takeda *et al.* (1984) and Eerola *et al.* (1984), agree that nickel dissolves in the slag as nickel oxide, NiO, over the oxygen partial pressure range of 10^{-11} to 10^{-6} atm., as

per Reaction 2.8.10 and Figure 2.8.9, where the slope of log $L_{Ni}^{s/m}$ and log p_{O2} supports that nickel is present in calcium ferrite slag as Ni^{2+}.

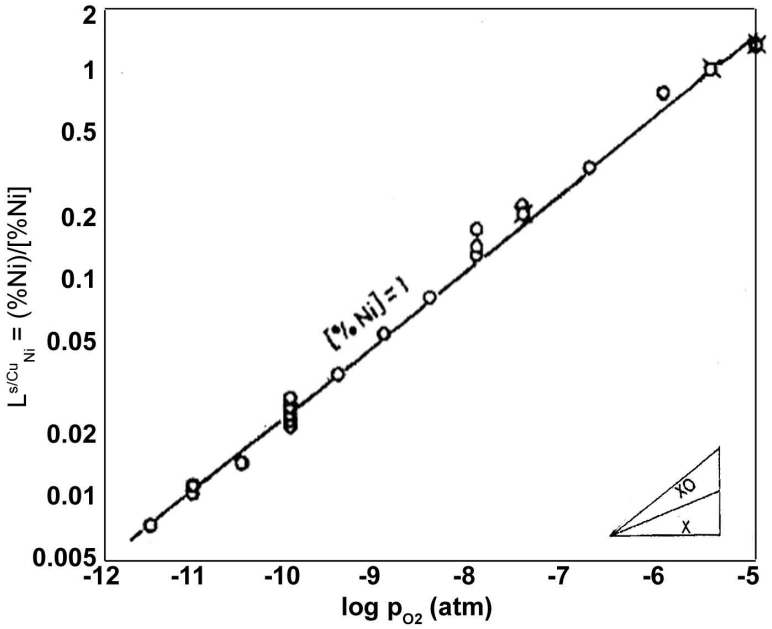

Figure 2.8.9: Distribution of nickel in calcium ferrite slag and copper as a function of oxygen partial pressure at 1250°C (Takeda, Ishiwata and Yazawa, 1984).

The distribution of nickel between iron silicate slag and copper and between calcium ferrite slag and copper has not always been measured at the desired conditions. Given that nickel dissolves in slag as NiO at converting conditions, the distribution of nickel between iron silicate slag and copper metal can be predicted from Equation 2.8.13 at 1300°C and an oxygen partial pressure of 10^{-6} atm. and from Equation 2.8.14 for calcium ferrite slag at the same conditions. Referring back to the lead distribution section, Equations 2.8.13 and 2.8.14 are derived from Equation 2.8.2.

$$L_{Ni}^{s/m} = \frac{1.88[\gamma^{o}_{Ni}]}{(\gamma_{NiO})} \quad \textbf{… Iron Silicate Slag} \qquad \textbf{Equation 2.8.13}$$

$$L_{Ni}^{s/m} = \frac{1.84[\gamma^{o}_{Ni}]}{(\gamma_{NiO})} \quad \textbf{… Calcium Ferrite Slag} \qquad \textbf{Equation 2.8.14}$$

Equations 2.8.13 and 2.8.14 assume that the activity coefficients of nickel and nickel oxide are not a function of oxygen partial pressure and temperature. The original activity

coefficient data extracted from literature for both iron silicate and calcium ferrite slags is shown in Tables 2.8.9 and 2.8.10, respectively, along with the experimental conditions and standard states used for Ni and NiO.

Table 2.8.9: Activity coefficients of nickel in copper and nickel oxide in iron silicate slag extracted from literature at various conditions

Reference	Temperature (^oC)	Oxygen Partial Pressure (atm.)	Standard State of Ni/NiO	Activity Coefficient [γ^o_{Ni}]	Activity Coefficient (γ_{NiO})
Takeda, Ishiwata & Yazawa (1984)	1250	10^{-7}	Liquid/ Solid	2.2	5
Kashima, Eguchi & Yazawa (1978)	1300	10^{-7}	Liquid /Liquid	2.2	3
Yazawa (1980)	1300	10^{-7}	Liquid /Liquid	2.2	4
Grimsey & Biswas (1976)	1300	10^{-7}	Liquid /Liquid	2.2	2.59 ± 0.23
Wang, Kurtis & Toguri (1973)	1250	10^{-7}	Liquid /Liquid	2.2	3.7 ± 0.84
Holzheid, Palme, Chakraborty (1997)	1300	10^{-7}	Liquid /Liquid	2.47	2.7 ± 0.52

Table 2.8.10: Activity coefficients of nickel in copper and nickel oxide in calcium ferrite slag extracted from literature at various conditions

Reference	Temperature (^oC)	Oxygen Partial Pressure (atm.)	Standard State of Ni/NiO	Activity Coefficient [γ^o_{Ni}]	Activity Coefficient (γ_{NiO})
Takeda, Ishiwata & Yazawa (1984)	1250	10^{-11} - 10^{-6}	Liquid /Solid	2.2	3-12
Eerola, Jylha & Taskinen (1984)	1250	10^{-11} - 10^{-6}	Liquid /Liquid	2.8	1.4 - 4.3

As seen in Tables 2.8.9 and 2.8.10, Takeda *et al.* (1984) assumed the reference standard state of nickel oxide to be solid whilst all other authors have assumed liquid standard state. However, the activity coefficient data needs to be standardised to the same reference standard state before any comparison can be made. The activity coefficient of NiO(l) in iron silicate slag was recalculated for Takeda *et al.* (1984) at the same conditions (i.e. 1250^{o}C and an oxygen partial pressure of 10^{-7} atm) using Equation 2.8.2 and the distribution data, which had to be extrapolated from the graph of log $L_M^{s/m}$ and log p_{O2} as raw data was not provided by the authors. In Equation 2.8.2, the oxygen partial pressure, $L_M^{s/m}$, (n_T), $[N_T]$ and γ^o_{Ni} remain constant, thus simplifying the equation to Equation 2.8.15.

$$L_M^{s/m} = \frac{(6.56\times10^{-4})K}{(\gamma_{MOv})}$$
$$\therefore \gamma_{MOv} = 1.87\times10^{-3}K$$

Equation 2.8.15

The data for the Gibbs free energy of formation of nickel oxide with reference to the liquid standard state at 1250°C was obtained using HSC Chemistry for windows as shown below:

$$NiO(s) = NiO(l)$$
$$\Delta G^o_{1250oC} = \sum \Delta G_{f\ \mathrm{Products}} - \sum \Delta G_{f\ \mathrm{Reactants}}$$
$$\Delta G^o_{1250oC} = \Delta G_{NiO(l)} - \Delta G_{NiO(s)} = -89.25 - (-103.62) = 14.37kJ = 14370J$$

According to Takeda *et al.* (1984) for the NiO(s) formation reaction, the Gibbs free energy of formation is given by Equation 2.8.16.

$$Ni(l) + \frac{1}{2}O_2(g) \rightarrow NiO(s)$$
$$\Delta G^o / J = -249400 + 92.84T(K)$$
$$\Delta G^o_{1250oC} = -1.08\times10^5 J$$

Equation 2.8.16

Thus the recalculated Gibbs free energy of formation of nickel oxide with reference to the liquid standard state is given by Equation 2.8.17.

$$\Delta G^o_{1250oC} = -1.08\times10^5 + 14370$$
$$\Delta G^o_{1250oC} = -9.36\times10^4 J$$

Equation 2.8.17

Thus K = 1627.5 and the activity coefficient of NiO(l) in iron silicate slag was recalculated to be 3.5.

Similar calculations as per above were carried out to recalculate the activity coefficient of NiO(l) in calcium ferrite slag for Takeda *et al.* (1984). As seen in Table 2.8.10, the activity coefficient of nickel oxide is given in the oxygen partial pressure range of 10^{-11} to 10^{-6} atm. The recalculated values were also calculated within this oxygen partial pressure range. From the calculations, it was determined that $\gamma_{NiO(l)}$ in calcium ferrite slag within the oxygen partial pressure range of 10^{-11} to 10^{-6} atm varied between 1.05-4.13. These values are in excellent agreement with Eerola *et al.* (1984).

Many authors, including, Takeda *et al.* (1984), Kashima *et al.* (1978), Wang *et al.* (1973), Holzheid *et al.* (1997) and Yazawa (1980), who have studied the affects of oxygen partial pressure on the distribution ratio of nickel between the silicate slag and copper, have assumed constant (γ_{NiO}) and [γ^{o}_{Ni}], however Grimsey and Biswas (1976) were the only authors to study the relationship between the activity coefficient of NiO(l) and oxygen partial pressure. Grimsey and Biswas (1976) found that at 1300^{o}C and between oxygen partial pressures of 10^{-9} and 10^{-7} atm., the activity coefficient of NiO(l) in iron silicate slag remains constant at 2.6±0.2. The activity coefficient value calculated by Grimsey and Biswas (1976) for NiO(l) is in agreement with the recalculated activity coefficient of NiO(l) for Takeda *et al.* (1984)

Both Takeda *et al.* (1984) and Eerola *et al.* (1984) found the activity coefficient of NiO(l) in the ferrite slag to vary with oxygen partial pressure. Over the oxygen partial pressure range of 10^{-11} to 10^{-6} atm, Takeda *et al.* (1984) found $\gamma_{NiO(l)}$ to increase from 1.05 to 4.13 whilst Eerola *et al.* (1984) found $\gamma_{NiO(l)}$ to increase from 1.4 to 4.3. When comparing the recalculated $\gamma_{NiO(l)}$ with the original $\gamma_{NiO(s)}$ as determined by Takeda *et al.* (1984) it is evident that $\gamma_{NiO(s)}$ is more dependant on oxygen partial pressure than $\gamma_{NiO(l)}$, with $\gamma_{NiO(s)}$ increase from 3 to 12 in oxygen partial pressure range of 10^{-11} to 10^{-6} atm. whilst $\gamma_{NiO(l)}$ increased from 1.05 to 4.13 within the same oxygen partial pressure range. At any given oxygen partial pressure, the activity coefficient of NiO(l) is a factor of 3 smaller then $\gamma_{NiO(s)}$ due to the decrease in the K-value by a factor of 3, for NiO(s), where K = 5060.9 to NiO(l), where K = 1627.5. However Takeda *et al.* (1984) and Eerola *et al.* (1984) agree that the observed increase in $\gamma_{NiO(l)}$ with increase in oxygen partial pressure, is not in accord with reasonable theoretical expectations and is unlikely to be true. As explained in Section 2.7.3, nickel oxide is considered a neutral oxide and its distribution is little affected by the basicity of the slag. Nickel oxide distributes similarly in both iron silicate slag and calcium ferrite slag. Thus if the activity coefficient of nickel oxide in iron silicate slag is independent of oxygen partial pressure, then it is expected that it will be also be independent of oxygen partial pressure in calcium ferrite slag. Both Takeda *et al.* (1984) and Eerola *et al.* (1984) calculated γ_{NiO} using Equation 2.8.2 and experimental distribution data. Thus with such a small increase in the $\gamma_{NiO(l)}$ in the oxygen partial pressure range of 10^{-11} to 10^{-6} atm, it is highly likely this trend observed can be accounted for by uncertainties in experimental and analytical techniques used to measure both the distribution data and the thermodynamic data required to calculate (γ_{NiO}). Thus constancy of the activity coefficient of NiO(l) in calcium ferrite slag with oxygen partial

pressure is assumed in this thesis and $\gamma_{NiO}(l)$ in calcium ferrite slag taken from Takeda *et al.*'s (1984) data is 4.13 and from Eerola *et al.*'s (1984) data is 4.3.

Holzheid *et al.* (1997) and Wang *et al.* (1973) measured the effects of temperature on the activity coefficient of NiO(l) in iron silicate slag and found ($\gamma_{NiO(l)}$) to be independent of temperature in the range of 1250-1350°C. Wang *et al.* (1973) found ($\gamma_{NiO(l)}$) in iron silicate slag to be a constant value of 3.7±0.8 whilst Holzheid *et al.* (1997) found ($\gamma_{NiO(l)}$) to be 2.7±0.5. The activity coefficient values of NiO(l) in iron silicate slag determined by both sets of authors is in good agreement and within experimental error.

Takeda *et al.* (1984) measured the effects of temperature on the activity coefficient of NiO(l) in calcium ferrite slag in the range of 1350-1250°C and found it to be negligible. They found that between 1250-1350°C, $\gamma_{NiO(l)}$ in the ferrite slag was a constant value of 4.6±0.6.

Table 2.8.11 lists the correlations found in literature on the effects of temperature on the activity coefficient of Ni(l) in copper. Nagamori *et al.* (1982) found the activity coefficient of Ni(l) in copper to be 2.7 at 1200°C and 2.3 at 1300°C. Eerola *et al.* (1984) calculated $\gamma^{o}_{Ni(l)}$ to be 3.0 at 1200°C and 2.8 at 1300°C. Taking into account uncertainties in experimental and thermodynamic data used to derive the relationship between temperature and the activity coefficient of nickel in copper, the relationships indicate that temperature in the range of 1200-1300°C has little affect, on the activity coefficient of Ni(l) in copper.

Table 2.8.11: Correlations between activity coefficient of nickel in copper and temperature

Reference	Activity Coefficient Relationship [γ^{o}_{Ni}]
Eerola, Jylha & Taskinen (1984)	$e^{1639/T(K)}$
Nagamori & Chaubal (1982)	$10^{(1430/T(K))-0.546}$

It has been seen that the effects of oxygen partial pressure and temperature on activity coefficient of Ni(l) in copper and NiO(l) in both iron silicate and calcium ferrite slag are negligible, the distribution ratios of nickel between the silicate slag and copper metal were calculated for each study using Equation 2.8.13 and the activity coefficient data in Table 2.8.9 and using Equation 2.8.14 and Table 2.8.10 for calcium ferrite slag. The calculated distribution data for both slags at standardised conditions of 1300°C and oxygen partial

pressure of 10^{-6} atm. is shown in Table 2.8.12. As is evident in Table 2.8.12, within experimental error, the distribution ratios of nickel calculated for each study as well as $\gamma_{NiO(l)}$ for both the silicate and ferrite slag are in good agreement. In general the distribution ratio of nickel between iron silicate slag and copper is 1.35 ± 0.3 and $\gamma^{o}_{Ni(l)}$ and $\gamma_{NiO(l)}$ are 2.3 ± 0.2 and 3.5 ± 0.6, respectively. For calcium ferrite slag, the distribution ratio of nickel is 1.09 ± 0.2 and $\gamma^{o}_{Ni(l)}$ and $\gamma_{NiO(l)}$ are 2.3 ± 0.2 and 4.2 ± 0.1, respectively. When comparing the distribution of nickel in both the silicate and ferrite slags, it is evident that the nickel distribution ratios and $\gamma_{NiO(l)}$ for both the silicate and ferrite slags are very similar, thus indicating that the solvent slag has little effect on the distribution of nickel in a slag-copper system, as is expected for neutral oxides (Section 2.7).

Table 2.8.12: Calculated distribution ratios of nickel between iron silicate slag and copper metal and between calcium ferrite slag and copper at 1300°C and oxygen partial pressure of 10^{-6} atm.

Reference	Distribution Coefficient ($L_{Ni}^{s/m}$)	
	Calcium Ferrite Slag	Iron Silicate Slag
Takeda, Ishiwata & Yazawa (1984)	0.98	1.18
Kashima, Eguchi & Yazawa (1978)	-	1.38
Yazawa (1980)	-	1.03
Grimsey & Biswas (1976)	-	1.60 ± 0.14
Wang, Kurtis & Toguri (1973)	-	1.15 ± 0.27
Holzheid, Palme, Chakraborty (1997)	-	1.76 ± 0.35
Eerola, Jylha & Taskinen (1984)	1.20	-

2.8.4 Summary

Listed in Table 2.8.13 are a summary of the activity coefficient data of the elements and their oxides in both the iron silicate slag and copper system and in the calcium ferrite slag and copper system at 1300°C and an oxygen partial pressure of 10^{-6} atm. Also listed in the table at the same conditions are the distribution ratios of nickel, lead and antimony between slag and copper for both the silicate and ferrite slags. The activity coefficient and distribution

values for all elements given in Table 2.8.13 was selected as these values were in good agreement with majority of the literature reviewed in this section.

Table 2.8.13: Summarised data for the distribution of nickel, lead and antimony between slag and copper at 1300°C and oxygen partial pressure of 10^{-6} atm.

		Iron Silicate Slag		Calcium Ferrite Slag	
	$[\gamma^{o}_{X}]$	(γ_{XO})	$(L_X^{s/m})$	(γ_{XO})	$(L_X^{s/m})$
Ni/NiO	2.3 ± 0.2	3.5 ± 0.6	1.35 ± 0.3	4.2 ± 0.1	1.09 ± 0.2
Pb/PbO	4.8 ± 0.02	0.3 ± 0.1	4.4 ± 1.3	3.1 ± 0.8	0.4 ± 0.02
$Sb/SbO_{1.5}$	0.03 ± 0.01	2.4 ± 0.9	0.15 ± 0.04	0.5 ± 0.2	0.61 ± 0.03

It can be concluded that lead, antimony and nickel dissolve in both iron silicate and calcium ferrite slag as oxides at 1300°C and an oxygen partial pressure of 10^{-6} atm. However the distribution ratio between slag and copper metal differs depending on the slag that is employed, such that:

- The distribution of lead between slag and copper highly favours the slag phase when iron silicate slag is used whilst favouring the metal phase when calcium ferrite slag is used. The distribution ratio of lead in iron silicate slag is an order of magnitude greater than that in calcium ferrite slag whilst the activity coefficient of lead oxide in iron silicate slag is an order of magnitude lower than that of calcium ferrite slag.
- The reversed behaviour is true for antimony. The distribution ratios of antimony are much higher for calcium ferrite slag in comparison to iron silicate slag.
- The distribution of nickel, which is considered a neutral oxide, is similar in both the ferrite and the silicate slags.

In accordance to the acid-base theory of slags, discussed in detail in Section 2.7, basic ferrite slag is superior for the removal of acidic oxides whereas the acidic silicate slag best removes basic oxides. The distribution of neutral oxides is not affected by the basicity of the slag. The behaviour of all three oxides is in accord with the thermodynamic predictions discussed in Chapter 2.7.

2.9 FERROUS CALCIUM SILICATE SLAG

2.9.1 Phase Equilibria and Liquidus Surface of FCS Slag

Ferrous calcium silicate slag (FCS slag) is located in the FeO_x-CaO-SiO_2 system. It was first recognised by Yazawa *et al.* (1999) as having the potential to become the third copper converting slag with the ability to solve the difficulties associated with both iron silicate and calcium ferrite slags as well as presenting the additional advantage of lower dissolution loss of oxidic copper in the continuous converting process. The nominal composition of FCS slag is located on the tie line between '$FeO+Fe_2O_3$' and calcium silicates, especially close to the dicalcium silicate composition containing high FeO_x. The preferred composition of FCS slag is shown by the arrow in Figure 2.9.1, positioned at the small liquidus "neck" region between the Ca_2SiO_4-FeO_x and $CaSiO_3$-FeO_x tie lines (dashed lines). Also shown in Figure 2.9.1 are the locations of the iron silicate and calcium ferrites slags in the ternary FeO_x-CaO-SiO_2 system, represented by F and CF, respectively. A detailed discussion on the phase equilibria of these slags is given in Section 2.3.

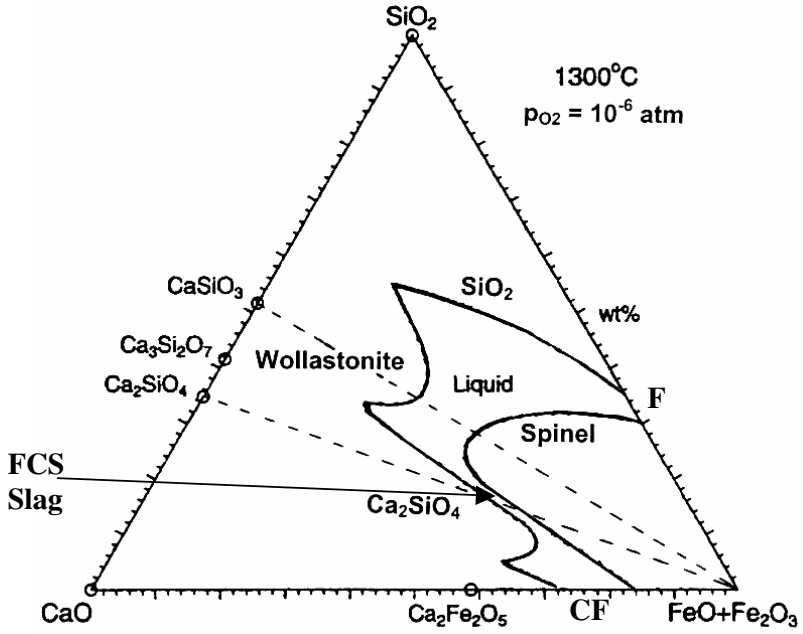

Figure 2.9.1: Liquid region in the FeO_x-SiO_2-CaO system at 1300°C and oxygen partial pressure of 10^{-6} atm (Kongoli, McBow and Yazawa, 2006)

F = Iron silicate Slag FCS = Ferrous Calcium Silicate Slag CF = Calcium Ferrite Slag

Copper smelting and converting processes are carried out at oxygen partial pressures varying between 10^{-8} to 10^{-5} atm. as illustrated by the Yazawa Chemical Potential Diagram (Figure 2.2.4). The oxygen partial pressure at which the Mitsubishi C-furnace operates is 10^{-6} atm. whereas the Kennecott Flash converter operates at an oxygen partial pressure of $10^{-5.5}$ atm. However the phase relations of the FeO_x-CaO-SiO_2 slag system have never been studied at these oxygen partial pressures. Based on quantitative model predictions using the Flogen model (discussed in Section 2.3), Yazawa and Kongoli (2001) summarised the effects of oxygen partial pressure and temperature on the liquid region of the FeO_x-CaO-SiO_2 system. Whilst the effects of oxygen partial pressure and temperature on the liquid region of the FCS slag have not been experimentally determined, the model predictions using the Flogen software have been validated with existing experimental data of iron silicate slag under known conditions at several temperatures and oxygen partial pressures. One such validation of the model predictions against existing experiment data by various investigators was of the liquid region of the FeO-Fe_2O_3-SiO_2-CaO system at 1300^{o}C and oxygen partial pressures of 10^{-8}, 10^{-7}, 10^{-6} atm. The comparison of the model with the experimental data is illustrated in Figures 2.9.2, 2.9.3 and 2.9.4. As can be seen in all three figures, the agreement between the model predictions and experimental data is within experimental uncertainty. There is however some disagreement between the Flogen model and the data of Tsukihashi (2003) at the magnetite saturation boundary of the ternary system at an oxygen partial pressure of 10^{-6} atm. However as the model agrees with Takeda *et al.* (1980) and Takeda's (2001) data in Figure 2.9.4, it can be assumed that there exists several unavoidable experimental uncertainties in Tsukihashi's (2003) results, including error in experimental techniques, control of experimental conditions and error in analytical techniques used by the investigators. Nonetheless, overall, the accuracy of the model data when compared to experimental data is in good agreement and thus the model can be used with confidence to discuss the liquid region of ferrous calcium silicate slag.

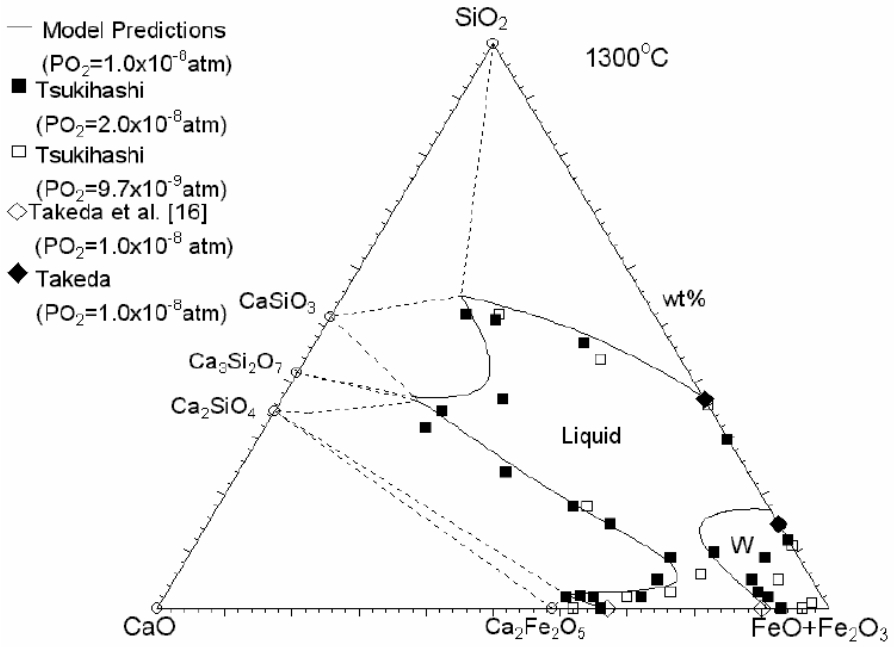

Figure 2.9.2: Liquid region of FeO_x-SiO_2-CaO slag at 1300°C and oxygen partial pressure of 10^{-8} atm according to model predictions and available experimental data (Kongoli, McBow, Yazawa, Takeda, Yamaguchi, Budd and Llubani, 2006)

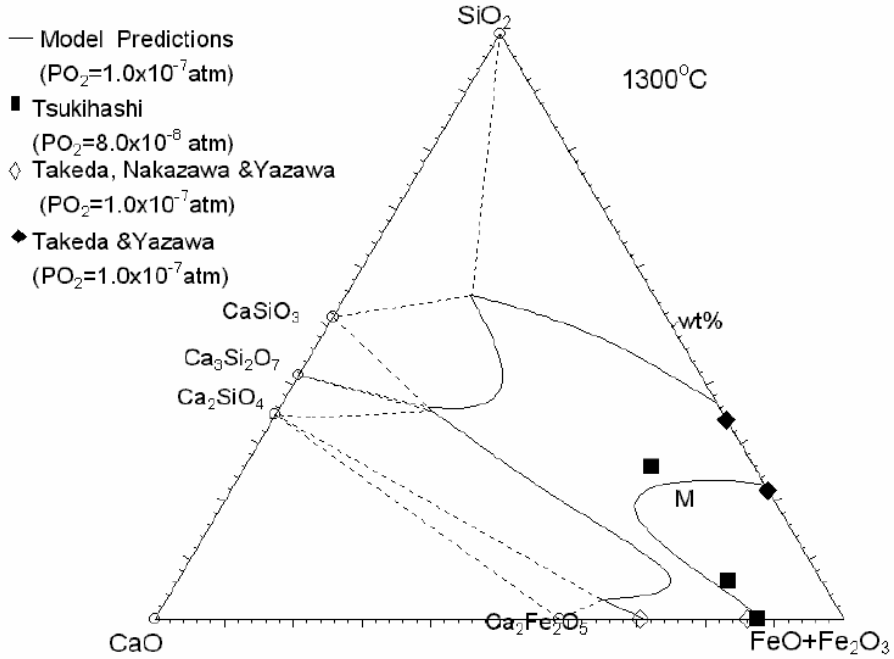

Figure 2.9.3: Liquid region of FeO_x-SiO_2-CaO slag at 1300°C and oxygen partial pressure of 10^{-7} atm according to model predictions and available experimental data (Kongoli, McBow, Yazawa, Takeda, Yamaguchi, Budd and Llubani, 2006)

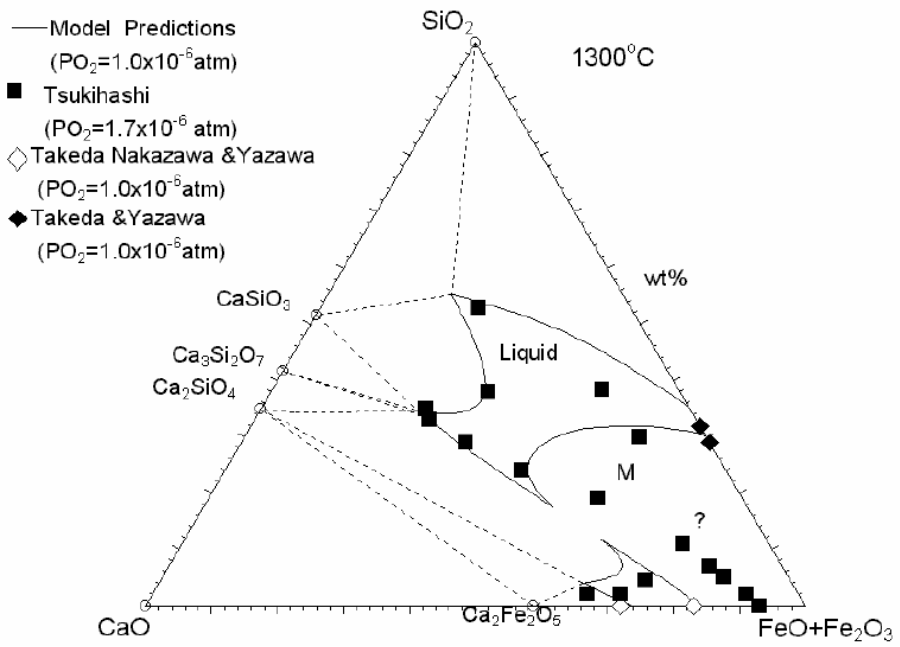

Figure 2.9.4: Liquid region of FeO_x-SiO_2-CaO slag at 1300°C and oxygen partial pressure of 10^{-6} atm according to model predictions and available experimental data (Kongoli, McBow, Yazawa, Takeda, Yamaguchi, Budd and Llubani, 2006)

Based on Yazawa and Kongoli's (2001) model predictions, the effects of oxygen partial pressure and temperature on the liquid region of the FeO_x-CaO-SiO_2 system is summarised in Figures 2.9.5 and 2.9.6, respectively. Figure 2.9.5 describes the homogeneous liquid region of the slag at l300°C and oxygen partial pressures of 10^{-7}, 10^{-6} and 10^{-5} atm. as experienced in copper smelting and converting operations. Figure 2.9.6 illustrates the effect of temperature on the homogeneous liquid region at oxygen partial pressure of 10^{-6} atm., the oxygen partial pressure of most converting operations. Figure 2.9.5 is compiled from taking a section along the lines of constant Fe/SiO_2 ratios from the liquid region boundaries in the ternary FeO_x-CaO-SiO_2 system at an oxygen partial pressure of 10^{-6} atm. and is plotted against the wt% CaO. Both Figures 2.9.5 and 2.9.6 indicate that four primary crystals of SiO_2, magnetite (Fe_3O_4), Ca_2SiO_4 and wollastonite ($CaSiO_3$) limit the liquid region of the 'FeO-Fe_2O_3'-CaO-SiO_2 slag system at conditions of oxidative converting.

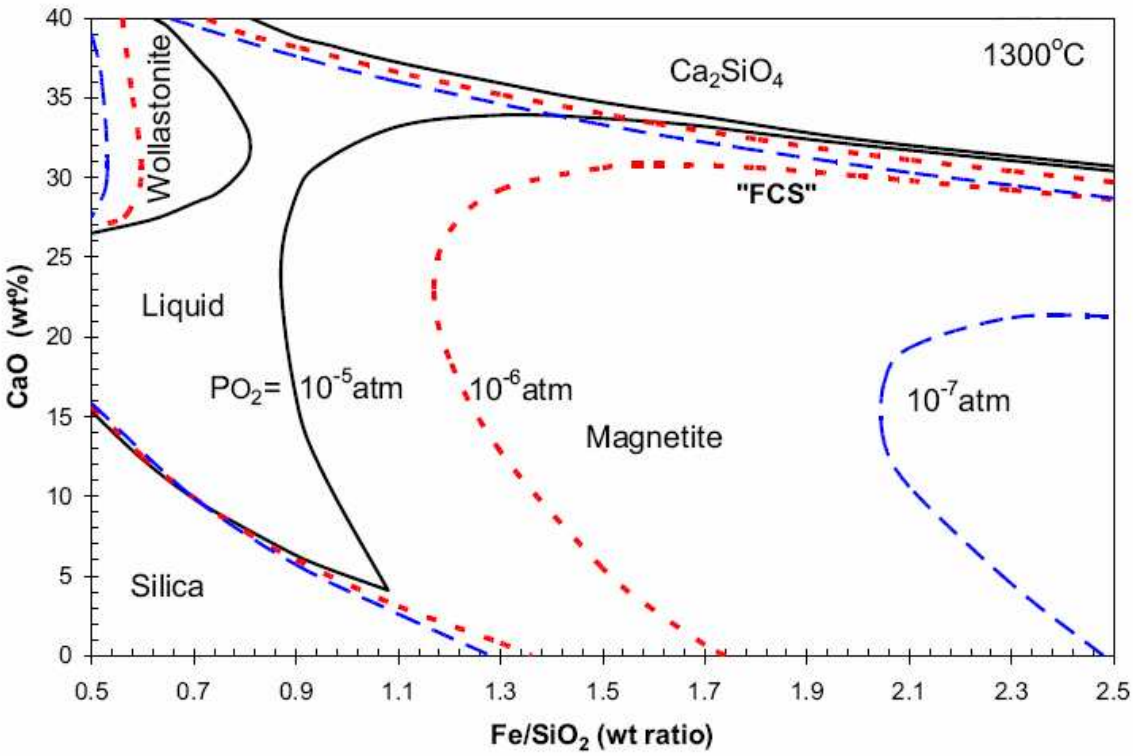

Figure 2.9.5: Effects of oxygen partial pressure on the homogenous liquid region of 'FeO-Fe_2O_3'-SiO_2-CaO system at 1300°C (Kongoli, McBow and Yazawa, 2006)

In Figure 2.9.5, the liquid region and thus the range of composition over which the slag is liquid has considerably decreased as oxygen partial pressure increases 10^{-7} atm. to 10^{-5}atm. The decrease in the liquid region is most significant at the magnetite saturation boundary. It is also interesting to note, that there is no significant change in the wollastonite and SiO_2 saturation boundaries with oxygen partial pressure. This is because these phases contain no Fe^{2+} or Fe^{3+} and so are unaffected by changes in oxygen partial pressure. Although Ca_2SiO_4 does not contain ferrous or ferric iron, as illustrated in Figure 2.9.5, an increase in oxygen partial pressure, however, slightly increases the liquid region near the Ca_2SiO_4 saturation boundary, which corresponds to the area of FCS slag.

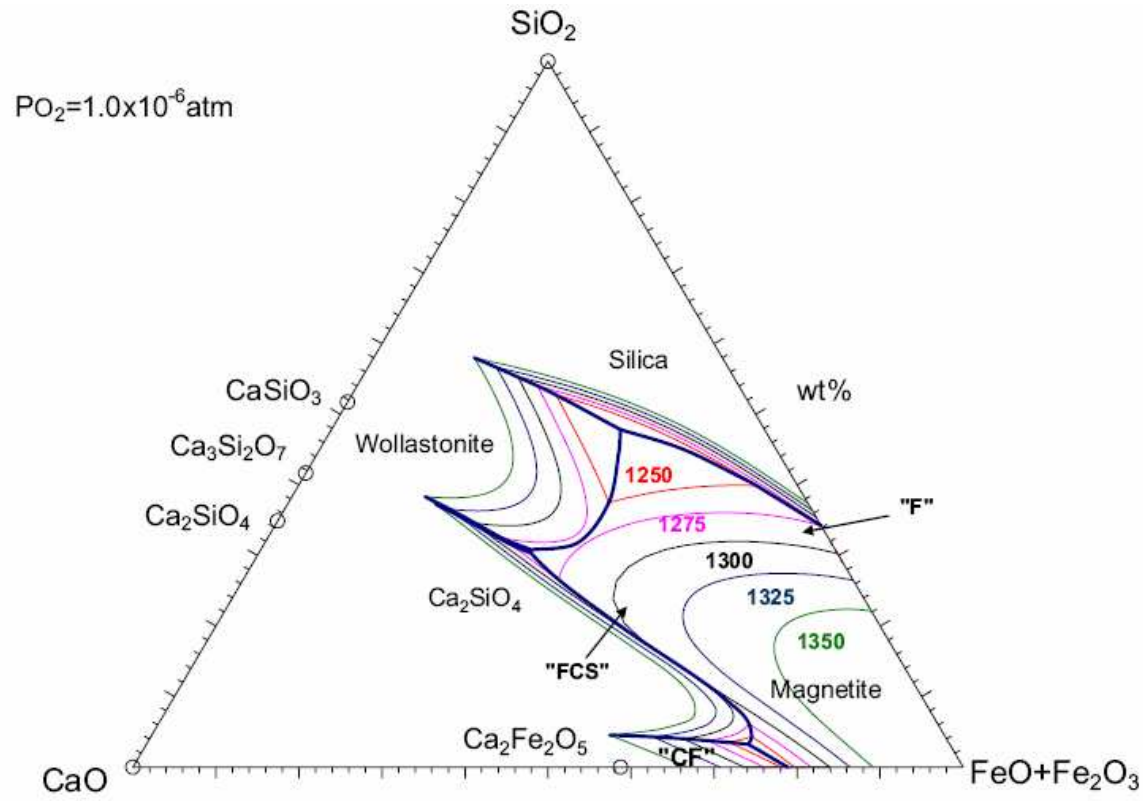

Figure 2.9.6: Effects of temperature on the homogeneous liquid region of 'FeO-Fe_2O_3'-SiO_2-CaO system at oxygen partial pressure of 10^{-6} atm (Kongoli, McBow and Yazawa, 2006)

Figure 2.9.6 shows that decrease in temperature decreases the liquid region on the magnetite and wollastonite surface. Thus, if the slag composition is situated close to the magnetite boundary, a small decrease in liquidus temperature results in increase in the likelihood of magnetite precipitation during converting. Process temperature has no major affect on the SiO_2 and Ca_2SiO_4 surfaces. As seen in Figure 2.9.6, the compositional range in which ferrous calcium silicate slag (as labelled) is a homogenous melt, is greatly depended on the process temperature, such that, below 1300^oC a homogeneous FCS slag is not available and FCS slag could either precipitate Fe_3O_4 spinel or dicalcium silicate, depending on which way the composition deviation occurs. However with an increase in temperature, the slag liquid region also increases and at 1300^oC a small liquid region exists near the Ca_2SiO_4 surface where FCS is situated.

In general, Figures 2.9.5 and 2.9.6 conclude that the liquid region decreases with the decrease of temperature and increase of oxygen partial pressure and it decreases drastically on the magnetite surface even for a slight decrease in temperature or a slight increase in the oxygen partial pressure. Both figures clearly demonstrate that whilst at 1300°C and oxygen partial pressure ranging between 10^{-6} and 10^{-5} atm., a liquid FCS slag is available, control of the slag composition to ensure a liquid melt is very difficult and virtually impossible and application of the slag for converting operations is impractical. However, in practice, converter slags contain a significant amount of dissolved copper as Cu_2O. The copper oxide content of iron silicate and calcium ferrite slag ranges from 15-17 wt% whereas it is believed that up to 10 wt% of copper oxide is dissolved in FCS slag at an oxygen partial pressure of 10^{-6} atm. and 1300°C (Yazawa *et al.*, 2001). The effects of the addition of copper oxide on the liquid region of FCS slag are demonstrated in Figures 2.9.7 and 2.9.8 at 1300°C and oxygen partial pressure of 10^{-6}atm. As observed, with zero copper oxide, the liquid region where FCS is located is very narrow however when the FCS is in equilibrium with copper and contains up to 10 wt% of copper oxide (Figure 2.9.8), the addition of copper oxide to slag increases the slag liquid region at the silica, wollastonite and magnetite phase boundaries. Thus when FCS slag is in equilibrium with copper metal, as is the case for both the Kennecott Flash converter and the Mitsubishi C-furnace, a homogeneous liquid FCS slag is available at 1300°C and an oxygen partial pressure of 10^{-6} atm. for application in converting.

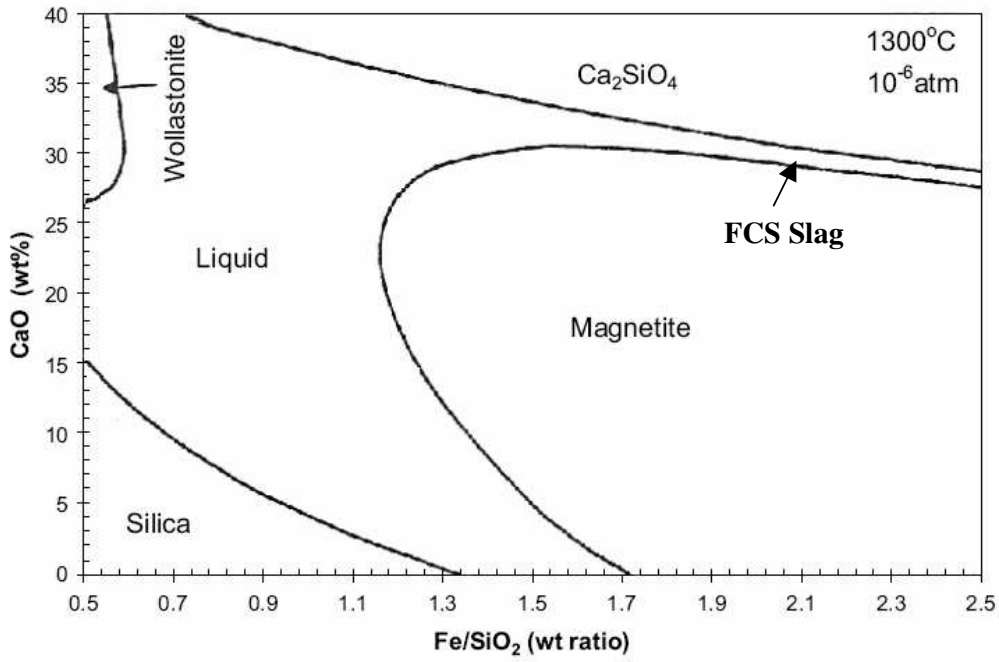

Figure 2.9.7: Liquid region of FeO_x-SiO_2-CaO slag with 0% Cu_2O at 1300°C and oxygen partial pressure of 10^{-6} atm (Kongoli, McBow and Yazawa, 2006)

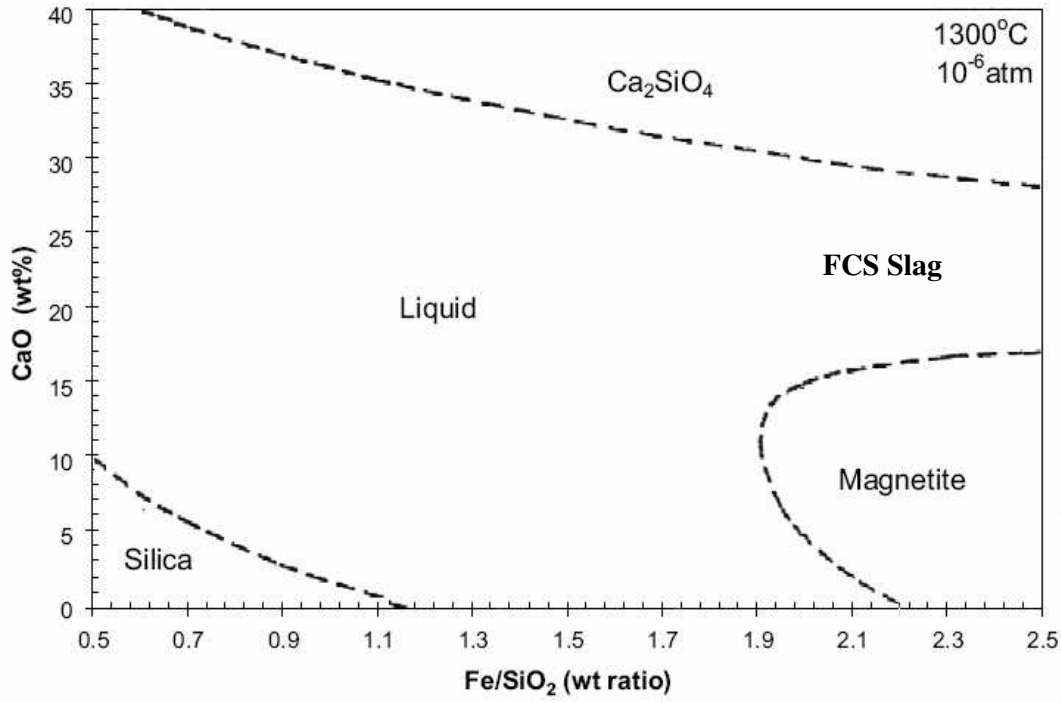

Figure 2.9.8: Liquid region of FeO_x-SiO_2-CaO slag with 10% Cu_2O at 1300°C and oxygen partial pressure of 10^{-6} atm (Kongoli, McBow and Yazawa, 2006)

Yazawa and Kongoli (2001) also demonstrated the combined effects of Cu_2O and CaO additions to FCS slag at a fixed Fe/SiO_2 ratio of 2.3 and an oxygen partial pressure of 10^{-6} atm. on the slag liquidus temperature as illustrated in Figures 2.9.9. The liquidus temperatures at the maximum dissolution of Cu_2O in slag at an oxygen partial pressure of 10^{-6} atm. are illustrated by lines labelled Cu-saturation. Observations of Figure 2.9.9 indicate that at an oxygen partial pressure of 10^{-6} atm., without the presence of copper oxide in slag, an increase in the slag CaO content, results in the decrease in the liquidus temperature, with the liquidus temperature being the lowest when CaO content ranges between 20-30 wt% CaO, before a rapid increase in temperature is observed. This increase in the slag liquidus temperature above approximately 30 wt% CaO results in the precipitation of Ca_2SiO_4, which is evident in Figure 2.9.7. Figure 2.9.7 illustrates that the fixed Fe/SiO_2 ratio of 2.3, above 30wt% CaO in slag, the slag is in the Ca_2SiO_4 saturation surface, such that precipitation of Ca_2SiO_4 in slag is inevitable. Below 20% CaO, the slag is troubled by magnetite precipitation. As shown in Figure 2.9.9, the liquidus temperature is further reduced for an increase in CaO content when the slag is in equilibrium with copper, the maximum decrease is observed when the dissolved copper oxide content of the slag is approximately 10 wt% Cu_2O and CaO content of slag ranges between 20-30 wt%. The 'V'-shaped region in Figure 2.9.9 at copper saturation, where

CaO content in slag ranges between 20-30 wt% CaO, signifies the slag composition when the slag liquidus temperature is at its lowest. This region is representative of the 'neck' of the slag liquidus region in Figure 2.9.8, where FCS slag is located.

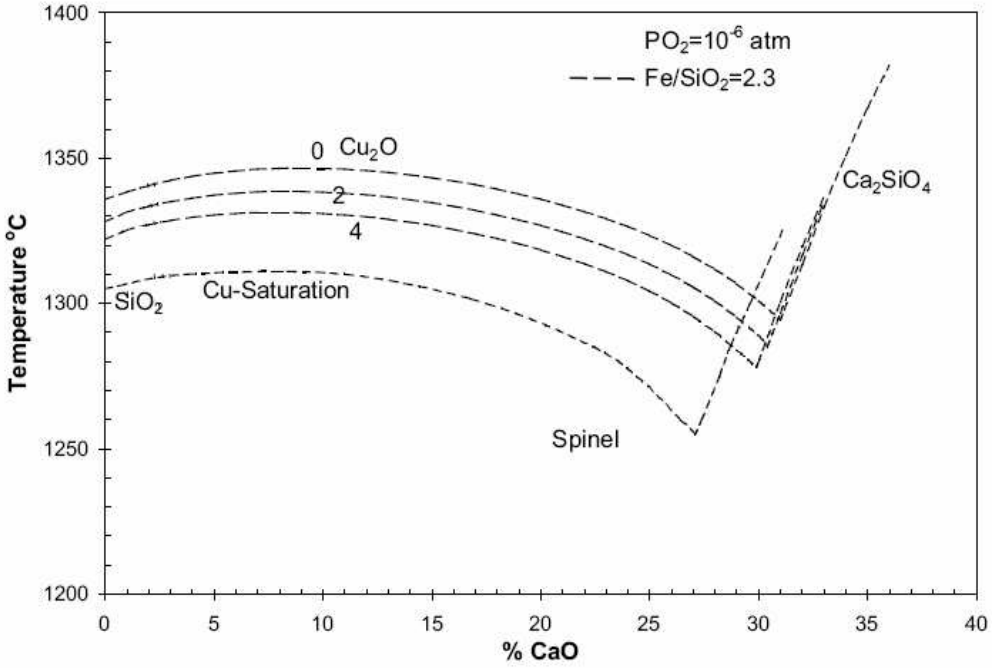

Figure 2.9.9: Effects of Cu_2O on the liquidus temperature at oxygen partial pressure of 10^{-6} atm and Fe/SiO_2 ratios of 2.3 (Kongoli, McBow and Yazawa, 2006)

In equilibrium with copper metal, the presence of copper oxide in FCS slag increases the slag liquid region especially at the magnetite, silica and wollastonite saturation boundaries. The presence of copper oxide in FCS slag ensures that the slag liquid region is wide enough for practical applications. Furthermore, the slag liquidus temperature also decreases with the addition of copper oxide to slag, with the temperature being the lowest when FCS slag is saturated with copper oxide and the slag CaO content ranges between 20-30 wt%. Thus in order to have a wide enough liquid range at low enough temperatures to ensure the slag is a homogeneous liquid at converting conditions and is practically useful, the lowest possible liquidus temperature is desired and thus when in equilibrium with copper, the CaO content of FCS slag needs to be between 20-30 wt%. Ideally ferrous calcium silicate slag is situated in the 'neck' of the liquidus region of Figure 2.9.8, between the magnetite and Ca_2SiO_4 saturation boundaries, where the Fe/SiO_2 ratio ranges between 1.9-2.5. A high Fe/SiO_2 ratio is desired to ensure low volume of slag is produced and handled during production. Whilst the liquid region of FCS slag is not as wide as the liquid region of both

iron silicate and calcium ferrite slags, a homogeneous FCS slag melt can be successfully implemented for copper converting, when in equilibrium with copper.

2.9.2 Dissolution of Copper and Other Neutral Minor Elements in FCS Slag

The loss of copper to slag is either caused by entrainment or dissolution. The dissolution loss of copper to slag in converting operations is predominantly in the form of oxidic copper. According to Yazawa *et al.* (1999), when compared to iron silicate and calcium ferrite slags, the oxidic dissolution loss of copper in ferrous calcium silicate slag will be lower both in terms of %Cu in slag and the total copper lost when taking into account the amount of slag produced. The predicted distribution behaviour of a neutral oxide, such as Cu_2O, in all three slags has been discussed and explained in Section 2.7 using the regular solutions ternary model. The general conclusion drawn from the discussion is that the dissolution of a neutral oxide in both the silicate and ferrite slags is very similar and is unaffected by the solvent slag as is indicated by the similarity in the activity coefficient values of the oxide in both slags. However for FCS slag, the activity coefficient of the neutral oxide is slightly higher than both iron silicate and calcium ferrite slags and lower dissolution loss of copper oxide and other neutral metal oxides to FCS slag are expected, since the solubility of an oxide in slag is inversely proportional to its activity coefficient. At present, experimental data on the dissolution of copper oxide in FCS slag is very limited whilst literature on the distribution of other elements with neutral oxides in FCS slag were not available. Nonetheless using existing data on the oxidic dissolution of copper in the ternary FeO_x-CaO-SiO_2 system, it is possible to validate the regular solutions model predictions on the distribution of neutral elements between FCS slag and copper.

Takeda (1994) has studied the oxidic dissolution loss of copper to slag between CaO-SiO_2-FeO_x slag and copper metal at 1300^{o}C and oxygen partial pressures ranging between 10^{-12} and 10^{-4} atm. Ojima *et al.* (2003) also studied the oxidic dissolution of copper in the FeO_x-CaO-SiO_2 slag system (including iron silicate and calcium ferrite slag) when equilibrated with copper metal. They performed both laboratory and pilot plant tests to determine the suitability of iron silicate, calcium ferrite and a ternary FeO_x-SiO_2-CaO slag to a new continuous converting process of bath smelting using a flash smelting furnace with use of a top submerged lance. A similar study was also performed by Vartiainen *et al.* (2003), who

conducted pilot plant tests to directly produce blister copper from concentrates using flash smelting. The authors used iron silicate, calcium ferrite and FCS slag with CaO/SiO_2 ratios varying between 1 and 3, to determine the most feasible slag for application on a commercial scale. The tests by both Ojima *et al.* (2003) and Vartiainen *et al.* (2003) were conducted at 1300°C and an oxygen partial pressure between $10^{-4.8}$ to 10^{-5} atm. Such a high oxygen partial pressure was used in order to ensure blister copper with less than 0.1 wt% S was produced in both new technologies. As explained in Section 2.2.1, the sulphur content of blister copper is inversely proportional to the oxygen partial pressure of the system, thus as the oxygen partial pressure increases, the sulphur content in blister decreases and it is desired by most operators to achieve blister copper with less than 0.1wt% S. High sulphur blister requires extended anode furnace blowing for de-sulphurisation which is not economical. Vartiainen and co-authors (2003) found that if the CaO/SiO_2 ratio in the FCS slag is higher than 1.5, the CaO content in a FeO_x-CaO-SiO_2 slag is higher than 20 wt% and the copper content in slag is at least 8 wt%, then the slag is molten at an oxygen partial pressure of $10^{-4.8}$ atm. and temperatures between 1250-1350°C. The slag compositions used by Vartiainen *et al.* (2003), Takeda (1994) and Ojima *et al.* (2003) are illustrated in Figure 2.9.10 and correspond to the compositions in Table 2.9.1.

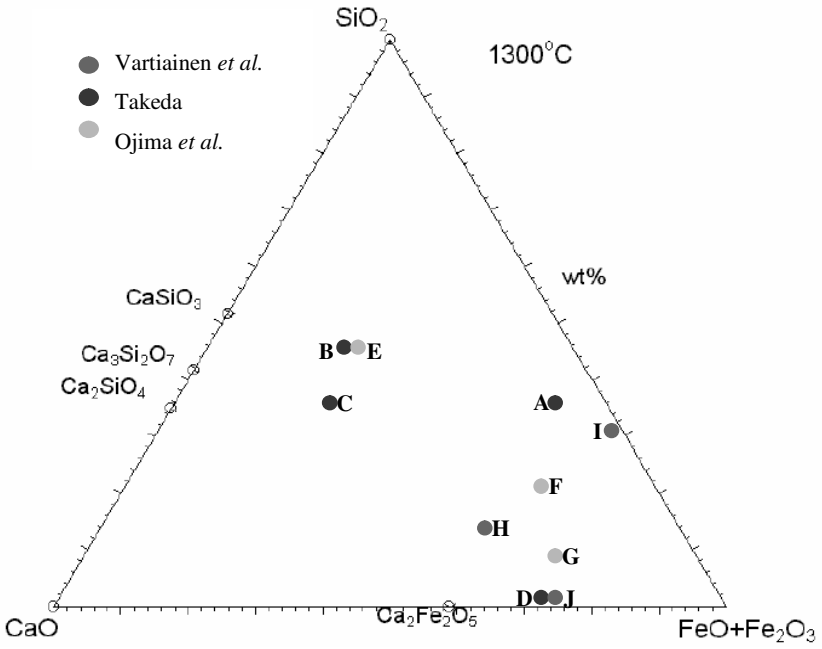

Figure 2.9.10: Comparison of the slag compositions employed by Vartiainen *et al.* (2003), Takeda (1994), Ojima *et al.* (2003) for experimentation.

Table 2.9.1: Slag compositions employed by Takeda (A-D), Ojima *et al.* (E-G) and Vartiainen *et al.* (H-J). *Q = %CaO/(%CaO + %SiO_2)* *R = %FeO_x in slag*

Slag	Q-ratio	R
A- Iron Silicate slag (FeO_x-SiO_2)	0.1-0.2	55-59
B- FeO_x-CaO-SiO_2	0.38-0.44	18-22
C- FeO_x-CaO-SiO_2	0.5-0.55	20-24
D- Calcium Ferrite slag (FeO_x-CaO)	1	70-74
E- FeO_x-CaO-SiO_2	0.5	29
F- FeO_x-CaO-SiO_2	0.44-0.55	62
G- Ferrous Calcium Silicate slag	0.7	70
H- Ferrous Calcium Silicate slag	0.67	58
I- Iron Silicate slag	0	68-70
J- Calcium Ferrite slag	1	72-75

In Figure 2.9.10 and Table 2.9.1, it is evident the Vartiainen and co-authors (2003) were the only investigators to determine the dissolution of copper oxide in ferrous calcium silicate slag as located in the 'neck' of the liquid region in Figure 2.9.1. This composition in Figure 2.9.10 is represented by 'H'. Ojima *et al.* (2003) did however examine slag composition close to this region at composition 'G'.

Although the slag compositions in the ternary FeO_x-CaO-SiO_2 system studied by Takeda (1994) do not extend to the FCS slag compositions, their investigation provides an indication of the copper solubility in FCS slag in comparison to the ferrite and silicate slags. The activity coefficient data for copper oxide as determined by Takeda (1994) is illustrated in the ternary FeO_x-CaO-SiO_2 system in Figure 2.9.11 at 1300^{o}C and an oxygen partial pressure between 10^{-8}-10^{-6} atm. In general copper solubility in slag is lowest at high Q-ratios (activity coefficient of copper oxide is large) and low R-ratio and highest in slag with low Q-ratios and high R-ratio (activity coefficient of copper oxide is small).

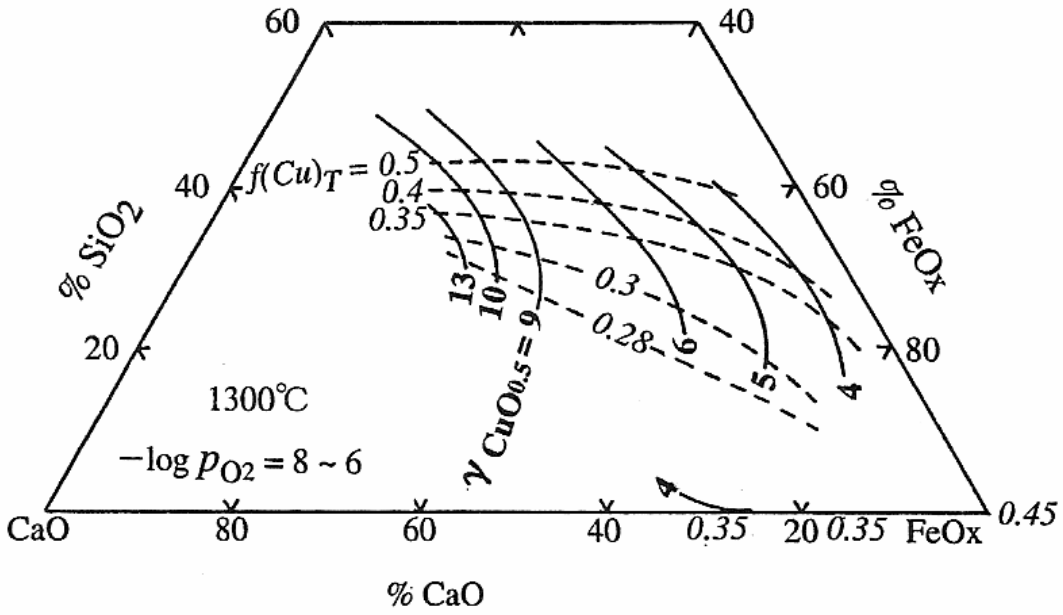

Figure 2.9.11: Activity coefficient of $CuO_{0.5}$ (solid lines) and total dissolution loss function f(Cu)T (dashed lines) in FeO_x-SiO_2-CaO system (Takeda, 1994)

Whilst the activity coefficient data does not extend to the FCS slag region, it does give the initial indication that the activity coefficient of copper oxide is between 6-9. At the same conditions, $\gamma_{CuO0.5}$ for iron silicate and calcium ferrite slags is 3.5 and 4.0, respectively. Since the copper content (wt%Cu) in slag is inversely proportional to $\gamma_{CuO0.5}$, lower dissolution copper loss to slag in FCS slag than both iron silicate and calcium ferrite slag on a (%Cu) basis is expected. The experimental data is Figure 2.9.11 validates the thermodynamic predictions from the regular solutions model that FCS slag has a lower solubility of copper and other neutral elements than iron silicate and calcium ferrite slags. The general trend of the activity coefficient curves in Figure 2.9.11 are similar to the thermodynamic model in Figure 2.7.5, however the strong concave nature of the isobars is not apparent for the experimental $\gamma_{CuO0.5}$ values since at 1300°C and an oxygen partial pressure between 10^{-8}-10^{-6} atm, the liquid region of the ternary slag system is limited by the SiO_2, magnetite (Fe_3O_4), Ca_2SiO_4 and wollastonite ($CaSiO_3$) boundaries (Figure 3.9.1) and thus the experimental data for $\gamma_{CuO0.5}$ is only available for compositions within the liquid region.

A comparison of the copper content in iron silicate, calcium ferrite and FCS slag as a function of oxygen partial pressure from Vartiainen and co-author's (2003) investigation is illustrated in Figure 2.9.12. Whilst there is substantial scatter in the results, the general trend in the data indicates that at the same oxygen partial pressure, the copper content in iron

silicate slag is higher than in FCS slag. A similar conclusion was also drawn by Takeda (1994) on the dissolution of copper in the silicate and ternary slags. In should be noted that FCS slag in Figure 2.9.12, represents FCS slags with CaO/SiO_2 ratio ranging between 1.5 and 2. Due to the lack of data available for calcium ferrite slag in Figure 2.9.12, a valid conclusion cannot be made on the copper content of the ferrite slag; however it appears that the dissolution of copper in calcium ferrite slag is similar to FCS slag at high oxygen partial pressures.

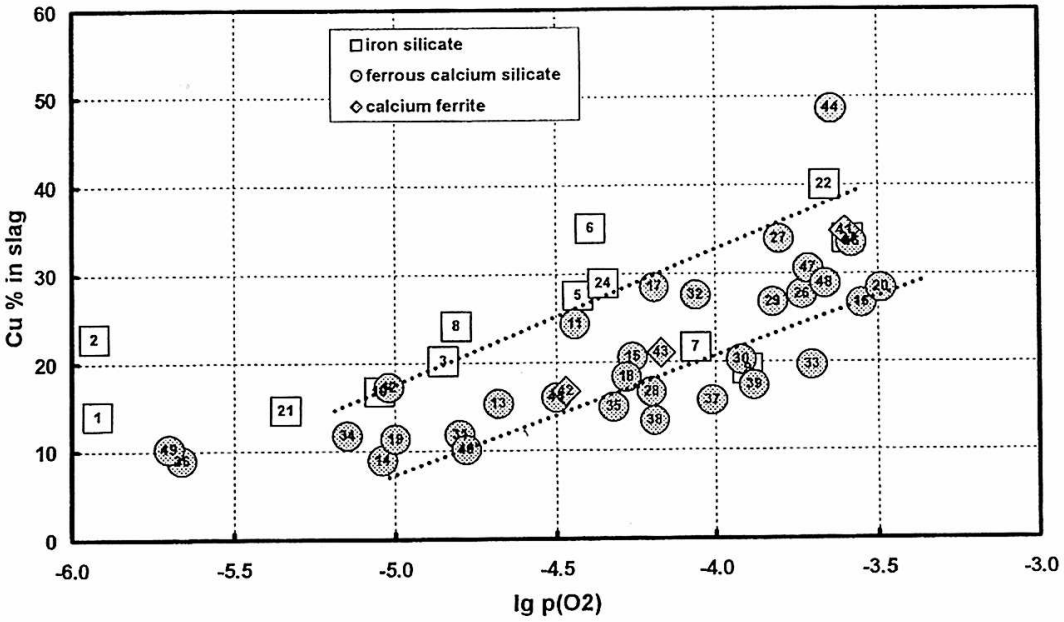

Figure 2.9.12: %Cu in slag as a function of oxygen partial pressure in blister copper for various slag systems (Vartiainen, Kojo and Rojas, 2003).

From the laboratory tests Ojima and co-authors (2003) found that a ternary slag with a Q-ratio of 0.5 had the smallest copper oxide content at the desired conditions, however, when the laboratory experiments were upgraded to pilot plant scale, the tests were interrupted due to foaming of the slag, with the first trial period lasting only 4 days. The pilot tests were resumed using a ternary slag with a higher Q-ratio of 0.7 that is, lower silica in slag. The change in slag composition proved to be successful, such that the test period was extended to 16 days and no slag foaming was observed. No reason was given by the authors for the slag foaming, or why raising the Q-ratio eliminated it. All other conditions in the pilot plant tests were kept unchanged, including temperature, oxygen partial pressure and gas flow-rate. The investigators also observed a decrease in the copper dissolution loss to the ternary slag with a lower silica content, such that at 1300^{o}C and the target oxygen partial pressure ($10^{-4.8}$ to 10^{-5}

atm.), the %Cu in slag with Q = 0.44-0.5 was 23% whilst in slag with Q = 0.7 the copper lost to slag was approximately 19%.

Table 2.9.2, compares the copper content in slag for various Q-ratios and %FeO_x in slag at similar conditions as determined by Vartiainen *et al.* (2003), Takeda (1994) and Ojima *et al.* (2003). For iron silicate and calcium ferrite slags, the results of all three investigators are in good agreement, taking into account experimental uncertainty. The results for the ternary slags are, however, very different even for similar Q-ratios, such that for a Q-ratio of roughly 0.5, Takeda found the solubility of copper is slag to be between 6-9.5% whilst for a similar Q-ratio, Ojima *et al.* (2003) found the % Cu in slag to be 7% for the laboratory experiments and 23% for the pilot plant experiments. Whilst for the laboratory experiments the copper content in slag is similar for both Takeda (1994) and Ojima *et al.* (2003), the pilot scale tests differ greatly. It is possible that the higher copper content of the slag in the pilot scale tests is a result of copper entrainment and not copper dissolution; however the authors have not documented citing copper entrainment in slag. The difference in the dissolution of copper in the ternary slags could also be a result of the iron oxide content of the slag. The FeO_x content of the slag used by Takeda (1994) and Ojima *et al.* (2003) in the laboratory experiments was very low (18-24%) when Q = 0.5 whilst the FeO_x content of the slag used by Ojima *et al.* (2003) is approximately 62% for the pilot plant tests. In general, copper solubility in the ternary slags increases as the slag FeO_x content increases. This relationship is evident in Figure 2.9.11 where the activity coefficient of copper oxide in slag increases with increasing Q-ratio and with decreasing FeO_x content of the slag. On any tie-line between FeO_x and CaO-SiO_2 binary, an increase in the iron oxide content of the slag, results in a decrease in the activity coefficient value of copper oxide, which results in an increase in the copper oxide content of the slag. Thus whilst the Q-ratio plays a vital role in determining the solubility of copper oxide in the ternary slag, so does the iron oxide content of the slag.

In order to ensure the maximum recovery of copper and thus reduce the dissolution loss of copper to slag, a slag with Q = 0.5 and low FeO_x content is required. However, a slag of low FeO_x content has as a very high melting point as it is close to the liquidus composition saturated with dicalcium silicate. A slag of composition saturated with $2CaO.SiO_2$ and low in FeO_x does not melt at 1300^oC and leads to a highly viscous slag, which can result in operational difficulties such as slag foaming, taphole blockage and copper metal entrainment. Increasing the FeO_x content and the Q-ratio of the slag will not only decrease the slag viscosity but also its melting point, ensuring the slag is liquid at operating conditions however

at the expense of copper loss to slag since increasing the slag FeO_x content, increases copper dissolution in slag. Ferrous calcium silicate slag as confirmed earlier has lower dissolution loss of copper to slag when comparing to both iron silicate and calcium ferrite slag and at 1300°C and 10^{-6} atm. will not jeopardise the physical properties of the slag which are of equal importance at operating conditions. Based on the behaviour of copper oxide in FCS slag, it is also expected that the distribution of other neutral elements such as NiO and CoO to the slag will be slightly lower in a FCS slag/copper system than both calcium ferrite and iron silicate slags at converting conditions.

Table 2.9.2: A comparison of the %Cu in slag for various Q-ratios and $\%FeO_x$ in slag at 1300°C and oxygen partial pressure of $10^{-4.8}$ to 10^{-5} atm.

	Vartiainen *et al.* (2003)	**Takeda *et al.* (2003)**	**Ojima *et al.* (2003)**
Q = 0.38-0.44 FeO_x = 18-22%		9.5	
Q = 0.5-0.55 FeO_x = 20-24%		6	
Q = 0.44-0.5 FeO_x = 62%			23 (Pilot test)
Q = 0.5 FeO_x = 29%			7 (Lab test)
Q = 0.67 FeO_x = 57%	12-13		
Q = 0.7 FeO_x = 70%			19 (Pilot test)
Calcium Ferrite	16	17	17 (Lab test)
Iron Silicate	22	21	24 (Lab test)

The total dissolution loss of copper to slag, which is a function of the total amount of slag, V, produced, is also of vital importance when selecting a slag system. This relationship was studied by Yawaza *et al.* (1999) and is illustrated in Figure 2.9.11 as the total dissolution loss function, $f(Cu)_T$ (dashed lines). The total amount of slag produced is inversely proportional to the iron content of the slag according to Equation 2.9.1 (Yazawa *et al.*, 1999).

$$(Cu)_T = (\%Cu) \times V = c' / [\gamma_{CuO_{0.5}} (\%FeO)]$$
$$f(Cu)_T = 100 / [\gamma_{CuO_{0.5}} (\%FeO)] \qquad \textbf{Equation 2.9.1}$$

As explained above, to ensure a slag of low wt% Cu, the FeO content of the slag needs to be low. Adding more flux lowers the wt% FeO in the slag but produces more slag. The higher the Fe content of the slag, the lower the amount of slag produced and if flux addition is high, the amount of slag formed is also high. Thus whilst the copper content in slag may be

low, the total amount of copper in slag is high and the direct recovery of copper to blister copper is poor as a large amount of copper goes to slag.

In Figure 2.9.11 on a tie-line between FeO_x and $CaO\text{-}SiO_2$ binary, where Q = 0.5 and FeO_x = 24-29%, the activity coefficient of copper in a slag is high but the total dissolution loss of copper in slag is also high ($f(Cu)_T$ = 0.35-0.4 when $\gamma_{CuO0.5}$ = 13). Increasing the FeO_x content of the slag decreases the total dissolution amount of copper in slag. In the region of FCS slag composition, $f(Cu)_T$ varies between 0.3 and 0.28. For calcium ferrite slag $f(Cu)_T$ is 0.35 and that for iron silicate slag is approximately 0.45. Thus at similar converting conditions, FCS slag not only has a lower copper content in slag but also the total dissolution loss of copper is lower than both iron silicate and calcium ferrite slag. Such values once again support Yazawa and co-author's (1999) prediction on the dissolution loss of copper in ferrous calcium silicate slag.

2.9.3 Dissolution of Basic and Acidic Minor Elements in FCS Slag

The predicted distribution behaviour of acidic and basic oxides in FCS slag has been discussed in detail in Section 2.7.4. However there exists limited experimental data on minor element distribution in ferrous calcium silicate slag to support the predictions. Although, the distribution of PbO in the ternary $FeO_x\text{-}SiO_2\text{-}CaO$ slag system has been investigated by Takeda and Yazawa (1989) at 1300^{o}C and the activity coefficients of PbO in the ternary system are reproduced in Figure 2.9.13. In Figure 2.9.13, at the composition of iron silicate slag γ_{PbO} = 0.3 and for calcium ferrite slag γ_{PbO} is between 3 and 4. For the composition of ferrous calcium silicate slag, γ_{PbO} is between 1 and 2. This reconfirms that whilst the interactions between PbO and SiO_2 in the FCS slag are not as strong as those between PbO and SiO_2 in iron silicate slag, the removal of PbO in FCS slag is nonetheless more efficient than in calcium ferrite slag. The line trends of the γ_{PbO} isobars in Figure 2.9.13 are similar to the thermodynamics model in Figure 2.7.6 (Section 2.7).

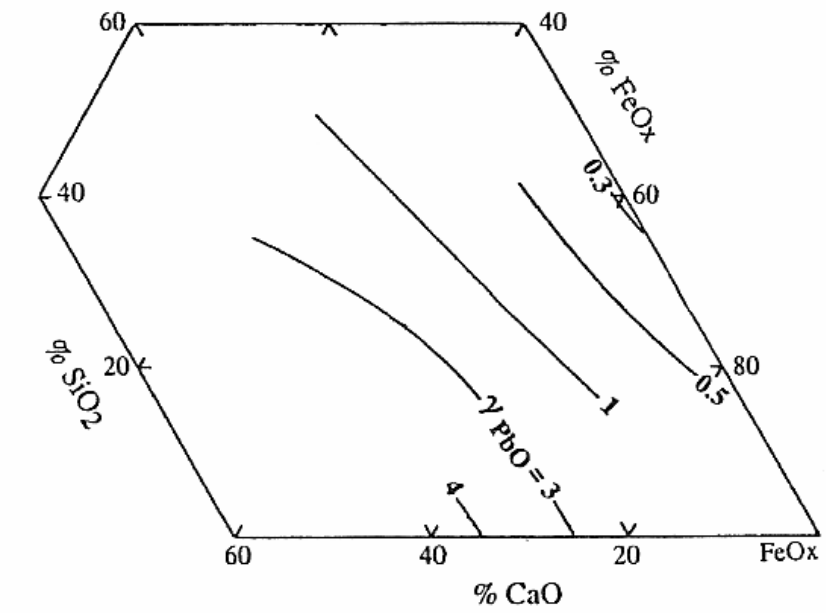

Figure 2.9.13: Activity coefficient of PbO (solid lines) in slag (Takeda and Yazawa, 1989)

In agreement with Takeda and Yazawa (1989) are the results on lead distribution by Vartiainen *et al.* (2003). Figure 2.9.14 illustrates the distribution coefficient of lead between slag and blister copper for iron silicate, calcium ferrite and FCS slag as a function of sulphur content in blister copper (i.e. as a function of oxygen partial pressure). Vartiainen *et al.* (2003) indicate that the lower the sulphur content in blister, the higher the oxygen partial pressure and the target sulphur content in blister copper set by the operators in the direct-to-blister flash smelting pilot plant testing is 0.1wt%. In general the distribution coefficient of lead between slag and blister is lower in the FCS slag than in iron silicate slag. The distribution coefficient of lead between calcium ferrite slag and blister copper is also given in Figure 2.9.14. In comparison with calcium ferrite slag, $L_{Pb}^{slag/Cu}$ for FCS slag is higher at the same oxygen partial pressure (i.e. the sulphur content), indicating a greater ability to remove lead from blister copper. It should be kept in mind that a comparison between the results from Takeda and Yazawa (1989) and Vartiainen *et al.* (2003) work cannot be made, as the experimental conditions and the ternary slag composition used by the two sets of investigators are different. Takeda and Yazawa's (1989) results are based on the oxygen partial pressure of 10^{-6} atm. and the oxygen partial pressure used by Vartiainen and co-authors (2003) for the pilot plant tests was highly oxidising, oxygen partial pressure of $10^{-4.74}$ atm. The FCS slag composition applied by Vartiainen *et al.* (2003) is situated in the 'neck' of the liquid region, as defined by Yazawa *et al.* (1999). The data presented by Takeda and Yazawa (1989) in Figure 2.9.13 is for various compositions within the FeO_x-CaO-SiO_2 system. This work was

compiled much earlier (1989) than when FCS slag was proposed for copper converting (1999) and hence gives an approximate value of γ_{PbO} in FCS slag. Nonetheless, even though the numerical data by Takeda and Yazawa (1989) and Vartiainen *et al.* (2003) cannot be compared, the general behaviour of the basic oxide in the three slags is in agreement with one another as well as with the thermodynamic predictions.

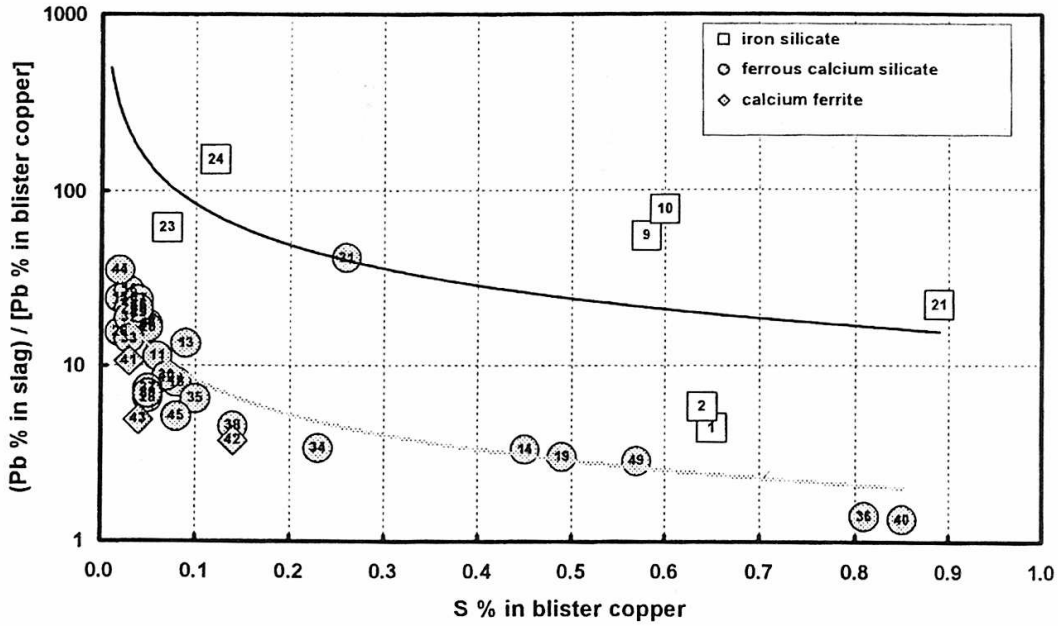

Figure 2.9.14: Distribution coefficient of Pb as a function of %S in blister copper. (Vartiainen, Kojo and Rojas, 2003)

Although a ternary diagram is not available for the AO-BO-MO system when MO is an acidic oxide, it is expected that the removal of acidic oxides such as arsenic and antimony with application of FCS slag will be similar to calcium ferrite slag but more superior to iron silicate slag. The activity coefficient data for the acidic arsenic oxide, as determined by Yazawa *et al.* (1999) is demonstrated in the ternary FeO_x-SiO_2-CaO slag in Figure 2.9.15, in order to support the predicted behaviour of acidic oxides in the three slags.

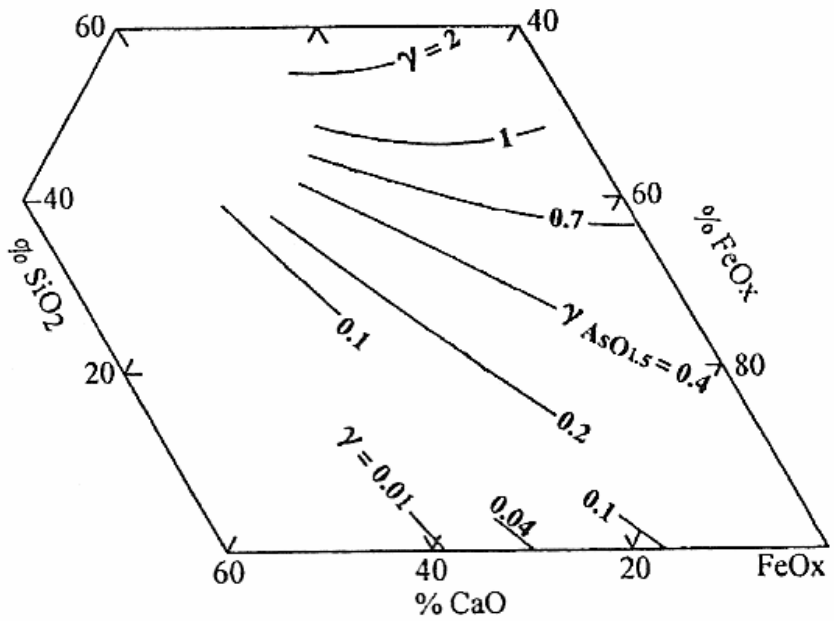

Figure 2.9.15: Activity coefficient of $AsO_{1.5}$ (solid lines) in slag (Yazawa, Takeda and Nakazawa, 1999)

As expected, the trends of γ_{PbO} and $\gamma_{AsO1.5}$ are opposite, such that γ_{PbO} increases from FeO_x-SiO_2 binary to FeO_x-CaO binary slags and for $\gamma_{AsO1.5}$ the opposite effect is observed and $\gamma_{AsO1.5}$ increases from FeO_x-CaO slag to FeO_x-SiO_2 slag. The $\gamma_{AsO1.5}$ in iron silicate slag is approximately 0.7-1 and for calcium ferrite slag $\gamma_{AsO1.5}$ is between 0.04 and 0.1, depending on the slag composition. In the area of ferrous calcium silicate slag, $\gamma_{AsO1.5}$ is estimated to be 0.1. Hence, as predicted, the removability of arsenic to FCS slag is similar to calcium ferrite slag but better than iron silicate slag.

Vartiainen *et al.* (2003) calculated the distribution coefficients of arsenic between slag and blister copper and the results are in agreement with Yazawa *et al.* (1999). The results for $L_{As}^{slag/Cu}$ are illustrated in Figure 2.9.16 for both FCS slag and iron silicate slag. Observations of Figure 2.9.16 indicate that the arsenic distribution coefficient between ferrous calcium silicate slag and blister copper is much higher than that of iron silicate slag. In ferrous calcium silicate slag the arsenic distribution coefficient increases with an increasing CaO/SiO_2 ratio in the slag. At a given Fe/SiO_2 ratio, when the CaO/SiO_2 ratio of the slag increases the distribution coefficient of arsenic, $L_{As}^{slag/Cu}$ increases.

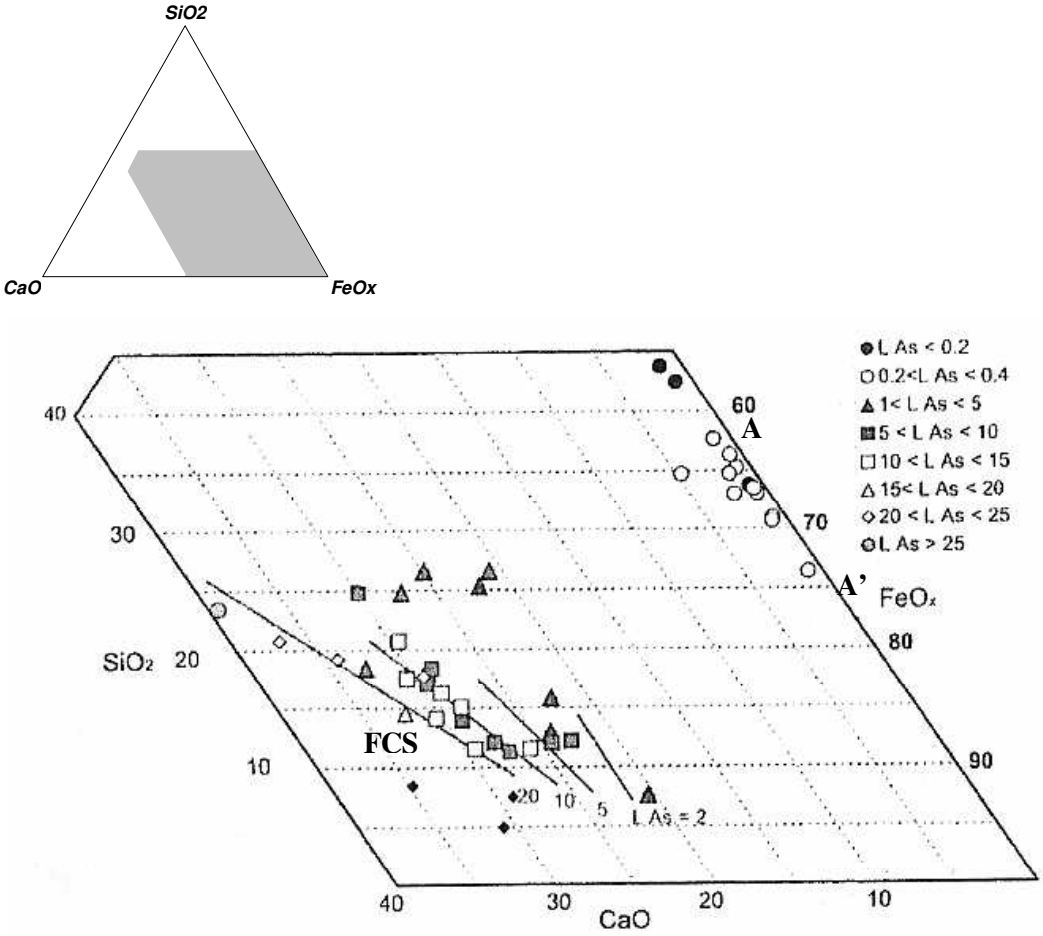

Figure 2.9.16: Distribution coefficient of As, $L_{As}^{slag/Cu}$, in FeO_x-SiO_2-CaO system at constant copper content in slag. AA' = Iron silicate slag (Vartiainen, Kojo and Rojas, 2003)

2.10 SUMMARY TO LITERATURE

Despite the significant potential of FCS slag for application in continuous copper converting operations, there is very limited knowledge on the slag. The phase equilibria and liquidus surface of FCS slag at 1300^{o}C and an oxygen partial pressure of 10^{-6} atm. has been reported, generated by the Flogen thermodynamic model. It was verified that within the FeO_x-CaO-SiO_2 slag system, when in equilibrium with copper, a homogenous liquid slag does exist in the region of high FeO_x, close to the dicalcium silicate saturation boundary. Yazawa *et al.* (1999) predicted that FCS slag has the potential to effectively remove acidic and basic oxides from blister copper, as well as a higher recovery to copper of elements with neutral oxides such as nickel and copper. However there is no experimental data on the distribution of minor elements between FCS slag and copper system under continuous converting conditions. There is a single study on the distribution of lead and arsenic between FCS slag and copper by Vartiainen *et al.* (2003), although it was conducted at an oxygen partial pressure of $10^{-4.74}$ atm. which is much more oxidizing than that experienced in continuous converting. This study supported the predictions that FCS slag would be superior to calcium ferrite slag in removing lead from copper and superior to iron silicate slag in removing arsenic from copper.

It has been stated by Takeda (2001) that FCS slag will be 'mild' on the magnesia-chrome refractories; however there are no experimental studies to support such a statement.

There is a clear need for an experimental study of FCS slag which will examine both:

- minor element distributions between the slag and copper under copper converting conditions,

- The extent of slag attack on magnesia-chrome refractories.

Thus, there is potential to study such topics in order to verify the applicability of FCS slag to continuous copper converting.

3.0 RESEARCH AIMS

This research project aims to determine and quantify the nature of the interactions between ferrous calcium silicate (FCS) slag and magnesia-chrome refractory bricks and to determine the distribution of antimony, lead and nickel, between FCS slag and copper under continuous copper converting conditions. The objectives of the research will be fulfilled by investigating the following questions, all at 1300^{o}C and an oxygen partial pressure of 10^{-6} atm.:

1. Does FCS slag attack magnesia-chrome refractories more or less aggressively than calcium ferrite slag?
2. What is the mechanism of the observed attack on the refractories?
3. How does the extent of slag attack vary with temperature?
4. What are the distribution ratios of antimony, lead and nickel between FCS slag and copper?
5. Are the observed distribution ratios in accord with thermodynamic predictions?

4.0 EXPERIMENTAL SECTION

4.1 INTRODUCTION

Two distinct types of experiments were employed to address the research questions outlined in Chapter 3. They are outlined below and discussed in detail in Section 4.5.

A) Slag/brick Experiments

These experiments were developed to address research questions 1-3 and involved placing FCS slag in small crucibles made from magnesia-chrome refractory at 1300^{o}C and at an oxygen partial pressure of 10^{-6} atm. for 8 hours. The experiments were repeated for 32 hours of contact time, keeping all other conditions constant, to observe the effects of time on the rate and extent of slag attack. All tests were repeated for the same conditions and for the same times using calcium ferrite slag for comparison. The experiments were also conducted at 1400^{o}C and an oxygen partial pressure of 10^{-6} atm. for 8 hours using FCS slag to determine how a change in temperature affects the nature and severity of the wear caused to the magnesia-chrome refractory. A more thorough explanation of the reasons for conducting the experiments at 1400^{o}C as well as at 32 hours is given in Chapter 5.1. After exposure to hot slag, the slag/refractory sample was sectioned and examined using QEM SEM (Quantitative Evaluation of Materials using Scanning Electron Microscopy) to determine:

- The general nature of any slag attack,
- The phases in the refractory that are attacked,
- Whether any phase transformations occurred and
- Whether or not new phases formed on the refractory/slag interface.

B) Minor Element Distribution Experiments

These experiments were conducted to answer research questions 4 and 5. They involved adding a small amount of a minor element oxide in FCS slag and equilibrating it with copper metal at 1300^{o}C and an oxygen partial pressure of 10^{-6} atm. for 4, 8 and 16 hours to determine if time is affecting the distribution results to ensure that equilibrium had been reached. The experiments were repeated by alloying the copper metal with a small amount of a minor element metal and equilibrating with FCS slag under the same conditions and experimental times to reach equilibrium from both directions. By conducting the experiments

from "both sides" it is possible to ensure that true equilibrium is reached. It is possible for distribution reactions which proceed very slowly to appear to be at equilibrium, when in fact they are not. Approaching experiments from both sides therefore eliminates this possibility. The oxides added to slag were lead oxide, representing basic oxides, antimony oxide representing acidic oxides and nickel oxide, representing neutral oxides. The metals alloyed with copper were therefore lead, antimony and nickel. The FCS slag and the copper were analysed using ICP-AES (Inductively Coupled Plasma Atomic Emission Spectrometry).

This chapter discusses all experiments in terms of the equipment and materials used, the experimental method employed, the analytical procedure for the sample analysis and the possible errors in both the experimental and analytical techniques used.

4.2 SCOPE & LIMITATIONS

The conditions employed in these experiments were largely influenced by those applicable to Kennecott flash converting. These conditions are also similar to those in the Mitsubishi converting process and thus the results of this research will also be relevant to the users of the Mitsubishi technology. Some limitations were experienced, including:

- *Temperature & Oxygen Partial Pressure:* Whilst the flash converting process operates at an oxygen partial pressure of approximately $10^{-5.5}$ atm. and 1250^{o}C, the experiments were conducted at an oxygen partial pressure of 10^{-6} atm. and 1300^{o}C for the reasons outlined below:

    1. The only phase equilibria data available for the FCS slag is a thermodynamic model at an oxygen partial pressure of 10^{-6} atm. and 1300^{o}C but is not reported for an oxygen partial pressure of $10^{-5.5}$ atm. and 1250^{o}C.
    2. The limited experimental data on minor element distribution that is available for FCS slag was determined at 1300^{o}C and an oxygen partial pressure of 10^{-6} atm. Most data on calcium ferrite slag is also at 1300^{o}C and an oxygen partial pressure of 10^{-6} atm.

- *Slag Composition:* There is limited experimental data on the dissolution of copper oxide in FCS slag, as detailed in Section 2.9. However, based on a thermodynamic model on the phase equilibrium of FCS slag, investigators have determined that the maximum dissolution of copper oxide in FCS slag at an oxygen partial pressure of 10^{-6} atm. and 1300^{o}C is approximately 10 wt% Cu_2O. Copper oxide (Cu_2O) was added to FCS slag in contact with the refractory to get a slag composition similar to that which would exist in equilibrium with copper. For the minor element distribution experiments, the Cu_2O content of the FCS slag was approximately 4 wt% prior to experiments as the slag was in contact with copper metal, allowing further dissolution to occur during experiments.

4.3 FURNACE SET-UP

The furnace set-up for both the slag/brick and minor element distributions was the same and so the description below addresses both types of experiments.

4.3.1 Experimental Apparatus

Figure 4.3.1 illustrates the vertical tube furnace used to carry out slag/brick and minor element distribution experiments and Figure 4.3.2 illustrates the experimental apparatus used. All the numbers shown in brackets in Figures 4.3.1 and 4.3.2 correspond to those in the following description.

The furnace (3) is heated by four silicon carbide resistance elements (6). The power to the elements is controlled by a Eurotherm 2400 series programmable digital auto-tune PID temperature controller. The temperature is sensed by Pt vs. Pt/13% Rh thermocouples. High Grade ceramic fibre insulation, commonly known at Kaowool (13), lines the inside of the furnace.

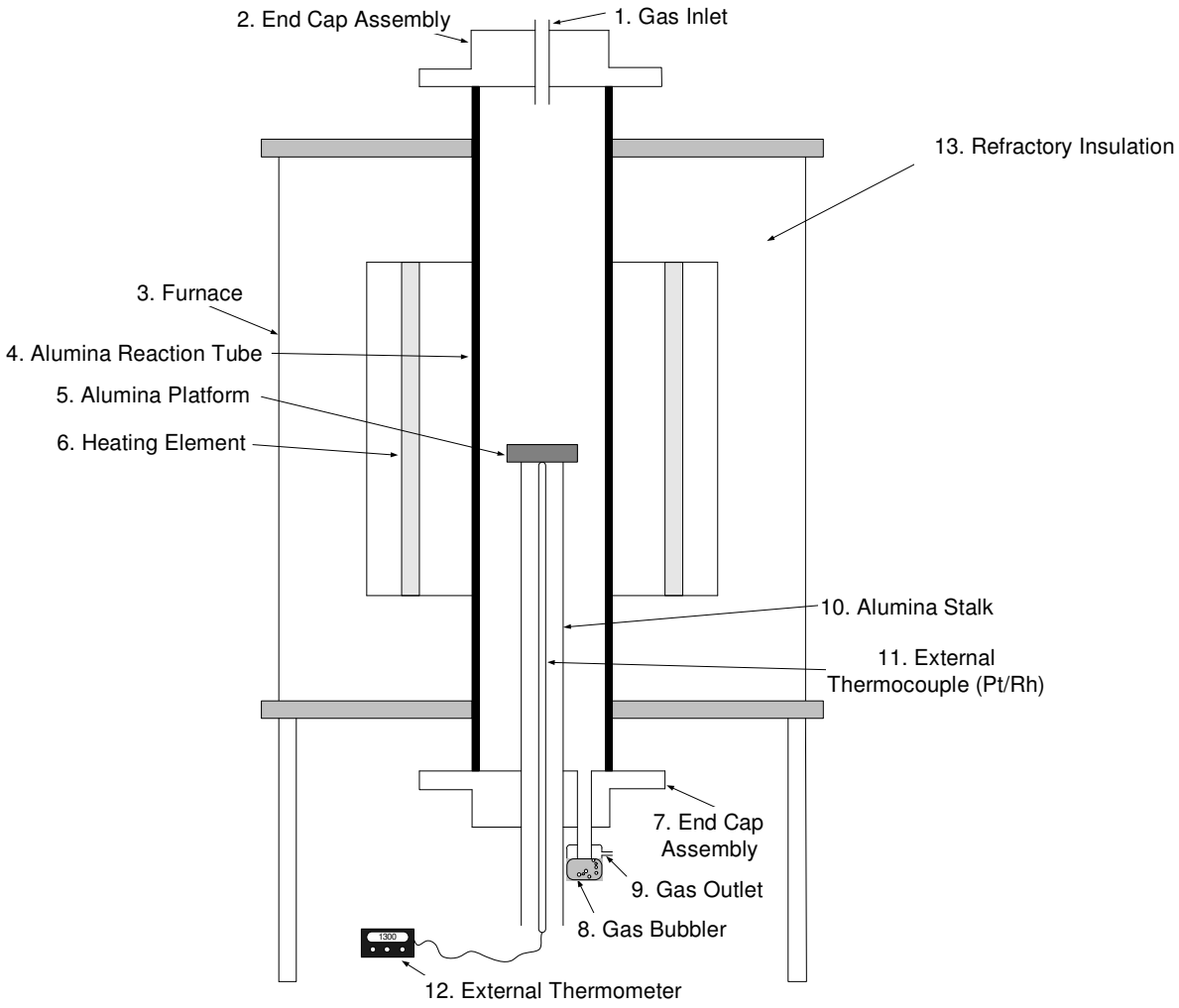

Figure 4.3.1: Vertical tube furnace used in the slag/brick and minor element distribution experiments.

An open-ended recrystallised alumina tube (4) runs vertically down the centre of the furnace. The dimensions of the tube are an outer diameter of 65mm, wall thickness of 3mm and a height of 1m. The open ends of the alumina tube were sealed with an end cap assembly (2 & 7) held in place with high temperature Viton o-rings. The gas is passed through the furnace via silicon tubing from the top (1) and exits from the bottom (9) however at the entry and exit ports, alumina tubes were used to allow gas to enter and exit the furnace. The entry points for the alumina tubes in the top and bottom end caps were also sealed with Viton o-rings. An alumina tube closed at the one end was used as a stalk to lift the sample from the bottom of the furnace (10). The closed end of the stalk holds the sample platform (5) which is also made of alumina cement and the open end is used to place a thermocouple (11) inside the furnace. The outlet gas was passed through a gas bubbler (8) containing di-n-butyl phthalate to prevent the back diffusion of oxygen from the atmosphere.

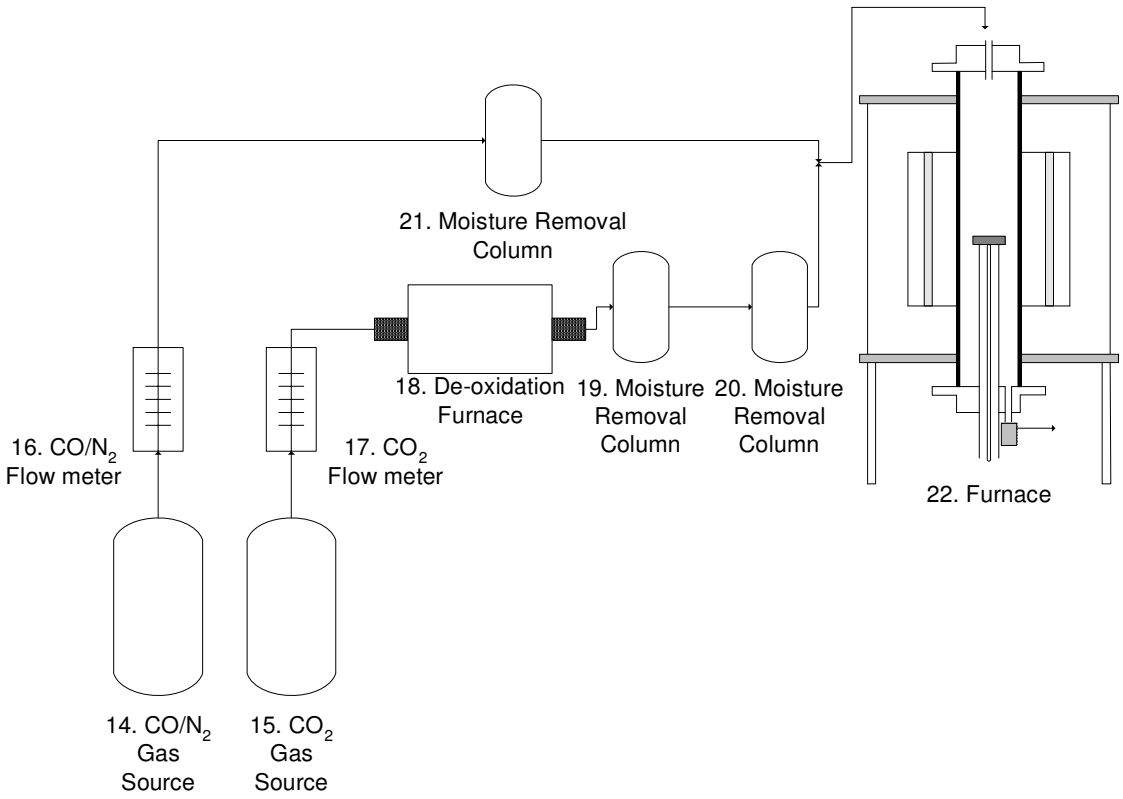

Figure 4.3.2: Experimental apparatus including gas sources, flow-meters, gas cleaning units and furnace

Prior to entering the furnace, the gases were cleaned to remove moisture and oxygen. The CO/N_2 gas was passed through a column of silica beads (21) and the CO_2 gas was passed through 3 successive cleaning columns as shown in Figure 4.3.2 as it was of food grade (i.e. 99.5% CO_2 with less than 100 vpm H_2O). The first column contained copper turnings heated to 600°C in a horizontal tube furnace (18) to remove most of the moisture and oxygen from the gas (Equation 4.3.1). The second and third columns consisted of silica gel (19) and anhydrous magnesium perchlorate (20), respectively, which removed any remaining traces of moisture.

$$2Cu + \frac{1}{2}O_2 = Cu_2O$$

$$\Delta G^o_{600^0C} = -105\,\text{kJ/mole} \qquad \textbf{Equation 4.3.1}$$

$$K_{600^0C} = 1.82 \times 10^6$$

Glass capillary flow-meters were used to control the flow rates of 5% CO/N_2 speciality gas (16) and CO_2 gas (17). A CO/N_2 gas mixture was used as the required flow-rate of CO was very small (5.53 cm^3/min when total flow rate of gas to furnace was 400 cm^3/min) and thus required a carrier gas. The gas flow-rate calculations are given in Appendix 1.

4.3.2 Hot Zone Calibration

The hot-zone calibration measurements were taken by placing a Pt vs. Pt 13% Rh thermocouple, which had marked 1cm increments, inside the alumina tube. The temperature was measured using an external thermometer (12). The furnace temperature was controlled at 1300°C and the thermocouple was moved incrementally along the length of the hot alumina tube and the temperature was measured at each increment. The hottest zone in the reaction area was found to exist at 49-52 cm from the bottom of the furnace tube. The maximum temperature that was achieved within this zone was 1277°C when the furnace internal thermocouple was measuring 1300°C and the hot-zone was at 1300°C when the internal thermocouple was measuring 1325°C. The temperature profile is illustrated in Figure 4.3.3.

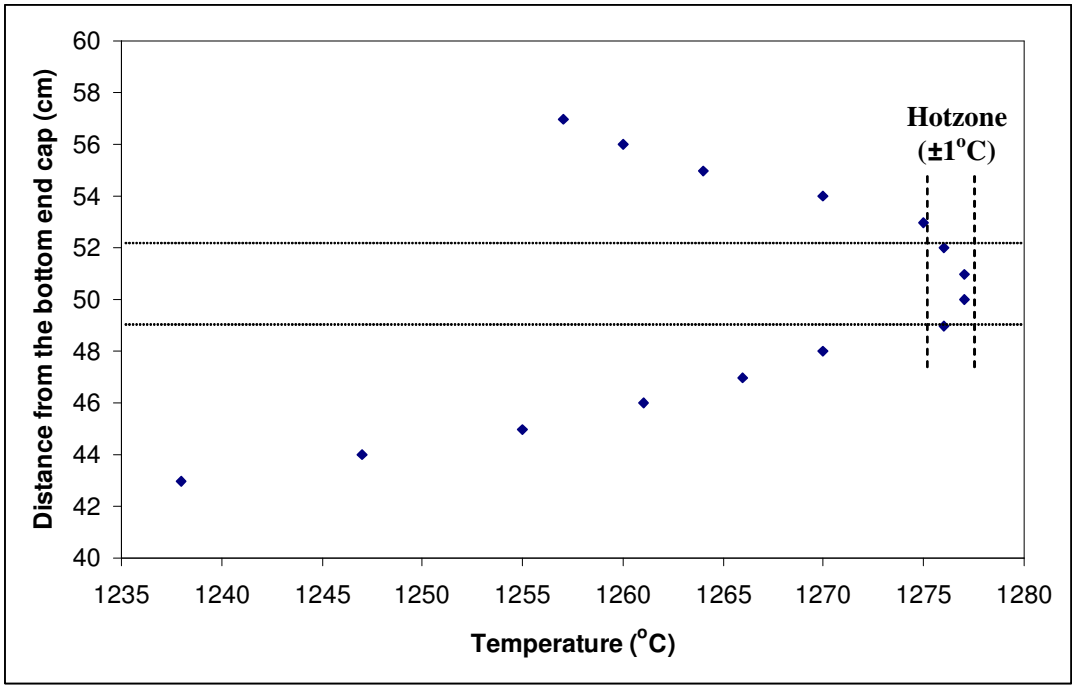

Figure 4.3.3: Temperature profile of the vertical tube furnace

4.3.3 Temperature Control

The furnace was fitted with two Pt vs. Pt 13% Rh thermocouples connected to the Eurotherm 2400 temperature controller. Both thermocouples are fitted outside the furnace tube, close to the heating elements. The furnace was also fitted with an external Pt vs. Pt 13% Rh thermocouple positioned inside the alumina platform stalk to accurately measure the temperature in the hot-zone and that of the sample.

4.3.4 Furnace Atmospheric Control

Due to the difference in the oxygen partial pressure inside the furnace during experiments (oxygen partial pressure of 10^{-6} atm.) and the oxygen content of the ambient atmosphere surrounding the furnace, which is approximately four orders of magnitude greater, there exists a considerable driving force for the back diffusion of oxygen when gases exit the furnace during experimentation. In order to prevent such oxygen back diffusion and isolate the reaction zone inside the furnace from the outside atmosphere, the gases were passed through a gas bubbler containing di-n-Butyl Phthalate (DBP, $C_6H_4(COO.C_4H_9)_2$) which has a very low vapour pressure (0.01 mm Hg at 20^{o}C).

All gas seals and tube connections were checked for tightness by placing soapy water on all the seals. If the soapy water bubbles at any seal, there is a leak present. For further confirmation, the gas exit port at the bubbler was sealed and the gas flow was switched off. The pressure inside the furnace was observed with a manometer and found not to decrease.

Once the seals around the furnace and the experimental train were inspected for gas tightness, an oxygen probe was installed into the furnace through the top end-cap to confirm that the oxygen partial pressure inside the furnace at 1300^{o}C was 10^{-6} atm. The insertion point of the oxygen-probe into the top end-cap was sealed using Viton o-rings to ensure a gas tight seal. The specifications of the probe are detailed in Appendix 2.

Following installation of the oxygen probe, the furnace was heated to 1300^{o}C and the CO/N_2 and CO_2 gases were supplied to the furnace at the flow rates established previously. An external thermocouple was also connected to the furnace from the bottom end-cap as described previously to measure the temperature inside the furnace tube. The furnace was left

running for 1 hour once the furnace temperature reached 1325°C and the temperature measured from the external thermocouple reached 1300°C at the hot-zone. The EMF voltage recorded from the voltmeter was measured at 413 mV giving an oxygen partial pressure of 1.06×10^{-6} atm. The oxygen partial pressure inside the furnace was continuously measured throughout the slag/brick and minor element distribution experiments to ensure no major fluctuations in conditions occurred. The EMF readings varied between 413 to 417 mV throughout all measurements taken by the oxygen probe, that is, the oxygen partial pressure fluctuated between 9.46×10^{-7} atm. to 1.06×10^{-6} atm. inside the furnace. The measured oxygen partial pressure is within the error band of the expected oxygen partial pressure given the errors in all variables that affect oxygen partial pressure. The related errors in oxygen partial pressure measurements are discussed in Section 4.7.

4.4 MATERIALS

4.4.1 Slag

The composition of FCS slag was calculated on the basis of a slag Fe/SiO_2 ratio of 2.3 and CaO content between 20 to 30wt%. For the slag/brick experiments, approximately 10 wt% copper oxide was added to the slag as no copper was present during experiments for slag/metal equilibration. In the case of the distribution experiments, 4wt% Cu_2O was added to the slag, allowing further dissolution to occur during experiments. As discussed in Section 2.9, when FCS slag and copper metal are at equilibrium at an oxygen partial pressure of 10^{-6} atm. and 1300°C, the copper oxide content in slag is approximately 10wt%. In case of the distribution experiments, small amounts (1-1.5 wt%) of each minor element oxide (NiO, PbO, $SbO_{1.5}$) were added to separate samples of FCS slags for equilibration with copper. The amount of the element oxide added to slag was assumed to be within its saturation limits in FCS slag as discussed in the next section. Two master slags of varying CaO composition were used for the slag/brick experiments in order to determine whether slag composition had an effect on refractory wear. Since FCS slag is located near the dicalcium silicate surface, a CaO content close to the dicalcium silicate boundary was selected. The second slag composition had a CaO composition midway between the magnetite and Ca_2SiO_4 saturation boundaries. The Fe/SiO_2 ratio is both cases was kept constant at 2.3. For both slag/brick and minor element distribution experiments, the master slags were prepared from $CaCO_3$, which was calcined in a muffle furnace at 1000°C in air for 5 hrs, SiO_2, produced by grinding silica glass

and AR-grade Fe_2O_3 and Cu_2O. Appropriate amounts of each were ground together to mix them, then packed in a magnesia crucible. The FCS slag was then melted for a total of 8 hours at 1300^oC and oxygen partial pressure of 10^{-6} atm. in the tube furnace. The slag was initially held at 1000^oC for 3 hours to allow the slag to equilibrate with the atmosphere whilst in a solid state and was then heated at 1300^oC for 5 hours. The slag sample was lowered to the cool zone and cooled in a $CO_2/CO/N_2$ atmosphere for 10 minutes following the melting time, and then was cooled in air to 25^oC. The heating curve for preparation of the master slags in shown in Figure 4.4.1.

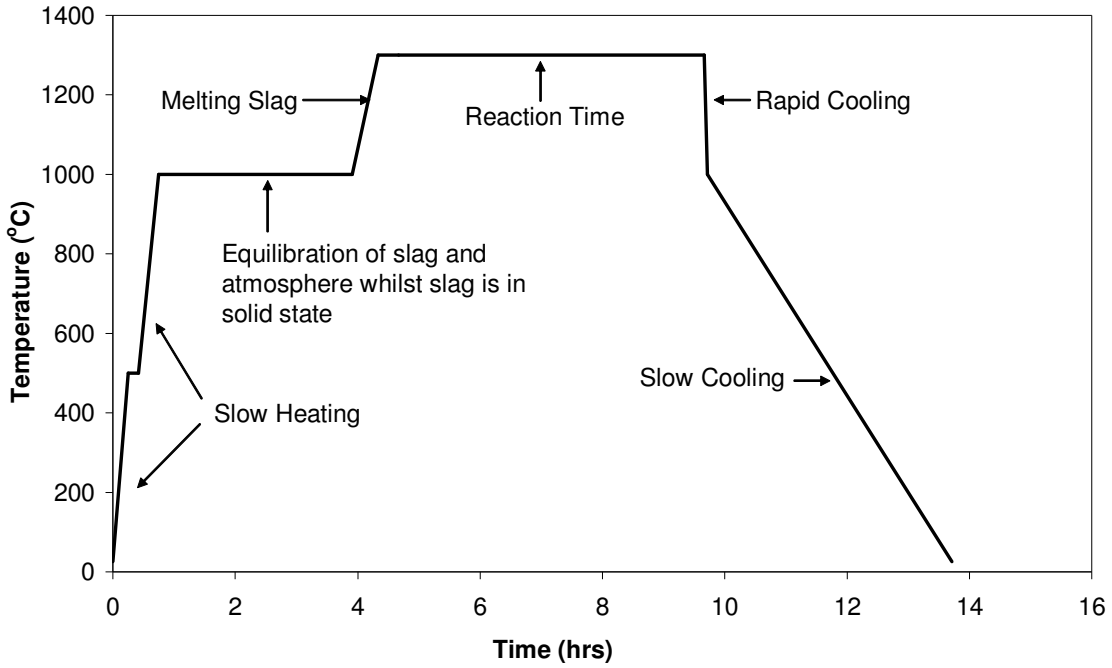

Figure 4.4.1: Heating curve for master slag preparation

The cooled slag was removed from the crucible, ground using a ring grinder and mixed to ensure homogeneity. The slag composition was analysed using the ICP-AES analysis technique and titrations were used to determine the ferrous iron (Fe^{2+}) content. The composition of the slag is shown in Table 4.4.1 and Figure 4.4.2. The solubility of magnesia in FCS slag at 1300^oC and an oxygen partial pressure of 10^{-6} atm. is not reported in literature; however analysis of the slag does indicate very minor dissolution of the magnesia crucible containing the slag melt.

Table 4.4.1: Slag composition used in both slag/brick and minor element distribution experiments

	$Fe_{(T)}$	Fe^{2+}	CaO	SiO_2	MgO	Cu_2O	Sb_2O_3	PbO	NiO
FCS Slag									
MS-21 (incl. $SbO_{1.5}$)	35.0	9.4	26.7	18.6	0.6	3.5	1.48		
MS-22 (incl. PbO)	35.1	9.8	26.2	17.6	0.9	3.6		1.22	
MS-23 (incl. NiO)	33.7	9.3	28.0	18.0	0.4	3.5			1.04
MS-24 (element free)	36.6	14.0	24.1	18.7	1.3	4.1	-	-	-
MS-4 (slag/brick)	35.9	10.5	23.1	16.4	0.9	9.8	-	-	-
MS-5 (slag/brick)	32.9	9.3	27.3	15.0	1.8	9.8	-	-	-
Calcium Ferrite Slag									
MS-CF	46.7	-	17	-	1.2	15.1	-	-	-

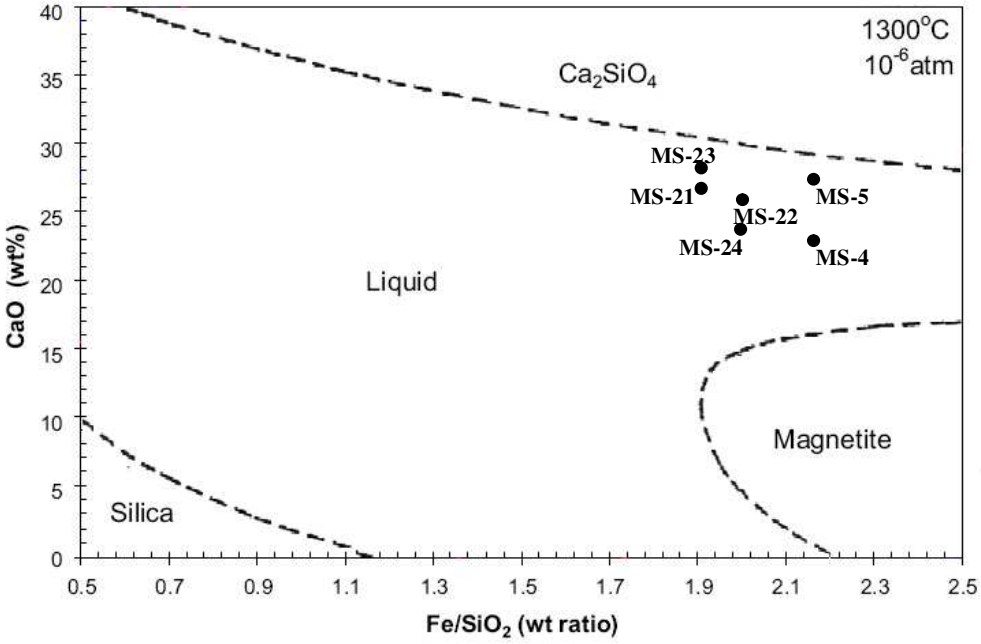

Figure 4.4.2: Liquid region of FeO_x-SiO_2-CaO slag with 10% Cu_2O at 1300°C and an oxygen partial pressure of 10^{-6} atm with experimental slag compositions (Kongoli, McBow and Yazawa, 2006).

Calcium ferrite slag was produced using calcined $CaCO_3$, Fe_2O_3 and Cu_2O heated in a magnesia crucible in a CO_2 atmosphere at 1300°C inside a muffle furnace for 4 hours. Following the melting time, the slag was removed from the crucible and ground in a ring grinder to achieve intimate mixing. Magnesia crucibles are well known in literature to be attacked by calcium ferrite slag and thus to minimise attack of the crucible and the amount of magnesia dissolved in the slag, the slag was heated for 4 hours rather than the 8 hours used for FCS slag. The ferrite slag composition was also analysed using ICP-AES analysis. The composition of calcium ferrite slag is also shown in Table 4.4.1 (MS-CF).

4.4.2 Saturation of NiO, PbO and $SbO_{1.5}$ in FCS slag

If the amount of oxide added to the slag exceeds its saturation limits, it affects the reliability of the distribution data. The oxide which does dissolve takes part in distribution behaviour, but that which does not dissolve mostly remains in the slag. When the slag is analysed by wet chemical methods the reported analysis for the metal in slag will be comprised of both the dissolved and the undissolved oxide. This therefore systematically biases the distribution ratio in favour of the slag. Distribution data affected by saturation effects cannot be accepted as reliable. Grimsey *et al.* (1976), found nickel solubility of up to 10 wt% (13wt% NiO) in silica saturated iron silicate slag at 1300°C and an oxygen partial pressure of 10^{-7} atm. They found the solubility of nickel to increase with increasing oxygen partial pressure and thus it is expected that at the desired experimental conditions in the current research, that is, 1300°C and an oxygen partial pressure of 10^{-6} atm., nickel solubility in slag will be higher. Based on this and the expected thermodynamic prediction that the dissolution of nickel oxide in both the iron silicate and FCS slag is similar, the amount of NiO (>1.5 wt%) added to FCS master slag samples should be well within the saturation limits. Takeda *et al.* (1984) and Eerola *et al.*, (1984) added approximately 1.5wt% nickel oxide to slag and did not report saturation issues. No data on the saturation limits of antimony and lead in FCS slag were found in the literature. Takeda *et al.* (1984), Eerola *et al.* (1984), Takeda *et al.* (1983) and Acuna and Yazawa (1987) and Kim and Sohn (1991), who all studied the distribution of lead and antimony in calcium ferrite slag at 1250°C and an oxygen partial pressure of 10^{-6} atm., added approximately 1.5 wt% of lead oxide and antimony oxide, respectively, in slag and did not report any saturation issues. Therefore the amount of PbO or $SbO_{1.5}$ added to FCS slag master samples was kept below 1.5 wt%.

4.4.3 Metal

Small amounts (1.2 – 1.4 wt%) of nickel, lead and antimony were alloyed with separate samples of copper for equilibration with FCS slag free of minor elements in the distribution experiments to reach equilibrium from both the metal and slag phases.

4.4.4 Refractory Brick

The slag was held in a crucible made from Radex DB-605 direct bonded magnesia-chrome refractory brick. The refractory was cut into a cylinder using a diamond tipped core drill of dimensions: 21mm OH x 12 mm OD. A 16mm IH x 5mm ID hole was then drilled into the sectioned brick using a 5mm silicon-carbide drill bit (Figure 4.4.2). Larger crucibles of dimensions 29mm OH x 18mm OD with 4mm wall thickness were made from the refractory brick in order to ensure that a slag/brick interface remained for inspections following experiments when both 32 hours contact time and a temperature of 1400^{o}C were used. After cutting, the brick crucibles were ultrasonically cleaned for 1 hour to remove any small detached particles and dried for 2 hours at 60^{o}C.

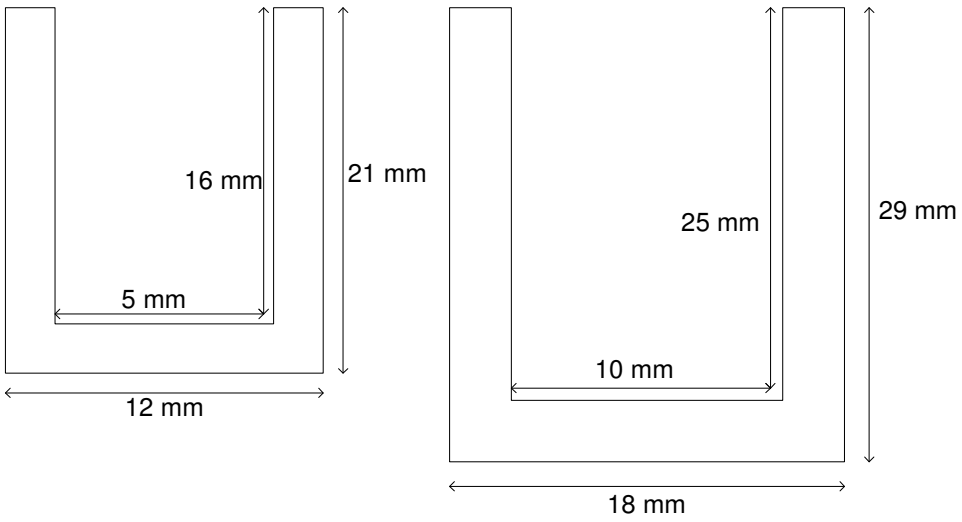

Figure 4.4.3: Dimensions of the magnesia-chrome refractory crucibles used in the slag/brick experiments (not to scale).

4.5 EXPERIMENTAL PROCEDURE

4.5.1 Slag/Brick Experiments

The slag was held in a crucible made from Radex DB-605 refractory brick and it was placed inside a magnesia crucible to contain any slag which may penetrate through the brick crucible during experimentation.

A mass of 1 gram of FCS slag for the 8 hour experiments and 5 grams of slag for the 32 hours and 1400^{o}C experiments were measured using an electronic balance to ±0.001 grams, and packed in the refractory crucibles and placed inside the magnesia crucible. The sample was then raised into the hot zone of the furnace. After the sample was position in the hot-zone, the end-cap assembly as well as the connecting silicon tubing to the bubbler were sealed. The sample was then slowly heated to 1300^{o}C to restrict thermal shock damage to the refractory and magnesia crucibles, the furnace and its components. The heating curve is illustrated in Figure 4.5.1. At the end of the experimental times, the sample was lowered from the furnace hot zone and rapidly cooled to 1000^{o}C in a $CO_2/CO/N_2$ atmosphere, such that the slag was fully solid. From 1000^{o}C, the sample was cooled slowly to 25^{o}C in air to avoid thermal shock damage of the furnace components and the brick crucible. Once the furnace was cooled to 25^{o}C, the sample was removed from the furnace and sectioned for analysis.

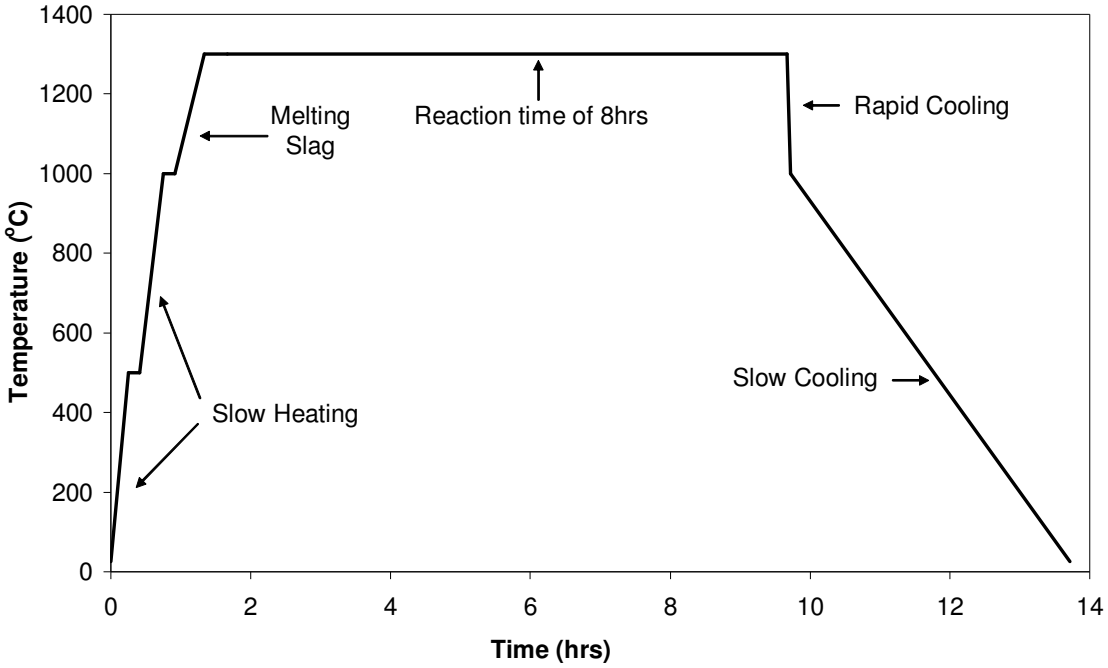

Figure 4.5.1: Heating curve for the slag/brick and minor element distribution experiments

The experiments were repeated using the above technique and under the same conditions using calcium ferrite slag for 8 and 32 hours for comparison with FCS slag. The experimental conditions for each experiment are listed in Table 4.5.1.

Table 4.5.1: The experimental conditions of slag/brick experiments

EXPERIMENT	TEMPERATURE (^{O}C)	OXYGEN PARTIAL PRESSURE (ATM)	EXPERIMENT TIME (HOURS)	SLAG COMPOSITION
SB-4	1300	10^{-6}	8	MS-4
SB-5	1300	10^{-6}	8	MS-5
SB-12	1300	10^{-6}	8	MS-CF
SB-14	1300	10^{-6}	32	MS-5
SB-15	1300	10^{-6}	32	MS-CF
SB-1400	1400	10^{-6}	8	MS-5

4.5.2 Minor Element Distribution Experiments

The arrangement of the crucible within the furnace is shown in Figure 4.5.2. The magnesia crucible containing the FCS slag and copper was covered with an inverted alumina crucible to minimise volatilisation losses, which were expected to be an issue with the samples containing lead and antimony.

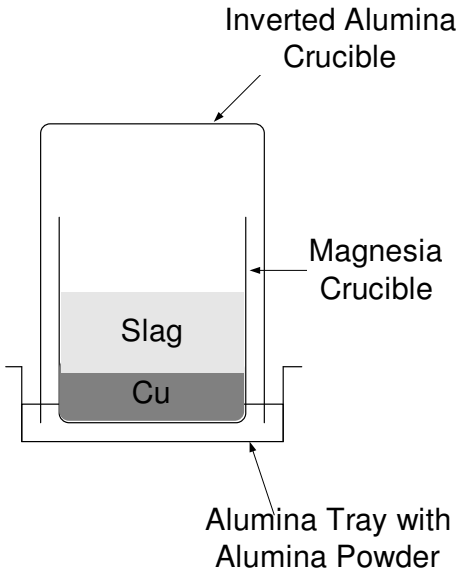

Figure 4.5.2: Arrangement of the crucible for the minor element distribution experiments

A mass of 5 grams of FCS slag and 7 grams of copper were measured to ±0.001 grams and placed in a magnesia crucible, covered with an alumina crucible then raised into the hot zone of the furnace. The sample was slowly heated to 1300^{o}C to restricted thermal shock damaged to the magnesia crucible, the furnace and its components. The heating curve is similar to the slag/brick experiments (Figure 4.5.1) however the reaction time varies according to the minor element distribution equilibration times of 4, 8 and 16 hours. After the required equilibration time, the crucible was quickly lowered into the cool zone of the furnace for rapid cooling. The sample was cooled to room temperature in a $CO_2/CO/N_2$ atmosphere for 10 minutes following the equilibration time, and then was cooled in air. Once the furnace was cooled to 25^{o}C, the sample was removed from the furnace and broken up to recover copper and slag. The copper was cleaned using a rotary sander and the slag was ground in a ring grinder. The slag and the copper were analysed using ICP-AES.

4.6 ANALYSIS OF SAMPLE

4.6.1 Slag/brick Experiments

Following the completion of the experiments, the slag/brick crucible samples were sectioned using a diamond saw as shown in Figure 4.6.1.

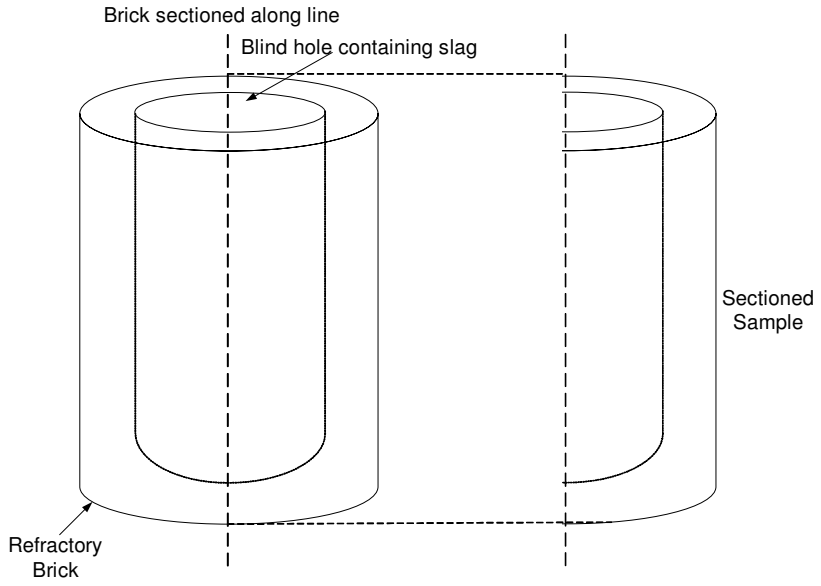

Figure 4.6.1: Sectioning of the slag/brick sample

The samples were then ultrasonically cleaned for 1 hour to remove any particles and residue left within the pores of the sample and dried at 60^{o}C for 1 hour. One of the sample halves was cast in epoxy resin under a vacuum. Once the resin had cured, the sample was polished to 1μm using a diamond impregnated polishing pad. The sample was polished to attain a suitable surface for the Scanning electron microscopy (SEM). Compositional analysis on the sample was performed using EDS (Electron Dispersive Spectroscopy). The elemental composition of the sample was measured via point scans and along a line. In a line scan analysis, the SEM electron beam is scanned along a preselected line across the sample while x-rays are detected for discrete positions along the line. Analysis of the x-ray energy spectrum at each position provides plots of the relative elemental concentration for each element versus position along the line.

4.6.2 Minor element distribution Experiments

All samples were analysed using an Inductively Coupled Plasma - Atomic Emission Spectrometer. The slag samples were analyzed for total iron, calcium, silicon and copper as well as for the minor elements antimony, nickel and lead whilst the metal samples were analyzed for copper, antimony, nickel and lead. The slags were dissolved using the borate fusion technique whereas the metal samples were dissolved using mixed acid digestion with a mixture of HNO_3, HF and $HClO_4$. The ferrous iron content of the slags were determined using wet chemical analysis, which involved mixing the sample in sodium carbonate and digesting in hydrochloric acid in an inert atmosphere. The mixture was then titrated using potassium dichromate ($K_2Cr_2O_7$) standard solution and a sodium diphenylamine-4-sulfonic acid indicator solution.

4.7 ERROR ANALYSIS

An error analysis is required for the minor element distribution experiments as relative error encountered during experiments affects accuracy of the distribution data. The main sources of error during experiments are fluctuations in experimental temperature and oxygen partial pressure measurements as well as the error in the analytical technique used for chemical analysis. According to Equation 4.7.1, the distribution of an element X between slag and metal is effected by K, which is a function of temperature, oxygen partial pressure and slag and metal composition. Thus uncertainties in temperature, oxygen partial pressure and chemical analysis measurements will affect the accuracy of the distribution data.

$$L_X^{s/m} = \frac{(\%X)}{[\%X]} = \frac{K_1(n_T)[\gamma_X]p_{O2}^{\nu/2}}{[n_T](\gamma_{XO\nu})} \qquad \textbf{Equation 4.7.1}$$

4.7.1 Furnace Temperature

A 4cm long hot-zone was found in the furnace with temperature variation of 1°C during the hot-zone calibration experiments. The temperature recorded by the external thermocouple during experiments fluctuated by ± 3°C. Using the Gibbs free energy data for Sb_2O_3, PbO and NiO, the relative error caused by temperature uncertainty in the slag/metal

distribution calculations was approximated. For the oxidation reactions of $Sb/SbO_{1.5}$, Pb/PbO and Ni/NiO, the respective values of equilibrium constant (K) within the temperature range of 1300 ± 3°C are given in Table 4.7.1 along with the variation of the equilibrium constant with the temperature range (i.e. relative error as a result of temperature uncertainty).

Table 4.7.1: Equilibrium constant (K) within the temperature range of 1300 ± 3°C for oxidation reactions of $Sb/SbO_{1.5}$, Pb/PbO and Ni/NiO.

Reactions	Equilibrium constant (K) with temperature fluctuations of 1300 ± 3°C			Relative Error (%)
	1297°C	1300°C	1303°C	
$Sb + \frac{3}{4}O_2(g) = SbO_{1.5}$	5.386×10^4	5.115×10^4	4.859×10^4	± 5.15
$Ni + \frac{1}{2}O_2(g) = NiO$	2.063×10^3	1.994×10^3	1.928×10^3	± 3.38
$Pb + \frac{1}{2}O_2(g) = PbO$	2.913×10^2	2.836×10^2	2.762×10^2	± 2.66

4.7.2 Gas Composition

The CO_2 and CO/N_2 gas flow-rates calculated in Section 4.3 were calibrated individually using a 100 cm^3 capacity bubble flow meter. The time required in seconds for 100cm^3 of each gas to pass through the bubble flow-meter was calculated using Equation 4.7.2.

$$t = 60\frac{100}{V} \qquad \textbf{Equation 4.7.2}$$

where t is the time in seconds and V is the total flow-rate of each gas in cm^3/min.

The required times for CO_2 and CO/N_2 gases to flow through the bubble flow-meter are given in Table 4.7.2. Also given in Table 4.7.2 are the total gas flow-rates necessary to obtain an oxygen partial pressure of 10^{-6} atm. at 1300°C. The bubble flow meter has a quoted error of ± 0.2 cm^3 (± 0.2%). The readings taken from the bubble flow meter scales had an error of ± 0.2 cm^3 (± 0.2%) whilst the relative error in the time readings using repeat trails was ± 0.22 sec (± 0.22%). The gas flow-rates were controlled using U-tube manometers using pressure difference as a control mechanism. The flow to the U-tube manometers was controlled using flow meters. The error in the flow-meters was ± 0.3% whilst the error in the

U-tube readings was ± 0.2mm (± 0.2%). The total relative error in measuring the flow-rate of each gas was ± 1.12% (± 2.24% in total).

Table 4.7.2: The flow-rates of CO_2 and CO/N_2 required for an oxygen partial pressure of 10^{-6} atm at 1300°C as well as the bubble flow meter times in seconds.

Gas	Gas flow-rate at 1300°C and 10^{-6} atm	Time (sec) taken for a 100cm^3 of gas to flow
CO_2	394.49 cm^3/min	15.21 sec
CO/N_2	110.13 cm^3/min	54.48 sec

The relative error in the oxygen partial pressure measurements was calculated by firstly using the total relative error in the gas flow-rate measurements (± 1.12%) to determine the fluctuations in the required gas flow-rates. The flow-rates were then used in the gas flow-rates calculations (Section 4.3) to determine the adjusted oxygen partial pressure once error in the gas flow-rates was accounted for. The relative error calculated in the oxygen partial pressure measurements is ± 4.95%.

When comparing to the fluctuations in oxygen partial pressure measured using the oxygen probe, the calculated relative error is in excellent agreement. As mentioned previously, the oxygen partial pressure measured using the oxygen probe varied between 9.46 x 10^{-7} atm. to 1.06 x 10^{-6} atm. and according to the relative percent error calculated, the oxygen partial pressure varied between 9.50 x 10^{-7} atm. to 1.05 x 10^{-6} atm.

4.7.3 Slag & Alloy Composition

The error in the ICP-AES analysis technique used by Spectrometer Services was ± 5% relative for the analysis of Sb_2O_3, PbO and NiO content in slag as well as for the content of antimony, lead and nickel in the metal phase. For all other components of slag (Fe, SiO_2, CaO and Cu_2O) the relative error in analysis was ± 3%. The higher error in the analysis of the minor elements in both the slag and metal phases is a result of the low contents of the elements in both phases.

5.0 RESULTS & DISCUSSION

5.1 BRICK WEAR EXPERIMENTS

5.1.1 Virgin Magnesia-Chrome Refractory

A detailed discussion on the phases present in magnesia-chrome direct-bonded refractories is given in Chapter 2.4. In order to observe and confirm the microstructure of the refractory brick to be used in this research, the samples of the virgin brick were examined using SEM (Scanning Electron Microscope) backscattered electron (BSE) imaging. The BSE images use a greyscale to reflect the average atomic weight of each microscopic volume irradiated by the electron beam. The compositions of the phases within the refractory prior to experimentation were determined using EDX (Energy Dispersive X-ray) analysis. The analysis consisted of many point scans of the various phases within the brick, to compile an average composition for each phase. As detailed in Section 2.4, the microstructure of a virgin magnesia-chrome direct-bonded refractory consists of two phases, the periclase and the chromite spinel, which are essentially MgO and Cr_2O_3, respectively, with minor amounts of Al_2O_3, Fe_2O_3, CaO and SiO_2 impurities. The major impurities in the bricks are Fe_2O_3 and to a lesser extent Al_2O_3.

The BSE images in Figures 5.1.1-5.1.3 reveal three distinguishable features. The dark-grey coloured phase was shown by EDX analysis to be periclase, the light-grey coloured phase to be chromite-spinel and the black coloured features of the images are voids. Three types of chromite spinel grains are also evident in Figures 5.1.1-5.1.3. In descending order of size they are primary, secondary and exsolved chromite spinel phases. As was observed in Section 2.4, and confirmed here, within the brick's matrix, there is direct bonding between:

- Primary and secondary chromite grains with the periclase grains
- Chromite-chromite grains and
- Periclase-periclase grains.

The direct-bonded refractory also has a significant amount of voidage as shown in Figures 5.1.1-5.1.3. From the general observations of the microstructure shown in Figures 5.1.1-5.1.3, it has been deduced that the pore structure within the direct-bonded magnesia-chrome brick is open. This was also found by Fahey (2002) when studying the microstructure of the same refractory brick (Radex DB-605).

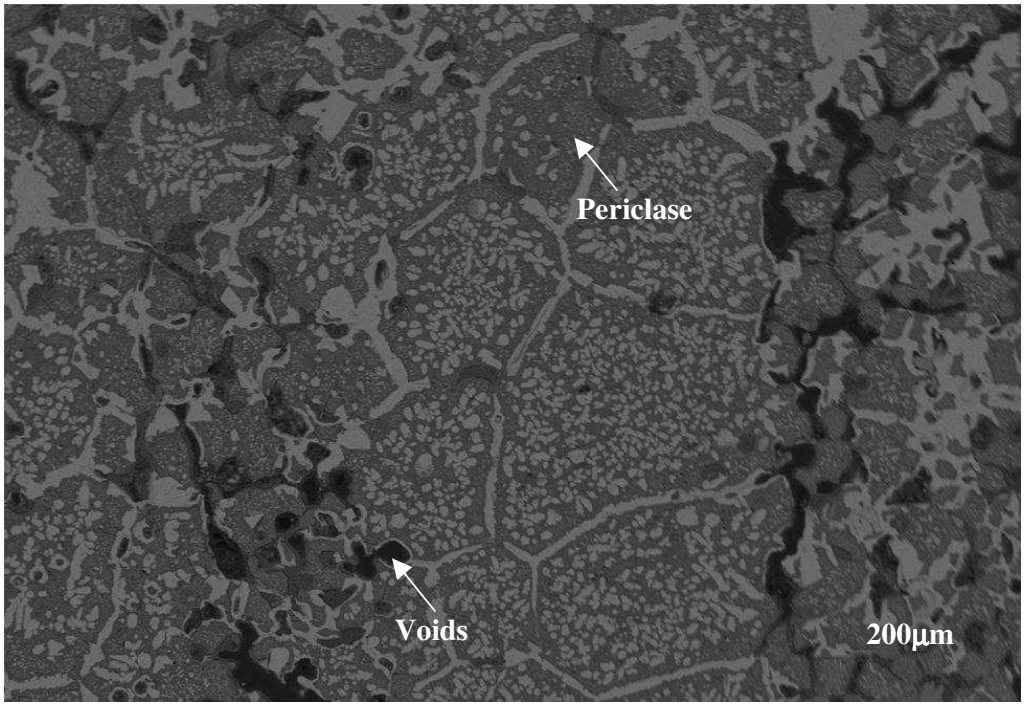

Figure 5.1.1: SEM backscattered electron image showing the periclase phase (dark grey) in a direct-bonded magnesia-chrome refractory brick

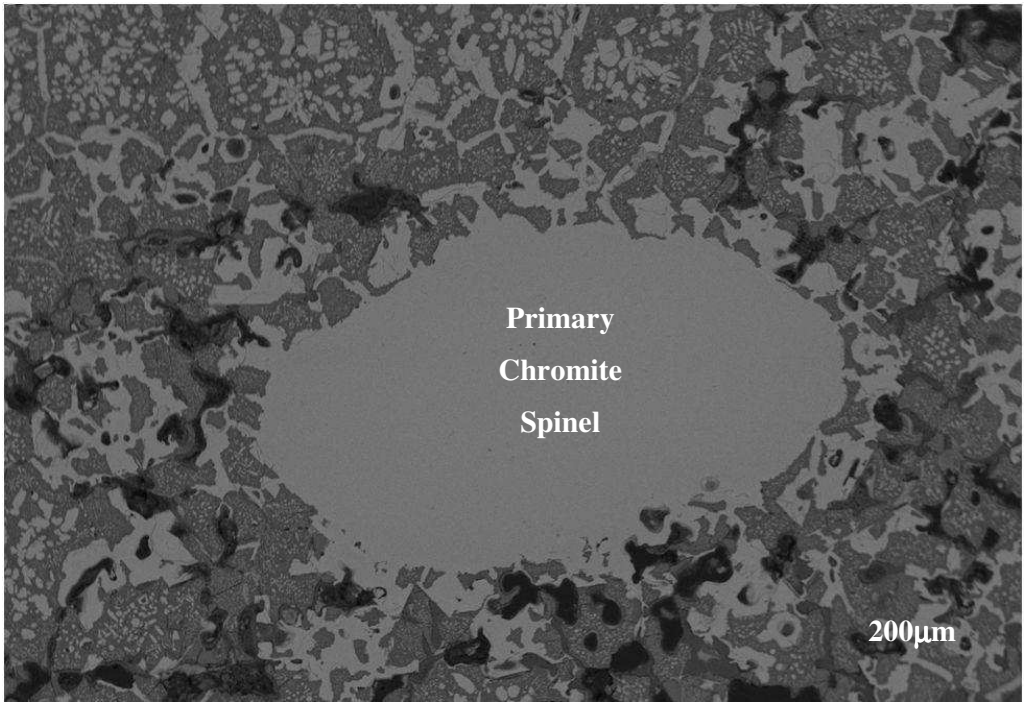

Figure 5.1.2: SEM backscattered electron image showing the primary chromite-spinel phase in a direct-bonded magnesia-chrome brick

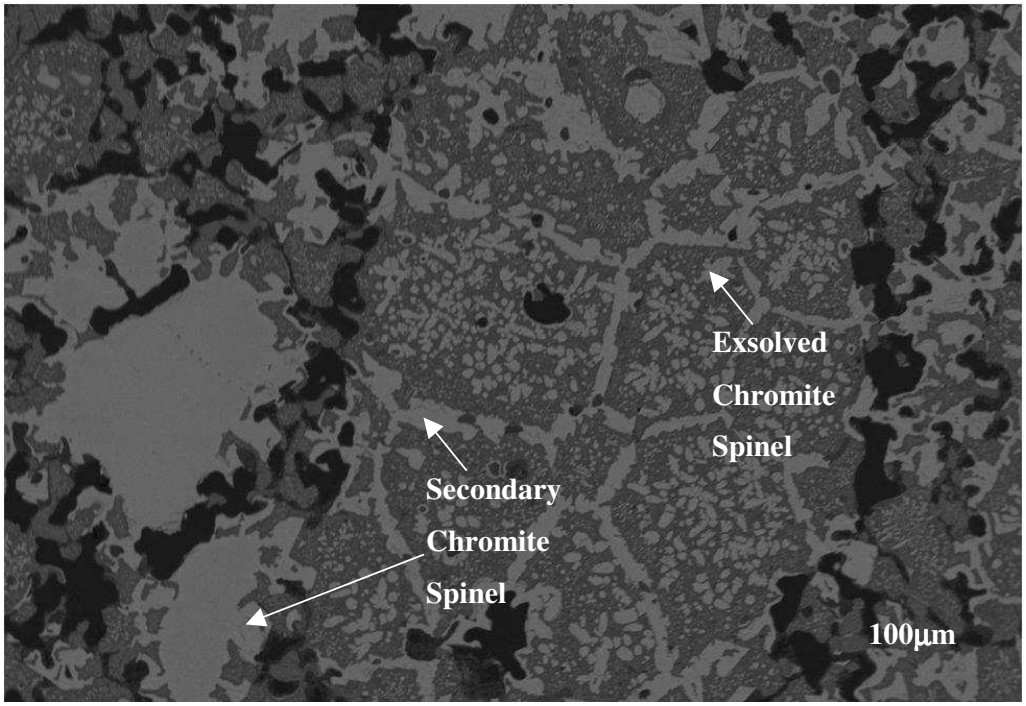

Figure 5.1.3: SEM backscattered electron image showing the secondary and exsolved chromite-spinel phase in a direct-boned magnesia-chrome brick

The composition of the periclase and chromite spinel phases in the unreacted magnesia-chrome refractory was measured using EDX analysis, in order to be able to compare the virgin refractory with the contacted sample and determine whether significant changes in composition resulted in either phase as a result of the interactions between species in the slag and the brick. The following two sections give the composition of the periclase and chromite spinel phases in the virgin magnesia-chrome refractory.

A) Periclase

The analysis consisted of several EDX point scans of the periclase grains, taking care to avoid chromite spinel inclusions. The point compositions were very similar and the average weight percent composition of periclase is illustrated in Table 5.1.1. The results are also reported as mole percent in order to determine the mole ratio of magnesium to oxygen. The phase is seen to consist essentially of magnesium and oxygen with minor amounts of iron and chromium and trace amounts of aluminium, silicon and calcium. Fahey (2002) found the mole ratio of magnesium to oxygen to be 0.96 with the presence of aluminium, iron and chromium as minor impurities, accounting for the shortfall of moles of magnesium compared to moles of oxygen. However the present results indicate a lower magnesium to oxygen ratio of 0.91 with

higher amounts of iron, aluminium and chromium than suggested by Fahey (2002) as well as the presence of calcium and silicon in trace amounts not seen by Fahey (2002). The slight variation in the findings between the two brick samples can be a result of differences in the original ore composition from which the two bricks were produced, as well as the rate of cooling of the brick and the way in which the exsolved chromite spinel precipitated from the periclase grains. Asides from the minor variations in the compositions of the two refractory samples, it can be concluded that the periclase phase of magnesia-chrome refractories is essentially impure MgO with minor amounts of iron, chromium, aluminium, silicon and calcium.

Table 5.1.1: Analysis of periclase in mole per cent

	Mg	**Al**	**Si**	**Ca**	**Cr**	**Fe**	**O**
Weight percent (Av.)	52.6	0.6	0.1	0.1	3.3	4.9	38.3
(Standard Deviation)	(0.7)	(0.3)	(0.1)	(0.1)	(0.9)	(0.9)	(0.3)
Mole percent	45.7	0.5	0.1	0.1	1.3	1.8	50.5

B) Chromite Spinel

Chromite spinel phase exists in three distinct forms, that is, primary, secondary and exsolved, also noted by Fahey (2002). The primary spinel grains are large and round whilst the medium sized secondary spinel grains exist around and between periclase grains, acting as a bonding phase. The exsolved chromite spinel exists within the periclase phase and, as discussed in Chapter 2.4, precipitates during manufacturing. The secondary chromite spinel appeared to be the most prevalent form. This observation was also made by Fahey (2002).

The composition of all three forms of chromite spinel was measured to compare any variations that may exist between the three spinel types. The analysis involved performing 10 point analyses each on 5 primary and 5 secondary chromite spinel grains. Since the exsolved chromite spinel phase is small, one point analysis per grain was conducted, with a total of twenty grains being analyzed. The average composition of the three spinel forms from the EDX analysis is illustrated in Table 5.1.2 and Figure 5.1.4. The current results vary from the findings by Fahey (2002) who found that there is no appreciable difference in the chemical composition of the three forms of chromite spinel. The present data shows that the iron content of the exsolved spinel is higher and the chromium content lower than both the primary and secondary spinel. The chemical compositions of the primary and secondary phases are

very similar. As previously mentioned, the slight variation in the findings between the two brick samples can be a result of the difference in the rate of cooling and therefore the way in which the exsolved chromite spinel precipitated from the periclase grains. Trace amounts of calcium and silicon in chromite spinel were observed in both this work and the work by Fahey (2002).

Table 5.1.2: Average composition (wt%) of the three different physical forms of chromite spinel in a magnesia-chrome brick at ambient temperature in weight percent

	Mg	**Al**	**Si**	**Ca**	**Cr**	**Fe**	**O**
Primary Chromite Spinel (Av.)	12.7	7.9	0.1	0.2	36.3	8.1	34.7
(Standard Deviation)	(0.7)	(0.2)	(0.0)	(0.1)	(0.8)	(0.6)	(0.2)
Secondary Chromite Spinel (Av.)	12.7	8.2	0.2	0.2	35.8	8.2	34.8
(Standard Deviation)	(0.6)	(0.4)	(0.1)	(0.1)	(0.8)	(0.4)	(0.3)
Exsolved Chromite Spinel (Av.)	13.3	7.1	0.1	0.2	29.9	15.9	33.6
(Standard Deviation)	(0.7)	(0.4)	(0.0)	(0.1)	(0.3)	(0.6)	(0.3)

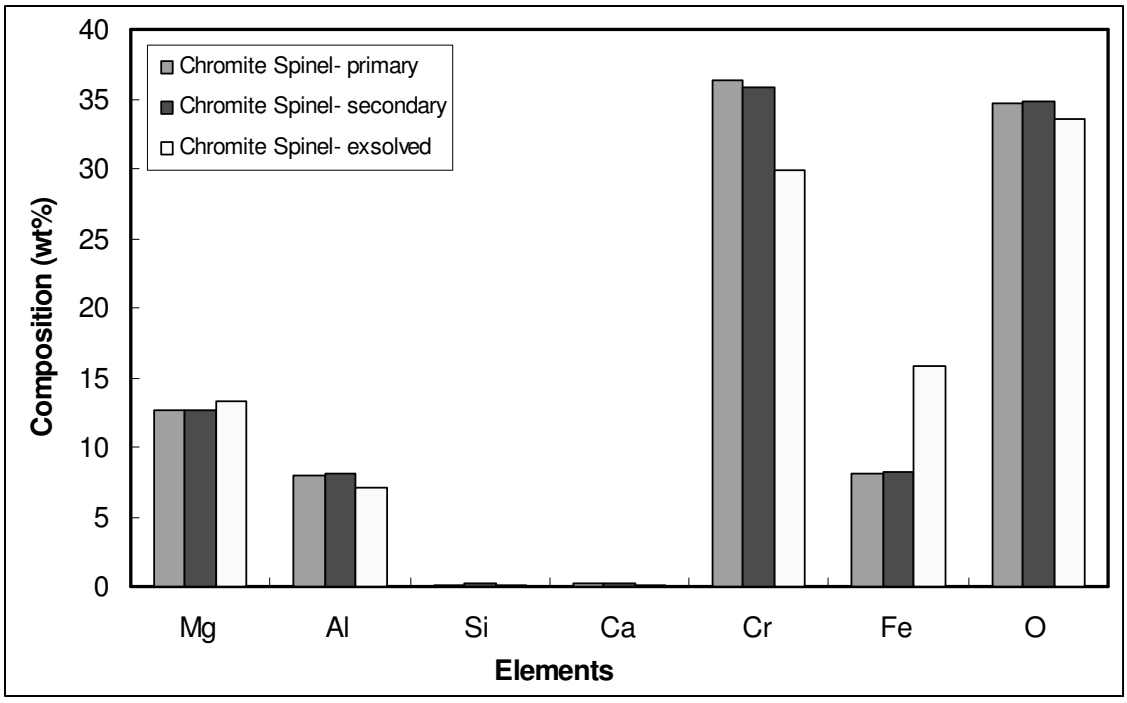

Figure 5.1.4: Comparison of composition of the three different forms of chromite spinel in a magnesia-chrome brick at ambient temperature.

5.1.2 Initial Slag Composition

In order to measure the effects of FCS slag and calcium ferrite slag on the magnesia-chrome refractories, it is necessary to determine the original composition of the slag. The compositions of both FCS slag and calcium ferrite slag used in the experiments are shown in Table 5.1.3. The slag compositions were determined using ICP-AES and the ferrous iron content of FCS using titrations as detailed in Chapter 4.6.2.

Table 5.1.3: Slag composition (wt%) used in both slag/brick experiments.

	$Fe_{(T)}$	Fe^{2+}	CaO	SiO_2	MgO	Cu_2O
FCS Slag						
MS-4	35.9	10.5	23.1	16.4	0.9	9.8
MS-5	32.9	9.3	27.3	15.0	1.8	9.8
Calcium Ferrite Slag						
MS-CF	46.7	-	17	-	1.2	15.1

As seen in Table 5.1.3, two FCS slag compositions were used to determine whether slag composition had an effect on refractory wear. The FCS slag compositions were selected from the phase diagram in Figure 2.9.8. Since FCS slag is located near the dicalcium silicate surface, a CaO content close to the dicalcium silicate boundary was selected. The second slag composition had a CaO composition midway between the magnetite and Ca_2SiO_4 saturation boundaries.

5.1.3 Mechanism of Refractory Wear- Reacted Samples

A) Experiments

Listed in Table 5.1.4 are the experimental conditions at which the slag/brick experiments were conducted. The experiments were initially conducted at 1300^{o}C and oxygen partial pressure of 10^{-6} atm for 8 hours, to determine the nature of slag attack caused by ferrous calcium silicate slag on magnesia-chrome refractories at converting conditions. These tests were conducted using two FCS slag compositions as mentioned previously. For comparison, the tests were repeated using calcium ferrite slag under the same conditions of

temperature, oxygen partial pressure and time. The experiments were repeated at 32 hours for both FCS and calcium ferrite slags, keeping all other conditions constant, in order to observe the effects of time on the rate and extent of slag attack. Finally, changes to the physico-chemical properties of FCS slag were induced by increasing the experimental temperature to 1400^{o}C, keeping all other conditions constant, including an oxygen partial pressure of 10^{-6} atm., contact time of 8 hours and slag composition.

Table 5.1.4: The experimental conditions of slag/brick experiments

Experiment	Temperature (^{o}C)	Oxygen Partial Pressure (atm)	Experiment Time (hours)	Slag Composition
SB-4	1300	10^{-6}	8	MS-4
SB-5	1300	10^{-6}	8	MS-5
SB-12	1300	10^{-6}	8	MS-CF
SB-14	1300	10^{-6}	32	MS-5
SB-15	1300	10^{-6}	32	MS-CF
SB-1400	1400	10^{-6}	8	MS-5

If refractory attack by FCS slag is a mass transfer controlled process then a higher temperature should accelerate the attack greatly as both slag viscosity and the rate of solid-state diffusion between species in the slag and the refractory are a function of temperature according to the Arrhenius relationship (Equation 5.1.1 and Equation 5.1.2).

The Arrhenius Relationship between the rate of solid state diffusion and temperature is given by Equation 5.1.1.

$$D = D_o \exp(-Q/RT) \qquad \textbf{Equation 5.1.1}$$

where T is temperature, D is the rate of diffusion, D_o is a constant, Q is the activation energy and R is the universal gas constant.

Equation 5.1.1 states that as temperature increases the rate of solid state diffusion also increases. The increase in rate of diffusion is controlled by the activation energy, which is the energy required for atoms to migrate from one lattice site to another. If the value of the activation energy is small then the rate increase will also be small. The activation energies for

solid state diffusion of some oxides in iron silicate, calcium ferrite and FCS slag and the magnesia-chrome refractories were found in literature at various temperatures and are given in Table 5.1.5.

Table 5.1.5: Activation energies for solid state diffusion of some oxides in iron silicate, calcium ferrite and FCS slag and the magnesia-chrome refractories (Kofstad, 1966) at various temperatures

Diffusion	Activation Energy (Q) kJ/mol	Coefficient (D_o)	Temperature Range (^oC)
Cr^{3+} in Cr_2O_3	255.7	0.137	1050-1550
Mg^{2+} in MgO	330.6	0.250	1425-1625
Fe^{2+} in MgO	174.1	0.000089	1000-1850

In Table 5.1.5, the activation energies for solid state diffusion are quite high, indicating that solid state diffusion rates are very temperature sensitive. However the data in Table 5.1.5 for Cr_2O_3 and MgO is self-diffusion data, i.e. the rate of solid state diffusion of the ions within the oxide in its own lattice. This is the only data available on solid state diffusion and thus will be used as an indication of the temperature sensitivity of solid state diffusion in the current process. The diffusion of Fe^{2+} in MgO was the only data available on solid state diffusion of the ions from one lattice site to another. Kofstad also reviewed the diffusion of Co^{2+} and Ni^{2+} in MgO in the temperature range of 1000-1850^{o}C and found that the activation energy of the diffusing ion decreased with increasing ionic radius of the ion. The ionic radius of Fe^{2+} is 78 pm, Co^{2+} is 74 pm and Ni^{2+} is 69 pm. The data for the self diffusion of Mg^{2+} and the diffusion of Fe^{2+} in MgO in Table 5.1.5 is in accord with the relationship between activation energy and the ionic radius of the diffusing ion. The ionic radius of Mg^{2+} is 72 pm. Table 5.1.5 shows that the diffusion of Fe^{2+} in MgO is both much slower (i.e. activation energy is lower) and less temperature sensitive than the self-diffusion of Mg^{2+}. Based on the same relationship, it can assumed that given the ionic radius of Fe^{3+} (64.5 pm) is higher than Cr^{3+} (63 pm), the activation energy for the diffusion of Fe^{3+} in Cr_2O_3 will be lower than the self diffusion of Cr^{3+} in Cr_2O_3 given in Table 5.1.5. With interdiffusion, the diffusing ions move in opposite directions at an equimolar rate and the rate of diffusion of the slowest moving ion sets the rate of the interdiffusion process. Therefore Fe^{3+} and Fe^{2+} determine the rate of interdiffusion between Fe^{3+} and Cr^{3+} in chromite spinel and between Fe^{2+} and Mg^{2+} in periclase.

According to Equation 5.1.2, the viscosity of liquids decreases exponentially with increase in temperature. The activation energy for the viscosity of FCS slag is not available in the literature; however it may be expected that this value will be between the activation energies for viscous flow for iron silicate and calcium ferrite slags at the same temperature increase, although closer to the value for iron silicate slag as FCS slag contains a significant amount of silica and thus its structure will most probably be closer to that of iron silicate. This data for the silicate and ferrite slag at a temperature increase from 1300°C to 1400°C is given in Table 5.1.6, from various sources.

$$\eta = A_A \exp(E_A / RT) \qquad \textbf{Equation 5.1.2}$$

where T is temperature, η is viscosity, A_A is a coefficient, E_A is the activation energy and R is the universal gas constant.

Table 5.1.6: Activation energies for viscous flow for iron silicate and calcium ferrite slags when temperature increases from 1300°C to 1400°C.

	Activation Energy (E_A) kJ/mol	**Coefficient (A_A)**
	Iron Silicate Slag	
Toguri *et al.*	85.0	0.14
Shiraishi *et al.* (1978)	67.6	0.36
Kauira *et al.* (1977)	77.5	0.15
	Calcium Ferrite Slag	
Sumita *et al.* (1980)	120.9	0.04
Saito *et al.* (2003)	128.9	0.01
Wright *et al.* (2001)	101.8	0.03

In general when comparing the activation energies for solid state diffusion to viscous flow, the activation energies for viscous flow are smaller, although the activation energies for calcium ferrite slag of the same order of magnitude to those of self-diffusion in the solid state. It is assumed that FCS slag is more like iron silicate slag so the activation energies for iron silicate slag are more likely to be appropriate to FCS slag. Thus viscous flow is less affected by temperature rise than solid state diffusion.

If refractory attack is chemically controlled and depends therefore on the activity of FeO and Fe_3O_4 in the slag and the intrinsic rate of the chemical reactions, then refractory attack should not increase significantly with increase in temperature. The effects of temperature on the activity of FeO and Fe_3O_4 in FCS slag are unreported however it is assumed that the temperature effects on the a_{FeO} and a_{Fe3O4} in FCS slag will be similar to that in calcium ferrite and iron silicate slags. Michal *et al.* (1952), Schuhmann *et al.* (1951) and Sehnalek *et al.* (1972), have studied the effects of temperature on the activity of FeO in iron silicate slag and found that it did not change significantly with an increase in temperature, for constant oxygen partial pressure and slag composition. For example, Michal *et al.* (1952) found that with temperature increased from 1250 to 1350^{o}C, a_{FeO} in a silica saturated iron silicate slag at an oxygen partial pressure of 10^{-8} atm was 0.36 and 0.37, respectively. Similarly Sehnalek *et al.* (1972) measured the activity of Fe_3O_4 in the silica saturated iron silicate slag at 1200 and 1300^{o}C and found a_{Fe3O4} to be 0.005 at 1200^{o}C and 0.004 at 1300^{o}C. The effects of temperature on the activity of FeO and Fe_3O_4 in calcium ferrite slag have been studied by Henao *et al.* (2006), Kongoli *et al.* (2003) and Takeda *et al.* (1980). All agree that at a given slag composition and oxygen partial pressure, there is no appreciable change in the a_{FeO} and a_{Fe3O4} in calcium ferrite slag with an increase in temperature of 100^{o}C. Takeda *et al.* (1980) found that as temperature increased from 1200 to 1300^{o}C, at a fixed slag composition and oxygen partial pressure, a_{FeO} is 0.34 at 1200^{o}C and 0.35 at 1300^{o}C. Similarly, Takeda *et al.* (1980) found a_{Fe3O4} to be 0.2 at both 1200^{o}C and 1300^{o}C.

B) Initial Observations

Once the samples were removed from the furnace following contact times listed in Table 5.1.4, they were inspected with the naked eye to distinguish whether any changes to the refractory were evident. These initial observations of the samples are detailed in this section.

1) 8 HOURS CONTACT TIME

For the slag samples which had been held in the magnesia-chrome refractory crucibles for 8 hours, the remaining FCS slag was approximately 4mm thick. The pool of calcium ferrite slag remaining in the crucible after experiments was approximately 2mm thick. The original dark brown colour of the magnesia-chrome refractory crucible had changed to black in the case of calcium ferrite slag, suggesting that the slag had penetrated right through the refractory material via the pore network. Calcium ferrite slag was also evident on the

magnesia crucible supporting the magnesia-chrome crucible. On the contrary, FCS slag/brick samples indicated no sign of FCS slag penetration through the refractory, as no colour differentiation was observed on the outer surface of the brick crucible and the magnesia crucible was free of any slag residue.

Comparison of the initial observations from the two experiments regarding the extent of slag penetration suggests that under similar conditions, calcium ferrite slag viscosity and slag/brick interfacial tension is much lower than that between FCS slag and the same refractory brick.

2) 32 HOURS CONTACT TIME

Following 32 hours of experimental time, calcium ferrite slag had not only penetrated the magnesia-chrome refractory crucible but also penetrated through the magnesia crucible safeguarding the sample and onto the supporting platform. FCS slag had penetrated further into the magnesia-chrome crucible with little slag remaining in the refractory crucible however no colour differential was evident on the outer surface of the crucible to signify complete penetration. FCS slag did not penetrate the magnesia crucible. Whilst there was no slag/brick interface present in the calcium ferrite slag sample because the slag had penetrated the brick, this was not the case for ferrous calcium silicate slag sample, where a distinct interface was observed. The attack of FCS slags and calcium ferrite on the refractory material is illustrated in Figures 5.1.5 and 5.1.6, respectively. It is evident that the level of penetration of FCS slag is far less severe than that of calcium ferrite slag even at extended experimental times. As observed in Figure 5.1.6, although calcium ferrite slag penetrated through the magnesia crucible, no degradation of the crucible is evident; suggesting that limited attack of the periclase phase in the refractory by the ferrite slag has occurred.

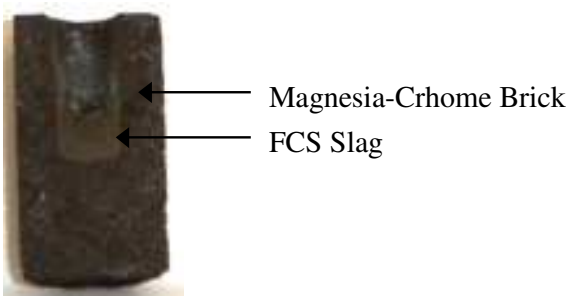

Figure 5.1.5: Magnesia-chrome brick in contact with FCS slag at 1300^{o}C, an oxygen partial pressure of 10^{-6} atm. for 32 hours.

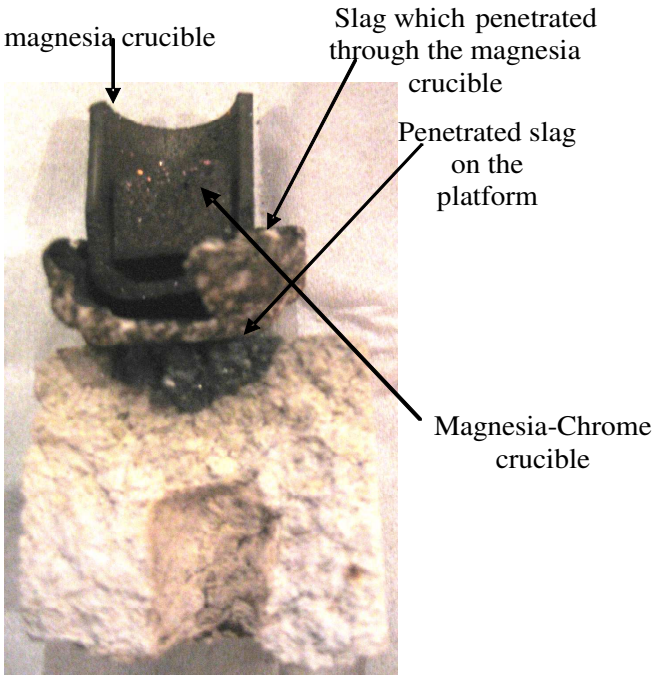

Figure 5.1.6: Attack by calcium ferrite slag at 1300°C, an oxygen partial pressure of 10^{-6} atm. for 32 hours.

3) 1400°C AND FCS SLAG

At 1400°C FCS slag had penetrated almost completely into the refractory, with only a small amount of slag remaining in the magnesia-chrome crucible. Similar to the case of calcium ferrite slag in the 8 hour test, the colour of the magnesia-chrome refractory had changed from dark brown to black on outer surface of the refractory crucible, suggesting increased slag penetration. Nonetheless, the magnesia crucible housing the sample was free of any slag residue and FCS slag did not penetrate or attack the magnesia crucible.

The only explanation for the increased penetration of slag into the refractory is that with an increase in temperature either or both slag viscosity and slag/brick interfacial tension have decreased. As per Equation 5.1.2, the relationship between the viscosity of liquids and temperature, an increase in temperature results in a decrease in viscosity. However the effects of temperature on the viscosity of FCS slag are unknown, with no data found in literature on the physical properties of the slag. Nonetheless, the decrease in viscosity with increase temperature in the range of 1200-1500°C was observed by Vartiainen and Sumita *et al.* for iron silicate and calcium ferrite slags respectively, at a fixed oxygen partial pressure. Vartiainen found that at a Fe/SiO_2 ratio of 1.44 and an oxygen partial pressure of 10^{-7} atm, the

viscosity of iron silicate slag decreased from 0.25 Pa.s at 1300°C to 0.09 Pa.s at 1400°C. Sumita *et al.* found that for calcium ferrite slag, the viscosity decreased from 0.03 Pa.s at 1300°C to 0.02 Pa.s at 1400°C. The viscosity of iron silicate slag is affected by temperature far more than calcium ferrite slag due to its structure of large complex silicate anions. With silica and lime both present in FCS slag, it is likely that the viscosity of FCS slag will be between iron silicate and calcium ferrite slags and be fairly sensitive to temperature.

Studies on the effects of temperature on the interfacial tension between FCS slag and magnesia-chrome refractory were not found in literature and neither were studies found for the silicate and ferrite slags. However, according to theory on the effects of temperature on the interfacial tension between solids and liquids, it decreases linearly with increasing temperatures (Verein Deutscher Eisenhuttenleute, 1995)

C) Microstructure

The slag/refractory samples were sectioned and polished to view under the SEM. A detailed procedure for the sample preparation for the SEM is given in Section 4.6. The BSE images of the microstructure of the refractory following contact with both FCS and calcium ferrite slags at various contact times are discussed in this section.

1) 8 HOURS CONTACT TIME

Observation of the brick after contact with FCS slag revealed reduction in porosity close to the slag/brick interface, due to slag penetration, whilst further from the interface slag penetration was not apparent. In comparison, the porosity in the refractory when in contact with calcium ferrite slag was reduced throughout the microstructure of the refractory. Figures 5.1.7 and 5.1.8 show the microstructure at the interface between slag and refractory, FCS and calcium ferrite slag, respectively. Since the cooling rate of the molten FCS slag was not very rapid, a 'glassy' single phase was not produced in the cooled sample, but rather a finely crystalline structure.

Under the same conditions and time, the microstructure of FCS slag and brick at the interface (Figure 5.1.7) is very different to the microstructure of the calcium ferrite slag/refractory samples (Figure 5.1.8). The boundary line (dashed lines) at the calcium ferrite slag/refractory interface is quite diffuse compared to the FCS slag/refractory interface. The

microstructure of the refractory after FCS slag contact is similar to that of the virgin magnesia-chrome brick; however slag penetration is evident from the presence of white specs within the microstructure in Figure 5.1.7, which are not present in the virgin refractory. This was the case for both tests SB-4 and SB-5. Analysis of such specs using EDX revealed that they contain copper (as Cu_2O) and calcium (as CaO). Whilst calcium is present in the original brick in very small amounts, copper (as Cu_2O) is a component of the slag and thus is a result of slag penetration.

The attack of calcium ferrite slag on magnesia-chrome brick at 1300^{o}C is very apparent after 8 hours of contact. In the slag phase of Figure 5.1.8 there are detached particles of the periclase phase whilst within the brick, attack of the chromite spinel phase is suggested by the decreasing grayscale colour of the grains from periphery to the centre. Copper and calcium, as Cu_2O and CaO, respectively (white specs) are also present in the brick in contact with the ferrite slag, further supporting slag penetration. Similar observations were also made by Fahey (2002). The ability of calcium ferrite slag to infiltrate and move through the brick pore network suggests low slag viscosity and low interfacial tension between calcium ferrite slag and magnesia-chrome refractory.

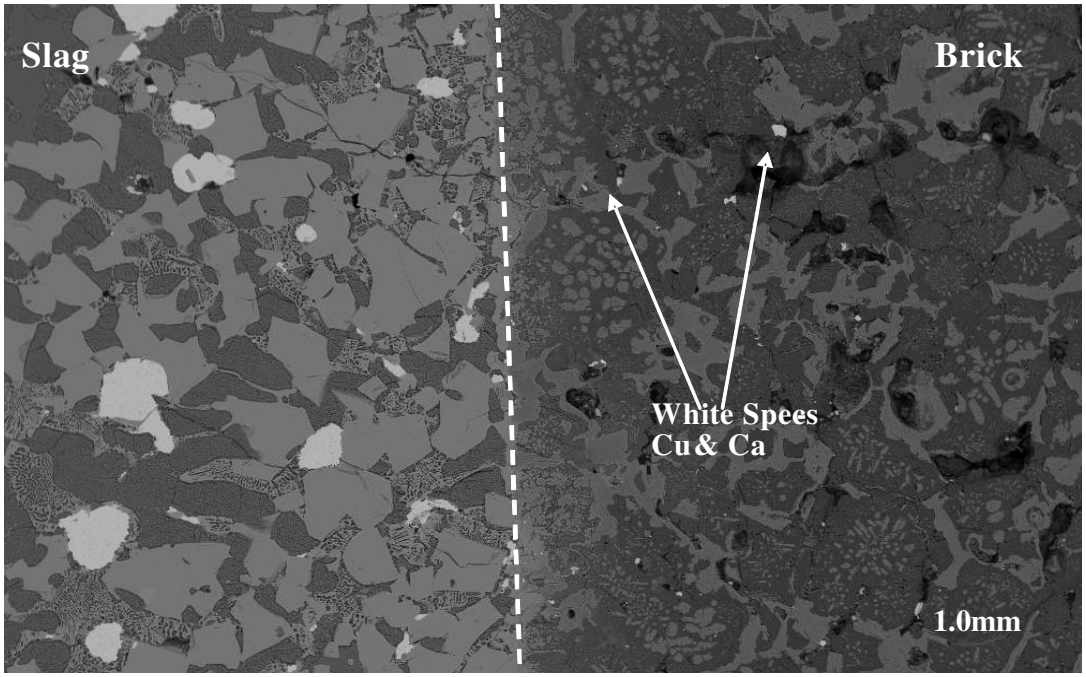

Figure 5.1.7: BSE image showing the microstructure at the slag/brick interface of FCS slag at oxygen partial pressure of 10^{-6} atm, 1300^{o}C for 8hrs

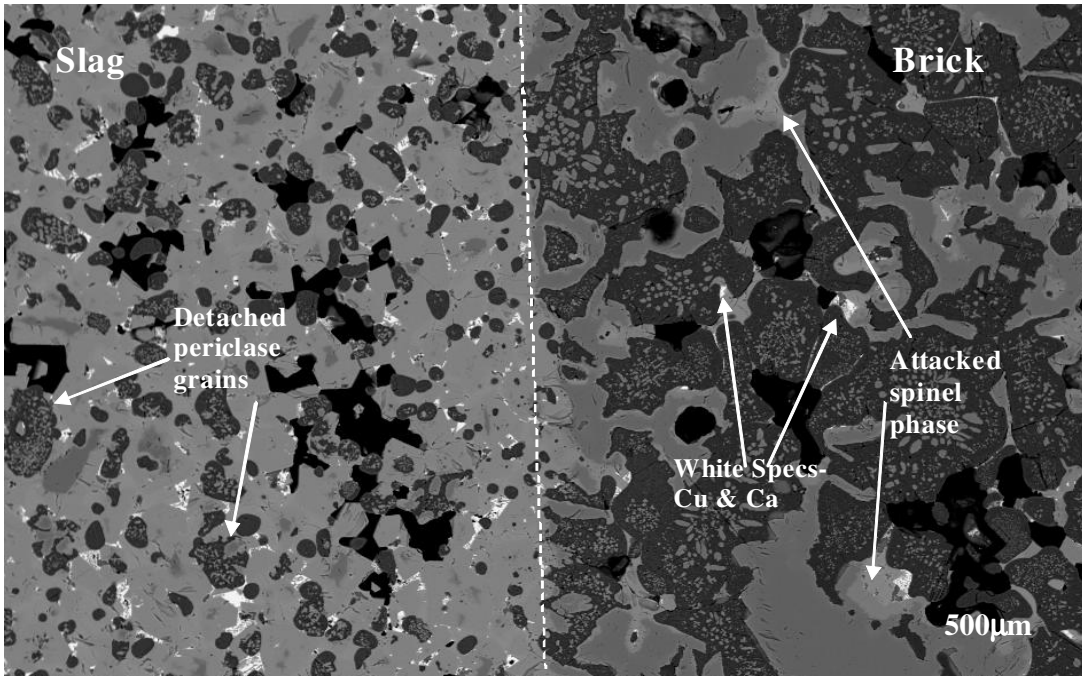

Figure 5.1.8: BSE image showing the microstructure at the slag/brick interface for calcium ferrite slag at oxygen partial pressure of 10^{-6} atm, 1300°C for 8hrs.

The general observation of the slag/refractory microstructure of calcium ferrite and FCS slag contained in magnesia-chrome refractory clearly indicates that interactions between calcium ferrite slag and brick have caused degeneration of the brick whilst only limited slag penetration of the brick is apparent in the FCS slag samples and there is no evidence of slag attack, such that no detached grains from the refractory are seen in FCS slag.

The location of the elements which comprise both the slag (FCS and calcium ferrite slags) and brick in the BSE images shown in Figures 5.1.7 and 5.1.8 are shown in Figures 5.1.9 and 5.1.10, respectively. The colour intensity key in Figures 5.1.9 and 5.1.10 represent the concentration levels of each element within both slag and brick. Black represents maximum concentration whilst white indicates zero concentration. The main constituents of FCS slag are iron, silicon, calcium and copper whereas those of calcium ferrite slag are iron, calcium and copper. For the refractory, the main constituents are chromium, magnesium and aluminum.

The evidence for FCS slag penetration in Figure 5.1.7 is confirmed in Figure 5.1.9. Minor amounts of silicon, calcium, copper and iron appear in the brick indicating some slag penetration into brick pores. There is also a minor concentration of aluminum from the brick in FCS slag as seen in Figure 5.1.9, which was not present in the initial slag. Small traces of

magnesium are seen in the slag phase and chromium is also present in very minor amounts in the FCS slag (Figure 5.1.9). This indicates that some interdiffusion between FCS slag and refractory components is occurring. Chemical reactions between the species in the slag and the refractory are not evident as there is no sign of new phases forming in the sample.

In the case of the calcium ferrite slag/refractory samples, images in Figure 5.1.10 support the findings of the BSE images in Figure 5.1.8. The copper and calcium diagrams in Figure 5.1.10 further confirm the EDX analysis that the white specs seen in Figure 5.1.8 are in fact calcium and copper, as CaO and Cu_2O, respectively, in the slag which has penetrated the refractory. The light grey rims surrounding some spinel grains in Figure 5.1.8 are the periphery of the chromite spinel grains enriched in iron as iron oxide, which were not present in the original grains. Fahey (2002) also found the lighter grey regions in the spinel phase to contain high levels of iron which appears to be more pronounced close to the slag/refractory interface. In the slag phase, chromium and aluminum from the brick are present in calcium ferrite slag; however both elements are not part of the initial slag composition. In the refractory, the concentration of both chromium and aluminum has decreased at the periphery of the chromite spinel grains especially close to the slag/refractory interface. Iron, a major component of the ferrite slag, appears to have interdiffused into the chromite spinel phase, in particular with chromium and aluminum, especially close to the slag/brick interface. Magnesium also appears in the slag phase but mainly as periclase grains and does not appear to be depleted close to the interface of the refractory as is the case with chromium and aluminum. Similar observations were also made by Fahey (2002) on the microstructure of the calcium ferrite slag/refractory interface. Fahey (2002) concluded that iron impregnation is associated with the loss of bonding of periclase grains. Fahey (2002) found that calcium ferrite slag acts a source of iron, causing degeneration of the chromite spinel bonding phase, possibly by interdiffusion which leads to volume changes, cracking and eventually debonding. As a consequence, periclase grains detach from the surface of the brick and appear in the slag phase. The conclusions drawn by Fahey (2002) are further supported in this research, where, as seen in Figures 5.1.8 and 5.1.10, the presence of periclase grains in slag and the iron enriched chromite spinel phase is clearly evident.

Main Components in Slag

Ca

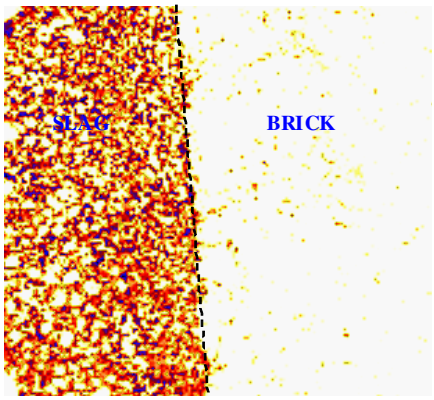

Cu

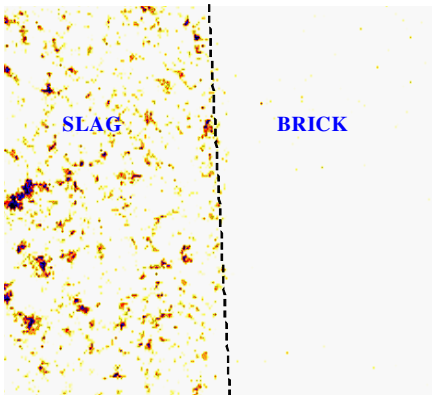

Fe

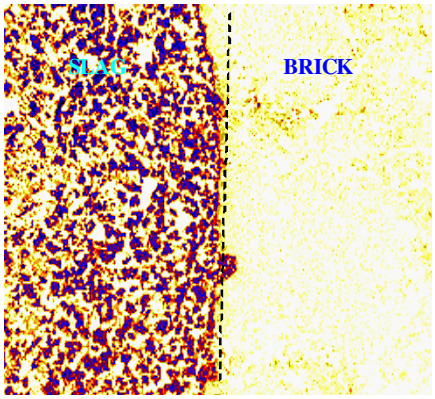

Si

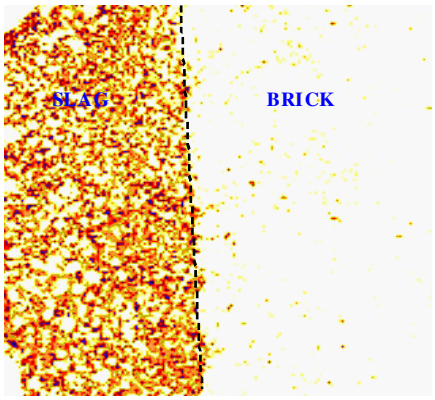

Main Components of refractory brick

Cr

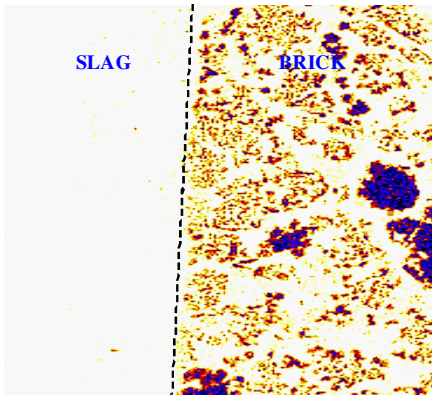

Mg

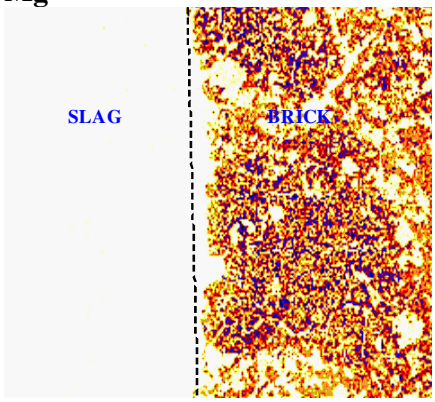

Al

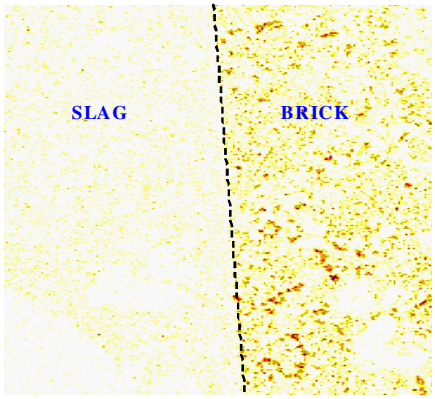

Figure 5.1.9: Elements scans (Al, Ca, Cr, Cu, Fe, Mg, Si) of the constituents of slag and brick to show their location after brick contact with FCS slag at 1300^{o}C and oxygen partial pressure of 10^{-6} atm for 8 hours

Main Components in Slag

Main Components in refractory brick

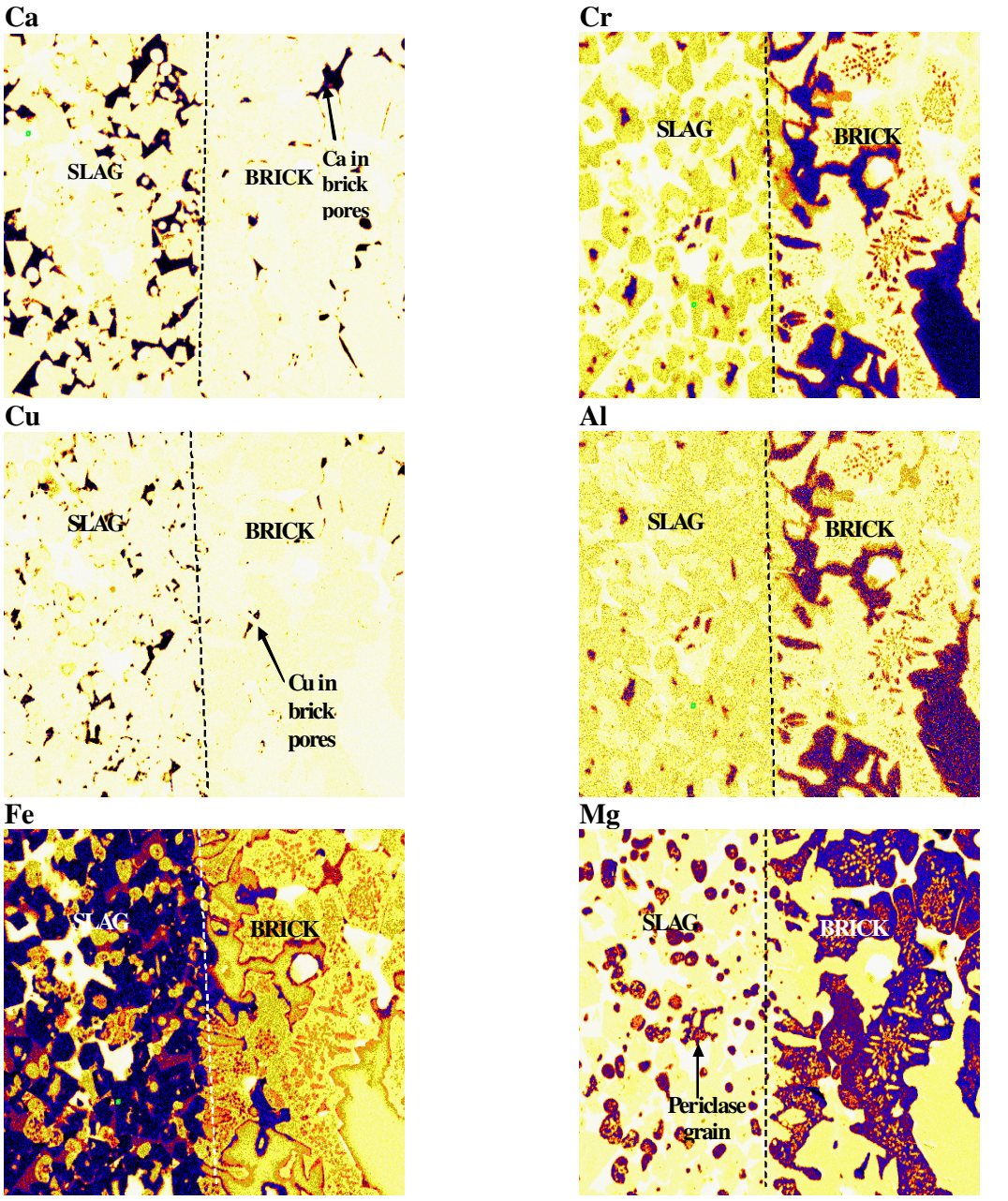

Figure 5.1.10: Elements scans (Al, Ca, Cr, Cu, Fe, Mg) of the constituents of slag and brick to show their location after brick contact with calcium ferrite slag at 1300^{o}C and oxygen partial pressure of 10^{-6} atm for 8 hours

Whilst the interactions between FCS slag and refractory is not as extreme as that between calcium ferrite slag and brick, the microstructure and element distribution images do indicate that there is some interactions and slag penetration. However the interactions between FCS slag and magnesia-chrome refractory is not obvious by observing the SEM images and a more detailed analysis is required of the compositional changes in slag and brick caused by reaction and/or diffusion, after experiments. This analysis is discussed later in this chapter.

2) 32 HOURS CONTACT TIME

Figures 5.1.11 and 5.1.12 show the microstructure of magnesia-chrome refractory in contact with ferrous calcium silicate slag and calcium ferrite slag, respectively, following 32 hours of contact time. The microstructure of FCS slag/refractory samples is not very different to that for 8 hours of contact time. In both cases, slag penetration is clearly evident from the presence of copper and calcium in the brick microstructure and very slight iron impregnation is evident on the chromite spinel grains close to the slag/brick interface. This iron impregnation was not seen in the 8 hour runs.

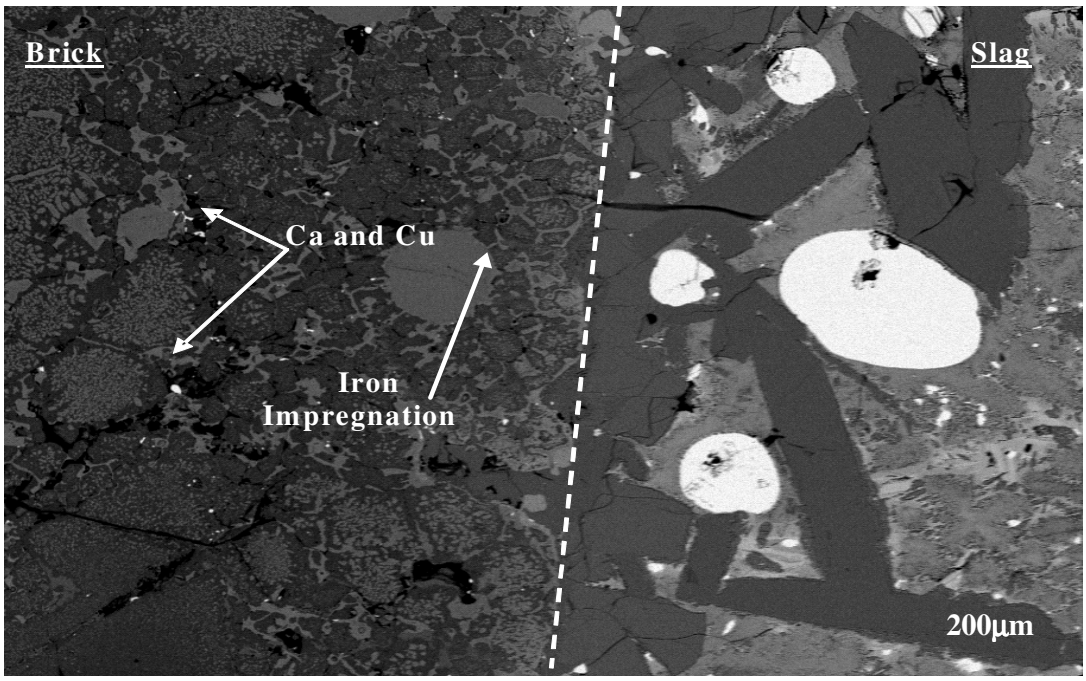

Figure 5.1.11: SEM (backscatter electrons) image showing the microstructure at the slag/brick interface of the FCS slag experiment at oxygen partial pressure of 10^{-6} atm, 1300°C for 32hrs.

Figure 5.1.12 shows the refractory brick following 32 hours of contact with calcium ferrite slag. The brick has severely disintegrated. There is no slag/brick interface as the slag had not only penetrated the refractory material but had also penetrated the magnesia crucible housing the sample and the platform holding the sample inside the tube furnace (Figure 5.1.6). It appears that the calcium ferrite slag preferentially attacks the chromite spinel phase, with iron enrichment evident in all spinel grains (light grey rims surrounding the grains). 'Holes' are present within the chromite spinel grains, which indicates that interactions between the penetrated slag and the chromite spinel phases have resulted in loss of bonding within the chromite grains, leading to the erosion of the spinel phase. Such erosion of the chromite spinel grains was not evident in the microstructure of the calcium ferrite slag samples after only 8 hours.

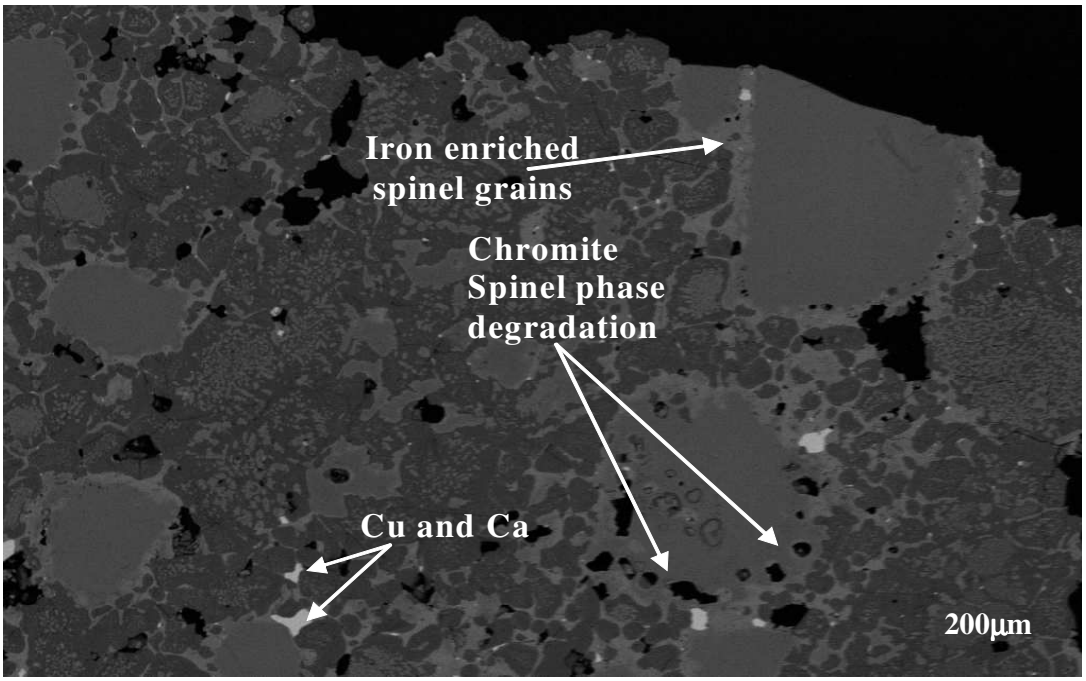

Figure 5.1.12: SEM (backscatter electrons) image showing the microstructure at the slag/brick interface of the calcium ferrite slag experiment at oxygen partial pressure of 10^{-6} atm, 1300^{o}C for 32hrs.

3) 1400°C AND FCS SLAG

The FCS slag/refractory interface after contact at 1400°C is shown in Figure 5.1.13. There is an increased attack of the refractory in comparison to that observed at 1300°C. Detached brick particles are present in the slag phase and copper and calcium from the slag appear within the microstructure of the refractory. EDX analysis conducted on the detached particles revealed them to be periclase. 'Hair-line' cracks are also evident in the refractory. Such crack propagation is likely to have resulted during the cooling of the slag/brick sample, when solidification of the penetrated slag caused structural and thermal expansion. Iron-enriched rims surrounding the chromite spinel grains were also noticed.

Within the refractory three zones were observed:

1. At the slag/refractory interface a zone rich in iron is present, confirmed using EDX analysis.
2. Further from the interface, a slag penetrated region is observed, where attack of the refractory by the penetrated slag is not evident.
3. Refractory with a microstructure similar to the original magnesia-chrome brick.

With an increase in temperature, FCS slag has become much more fluid and is able to more easily infiltrate the open porosity of the refractory. The increase in temperature has also increased the rate of interdiffusion between components in the slag and the refractory because at 1300°C iron impregnation was not evident in the microstructure of the FCS slag samples whereas it is at 1400°C. Iron impregnation, as well as the presence of the periclase grains in the slag, suggests that iron from the penetrated slag is preferentially diffusing into chromite spinel grains. As the secondary spinel grains act as a bonding phase, the outcome of this interdiffusion is detrimental, as it results in the deterioration of the secondary spinel, which results in weakened bonding between the chromite spinel and the periclase phases. The weakened bonding between these two phases in turn causes the brick to disintegrate. The fact that periclase grains appear in the slag and have not dissolved indicates that the attack of this phase is not as severe as that of the chromite spinel phase and there is a low solubility of MgO in the slag. It appears that the increase in temperature from 1300°C to 1400°C has not only resulted in the decrease in viscosity of FCS slag, allowing penetration, but also in the increase in the rate of interactions between slag and brick. Composition analysis of the slag and brick were conducted using EDX as well as line scans to determine changes in composition of the refractory and slag at the interface. This analysis is discussed later in the chapter.

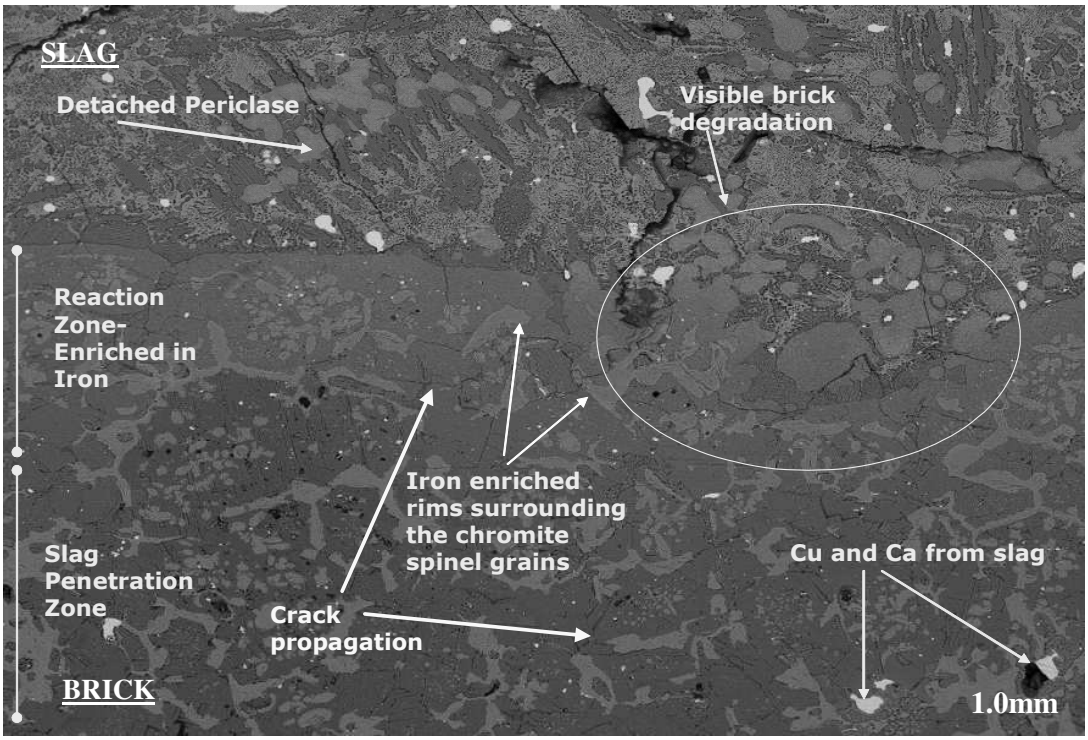

Figure 5.1.13: BSE image showing the microstructure at the slag/brick interface of the FCS slag experiment at oxygen partial pressure of 10^{-6} atm, 1400^{o}C for 8hrs.

D) EDX Analysis

Whilst the microstructure and element distribution images for the FCS slag/refractory samples indicate that there are some interactions and slag penetration taking place, the interactions between FCS slag and magnesia-chrome refractory are not very obvious from SEM BSE images. The effects of contact time on refractory wear are also not very noticeable from the SEM BSE images in the case of FCS slag. A more detailed analysis is required of the compositional changes in the brick in order to discuss and compare the wear of the refractory by FCS and calcium ferrite slags. The changes in composition of the periclase and primary chromite spinel phases were determined using EDX analysis. Primary chromite spinel grains where analyzed as these grains most comprised the refractory at the slag/refractory interface. The analysis of the chromite spinel grains involved taking 5 points scans each at the center and periphery of the grains close to the slag/brick interface, with a total of 3 grains analyzed. The analysis of the periclase phase consisted of taking 10 points scan of each grain with a total of 3 grains analyzed. The data from the EDX analysis is discussed in this section.

1) CHROMITE SPINEL AT 1300°C, OXYGEN PARTIAL PRESSURE OF 10^{-6} ATM.

Tables 5.1.7 and 5.1.8 compare the composition of the chromite spinel grains near the slag/refractory interface of calcium ferrite and FCS slag samples, respectively, at an oxygen partial pressure of 10^{-6} atm., 1300°C and contact time of 8 hours. The composition of the chromite spinel grains exposed to slag at the center and periphery is compared to the composition of the virgin grains (labeled as 'unreacted' in the tables and figures). Due to the similarity in the changes at the center and periphery of each spinel grain analyzed, the data in Tables 5.1.7 and 5.1.8 is an average together with the standard deviation. Figures 5.1.14 and 5.1.15 represent the results in Tables 5.1.7 and 5.1.8 graphically.

Table 5.1.7: Average composition (wt%) of chromite spinel grains in a magnesia-chrome refractory in contact with calcium ferrite slag at the slag/refractory interface at oxygen partial pressure of 10^{-6} atm., 1300°C for 8hrs

	Mg	**Al**	**Si**	**Ca**	**Cr**	**Fe**	**Cu**	**O**
Unreacted Chromite Spinel (Av.)	12.7	7.9	0.1	0.2	36.3	8.1	-	34.7
(Standard Deviation)	*(0.7)*	*(0.2)*	*(0.0)*	*(0.1)*	*(0.8)*	*(0.6)*	*(-)*	*(0.2)*
Periphery of Grain (Av.)	11.7	6.4	0.09	1.2	29.2	19.7	0.4	33.2
(Standard Deviation)	*(0.6)*	*(0.5)*	*(0.1)*	*(0.3)*	*(0.4)*	*(0.4)*	*(0.3)*	*(2.1)*
Center of Grain (Av.)	12.6	7.4	0.04	0.3	35.1	11.6	0.2	34.6
(Standard Deviation)	*(0.1)*	*(0.3)*	*(0.0)*	*(0.0)*	*(0.8)*	*(0.1)*	*(0.0)*	*(0.3)*

Table 5.1.8: Average composition (wt%) of chromite spinel grains in a magnesia-chrome refractory in contact with FCS slag at the slag/refractory interface at oxygen partial pressure of 10^{-6} atm., 1300°C for 8hrs

	Mg	**Al**	**Si**	**Ca**	**Cr**	**Fe**	**Cu**	**O**
Unreacted Chromite Spinel (Av.)	12.7	7.9	0.1	0.2	36.3	8.1	-	34.7
(Standard Deviation)	*(0.7)*	*(0.2)*	*(0.0)*	*(0.1)*	*(0.8)*	*(0.6)*	*(-)*	*(0.2)*
Periphery of Grain (Av.)	12.6	7.8	0.1	0.3	35.0	8.9	0.3	34.4
(Standard Deviation)	*(0.5)*	*(0.6)*	*(0.1)*	*(0.2)*	*(0.4)*	*(0.3)*	*(0.1)*	*(0.7)*
Center of Grain (Av.)	12.3	7.5	0.1	0.3	36.2	8.8	0.2	34.3
(Standard Deviation)	*(0.3)*	*(0.3)*	*(0.1)*	*(0.2)*	*(0.2)*	*(0.9)*	*(0.1)*	*(0.8)*

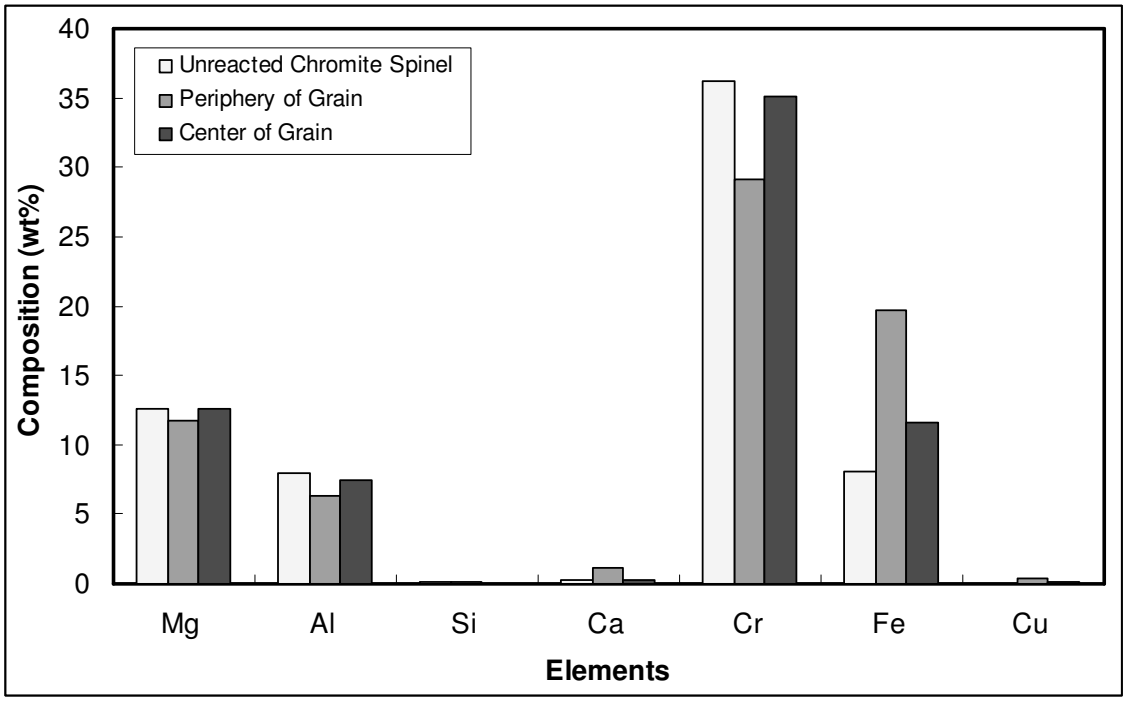

Figure 5.1.14: Comparison of composition of chromite spinel grains before and after reaction with calcium ferrite slag at oxygen partial pressure of 10^{-6} atm., 1300°C for 8hrs

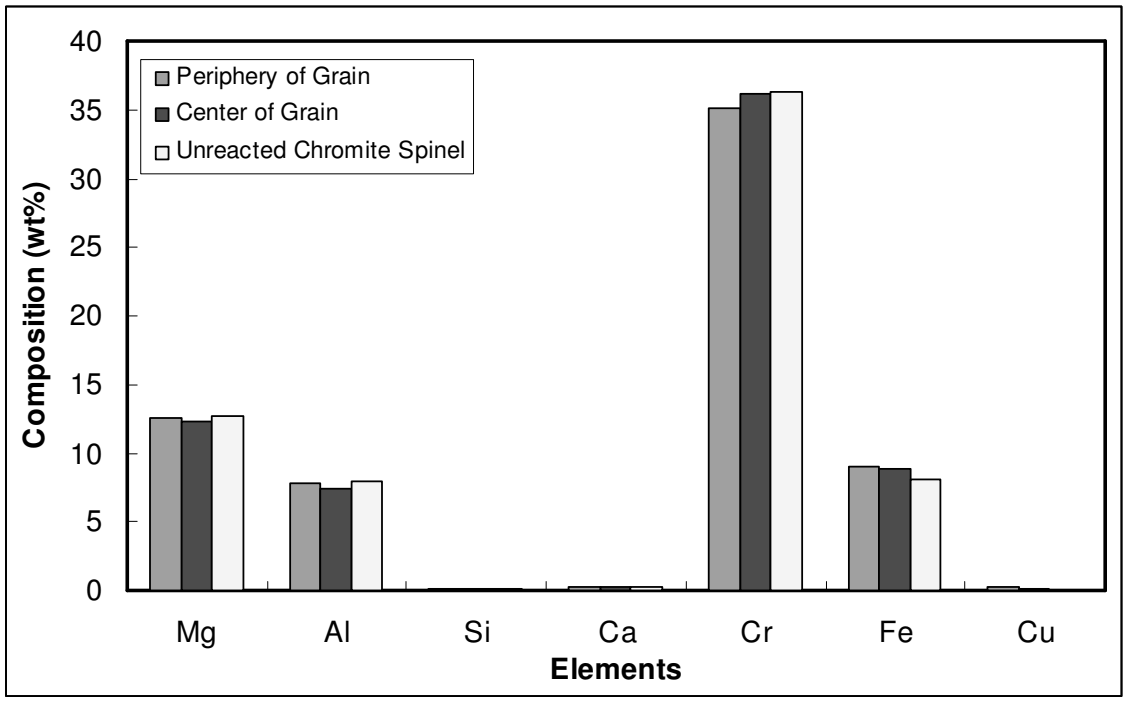

Figure 5.1.15: Comparison of composition of chromite spinel grains before and after reaction with FCS slag at oxygen partial pressure of 10^{-6} atm., 1300°C for 8hrs

The EDX analysis for both the FCS slag and calcium ferrite slag samples supports the qualitative data from the BSE images discussed previously. Figure 5.1.14 clearly shows that the chromite spinel phase of the refractory close to the calcium ferrite slag/refractory interface has depleted in chromium and aluminum and enriched in iron. This is much more severe at the periphery of the grains, which was in direct contact with calcium ferrite slag, than the center of the grains. Fahey (2002) made similar findings on the interactions between calcium ferrite slag and the chromite spinel phase of the refractory, proposing that solid-state diffusion is occurring between iron in the slag and chromium and aluminum in the chromite spinel phase.

Ions of different elements with similar ionic radius and the same charge can substitute for one another in a mineral structure. When two different cations occupy a particular position in a crystal, the ion with higher ionic radius forms a stronger bond with surrounding anions and is preferentially substituted. As seen in Table 5.1.9, the three elements that appear to be interdiffusing, chromium, aluminum and iron are all trivalent ions with similar ionic radii. Due to the higher ionic radius of Fe^{3+}, it is able to substitute for Cr^{3+} or Al^{3+} and form a stronger bond with anions in the chromite spinel structure.

Table 5.1.9: Ionic radii of selected ions

Ion	**Cr^{3+}**	**Fe^{3+}**	**Al^{3+}**
Ionic radius (pm)	63	64.5	53.5

In the current study three distinct zones in the chromite spinel phase in contact with calcium ferrite slag were identified, which were also observed by Fahey (2002):

- Zone 1: furthest from the interface, where the chromite spinel grains are approximately of the same composition as the un-reacted grains;
- Zone 2: an interdiffusion zone, where the chromium and aluminum contents of the spinel phase are decreasing whilst the iron content is increasing;
- Zone 3: Closest to the interface, adjacent to the slag, the periphery of the chromite spinel phase is close to composition of magnesioferrite ($MgO.Fe_2O_3$), with the molar ratio of Fe to Mg measured to be 1.9:1.

The magnesioferrite accompanied the interdiffusion between iron in calcium ferrite slag and chromium and aluminum in the chromite spinel. This conclusion was also drawn by Fahey (2002). Whilst in both the current study and the findings by Fahey (2002), a magnesioferrite phase is proposed to have formed, no distinct phase boundary which accompanies the formation of a new phase was observed in either study. The formation of this phase is discussed in detail later in the chapter and it will be seen that no phase boundary should form.

The attack on the refractory by FCS slag is very minor, with only a slight depletion of chromium and enrichment of iron in the chromite spinel grains as shown in Figure 5.1.15. A line scan analysis (Figure 5.1.16) of the chromite spinel grain in contact with FCS slag at the slag/refractory interface further supports the observation that limited interdiffusion takes place between iron in FCS slag and chromium in the chromite spinel phase. In Figure 5.1.16, there is only a slight gradient from the chromite spinel phase to the slag phase. No new phases of the periphery of the chromite grains were seen in the refractory in contact with FCS slag, such that, the molar ratio of Fe to Mg of the chromite phase following contact with FCS slag was similar to the virgin brick and no change in grayscale colour is evident in Figure 5.1.7.

As seen in Figure 5.1.15, there is no evidence of interdiffusion between silicon, calcium and copper in FCS slag and the species in the chromite spinel phase. If silicon, calcium and copper participated in interdiffusion, greater amounts of them would be expected in the chromite phase as they would be the diffusing species from the slag phase. The limited diffusion of silicon, calcium and copper from FCS slag into the chromite spinel grains is further supported by the lack of diffusion gradients evident in the line scan in Figure 5.1.16. The fact that silicon, calcium and copper have not interdiffused is expected as silicon is part of anions i.e. it is strongly bonded to oxygen, copper is a univalent ion and calcium is divalent so neither would interdiffuse with Cr^{3+}.

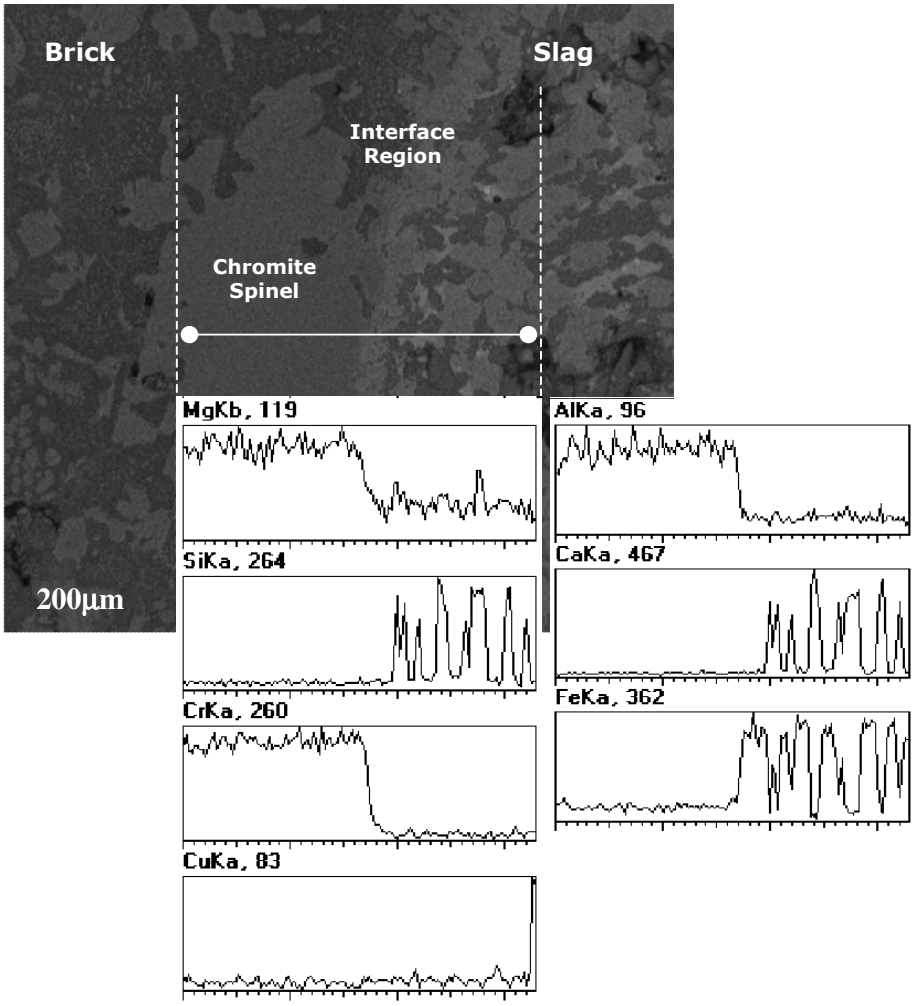

Figure 5.1.16: Line scan of chromite spinel at interface of brick contacted with molten FCS slag at 1300°C, oxygen partial pressure of 10^{-6} atm., 8 hours

Tables 5.1.10 and 5.1.11 compare the change in composition of the chromite spinel grains near the slag/refractory interface of calcium ferrite and FCS slag samples, respectively, at an oxygen partial pressure of 10^{-6} atm., 1300°C and contact time of 32 hours. Figures 5.1.17 and 5.1.18 represent the results in Tables 5.1.10 and 5.1.11 graphically.

Following 32 hours of contact, the chromium and aluminum contents of the chromite spinel grains have decreased to a very significant extent when in contact with calcium ferrite slag whilst the iron content has almost doubled. This is particularly the case at the periphery of the grains, indicating that with time, the attack of the chromite spinel phase by the ferrite slag has progressed much further than that observed after 8 hours of contact. Calcium ferrite slag has severely disintegrated the chromite spinel grains as a result of interdiffusion

following extended contact time. On the periphery of some chromite spinel grains in Figure 5.1.12, the Fe to Mg molar ratio was measured to be 2.1:1, close to that of magnesioferrite.

Following 32 hours of contact time, the chromium and aluminum content of the chromite spinel phase in contact with FCS slag has also decreased and the iron content has increased as shown in Table 5.1.11 and Figure 5.1.18, however not as significantly as with the calcium ferrite slag samples. Whilst interdiffusion between iron in FCS slag and chromium and aluminum in the brick continues to take place, brick degradation is not apparent as seen from the microstructure of the brick in Figure 5.1.11. Even following extended contact time, no magnesioferrite, with a Fe to Mg molar ratio close to 2:1, was evident the periphery of the chromite spinel grains in Figure 5.1.11.

The interdiffusion between iron, chromium and aluminum in the FCS slag/refractory samples is further illustrated by the line scan (Figure 5.1.19). The small diffusion gradients in Figure 5.1.19 confirm that interdiffusion is limited, even after 32 hours. Only a slight increase in iron content and decrease in chromium and aluminum content in the refractory is apparent at the FCS slag/refractory interface. Nonetheless, considering that with time the extent of interdiffusion between iron in FCS slag and chromium and aluminum in the spinel has progressed, the current results suggest that at 1300^{o}C, over operating times of years, the chromite spinel phase will degrade as a result of contact with FCS slag, although the rate of attack will be much slower than for calcium ferrite slag.

Table 5.1.10: Average composition (wt%) of chromite spinel grains in a magnesia-chrome brick in contact with calcium ferrite slag at the slag/brick interface at oxygen partial pressure of 10^{-6} atm., 1300^{o}C for 32hrs

	Mg	**Al**	**Si**	**Ca**	**Cr**	**Fe**	**Cu**	**O**
Unreacted Chromite Spinel (Av.)	12.7	7.9	0.1	0.2	36.3	8.1	-	34.7
(Standard Deviation)	*(0.7)*	*(0.2)*	*(0.0)*	*(0.1)*	*(0.8)*	*(0.6)*	*(-)*	*(0.2)*
Periphery of Grain (Av.)	10.4	3.4	0.2	2.6	17.7	31.5	0.07	28.3
(Standard Deviation)	*(0.4)*	*(0.5)*	*(0.2)*	*(0.7)*	*(0.8)*	*(0.6)*	*(0.1)*	*(1.9)*
Center of Grain (Av.)	11.2	7.6	0.01	0.8	34.5	8.6	0.03	32.8
(Standard Deviation)	*(0.3)*	*(0.1)*	*(0.0)*	*(0.6)*	*(0.6)*	*(0.3)*	*(0.0)*	*(0.5)*

Table 5.1.11: Average composition (wt%) of chromite spinel grains in a magnesia-chrome brick in contact with FCS slag at the slag/refractory interface at oxygen partial pressure of 10^{-6} atm., 1300°C for 32hrs

	Mg	**Al**	**Si**	**Ca**	**Cr**	**Fe**	**Cu**	**O**
Unreacted Chromite Spinel (Av.)	12.7	7.9	0.1	0.2	36.3	8.1	-	34.7
(Standard Deviation)	*(0.7)*	*(0.2)*	*(0.0)*	*(0.1)*	*(0.8)*	*(0.6)*	*(-)*	*(0.2)*
Periphery of Grain (Av.)	13.6	6.7	0.05	0.2	30.5	12.9	0.2	32.9
(Standard Deviation)	*(0.4)*	*(0.4)*	*(0.0)*	*(0.1)*	*(0.7)*	*(0.5)*	*(0.1)*	*(2.9)*
Center of Grain (Av.)	14.3	7.9	0.04	0.2	35.8	5.6	0.1	34.7
(Standard Deviation)	*(0.4)*	*(0.1)*	*(0.0)*	*(0.0)*	*(0.5)*	*(0.1)*	*(0.0)*	*(0.4)*

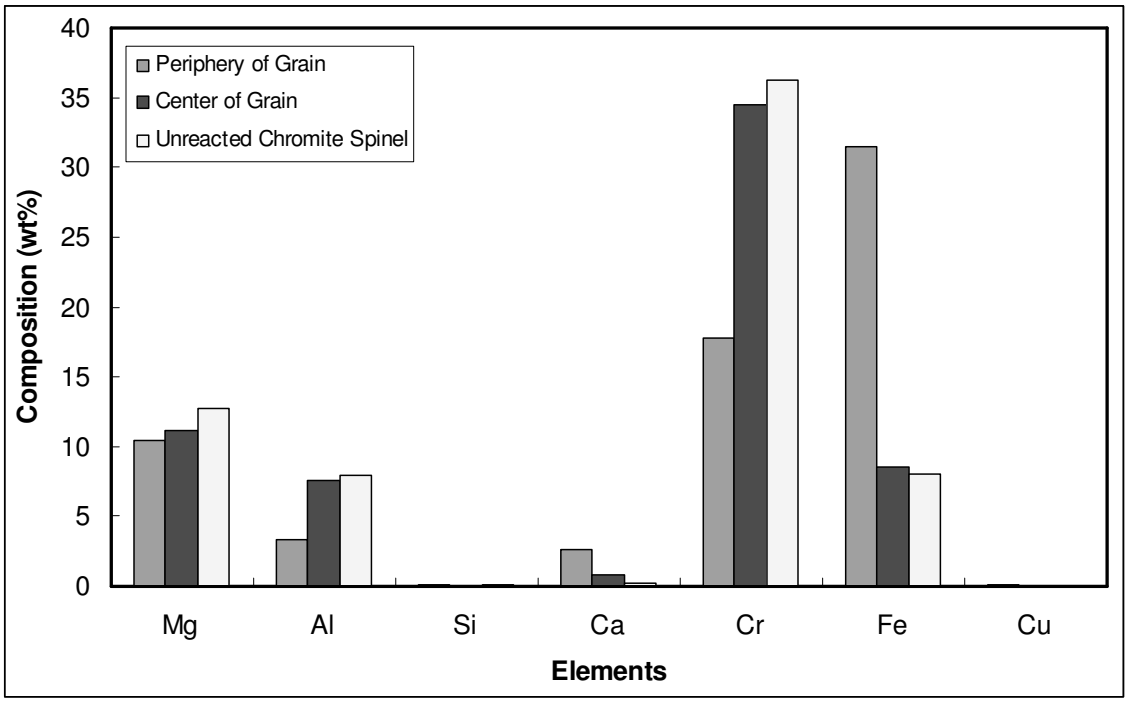

Figure 5.1.17: Comparison of composition of chromite spinel grains before and after reaction with calcium ferrite slag at oxygen partial pressure of 10^{-6} atm., 1300°C for 32hrs

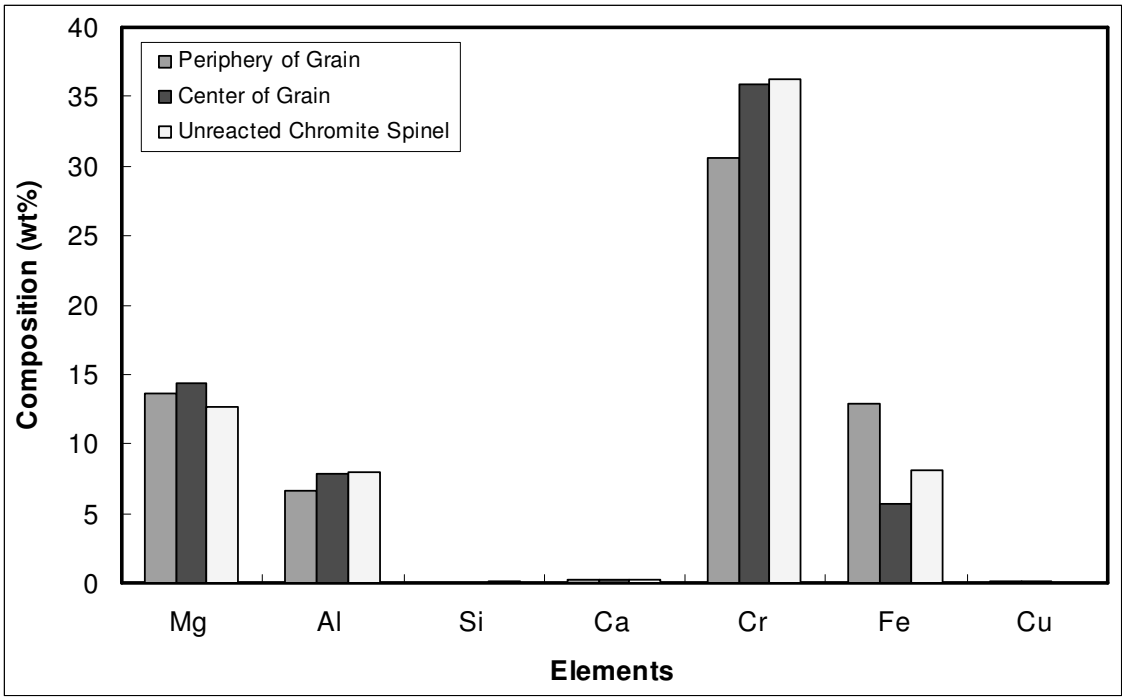

Figure 5.1.18: Comparison of composition of chromite spinel grains before and after reaction with FCS slag at oxygen partial pressure of 10^{-6} atm., 1300°C for 32hrs

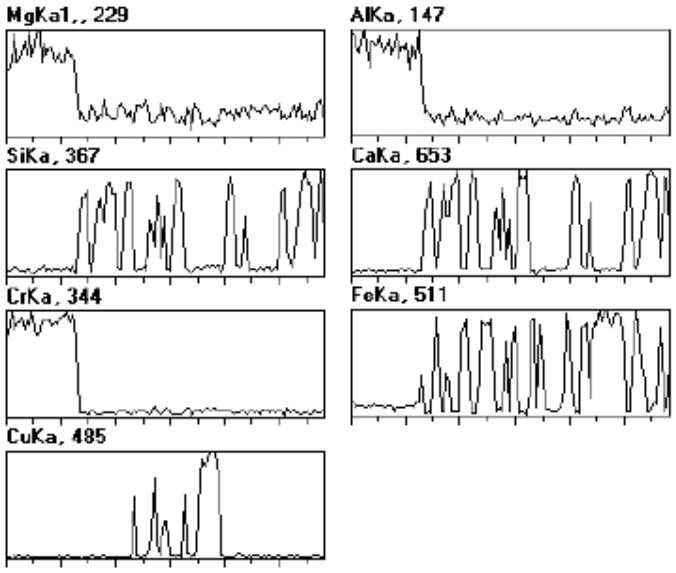

Figure 5.1.19: Line scan of chromite spinel at interface of refractory contacted with molten FCS slag at 1300°C, oxygen partial pressure of 10^{-6} atm., 32 hours.

2) MgO-Cr_2O_3-Fe_2O_3 SYSTEM AT 1300°C

It is clearly evident from the current data that iron oxide is the only species in either calcium ferrite or FCS slag which is interacting with the chromite spinel phase of the refractory. At 1300°C and an oxygen partial pressure of 10^{-6} atm, the Fe^{3+}/Fe^{2+} ratio and the mole fraction of FeO_x in calcium ferrite and FCS slag is given in Table 5.1.12. The Fe^{3+}/Fe^{2+} ratio and the mole fraction of FeO_x in iron silicate slag at similar conditions is also given. The Fe^{3+}/Fe^{2+} ratio of iron silicate and calcium ferrite slags was taken from Figures 2.3.4 and 2.3.5, respectively. The Fe^{3+}/Fe^{2+} ratio of FCS slag used for the slag/brick experiments was determined using titrations as detailed in Chapter 4.6.2. The mole fraction of FeO_x in FCS slag was calculated based on the slag composition analyzed using ICP-AES and that for iron silicate and calcium ferrite slags was calculated from slag compositions given in Mackey *et al.* (1982) and Kongoli *et al.* (2006), respectively. As seen in Table 5.1.12, the ferric ions are the dominating species of iron in both FCS slag and calcium ferrite slag both in terms of mole fraction and Fe^{3+}/Fe^{2+} ratio whilst ferrous ions are dominating in iron silicate slag.

Table 5.1.12: The Fe^{3+}/Fe^{2+} ratio of iron silicate, calcium ferrite and FCS slag at 1300°C and an oxygen partial pressure of 10^{-6} atm.

	Iron Silicate Slag	**Calcium Ferrite Slag**	**FCS Slag**
Fe^{3+}/Fe^{2+} ratio	0.3	3.0	2.4 ± 0.1
Mole Fraction of FeO_x	0.68	0.53	0.42

The activity coefficient of Fe_2O_3 in the calcium ferrite slag is small and the activity of Fe_3O_4 (an indirect measure of the theoretical activity of Fe^{3+}) is high, such that calcium ferrite slag acts as a source of supply for the interdiffusion between iron (Fe^{3+}) in slag and chromium (Cr^{3+}) in the chromite spinel phase of the refractory. Both in the current study and in Fahey's (2002) study, magnesioferrite formation accompanied the interdiffusion between species in the ferrite slag and the chromite spinel phase; however no phase boundary was evident. The likelihood of the formation of magnesioferrite at the periphery of the chromite spinel grains in contact with calcium ferrite slag as a result of interdiffusion can be discussed with application of the MgO-Cr_2O_3-Fe_2O_3 phase diagram at 1300°C, taken from Section 2.4 (Figure 2.4.1) and reproduced here (Figure 5.1.20). The brick composition is normalized to MgO+Cr_2O_3+Fe_2O_3 = 100 as these are the main components of the refractory.

Chromite spinel is shown in Figure 5.1.20 as a solid solution which extends from $MgO.Fe_2O_3$ to $MgO.Cr_2O_3$. When the chromite spinel is in contact with calcium ferrite slag, Cr^{3+} in the chromite phase is replaced by Fe^{3+} from the slag and the composition of the chromite spinel solid solution shifts towards '$MgO.Fe_2O_3$' (i.e. magnesioferrite). Once Cr^{3+} is completely replaced by Fe^{3+} in the chromite spinel, $MgO.Fe_2O_3$ results. As the MgO-Cr_2O_3-Fe_2O_3 system is a solid solution series, $MgO.Fe_2O_3$ results without a phase boundary between the magnesioferrite and the chromite spinel.

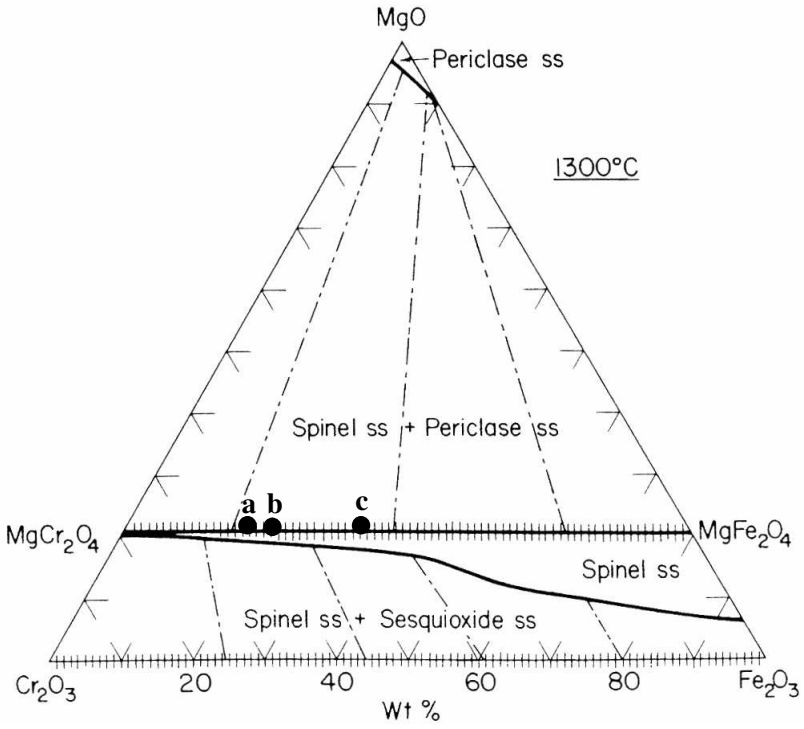

Figure 5.1.20: Phase Diagram of the System MgO-Cr_2O_3-Fe_2O_3 at 1300°C (Levin and McMurdie, 1975) *(a) = composition of the virgin chromite spinel, (b) = composition of chromite spinel after 8 hours contact with FCS slag, (c) = composition of chromite spinel after 32 hours contact with FCS slag.*

In Table 5.1.12, the Fe^{3+}/Fe^{2+} ratio of ferrous calcium silicate slag is very similar to that of calcium ferrite slags. The amount of Fe_2O_3 in FCS slag in terms of mole fraction is also considerable. The activities of FeO and Fe_3O_4 in FCS slag are not known. However it is expected that since the CaO content of FCS slag is lower than that in calcium ferrite slag and CaO/Fe_2O_3 interact strongly, a higher activity of Fe_2O_3 is expected. From the high activity of Fe_3O_4, high Fe^{3+}/Fe^{2+} ratio in slag and considerable mole fraction of FeO_x, one would expect FCS slag to attack the chromite spinel phases in the refractory to a similar extent to that seen with calcium ferrite slag. Whilst interdiffusion is taking place between Cr^{3+} in the chromite

phase and Fe^{3+} in FCS slag, the extent of interdiffusion was observed to be limited and no magnesioferrite product formation was seen on the periphery of the chromite spinel even at extended contact times. A possible explanation for the limited interdiffusion in the FCS slag/brick samples is that the activity of Fe^{3+} is lower at the interface than the bulk of the slag, which is likely for a viscous slag i.e. there is a significant mass transfer boundary layer on the slag side of the interface. As the contact time progressed, so did the extent of the interdiffusion between Fe^{3+} and Cr^{3+}, thus is it possible that over practical contact times of years in the converter, magnesioferrite may develop on the periphery of the chromite spinel phase in contact with FCS slag. The possibility of magnesioferrite as a result of the interdiffusion is also discussed with application of Figure 5.1.20.

In Figure 5.1.20, 'a' is the composition of the virgin chromite spinel, for brick composition normalized to $MgO+Cr_2O_3+Fe_2O_3 = 100$. As the slag/refractory contact time increases from 8 hours (b) to 32 hours (c), and interdiffusion between iron in FCS slag and chromium in the chromite spinel proceeds, the composition of the chromite spinel phases approaches that of magnesioferrite solid solution. Over time, the magnesium content of the chromite spinel grains does not change significantly as shown in Tables 5.1.8 and 5.1.11. Thus according to Figure 5.1.20, the formation of a magnesioferrite solid solution similar to that observed on the periphery of chromite spinel grains in contact with calcium ferrite slag is probable when FCS slag is in contact with the chromite spinel. However as the rate of interdiffusion is very slow it takes a long time for the solid solution to reach the magnesioferrite composition. Magnesioferrite on the periphery of the chromite grains in contact with calcium ferrite slag had formed after 8 hours of contact time at the same conditions.

3) PERICLASE AT 1300°C, OXYGEN PARTIAL PRESSURE OF 10^{-6} ATM.

Analysis of the periclase grains in contact with calcium ferrite slag at the slag/refractory interface at an oxygen partial pressure of 10^{-6} atm., 1300°C for 8 hours, given in Table 5.1.13 and Figure 5.1.21 shows that this phase has also changed in composition. In comparison to the virgin periclase (labeled 'unreacted in the tables and figures), the magnesium content of the periclase in contact with the ferrite slag (labeled 'reacted in the tables and figures) has decreased whilst the iron content has increased. This behaviour shows that interdiffusion is taking place between iron (Fe^{2+}) in the ferrite slag and magnesium (Mg^{2+}), since Fe^{2+} and Mg^{2+} have a same charge and a similar ionic radius, 78 and 72 pm,

respectively. Fahey (2002) also observed similar interactions between magnesium in the periclase and iron in the slag. Fahey (2002) found that a magnesioferrite product layer had formed on the periphery of the periclase grains in contact with the ferrite slag as a result of interdiffusion, although observation of his BSE images revealed no distinct phase boundary. It will be explained later that the formation of magnesioferrite from MgO does require a phase boundary, unlike the case for chromite spinel. No new phases were observed in the current calcium ferrite slag/refractory samples. Although, a region with a Fe to Mg molar ratio of 1:1, close to that of magnesiowustite solid solution, was observed on the periphery of the periclase grains in contact with calcium ferrite slag in the current samples.

Table 5.1.13: Average composition (wt%) of periclase grains in a magnesia-chrome brick in contact with calcium ferrite slag at the slag/refractory interface at oxygen partial pressure of 10^{-6} atm., 1300°C for 8hrs

	Mg	**Al**	**Si**	**Ca**	**Cr**	**Fe**	**Cu**	**O**
Unreacted Periclase (Av.)	52.6	0.6	0.1	0.1	3.3	4.9	-	38.3
(Standard Deviation)	*(0.7)*	*(0.3)*	*(0.1)*	*(0.1)*	*(0.9)*	*(0.9)*	*(-)*	*(0.3)*
Reacted Periclase (Av.)	43.3	0.3	0.3	0.3	3.5	18.4	0.5	36.2
(Standard Deviation)	*(0.2)*	*(0.4)*	*(0.1)*	*(0.1)*	*(0.7)*	*(0.7)*	*(0.3)*	*(1.8)*

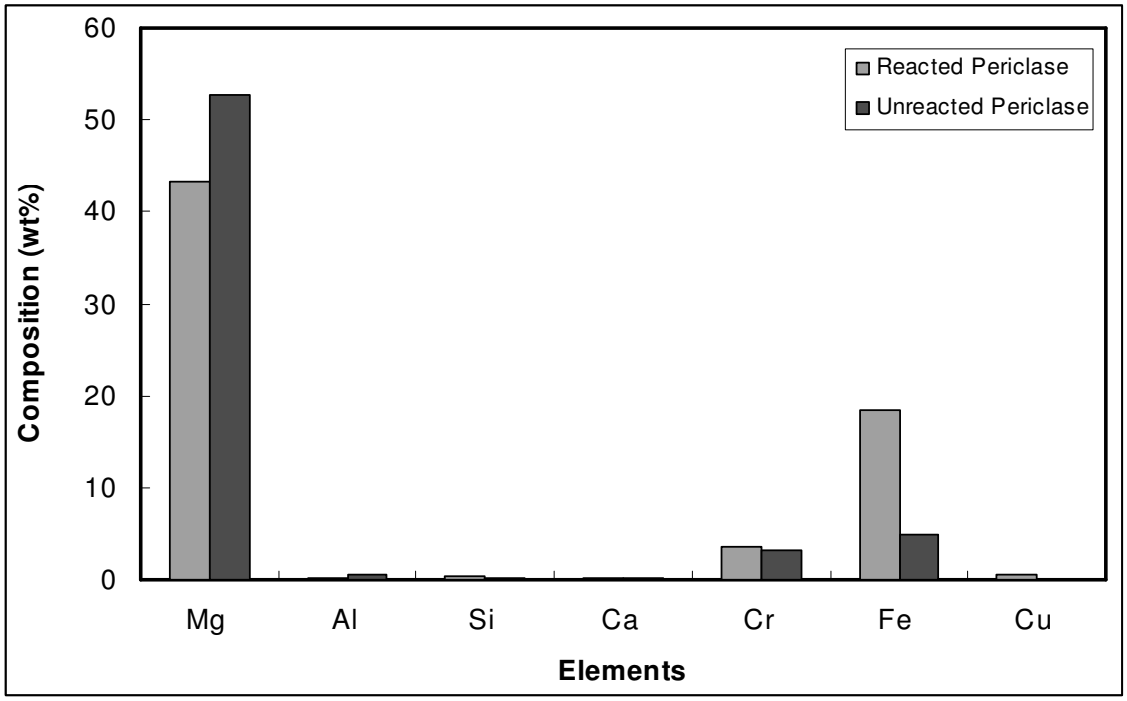

Figure 5.1.21: Comparison of composition of periclase grains before and after reaction with calcium ferrite slag at oxygen partial pressure of 10^{-6} atm, 1300°C for 8hrs.

As seen in Table 5.1.14 and Figure 5.1.22, when the periclase is in contact with FCS slag, there is also an increase in the iron content and decrease in the magnesium content of the periclase grains, again indicating that interdiffusion in taking place between iron (Fe^{2+}) in FCS slag and magnesium (Mg^{2+}) in the periclase. No magnesioferrite was observed on the periphery of the periclase in contact with FCS slag, although magnesiowustite solid solution, with Fe to Mg molar ratio of 1:1, was detected on the periphery of some periclase grains.

Table 5.1.14: Average composition (wt%) of periclase grains in a magnesia-chrome brick in contact with FCS slag at the slag/refractory interface at an oxygen partial pressure of 10^{-6} atm, 1300°C for 8hrs.

	Mg	**Al**	**Si**	**Ca**	**Cr**	**Fe**	**Cu**	**O**
Unreacted Periclase (Av.)	52.6	0.6	0.1	0.1	3.3	4.9	-	38.3
(Standard Deviation)	*(0.7)*	*(0.3)*	*(0.1)*	*(0.1)*	*(0.9)*	*(0.9)*	*(-)*	*(0.3)*
Reacted Periclase (Av.)	47.4	0.6	0.2	0.5	2.6	11.2	1.7	37.0
(Standard Deviation)	*(0.4)*	*(0.1)*	*(0.1)*	*(0.3)*	*(0.4)*	*(0.8)*	*(0.4)*	*(0.5)*

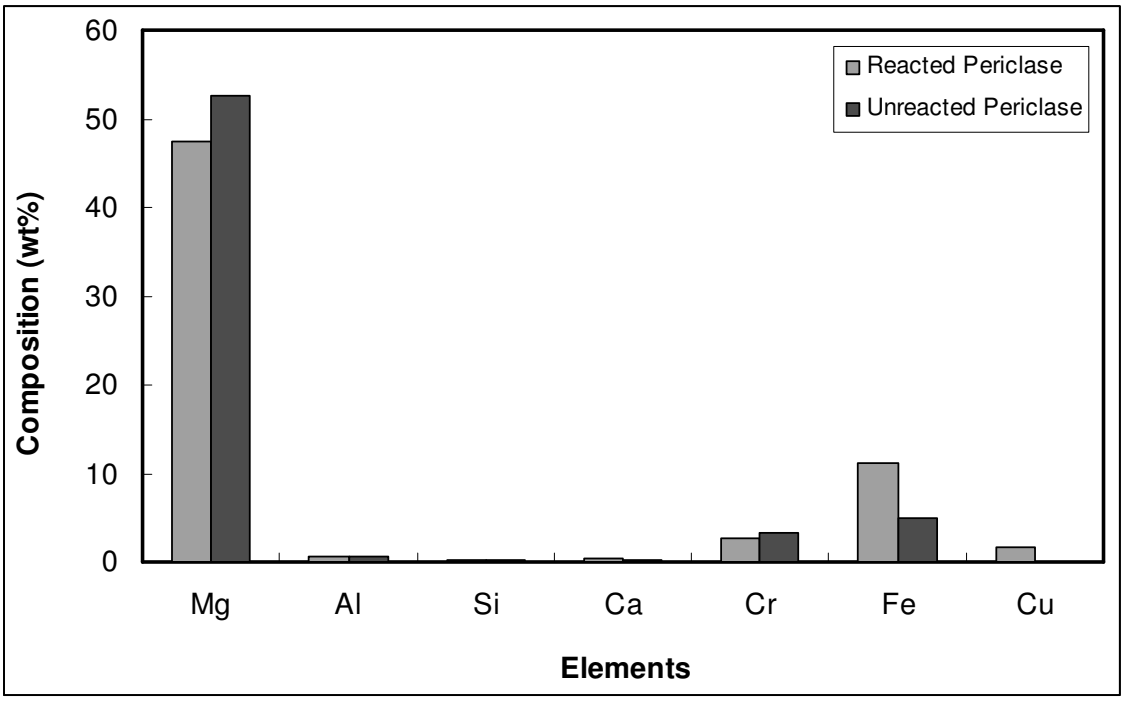

Figure 5.1.22: Comparison of composition of periclase grains before and after reaction with FCS slag at an oxygen partial pressure of 10^{-6} atm., 1300°C for 8hrs

The interdiffusion between iron in FCS slag and magnesium in periclase is further illustrated by the line scan analysis in Figure 5.1.23, taken over the interface between FCS slag and the periclase. Tracing the line scan from the slag to the periclase, the magnesium and iron content increase and decrease, respectively. These changes are less than for the calcium ferrite slag samples, signifying that the rate of diffusion between species in FCS slag and the periclase are not as rapid as with calcium ferrite slag.

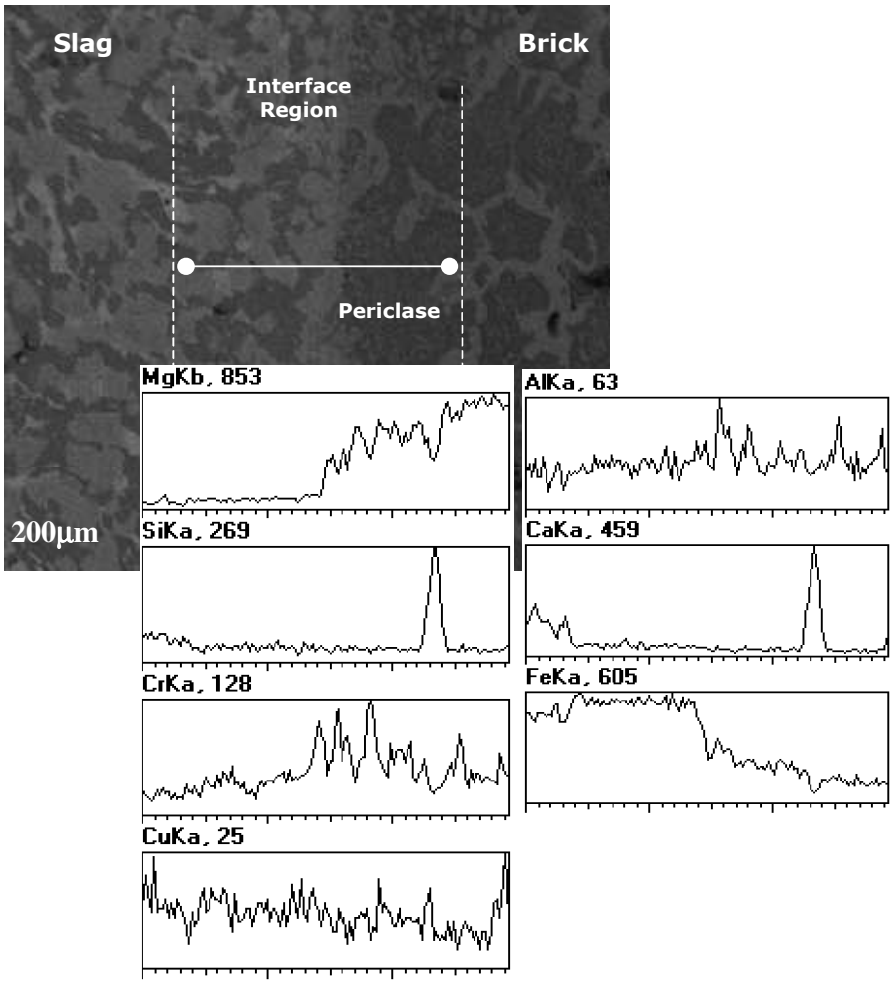

Figure 5.1.23: Line scan of periclase at interface of refractory contacted with molten FCS slag at 1300^{o}C and an oxygen partial pressure of 10^{-6} atm. for 8 hours

Following 32 hours of contact time, the magnesium and iron content of the periclase has not changed much with time when in contact with calcium ferrite slag, as seen in Table 5.1.15 and Figure 5.1.24. When comparing the iron enrichment and chromium and aluminum depletion in the chromite spinel phase in contact with the ferrite slag to the iron enrichment and magnesium depletion in the periclase phase, it is evident that:

- Following 32 hours of contact with calcium ferrite slag, the iron content of the chromite spinel at the periphery was almost double and the chromium content halve the content of the two species in the spinel after 8 hours, as seen in Tables 5.1.7 and 5.1.10.
- On the contrary, the iron content of the periclase has only increased by approximately 1 weight percent and the magnesium content only decreased by 1 weight percent from 8 hours of contact to 32 hours of contact with calcium ferrite slag, as evident in Tables 5.1.13 and 5.1.15.

Over time interdiffusion between iron in calcium ferrite slag and ions in the periclase is not as rapid as that observed in the chromite spinel. This is likely due to the fact that calcium ferrite slag contains very little Fe^{2+}, the interdiffusing species from slag to periclase. The current findings are supported by Yan *et al.* (2001) who also found that the dissolution rate of Cr_2O_3 (2.3×10^{-6} $g.cm^{-2}.s^{-1}$) in calcium ferrite slag is higher than the dissolution rate of MgO (1.1×10^{-6} $g.cm^{-2}.s^{-1}$). The current data further supports Fahey's (2002) findings that the chromite phase is preferentially attacked by the ferrite slag, with the spinel grains eroding after longer exposure times and the undissolved periclase grains appearing in the slag.

Table 5.1.15: Average composition (wt%) of periclase grains in a magnesia-chrome brick in contact with calcium ferrite slag at the slag/refractory interface at an oxygen partial pressure of 10^{-6} atm., 1300°C for 32hrs

	Mg	**Al**	**Si**	**Ca**	**Cr**	**Fe**	**Cu**	**O**
Unreacted Periclase (Av.)	52.6	0.6	0.1	0.1	3.3	4.9	-	38.3
(Standard Deviation)	*(0.7)*	*(0.3)*	*(0.1)*	*(0.1)*	*(0.9)*	*(0.9)*	*(-)*	*(0.3)*
Reacted Periclase (Av.)	42.2	0.1	0.3	0.5	3.7	19.3	0.5	35.8
(Standard Deviation)	*(0.6)*	*(0.1)*	*(0.0)*	*(0.3)*	*(0.2)*	*(0.4)*	*(0.2)*	*(1.2)*

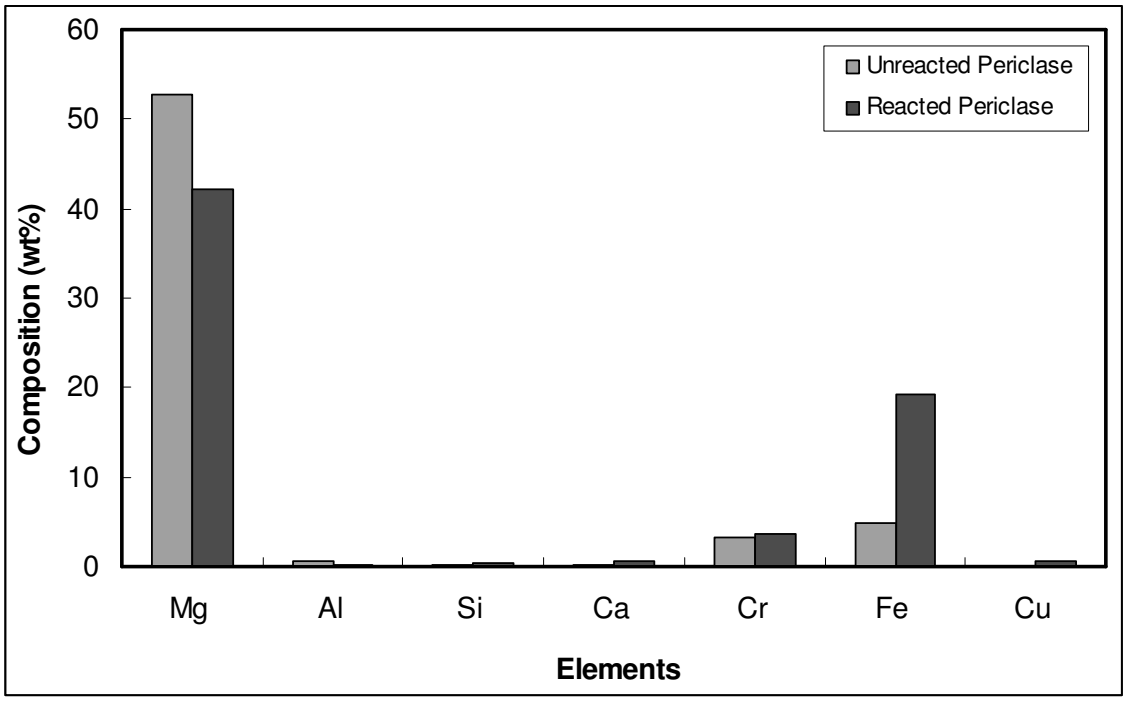

Figure 5.1.24: Comparison of composition of periclase grains before and after reaction with calcium ferrite slag at an oxygen partial pressure of 10^{-6} atm., 1300°C for 32hrs

Table 5.1.16 and Figure 5.1.25 shows the change in composition in periclase following contact with FCS slag for 32 hours at 1300°C and an oxygen partial pressure of 10^{-6} atm. Compared to that in contact with FCS slag for 8 hours, this phase has further depleted in magnesium and enriched in iron following 32 hours of contact with FCS slag. The average magnesium content of the periclase grains has decreased by approximately 3 wt% and the average iron content has increased by 4 wt%. Nonetheless, even following extended contact time, no magnesioferrite formation on the periclase phase was observed. However a magnesiowustite solid solution, with Fe to Mg molar ratio of 1:1 was detected on the periphery of some periclase grains.

Once again interdiffusion between magnesium in periclase and iron in FCS slag at 32 hours is illustrated by the line scan in Figure 5.1.26 where a gradual increase in the iron content and a gradual decrease in the magnesium content of the periclase grains results close to the slag/refractory interface.

Table 5.1.16: Average composition (wt%) of periclase grains in a magnesia-chrome brick in contact with FCS slag at the slag/brick interface at an oxygen partial pressure of 10^{-6} atm., 1300°C for 32hrs.

	Mg	**Al**	**Si**	**Ca**	**Cr**	**Fe**	**Cu**	**O**
Unreacted Periclase (Av.)	52.6	0.6	0.1	0.1	3.3	4.9	-	38.3
(Standard Deviation)	*(0.7)*	*(0.3)*	*(0.1)*	*(0.1)*	*(0.9)*	*(0.9)*	*(-)*	*(0.3)*
Reacted Periclase (Av.)	44.7	0.04	0.8	1.2	1.4	15.1	0.4	35.8
(Standard Deviation)	*(0.3)*	*(0.1)*	*(0.5)*	*(0.8)*	*(0.7)*	*(0.4)*	*(0.2)*	*(0.9)*

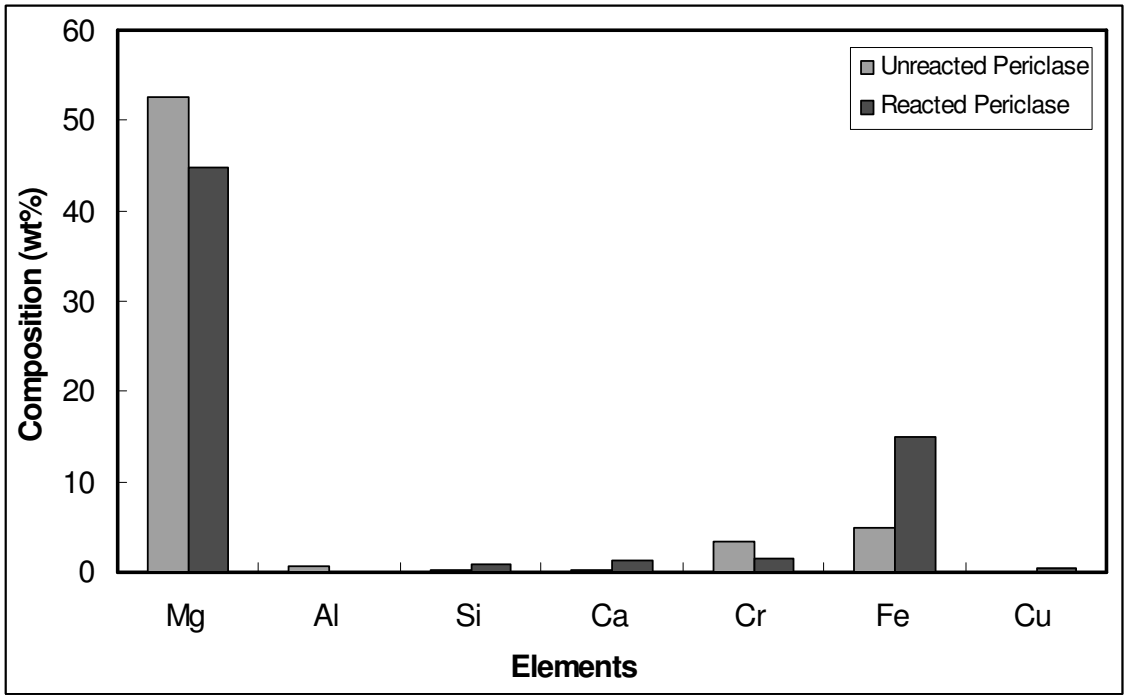

Figure 5.1.25: Comparison of composition of periclase grains before and after reaction with FCS slag at an oxygen partial pressure of 10-6 atm., 1300oC for 32hrs

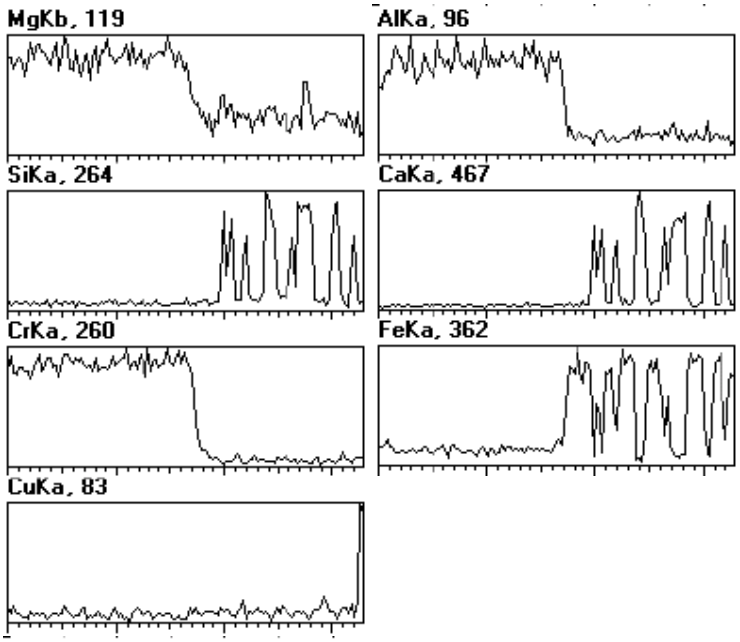

Figure 5.1.26: Line scan of periclase at interface of brick contacted with molten FCS slag at 1300°C and an oxygen partial pressure of 10^{-6} atm., 32 hours

When comparing the content of iron and magnesium in the periclase in contact with calcium ferrite slag to that in contact with FCS slag, it is evident that whilst interdiffusion between species in FCS slag and periclase has progressed with time, it is not at a very rapid rate. Following 32 hours of contact, the iron enrichment and magnesium depletion in periclase is much higher when the refractory is in contact with the ferrite slag. In the current samples, magnesiowustite solid solution was detected, however in the case of FCS slag only on the periphery of a few periclase grains in contact with the slag and for calcium ferrite slag; magnesiowustite was detected on almost all periclase grains in contact with the ferrite slag. This further indicates that rate of diffusion between iron in FCS slag and magnesium in periclase is slower than calcium ferrite slag.

4) MGO-FEO-FE_2O_3 SYSTEM AT 1300°C

Periclase is essentially impure MgO and when calcium ferrite slag is contact with this phase, Fahey (2002) found that magnesioferrite formed on the periphery of the grains as a result of interdiffusion between Mg^{2+} in the periclase and Fe^{2+} in the slag. No magnesioferrite was observed in the current calcium ferrite slag/refractory samples, however, a magnesiowustite solid solution was observed on the periphery of the periclase grains in contact with calcium ferrite slag. The likelihood of the formation of magnesioferrite and

magnesiowustite when periclase is in contact with calcium ferrite slag can be discussed by application of the MgO-FeO-Fe_2O_3 phase diagram at 1300^oC isotherm at various oxygen partial pressures, taken from Section 2.5 and reproduced here (Figure 5.1.27). In Figure 5.1.27 it can be seen that interactions between iron oxide in slag and magnesia in the refractory can result in the formation of magnesioferrite ($MgO.Fe_2O_3$) and magnesiowustite solid solution ($MgO.FeO$), the proportions of which vary according to the change in Fe^{3+}/Fe^{2+} ratio in slag, which is controlled by the oxygen partial pressure. As discussed in Section 2.3, at a given oxygen partial pressure, Fe^{3+}/Fe^{2+} ratio in slag is fixed. The oxygen partial pressure is fixed in the current system at 10^{-6} atm and was also fixed in the experiments conducted by Fahey (2002) at 3.7 x 10^{-4} atm (pure CO_2).

As discussed earlier, interdiffusion is only possible between elements which have the same ionic charge and a similar ionic radius. Thus Mg^{2+} will only interdiffusion with Fe^{2+}. At the oxygen partial pressure isobar of 10^{-6} atm, when MgO is in contact with slag of a Fe^{3+}/Fe^{2+} ratio appropriate to 10^{-6} atm., then the system must move along this isobar in Figure 5.1.27 , that is, the MgO by gaining Fe^{2+} by interdiffusion, will shift into the magnesiowustite phase field. With time and as interdiffusion progresses, it will shift down the isobar to higher iron contents until it reaches the magnesiowustite/magnesioferrite phase boundary. Magnesioferrite will precipitate as a separate phase with a distinct phase boundary, once the system reaches and passes the magnesiowustite/magnesioferrite boundary. As time progresses, the proportion of magnesioferrite will increase and the proportion of magnesiowustite will decrease until only the magnesioferrite remains. Thus the interactions between MgO in the refractory and iron oxides in the slag should first result in an MgO.FeO solid solution, before magnesioferrite can form. Since the interactions are taking place in solid state, within which ionic diffusion is slow, these phase changes will take a very long time.

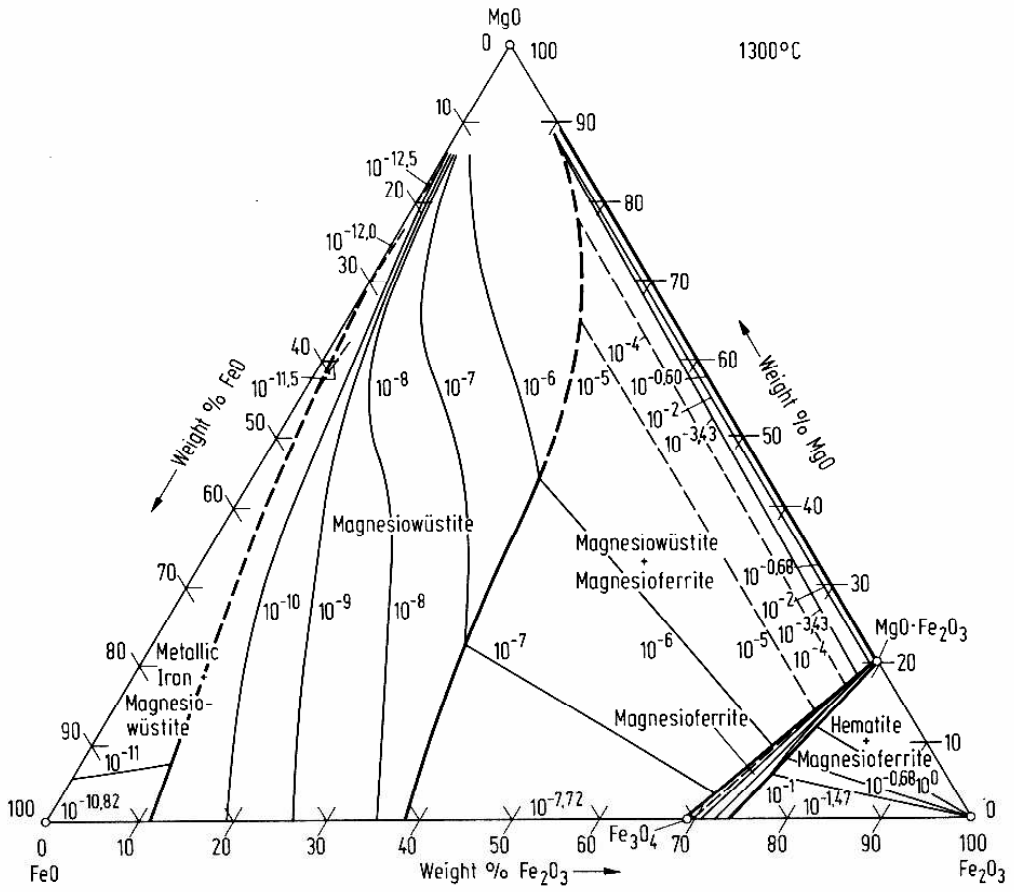

Figure 5.1.27: Phase diagram of the FeO-Fe_2O_3-MgO system along the 1300°C isotherm at various oxygen partial pressures (Levin and McMurdie, 1975).

The magnesiowustite solid solution observed in the current study, which had developed on the periphery of the periclase grains in contact with the ferrite slag thus is in accord with the FeO-Fe_2O_3-MgO phase equilibria. However, over longer contact times, once 'enough' iron interdiffusion into periclase has taken place and the phase is saturated with magnesiowustite, magnesioferrite will form at 1300°C and oxygen partial pressure of 10^{-6} atm.

In the case of Fahey's experiments, conducted at an oxygen partial pressure of 3.7 x 10^{-4} atm, this system must move close to the 10^{-4} atm isobar in Figure 5.1.27. At an oxygen partial pressure of 10^{-4} atm. much less iron needs to diffuse into MgO before magnesioferrite forms and the magnesioferrite formed will be very close to $MgO.Fe_2O_3$ along the $FeO.Fe_2O_3/MgO.Fe_2O_3$ solid solution continuum. Thus, at the conditions used by Fahey (2002), the likelihood of the formation of magnesioferrite on the periclase grains as a result of

contact with calcium ferrite slag is higher than under the experimental conditions used in this work. It is likely that the product layer Fahey (2002) observed is magnesioferrite. The lack of an observable phase boundary could be because magnesioferrite has precipitated as very small regions scattered through the material near the interface.

The formation of magnesioferrite and magnesiowusite when MgO is in contact with calcium ferrite slag has also been observed by Allen *et al.* (1995), Yamaguchi *et al.* (1994) and Sato *et al.* (1999) in air at 1300^{o}C and by Donald and Toguri (1997) at an oxygen partial pressure of 10^{-6} atm. and 1300^{o}C, as detailed in Section 2.5.2.

As evident in Figure 5.1.27, at 1300^{o}C and oxygen partial pressure of 10^{-6} atm., a magnesiowustite solid solution and a magnesioferrite solid phase should form when FCS slag is in contact with periclase. Similar to the case of calcium ferrite slag, whilst magnesiowustite was detected on some periclase grains, no magnesioferrite was observed on the periphery of the periclase phase in contact with FCS slag even at extended experimental times. However, as the contact time progressed, so did interdiffusion between Fe^{2+} and Mg^{2+}, thus is it possible that over contact times of years in the converter, magnesioferrite may develop on the periphery of the periclase phase.

5) FCS SLAG COMPOSITION - 8 HOURS OF CONTACT, 1300^{O}C AND OXYGEN PARTIAL PRESSURE OF 10^{-6} ATM

The FCS slag composition following 8 hours of contact with the refractory was also analyzed using EDX analysis. The results are reported in Table 5.1.17 and Figure 5.1.28 together with the initial slag composition. As evident in the BSE images in Figure 5.1.7, the cooling rate of the molten FCS slag was not rapid enough to form a 'glassy' phase in the cooled sample. Thus over 50 point scans were taken from the reacted slag samples both at the slag/refractory interface and further from the interface. It was noticed that the composition of the slag close to the interface was not significantly different to that far from the interface. The data in Table 5.1.17 and Figure 5.1.28 is an average of the point scans, together with the standard deviation. The lack of a composition gradient indicates that in the case of FCS slag and magnesia-chrome interactions, the diffusion of species from the slag into the refractory is most likely to be controlling the rate of change in the refractory.

Figure 5.1.28 shows that the magnesium and chromium content of FCS slag has increased following contact with the refractory, whilst the iron content has slightly decreased. Interdiffusion between magnesium and chromium from the periclase and chromite spinel, respectively, and the iron in the slag is causing the composition changes. The calcium and silicon content of the slag has not changed significantly whilst the copper content has slightly decreased. This decrease is within the standard deviation in the analyses. It was not expected that the content of calcium and silicon would vary following interactions with the refractory as neither component is involved in interdiffusion.

Table 5.1.17: Composition (wt%) of the reacted FCS slag following compared to the initial FCS slag composition after 8 hours of contact with refractory at 1300°C and oxygen partial pressure of 10^{-6} atm.

	Mg	**Al**	**Si**	**Ca**	**Cr**	**Fe**	**Cu**	**O**
Initial FCS Slag (Av.)	1.1	-	7.0	19.5	-	32.9	8.7	30.8
Reacted FCS Slag (Av.)	4.3	0.4	7.0	19.9	1.6	31.7	7.9	28.1
(Standard Deviation)	*(0.6)*	*(0.2)*	*(0.1)*	*(0.3)*	*(0.5)*	*(0.2)*	*(1.9)*	*(2.0)*

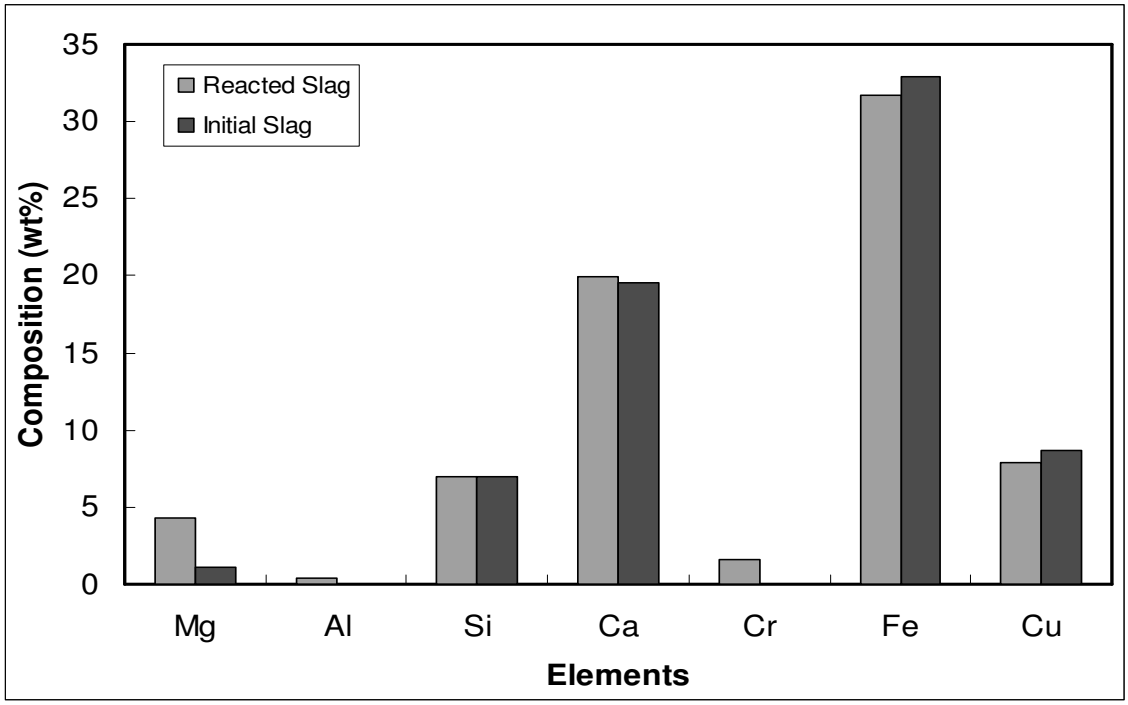

Figure 5.1.28: Composition of the reacted FCS slag compared to the initial slag composition after 8 hours of contact with refractory at 1300°C and oxygen partial pressure of 10^{-6} atm.

5.1.4 Comparison of the Refractory Wear by FCS, Calcium Ferrite and Iron Silicate slags at 1300°C

The results from this research support the conclusions made by Fahey (2002) on the wear mechanism caused by calcium ferrite slag. As detailed in Section 2.5.2, Fahey *et al.* (2004) found that due to low slag viscosity and low interfacial tension between calcium ferrite slag and magnesia-chrome refractories, calcium ferrite slag readily penetrated into the refractory via the voids within the structure of the brick. As the activity of Fe_3O_4 (which reflects the activity of Fe^{3+}) is high in calcium ferrite slag, iron (Fe^{3+}) from the penetrated slag preferentially interdiffuses with chromium (Cr^{3+}) in the chromite spinel phase and the chromium then dissolves into the ferrite slag. The interdiffusion and dissolution of chromium causes degeneration of the chromite spinel bonding phase and as a consequence, the periclase grains detach from the surface of the brick and appear in the slag phase. As chromite spinel is the main bonding phase within the magnesia-chrome bricks, the dissolution of the chromite is damaging to the integrity of the brick. Furthermore, the formation of magnesioferrite, which accompanies the interdiffusion between iron in calcium ferrite slag and chromium in the chromite spinel phase and magnesium in the periclase, contributes to brick degradation due to local volume expansion, which causes stress and leads to interfacial cracking.

As detailed in Section 2.5.1, refractory wear caused by iron silicate slag is far less severe than calcium ferrite slag, primarily due to the lack of attack by iron silicate slag on the chromite spinel bonding phase as well as due to the viscous behaviour of the silicate slag, which limits slag penetration. With the activity of FeO being high in the silicate slag (Table 5.1.12), it tends to attack the MgO in the periclase phase of the refractory. Interactions between periclase in the refractory and FeO in slag result in the formation of magnesioferrite formation as well as silicates such as forsterite ($2MgO.SiO_2$), olivine ($2MgO.2FeO.SiO_2$) and pyroxene ($MgO.FeO.SiO_2$). The presence of such silicates is a serious limitation to the refractory as these phases have a low melting point and soften at copper converting temperatures, making the brick weak and readily prone to attack by the slag. Despite the formation of silicate phases, attack of the periclase phase does not give rise to great disintegration of the brick as periclase is not the main bonding phase. In addition, reactions between iron silicate slag and the refractory occur largely at the interface due to the high viscosity of the silicate slag, which limits slag penetration and thus internal structural failure as experienced in refractories in contact with calcium ferrite slag is not apparent. Although the

silicate slag is superior to calcium ferrite slag in terms of refractory wear, as mentioned previously and discussed in detail in Section 2.2.2, iron silicate slag cannot be used for continuous copper converting due to its inherent magnetite precipitation problems.

It is clear that FCS is superior to calcium ferrite slag in terms of refractory wear. At similar conditions of 1300^{o}C and an oxygen partial pressure of 10^{-6} atm., the aggressiveness of calcium ferrite slag towards magnesia-chrome refractory bricks is much more pronounced than FCS slag, such that the refractory had eroded significantly when in contact with the ferrite slag for 32 hours. FCS slag attacked neither periclase nor the chromite spinel phases severely enough to cause brick degradation through the formation of new phases (i.e. magnesioferrite) or the dissolution of existing phases (i.e. chromite spinel bonding phase). The compositional data of FCS slag samples showed little sign of preferential attack of the chromite bonding phase, which is a significant cause of brick degradation in calcium ferrite slag samples.

The slag penetration of FCS slag into the refractory was also limited, with most interactions between slag and brick limited to being close to the slag/brick interface, indicating that FCS slag is a more viscous slag than calcium ferrite slag. Although viscosity data is not available for FCS slag, it is expected that the viscosity of this slag will be between that of iron silicate and calcium ferrite slags. With interactions occurring mostly at the slag/refractory interface and limited attack of the chromite bonding phase, the internal structural failure evident in refractories in contact with calcium ferrite slags, is highly unlikely with refractories in contact with FCS slag.

The current findings on refractory wear by FCS slag indicate that refractory wear, if any, caused by FCS slag will result predominantly from physical wear and not from chemical wear. However, although limited, FCS slag penetration is likely to densify the brick. As explained in Section 2.4, densification is caused by the accumulation of oxides, primarily lime and silica, a short distance behind the hot face as a result of slag penetration. Such oxides from the slag do not react with the brick phases. This densification can lead to thermal expansion spalling. Such spalling results from the build-up of stresses within the brick's structure caused by the differential expansion of the refractory, causing crack propagation and fracture. Whilst the current system was isothermal and spalling was not observed, thermal expansion spalling as a result of FCS slag penetration in a converter, where temperature fluctuations are probable, is also highly possible. Nonetheless, with both slag penetration and

slag/refractory interactions being not as significant as calcium ferrite slag, the use of FCS slag in a converter will result of a longer campaign life and thus reduce the costs involved in plant shut-down for brick re-lining.

5.1.5 Attack of Magnesia-Chrome Refractory by FCS Slag at 1400°C

In order to explain why FCS slag is less aggressive towards magnesia-chrome refractories than calcium ferrite slag, further slag/refractory experiments were designed to determine whether the slag's physico-chemical properties (i.e. viscosity) influence the extent of slag penetration and/or subsequent attack of the refractory. Changes to the physico-chemical properties of FCS slag were induced by increasing the experimental temperature to 1400°C keeping all other conditions constant, including oxygen partial pressure and slag composition. The EDX analysis from such experiments is discussed in this section.

1) CHROMITE SPINEL AT 1400°C, OXYGEN PARTIAL PRESSURE OF 10^{-6} ATM., FOR 8 HOURS

In Table 5.1.18 and Figure 5.1.29 the change in composition of the chromite spinel grains in contact with FCS slag at 1400°C, oxygen partial pressure of 10^{-6} atm for 8 hours at the periphery and the center of the grains is compared to the composition of the original grains. At the periphery of the grains, the spinel phase has significantly depleted in chromium and aluminum and enriched in iron. The composition of the contacted grains in the center is similar to that of the virgin grains. Similar to the case at 1300°C, as evident in Table 5.1.18 and Figure 5.1.29, at 1400°C, iron is the still the only species in FCS slag to be interdiffusing with species in the chromite spinel phase. The data in Table 5.1.18 and Figure 5.1.29, suggests that the presence of the periclase grains in FCS slag at 1400°C as seen in Figure 5.1.13, is a result of the loss of bonding between the periclase grains and the chromite grains. The deterioration of secondary spinel bonding phase is resulting from the interdiffusion between Cr^{3+} and Fe^{3+}. With the increase in the interdiffusion between iron in FCS slag and the chromium and aluminum in the chromite spinel phase, magnesioferrite formation was observed on the periphery of some chromite spinel grains at 1400°C.

Table 5.1.18: Average composition (wt%) of chromite grains in a magnesia-chrome brick in contact with FCS slag at the slag/brick interface at oxygen partial pressure of 10^{-6} atm., 1400°C for 8hrs

	Mg	Al	Si	Ca	Cr	Fe	Cu	O
Unreacted Chromite Spinel (Av.)	12.7	7.9	0.1	0.2	36.3	8.1	-	34.7
(Standard Deviation)	*(0.7)*	*(0.2)*	*(0.0)*	*(0.1)*	*(0.8)*	*(0.6)*	*(-)*	*(0.2)*
Periphery of Grain (Av.)	11.3	5.5	0.07	0.2	23.9	23.1	0.1	33.4
(Standard Deviation)	*(0.3)*	*(0.3)*	*(0.1)*	*(0.1)*	*(0.6)*	*(0.3)*	*(0.0)*	*(1.9)*
Center of Grain (Av.)	12.4	8.1	0.06	0.2	35.9	8.7	0.03	35.8
(Standard Deviation)	*(0.2)*	*(0.4)*	*(0.0)*	*(0.0)*	*(0.6)*	*(0.9)*	*(0.0)*	*(1.2)*

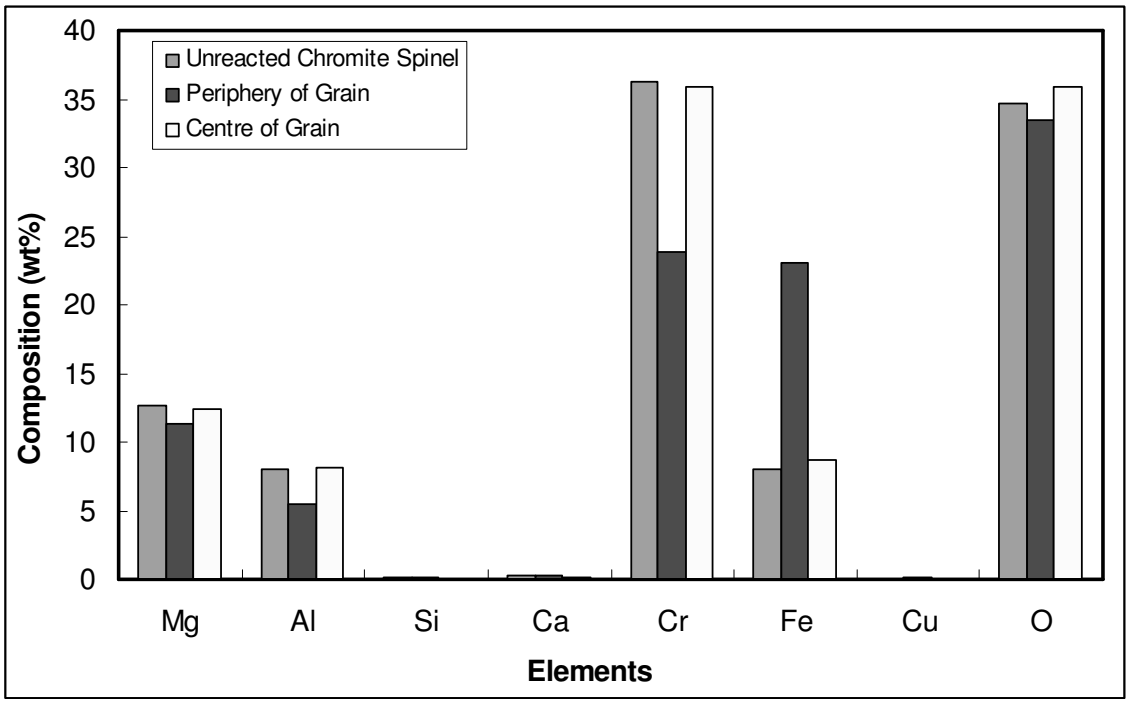

Figure 5.1.29: Comparison of composition of chromite spinel grains before and after reaction with FCS slag at oxygen partial pressure of 10^{-6} atm., 1400°C for 8hrs

When comparing the composition of the reacted chromite spinel grains at the periphery at 1300°C and 1400°C with the original grains, it is clearly evident that the interdiffusion between species in the slag and chromite phase at 1400°C has accelerated greatly (Figure 5.1.30). In Figure 5.1.30 it can be seen that, at 1400°C the iron content of the spinel phase is almost double that of the phase at 1300°C and the chromium content is almost half. The current results confirm that the attack by FCS slag is a mass transfer controlled process. With an increase in temperature, the slag viscosity has decreased, and so penetration

of FCS slag into the brick has increased, as is evident from the microstructure of the brick in Figure 5.1.13. However another observation is that an increase in temperature has also resulted in an increase in the degree of interactions between iron in slag and chromium and aluminum in the chromite spinel phase, presumably due to the higher rates of solid state diffusion. According to Bodsworth (2000) the effects of diffusion are readily seen by a change in concentration with time, such that if the rate of diffusion is slow, than the change in the concentration with time will be small. Given that for the same experimental time of 8 hours, the change in composition of the chromite spinel phase at 1400^{o}C is higher than at 1300^{o}C, it can be proposed that the rate of diffusion between species in the FCS slag and the refractory has increased at 1400^{o}C. If the diffusion rate remained unaffected by the increase in temperature, then whilst slag penetration would have increased, the average composition of the chromite spinel phases at the periphery would not be expected to change so dramatically. Furthermore, with a decrease in the slag viscosity and increase in the rate of diffusion, interdiffusion between the iron in FCS slag and the species in the chromite spinel phases is not only occurring at the slag/brick interface but also within the brick. As explained previously, whilst the degradation of the periclase phase is not very detrimental to the structure of the refractory, the disintegration of the chromite phase as a result of the increased rate of interdiffusion is damaging as this phase is the main bonding phase, the depletion of which will result in the degradation of the refractory. In comparison, at 1300^{o}C the interactions between FCS slag and the chromite spinel phase are largely taking place at the interface due to the higher viscosity of the slag, and at a much slower diffusion rate, therefore limiting interdiffusion between Cr^{3+} and Fe^{3+}.

The observed increase in the penetration of FCS slag into the refractory (i.e. decrease in slag viscosity) and the increase in the rate of solid state diffusion between iron in slag and the chromite spinel phase is in accord with Equations 5.1.1 and 5.1.2. Although viscosity of FCS slag has decreased and rate of solid state diffusion increased with increase in temperature, the effects of temperature are far greater on the rate of solid state diffusion. The decrease in slag viscosity resulted in slag penetrating further into the refractory however unlike calcium ferrite slag at 1300^{o}C, whilst FCS slag had penetrated further into the refractory; it had not penetrated out of the refractory even at 1400^{o}C. Nonetheless the increase in the rate of interdiffusion between FCS slag and the chromite spinel has resulted in similar compositional changes in the spinel phase to calcium ferrite slag at 1300^{o}C. This behaviour is in agreement with the predictions made earlier according to the activation energies for viscous flow (Table 5.1.6) and solid state diffusion (Table 5.1.5).

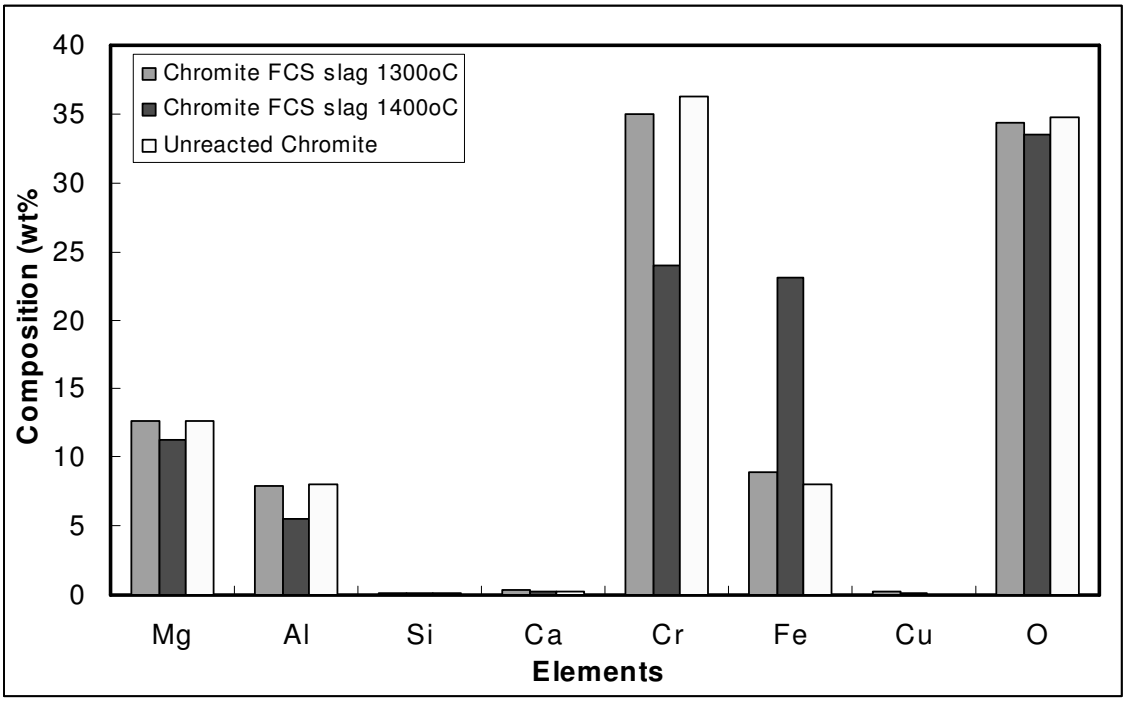

Figure 5.1.30: Comparison of composition of chromite spinel grains taken at the periphery before and after reaction with FCS slag at oxygen partial pressure of 10^{-6} atm., 1300°C and 1400°C for 8hrs

2) PERICLASE AT 1400°C, OXYGEN PARTIAL PRESSURE OF 10^{-6} ATM., FOR 8 HOURS

Table 5.1.19 and Figure 5.1.31, illustrate the composition of the periclase in contact with FCS slag at oxygen partial pressure of 10^{-6}atm., 1400°C for 8 hours along with the composition of the virgin periclase. Analysis of the periclase grains in contact with FCS slag at the slag/brick interface at oxygen partial pressure of 10^{-6} atm., 1400°C for 8 hours, shows that this phase has also depleted in magnesium and enriched in iron. Once again, interdiffusion of Fe^{2+} and Mg^{2+} is taking place, however a magnesioferrite product layer was not observed on the periphery of the periclase grains in contact with the FCS slag at 1400°C. Although close to the periphery of some periclase grains, magnesiowustite solid solution was detected.

Table 5.1.19: Average composition (wt%) of periclase grains in a magnesia-chrome brick in contact with FCS slag at the slag/brick interface at oxygen partial pressure of 10^{-6}atm., 1400°C for 8hrs.

	Mg	**Al**	**Si**	**Ca**	**Cr**	**Fe**	**Cu**	**O**
Unreacted Periclase (Av.)	52.6	0.6	0.1	0.1	3.3	4.9	-	38.3
(Standard Deviation)	*(0.7)*	*(0.3)*	*(0.1)*	*(0.1)*	*(0.9)*	*(0.9)*	*(-)*	*(0.3)*
Reacted Periclase (Av.)	33.3	0.7	0.2	0.3	3.6	27.6	0.2	36.3
(Standard Deviation)	*(0.4)*	*(0.3)*	*(0.4)*	*(0.6)*	*(0.4)*	*(0.8)*	*(0.2)*	*(2.5)*

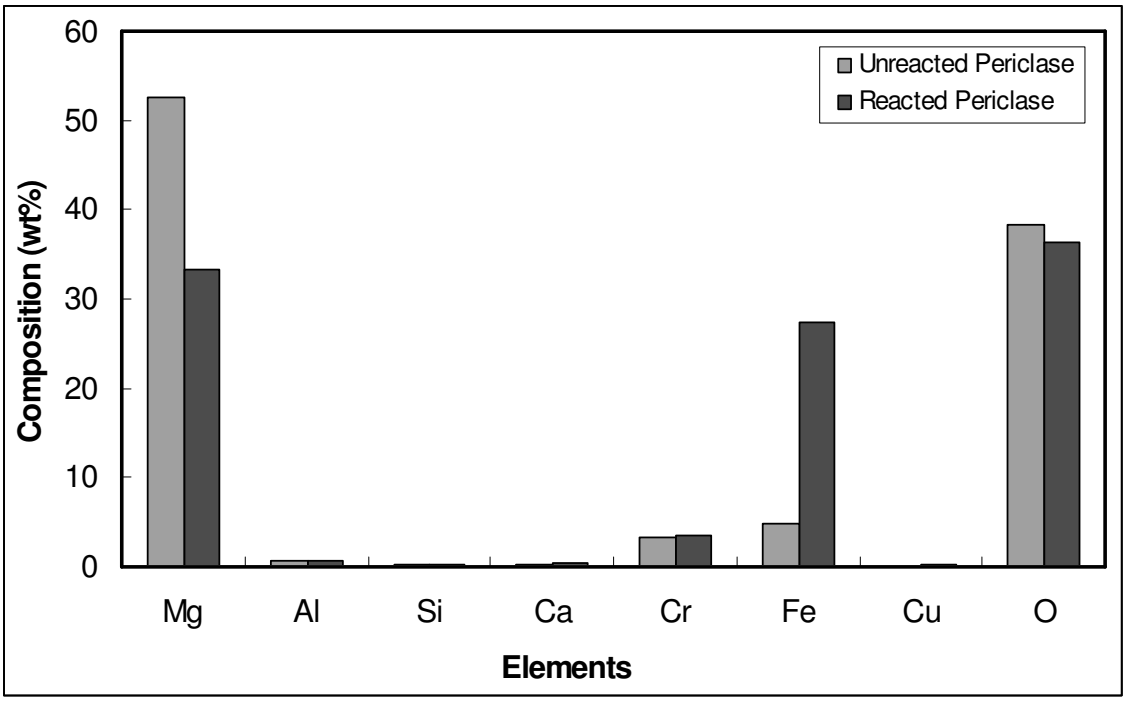

Figure 5.1.31: Comparison of composition of periclase grains before and after reaction with FCS slag at oxygen partial pressure of 10^{-6} atm., 1400°C for 8hrs

In Figure 5.1.32, it can be seen that at 1400°C, magnesiowustite and magnesioferrite are only stable under relatively oxidizing conditions and below the oxygen partial pressures of approximately $10^{-6.7}$ atm, no magnesioferrite phase forms.

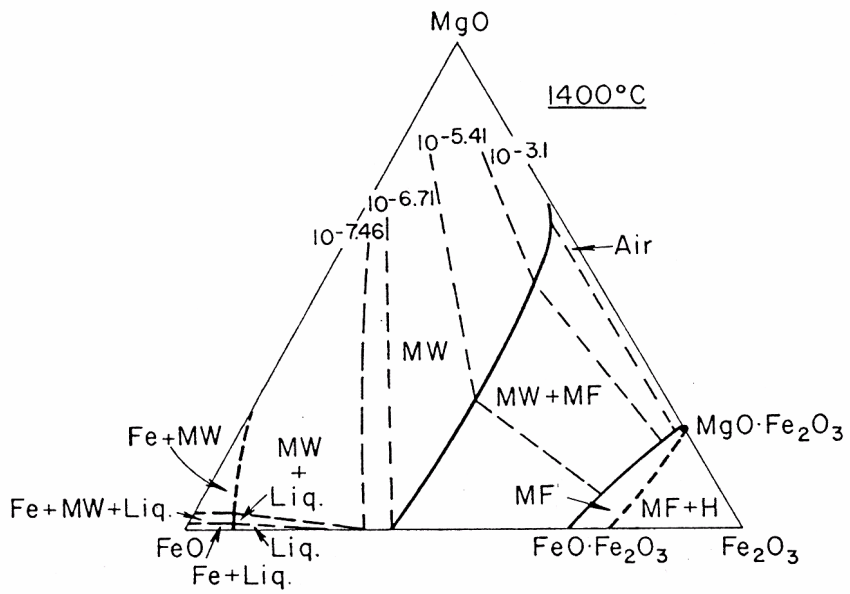

Figure 5.1.32: Phase diagram of the FeO-Fe_2O_3-MgO system along the 1400°C isotherm at various oxygen partial pressures (Levin and McMurdie, 1975).

At the current conditions, of 1400°C and oxygen partial pressure of 10^{-6} atm, magnesiowustite is stable over a wider range of conditions than at 1300°C and magnesioferrite could form however it will have a much lower MgO content than at 1300°C and the same oxygen partial pressure. At 1400°C magnesioferrite will almost be magnetite, the most magnesium-depleted end of the spinel solid solution.

When comparing the periclase phase at 1300°C and 1400°C, it can be seen in Figure 5.1.33, that the iron content of the periclase phase at 1400°C is almost double that at 1300°C, similarly the magnesium content at 1400°C is much lower than that at 1300°C. Similar to the case of the chromite spinel grains, with a 100°C increase in temperature not only has the slag viscosity decreased, allowing the slag to penetrate further into the refractory, but the rate of interdiffusion between iron in FCS slag and magnesium in the periclase phase has also increased.

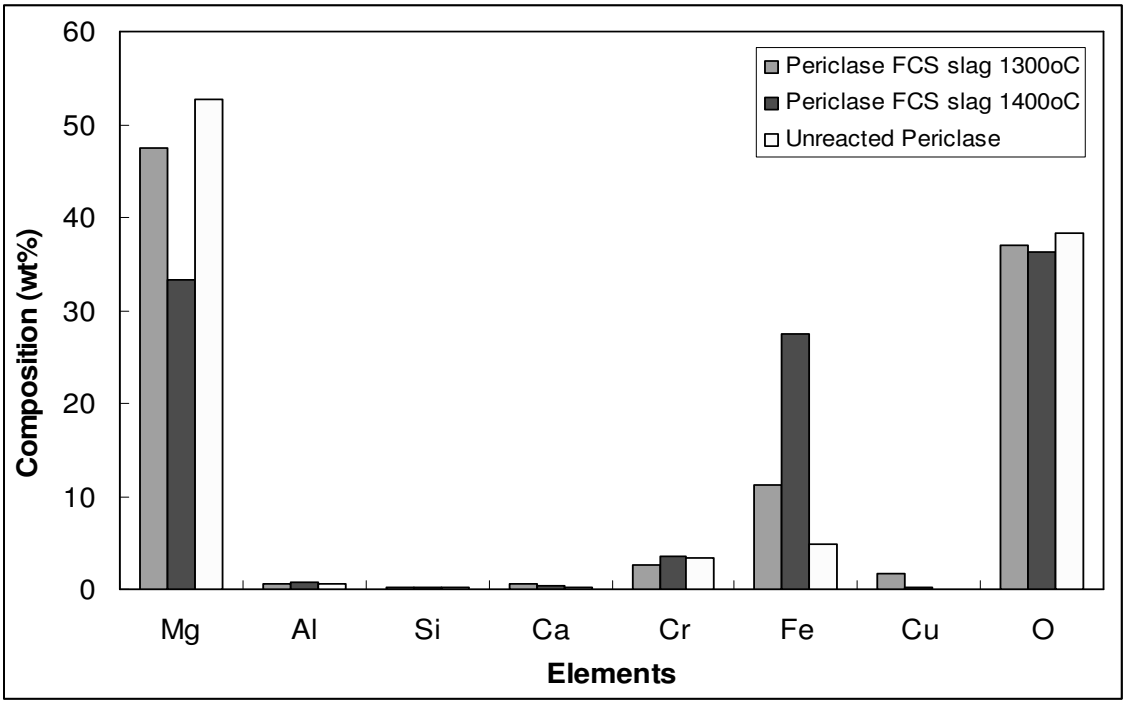

Figure 5.1.33: Comparison of composition of periclase grains before and after reaction with FCS slag at oxygen partial pressure of 10^{-6} atm., 1300°C and 1400°C for 8hrs

5.1.6 Suitability of FCS slag for Continuous Copper Converting

When comparing refractory wear caused by FCS slag at 1300°C and an oxygen partial pressure of 10^{-6} atm to that caused by calcium ferrite slag, the current findings clearly demonstrate that the refractory in contact with calcium ferrite slag had severely deteriorated (Figures 5.1.8 and 5.1.12), whilst attack on the refractory by FCS slag was not significant. Between 8 and 32 hours, the degree of interdiffusion between species in FCS slag and species in the brick had increased but not to the extent that a product layer of magnesioferrite was formed.

With an increase in temperature to 1400°C, not only had slag viscosity decreased and slag penetration increased but the rate of solid state diffusion between iron in FCS slag and species in the refractory had also increased significantly, such that the wear of the refractory was much more severe. However, no copper converting process operates at such high temperatures. Given that there is minimal attack of the refractory at 1300°C, FCS slag is suitable for use in copper converting at 1300°C where the slag viscosity is higher and the rate

of diffusion between FCS slag and refractory species is slow. The use of FCS slag will result in a longer campaign life as the life of the refractory bricks will be prolonged. In addition, less refractory material will be discarded to landfill and this will be environmentally beneficial by reducing concerns relating to the disposal of the Cr_2O_3 component of the magnesia-chrome refractories. Industrial users of the continuous copper converting processes will remain competitive and benefit financially (with lower operating cost and possibly increase profit) from reduced costs associated with refractory maintenance, including lost production and labour costs for refractory replacement work and the price of refractories themselves.

5.2 MINOR ELEMENT DISTRIBUTION

A detailed experimental procedure for the minor element distribution experiments is given in Chapter 4.0. In summary, all distribution experiments were conducted at 1300^{o}C and an oxygen partial pressure of 10^{-6} atm. for 4, 8 and 16 hours. Two series of experiments were conducted at the same conditions and experimental times for each minor element:

- The first series of experiments commenced with the metal oxide in FCS slag in contact with copper metal.
- The second series commenced with the metal in copper in contact with FCS slag.

The oxides added to slag were lead oxide representing basic oxides, nickel oxide representing neutral oxides and antimony oxide representing acidic oxides. The metals alloyed with copper were therefore lead, nickel and antimony. The FCS slag and the copper were analysed for their lead, nickel and antimony contents in each phase using ICP-AES analysis.

Listed in Table 5.2.1 are the concentrations of lead, nickel and antimony in each phase following the experimental times of 4, 8 and 16 hours. The oxides of lead, nickel and antimony in Table 5.2.1 are assumed to be PbO, NiO and $SbO_{1.5}$, respectively. These oxidation states of the three elements in FCS slag are based on the distribution behaviour of lead, nickel and antimony in iron silicate and calcium ferrite slag for a slag/copper system discussed in Chapter 2.8. It is assumed that at the same conditions, the oxidation states of the three elements in FCS slag will also be the same.

Table 5.2.1: Experimental distribution data for FCS slag at 1300°C and oxygen partial pressure of 10^{-6} atm.

	Time (hrs)	Pb (wt%)		Ni (wt%)		Sb (wt%)	
		Metal	Slag	Metal	Slag	Metal	Slag
M in Metal	**0**	**1.39**	**0**	**1.18**	**0**	**1.25**	**0**
	4	0.74	0.67	0.52	0.46	0.95	0.39
	8	0.67	0.59	0.52	0.38	0.94	0.42
	16	0.57	0.47	0.42	0.35	0.97	0.31
M in Slag	**0**	**0**	**1.13**	**0**	**0.82**	**0**	**1.24**
	4	0.36	0.52	0.22	0.26	0.57	0.54
	8	0.38	0.43	0.22	0.26	0.65	0.36
	8	0.42	0.39	0.22	0.25	0.66	0.39
	8	0.42	0.40	0.22	0.25	0.63	0.38
	16	0.33	0.33	0.22	0.23	0.56	0.32
	16	0.37	0.32	0.22	0.18	0.64	0.35
	16	0.37	0.32	0.22	0.18	0.73	0.27

Listed in Table 5.2.2 are the 'apparent distribution ratios' ($L_M^{s/m}$) of lead, nickel and antimony between FCS slag and copper at 1300°C and an oxygen partial pressure of 10^{-6} atm. at each time calculated using the raw data in Table 5.2.1 and Equation 5.2.1.

$$L_M^{s/m} = \frac{(\%M)}{[\%M]} \qquad \textbf{Equation 5.2.1}$$

In Equation 5.2.1, (%M) is the wt% of metal M in the slag phase and [%M] is the wt% of metal M in the copper. In Table 5.2.2 the term 'apparent distribution ratio' is used for these ratios as it is uncertain whether or not the data represents equilibrium conditions.

Table 5.2.2: 'Apparent' distribution ratios for lead, nickel and antimony between FCS slag and copper at 1300°C and oxygen partial pressure of 10^{-6} atm.

	Time (hrs)	$L_{Pb}^{s/m}$	$L_{Ni}^{s/m}$	$L_{Sb}^{s/m}$
M in Metal	**0**	0	0	0
	4	0.90	0.89	0.41
	8	0.89	0.73	0.44
	16	0.83	0.84	0.32
M in Slag	**0**	∞	∞	∞
	4	1.44	1.18	0.95
	8	1.12	1.18	0.55
	8	0.93	1.14	0.59
	8	0.95	1.14	0.60
	16	1.01	1.04	0.57
	16	0.85	0.82	0.55
	16	0.85	0.82	0.37

The accumulated percent relative error in the distribution ratios calculated in Table 5.2.2 is given in Table 5.2.3 for each element. As can be seen in Table 5.2.3, the relative error in the distribution experiments is the sum of the errors in each chemical analysis, in controlling temperature and in setting the oxygen partial pressure.

Table 5.2.3: Accumulated Percent Relative Error from distribution experiments of each element

Error in Distribution Measurements			
	Lead (Pb)	**Nickel (Ni)**	**Antimony (Sb)**
Temperature	± 2.66	± 3.38	± 5.15
Gas Composition	± 4.95	± 4.95	± 4.95
Analysis (Slag)	± 5.0	± 5.0	± 5.0
Analysis (Alloy)	± 5.0	± 5.0	± 5.0
Total Error	**± 17.61%**	**± 18.33%**	**± 20.10%**

A detailed discussion on the experimental and analytical uncertainties involved in distribution experiments is given in Section 4.7. In summary, according to Equation 5.2.2, and as discussed in Section 2.7.1, the distribution ratio $L_M^{s/m}$ is a function of the equilibrium constant K_1, which depends on temperature, the activity coefficients of γ^o_M and γ_{MO_v} in metal and slag, respectively and the oxygen partial pressure.

$$L_M^{s/m} = \frac{(\%M)}{[\%M]} = \frac{K_1(n_T)[\gamma^o{}_M]p_{O2}^{v/2}}{[n_T](\gamma_{MOv})} \qquad \textbf{Equation 5.2.2}$$

The activity coefficients of M and MO_v are a function of the interactions between the impurity M and the copper and the interactions between MO_v and the species in the slag, respectively. Thus γ^o_M and γ_{MO_v} are strongly affected by the chemical composition of the species in each of the metal and slag phases, respectively. Accordingly uncertainties in temperature, oxygen partial pressure and chemical analysis measurements will in effect affect the accuracy of the distribution data.

It can be seen in Table 5.2.3 that the relative error in the distribution experiments is approximately ± 20% for each element, which was the applied to all distribution data discussed in the following sections.

5.2.1 Distribution of Lead, Nickel and Antimony between FCS slag and Copper

A) Lead Distribution

The apparent distribution ratios of lead between FCS slag and copper shown in Table 5.2.2 are plotted in Figure 5.2.1, as a function of time, together with indicative relative error bars on some data points.

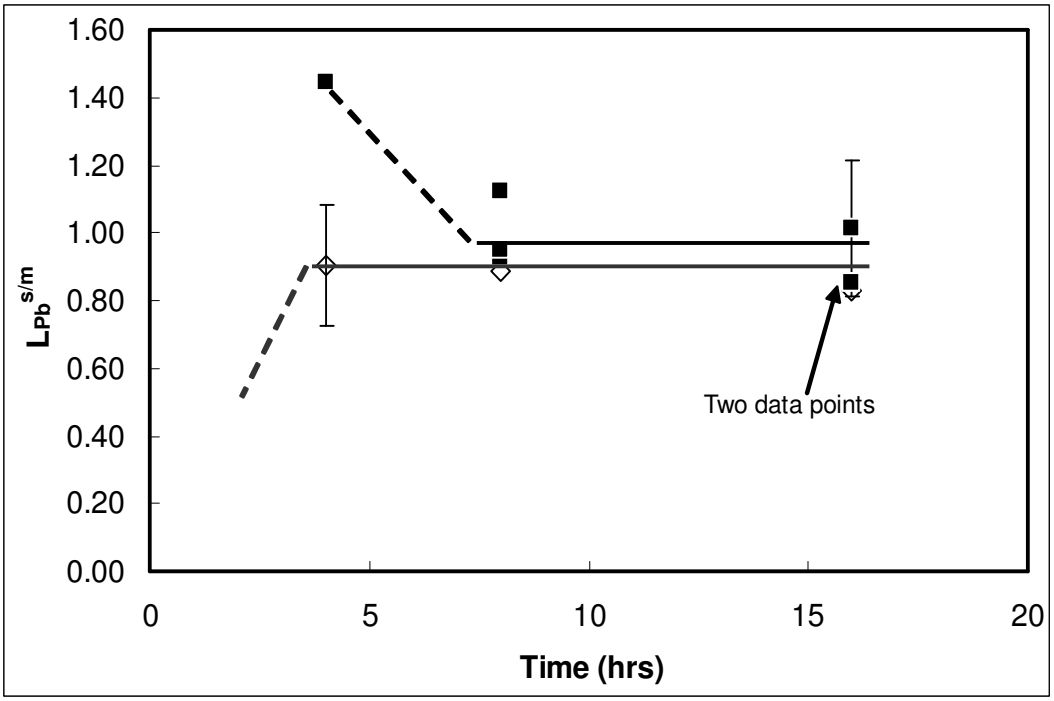

Figure 5.2.1: Apparent slag/copper distribution ratio of lead for FCS slag as a function of time at 1300°C and an oxygen partial pressure of 10^{-6} atm.
Filled squares = metal oxide initially in slag, unfilled diamonds = metal initially in copper.

As seen in Figure 5.2.1, equilibrium appears to have been approached more rapidly when lead is initially in copper. Equilibrium is achieved from the slag side following 8 hours of experimental times whilst it is achieved earlier, after 4 hours, from the metal side. However, the distribution ratios approaching equilibrium from the slag side are all a little higher than when approached from the copper side. The distribution ratio should be the same at equilibrium irrespective of which phase the minor element is in. One possible reason for the difference is the different standard used in ICP-AES for calibration to analyze the samples. Following experiments, the samples which initially had the metal in copper were sent for analysis at a much later date than the samples which initially had the metal oxide in slag. Thus, if different standards were used for analysis, this could cause a small systematic difference between the sets of data. Nonetheless, the difference between the two lines is within experimental uncertainty as indicated by the error bars in Figure 5.2.1 and thus is not significant. Both lines in Figure 5.2.1 represent the distribution ratio of lead between FCS slag and copper at equilibrium, when approached from the slag (top line) and metal (bottom line) sides. Since equilibrium was achieved after 8 hours when approaching equilibrium from the slag side, the top line is the average of the apparent distribution ratios calculated from the lead oxide in slag experiments at 8 and 16 hours in Table 5.2.2. From the metal side, equilibrium

was achieved after 4 hours and thus the bottom line is the average of the apparent distribution ratios calculated from the lead in copper experiments at 4, 8 and 16 hours in Table 5.2.2. As is evident in Figure 5.2.1, once equilibrium is achieved from both sides, all data points are within experimental error bars and there are no outliers. From Figure 5.2.1, the overall distribution ratio of lead between FCS slag and copper at 1300°C and an oxygen partial pressure of 10^{-6} atm., was taken as the average of all the apparent distribution ratios once equilibrium was achieved in Table 5.2.2 from both series of experiments, that is, $L_{Pb}^{s/m}$ = 0.93 ± 0.2. As previously mentioned, since equilibrium was not achieved at 4 hours, when approaching equilibrium from the slag side, at this time the apparent distribution ratio ($L_{Pb}^{s/m}$ = 1.44) was not included in the calculation of the average distribution ratio.

B) Nickel Distribution

In Figure 5.2.2, the apparent distribution ratios of nickel between FCS slag and copper shown in Table 5.2.2 are plotted as a function of time, together with indicative relative error bars on some data points.

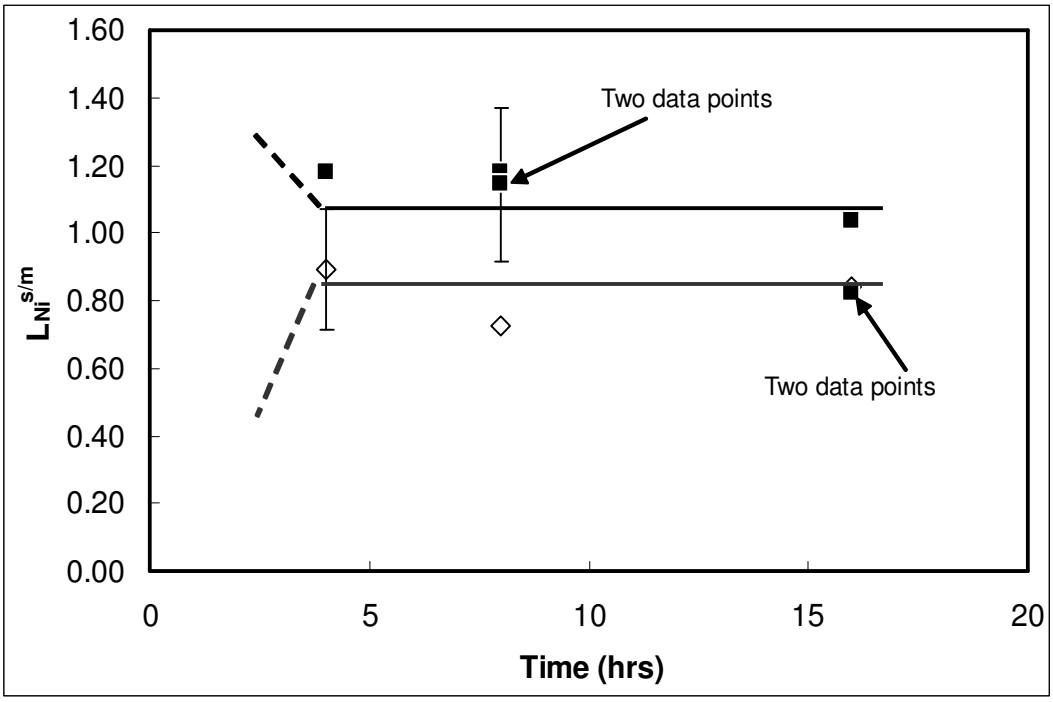

Figure 5.2.2: Apparent slag/copper distribution ratio of nickel for FCS slag as a function of time at 1300°C and an oxygen partial pressure of 10^{-6} atm.

Filled squares = metal oxide initially in slag, unfilled diamonds = metal initially in copper.

In Figure 5.2.2, equilibrium of nickel between FCS slag and copper is achieved after 4 hours, from both the slag and metal sides. With the exception of two data points, at 16 hours, when nickel oxide is initially in slag (i.e. $L_{Ni}^{s/m} = 0.82$), all other distribution data is within the error bars. Apart from being a result of experimental errors mentioned previously, the two outliers in Figure 5.2.2 could also be due to a loss of mass following experiments. The total mass of crucible, slag and copper before experiments was measured to be 12 grams and after experiments it was measured to be 11.9g, a loss of 0.1g. Significant mass loss was not experienced in any other experimental run for nickel. It is unlikely that the loss of mass is a result of volatilisation as at the experimental conditions, the vapor pressure of nickel is not high enough to result in volatilisation losses. Thus given that these two experimental runs experienced mass losses, which was not experienced in any other nickel distribution experiment, there is some doubt about their reliability. However, as the values are well within two standard deviations, the error in the data points is not of a major concern and can be ignored.

Once again, as seen in Figure 5.2.2, whilst equilibrium has been achieved, the apparent distribution ratio of nickel between FCS slag and copper at equilibrium is lower when approaching equilibrium from the metal side. As explained earlier, this discrepancy in the distribution ratios could possibly be a result of the different standards used for calibration in the ICP-AES analysis of the samples, which were also sent at different times as was the case for the lead samples. Nonetheless, given that the difference between the two lines is within experimental uncertainty, it is not significant. Both lines in Figure 5.2.2 represent the distribution ratios at equilibrium when approaching equilibrium from the slag (top line) and metal side (bottom line). Since equilibrium was achieved from both the slag and metal sides after 4 hours, the top line is the average of all the apparent distribution ratios calculated from the nickel oxide in slag experiments and the bottom line is the average of all the apparent distribution ratios calculated from the nickel in copper experiments in Table 5.2.2. The distribution ratio of nickel between FCS slag and copper at 1300^{o}C and an oxygen partial pressure of 10^{-6} atm., was taken as being 0.98 ± 0.2 at equilibrium from Figure 5.2.2. This overall distribution ratio is an average of all the apparent distribution ratios in Table 5.2.2, since equilibrium was achieved in 4 hours in both series of experiments and there are no outliers.

C) Antimony Distribution

The apparent distribution ratios of antimony between FCS slag and copper shown in Table 5.2.2 are plotted in Figure 5.2.3, as a function of time, together with indicative relative error bars on some data points.

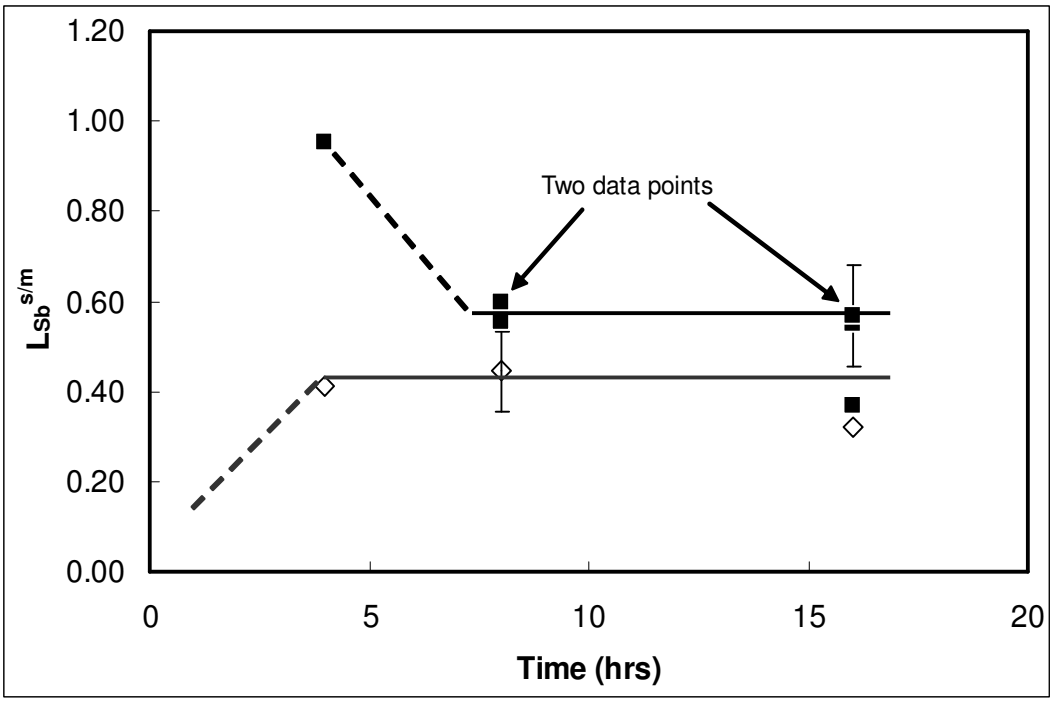

Figure 5.2.3: Apparent slag/copper distribution of antimony for FCS slag as a function of time at 1300°C and an oxygen partial pressure of 10^{-6} atm. Filled squares = metal oxide initially in slag, unfilled diamonds = metal initially in copper.

As seen in Figure 5.2.3, the equilibrium of antimony between FCS slag and copper is achieved after 4 hours, from the metal side and after 8 hours from the slag side. Similar to the case of lead and nickel distribution, the distribution ratios of antimony when approaching equilibrium from the slag side are higher than when approaching equilibrium from the metal side. This difference can again be accounted for by the possible use of different standards used for calibration in the ICP-AES analysis of the samples as once again the samples from the two series of experiments were sent for analysis at different times.

In Figure 5.2.3, there are 2 outliers at 16 hours; one is a distribution data point from experiments initially with antimony oxide in slag and the other is from experiments with antimony initially in copper. All other data points, once equilibrium has been achieved, are

within the error bars in Figure 5.2.3. Another possible cause for the two outliers, is insufficient control of volatilization of antimony. Volatilisation losses of antimony are a common occurrence at copper converting conditions as shown by Nagamori *et al.* (1982), Kim *et al.* (1996) and Yazawa *et al.* (1983). Whilst the samples were covered with an inverted alumina crucible to minimise volatilisation losses (Chapter 4.5), volatilisation losses were possible because there was a loss of mass of sample following experiments. Volatilisation generally results in the loss of material from the top phase in the crucible, that is, antimony oxide from FCS slag. As that material is lost by volatilisation, the slag/metal system seeks to re-equilibrate. However, if the rate of equilibrium is not rapid enough, the distribution of antimony is shifted to the metal phase, resulting in a decrease in the distribution ratio of antimony between FCS slag and copper. A loss of mass was experienced in all antimony experiments and it increased with time, being the highest following the 16 hours experimental times. At all 16 hours experiments, the total mass of crucible, slag and copper before experiments was measured to be 12 grams and after experiments it was measured to be 11.9g, a loss of 0.1g. However only two of the experiments conducted resulted in low distribution ratios of antimony in a slag/metal system, indicating that the system was not able to reach equilibrium in the given time following volatilisation. It is likely that this may have resulted due to systematic error such a slight fluctuation in temperature and oxygen partial pressure during experiments, which may have destabilized the distribution equilibrium of antimony in the slag/metal system and the system did not reach equilibrium in time, resulting in the two outliers. Consequently, due to the unreliability of these two data points at 16 hours, they were not considered when calculating the average distribution ratio. In Figure 5.2.3, the two lines are the average of the apparent distribution ratios at equilibrium, excluding the outliers, from the antimony oxide in slag experiments (i.e. data from the 8 and 16 hours experiments only) and the antimony in copper experiments calculated in Table 5.2.2, (i.e. data from 4, 8 and 16 hours experiments). The distribution ratio of antimony between FCS slag and copper at $1300^{o}C$ and an oxygen partial pressure of 10^{-6} atm., was taken as 0.54 ± 0.1 from Figure 5.2.3. This overall distribution ratio is an average of all the apparent distribution ratios once equilibrium has been achieved from Table 5.2.2 and does not include the apparent distribution ratio of 0.95 at 4 hours from the lead oxide is slag experiments, as equilibrium was not yet achieved as well as the apparent distribution ratios of 0.37 and 0.32 at 16 hours due to the uncertainty in their reliability as mentioned previously.

5.2.2 Comparison of the distribution of ratios

The experimentally determined distribution ratios of lead, nickel and antimony in FCS slag and copper at 1300°C and an oxygen partial pressure of 10^{-6} atm., are compared to the literature distribution data available for the same elements at the same conditions for iron silicate and calcium ferrite slags. This comparison is tabulated in Table 5.2.4 and Figure 5.2.4. Figure 5.2.4 shows graphically the relative differences in the distribution data of lead, nickel and antimony between the three slags in Table 5.2.4. The distribution data for the silicate and ferrite slags is extracted from Table 2.8.13, Section 2.8.4.

Table 5.2.4: Slag/copper distribution ratio of lead, nickel and antimony for FCS, iron silicate and calcium ferrite slags at 1300°C and an oxygen partial pressure of 10^{-6} atm. *(Source: Table 2.8.13, Section 2.8.4)*

	Iron Silicate Slag	**FCS Slag**	**Calcium Ferrite Slag**
	$L_M^{s/m}$	$L_M^{s/m}$	$L_M^{s/m}$
Pb/PbO	4.4 ± 1.3	0.93 ± 0.2	0.40 ± 0.02
Ni/NiO	1.35 ± 0.3	0.98 ± 0.2	1.09 ± 0.2
Sb/SbO$_{1.5}$	0.15 ± 0.04	0.54 ± 0.1	0.61 ± 0.03

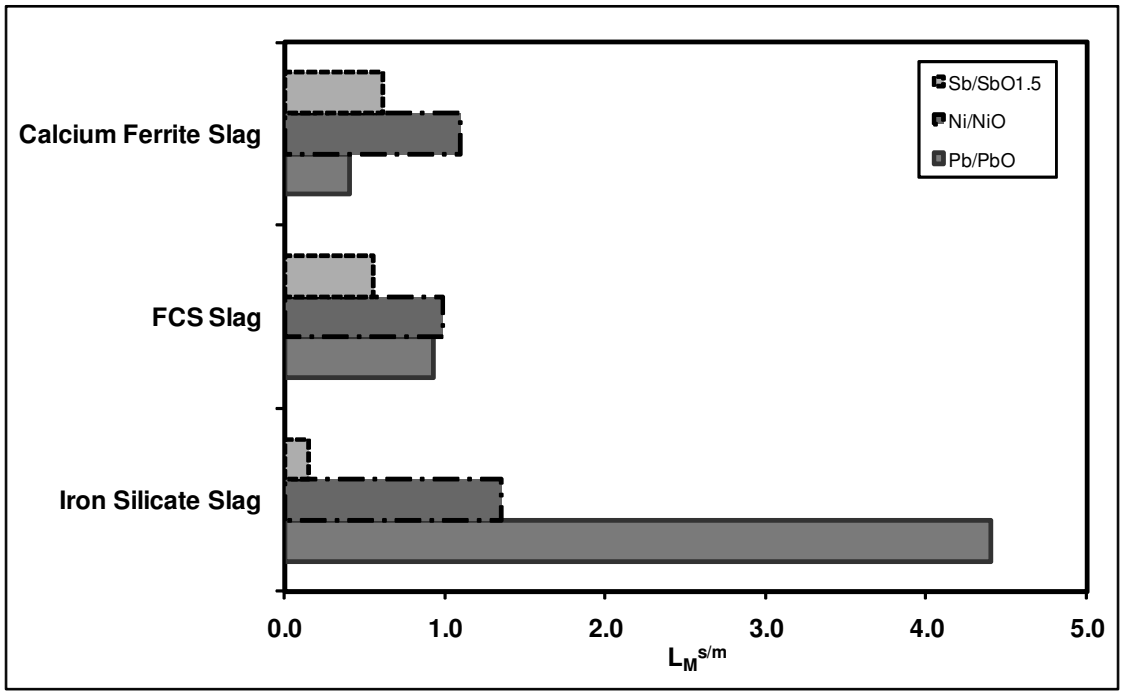

Figure 5.2.4: Slag/copper distribution ratio for nickel, lead and antimony for the three slags; iron silicate, FCS and calcium ferrite at 1300°C and an oxygen partial pressure of 10^{-6} atm.

When comparing the distribution ratio of lead in iron silicate, calcium ferrite and FCS slags in Figure 5.2.4, it is evident that lead distribution in the slag phase is highest in the silicate slag ($L_{Pb}^{s/m} = 4.4$) and lowest in the ferrite slag ($L_{Pb}^{s/m} = 0.4$). Lead distribution ratio in FCS slag is between the silicate and ferrite slag ($L_{Pb}^{s/m} = 0.93$). In the case of antimony distribution, within experimental error, the distribution of antimony in FCS slag ($L_{Sb}^{s/m} = 0.54$) is similar to that in calcium ferrite slag ($L_{Sb}^{s/m} = 0.61$). Antimony highly favors the metal phase when iron silicate slag is used, with $L_{Sb}^{s/m}$ being 0.15. The distribution ratio of nickel is very similar in the silicate ($L_{Ni}^{s/m} = 1.35$) and ferrite ($L_{Ni}^{s/m} = 1.09$) slags but slightly lower in FCS slag ($L_{Ni}^{s/m} = 0.98$).

Whilst the distribution ratio for lead is largest in iron silicate slag, the silicate slag cannot be used for continuous copper converting in the Mitsubishi C-furnace and the Kennecott-Outokumpu Flash converters due to its inherent magnetite precipitation problems. As discussed in Section 2.2.2, the equilibrium partial pressure of oxygen for magnetite saturation is calculated as approximately 10^{-6} atm. at 1300^{o}C and when the oxygen partial pressure rises above 10^{-6} atmospheres, solid magnetite will precipitate from iron silicate slag. Both the Mitsubishi C-furnace and the Kennecott-Outokumpu Flash converter operate either with pure oxygen or oxygen enriched air, where the oxygen partial pressure ranges between 10^{-6} to 10^{-5} atm., in order to reduce waste gas volume and maintain heat balance without excessive supplementary heat input. At present the Mitsubishi Corporation and KUCC use calcium ferrite slag in their converters. Whilst calcium ferrite slag is able to effectively remove elements with acidic oxides such as arsenic and antimony from blister copper, as shown in Figure 5.2.4, the removal of basic oxides such as lead oxide, to the ferrite slag is not very efficient, with a significant amount of the impurity distributing to the blister copper. This is of particular concern if lead is a major impurity in the converter feed. The insufficient removal of impurities from the blister copper results in a greater economic strain on the copper refining stages as well as producing poor quality copper. A study conducted by Zotkov *et al.* (1989) on the economic effects of the impurity levels in blister copper on fire refining, found that an increase in the impurity levels in the blister copper charged to the anode furnace leads to increased economic losses in fire refining. At present the Mitsubishi Timmins smelter removes lead from blister copper by charging silica flux and solid electric furnace slag to a rotary anode furnace prior to adding the blister copper to the furnace. The remaining sulphur and oxygen from blister copper is removed using air and ammonia, respectively, and the lead-

bearing iron silicate slag is skimmed off (Biswas and Davenport, 1980). The lead impurity in the anode copper is lowered from 0.6% to 0.15% which is further removed from the copper in electrolytic refining (Biswas and Davenport, 1980). If however lead is a major impurity in converter feed, greater amounts of the metal will distribute to blister copper with application of calcium ferrite slag. The inability of calcium ferrite slag to effectively remove lead presents a problem because the impurities pass through the blister copper fire refining stage and accumulate in the anode copper at levels which are unacceptably high for the subsequent stage of electrolytic refining. If the impurity concentration in the anode copper is too high, an excessive amount of floating "slime" forms in the electrolytic solution. The slime deposits on the surface of the cathodes, affects the copper quality, and decreases the energy efficiency of the electrolysis and the purity of the cathode copper produced (Biswas and Davenport, 1980). The presence of lead in cathode copper above 5ppm, which is the specification for the quality of cathode copper (Biswas and Davenport, 1980) can lead to cracking at the grain boundaries of solidified copper and also affects the electrical conductivity and annealability of the product. As the grade and quality of copper ores decrease with time, a slag which is able to remove all impurities from the converter effectively is most beneficial.

As discussed in Section 2.9.1, ferrous calcium silicate slag can also be successfully implemented for continuous copper converting, without the precipitation of magnetite, when FCS slag is in equilibrium with copper. In terms of minor element distribution, FCS slag can remove acidic oxides such as arsenic and antimony to the slag phase as efficiently as calcium ferrite slag whilst also being able to remove lead from the blister copper to a greater degree than the ferrite slag, as indicated by the distribution data in Figure 5.2.4. Therefore using FCS slag in copper converting operations which currently use calcium ferrite slag, will result in reduced operating and productions costs involved in refining blister copper in the anode and cathode furnaces. In addition, the recovery of valuable metals such as nickel and cobalt is also enhanced with the application of FCS slag. Nickel and cobalt are elements which form neutral oxides in terms of their interactions with species in slag. As evident in Figure 5.2.4, whilst only marginal, nickel distributes to a greater degree to the copper phase when FCS slag is applied than with use of both iron silicate and calcium ferrite slags. Nickel distribution is very similar in the ferrite and silicate slags at 1300^{o}C and oxygen partial pressure of 10^{-6} atm. Such elements are recovered from the copper during electrolytic refining as profitable by-products and thus it is aimed to distribute most of these valuable metals to the blister copper phase during copper converting in order to increase the profit margin of any smelter. Thus, the application of FCS slag in copper converting is also beneficial in the recovery of profitable

metals as over the production life of a smelter, a greater recovery of by-product metals is achievable by application of FCS slag in comparison to the silicate and ferrite slags. Although it may be argued that the slightly lower distribution ratio of nickel in FCS slag and copper than the ferrite slag is not very significant, nickel recovery is no worse when using FCS slag than it is when using calcium ferrite slag. Although not a minor element, the oxide of copper is also considered a neutral oxide. Thus based on the experimental data on the distribution of nickel between FCS slag and copper, the dissolution loss of copper as copper oxide to FCS slag will also be lower than both the silicate and ferrite slags at converting conditions, therefore resulting in a higher recovery of the metal as blister copper during converting.

5.2.3 Activity Coefficients of PbO, NiO and $SbO_{1.5}$ in Iron Silicate, Calcium Ferrite and FCS slag at 1300°C and oxygen partial pressure of 10^{-6} atm.

Listed in Table 5.2.5 are the calculated activity coefficients of lead oxide, nickel oxide and antimony oxide in iron silicate, calcium ferrite and ferrous calcium silicates slags at 1300°C and oxygen partial pressure of 10^{-6} atm. The activity coefficients of lead, nickel and antimony in copper are also given in Table 5.2.5. Liquid reference standard states are assumed for all species.

In Table 5.2.5, the activity coefficients of lead oxide, nickel oxide and antimony oxide in iron silicate and calcium ferrite slags were extracted from Table 2.8.13, Section 2.8.4. The activity coefficients of PbO, NiO and $SbO_{1.5}$ in ferrous calcium silicate (FCS) slag were calculated using Equation 5.2.3 at 1300°C and oxygen partial pressure of 10^{-6} atm, assuming liquid reference standard state for all three metals and their oxides.

$$L_M^{s/m} = \frac{(\%M)}{[\%M]} = \frac{K(n_T)[\gamma^o{}_M]p_{O2}^{v/2}}{[n_T](\gamma_{MOv})}$$

$$\therefore (\gamma_{MOv}) = \frac{K(n_T)[\gamma^o{}_M]p_{O2}^{v/2}}{[n_T]L_M^{s/m}}$$

Equation 5.2.3

In Equation 5.2.3, the activity coefficients of lead, nickel and antimony in copper were taken from Table 2.8.13, Section 2.8.4 of the literature review. It is assumed that as the impurities are present in small amounts in copper, γ_M will be constant; obeying Henry's Law

and will be the limiting activity coefficient γ^{o}_{M}. The distribution ratios of lead, nickel and antimony between slag and metal at equilibrium was obtained from experimental data in Table 5.2.4. The total number of moles of species (FeO, $FeO_{1.5}$, SiO_2, CaO, MgO, $CuO_{0.5}$ and XO_v) in FCS slag was calculated to be constant at 1.48 and 1.57 for copper metal. The composition of the slag used to calculate (n_T) is shown in Table 4.4.1, Section 4.4. The equilibrium constants, K, for Reaction Equations 5.2.4, 5.2.5 and 5.2.6 were taken from the HSC Chemistry for Windows database.

$$Pb_{(l)} + \frac{1}{2}O_{2(g)} \rightarrow PbO_{(l)}$$

$$\Delta G^{o}_{1300oC} = -73.863kJ \qquad \textbf{Equation 5.2.4}$$

$$K_{1300oC} = 2.836\times10^{2}$$

$$Sb_{(l)} + \frac{3}{4}O_{2(g)} \rightarrow SbO_{1.5(l)}$$

$$\Delta G^{o}_{1300oC} = -168.863kJ \qquad \textbf{Equation 5.2.5}$$

$$K_{1300oC} = 4.049\times10^{5}$$

$$Ni_{(l)} + \frac{1}{2}O_{2(g)} \rightarrow NiO_{(l)}$$

$$\Delta G^{o}_{1300oC} = -99.370kJ \qquad \textbf{Equation 5.2.6}$$

$$K_{1300oC} = 1.994\times10^{3}$$

Table 5.2.5: Summarised activity coefficient data for lead, nickel and antimony and their oxides at 1300°C and oxygen partial pressure of 10^{-6} atm. Liquid reference standard states are assumed for all elements and their oxides.

	[γ^{o}_{M}]	**Iron Silicate Slag**	**FCS Slag**	**Calcium Ferrite Slag**
		(γ_{MO})	**(γ_{MO})**	**(γ_{MO})**
Pb/PbO	4.8 ± 0.02	0.3 ± 0.1	1.4 ± 0.3	3.1 ± 0.8
Ni/NiO	2.3 ± 0.2	3.5 ± 0.6	4.5 ± 0.9	4.2 ± 0.1
Sb/$SbO_{1.5}$	0.03 ± 0.01	2.4 ± 0.9	0.6 ± 0.1	0.5 ± 0.2

In Table 5.2.5, the activity coefficient of lead oxide is lowest in iron silicate slag (γ_{PbO} = 0.3) and highest in calcium ferrite slag (γ_{PbO} = 3.1). The activity coefficient of PbO in FCS slag is between both the silicate and ferrite slags (γ_{PbO} = 1.3). Although, the activity coefficient of PbO in FCS slag has not been experimentally determined in literature, the activity coefficient of PbO in the ternary FeO_x-SiO_2-CaO slag system has been investigated experimentally by Takeda and Yazawa (1989) at 1300^{o}C and is shown in Figure 2.9.13, Section 2.9. Referring back to this figure, the authors found that in the vicinity of the composition of ferrous calcium silicate slag, γ_{PbO} is between 1 and 2, which is in agreement with the current experimental value.

The experimentally calculated activity coefficients for NiO in all three slag systems illustrate that the activity coefficient of NiO in the silicate (γ_{NiO} = 3.5) and ferrite (γ_{NiO} = 4.2) slags is very similar within experimental errors and is slightly higher in FCS slag (γ_{NiO} = 4.5). However, it is possible that this higher γ_{NiO} in FCS slag is due to experimental errors.

The activity coefficient of $SbO_{1.5}$ is highest in iron silicate slag ($\gamma_{SbO1.5}$ = 2.4) and lowest in calcium ferrite ($\gamma_{SbO1.5}$ = 0.5) slag. The activity coefficient of antimony oxide in FCS slag ($\gamma_{SbO1.5}$ = 0.6) is similar to the ferrite slags, within experimental errors. The behavior of the activity coefficients of PbO, NiO and $SbO_{1.5}$ in iron silicate, calcium ferrite and FCS slag at similar conditions, is in agreement with the distribution of the three elements in the ferrite, silicate and FCS slags discussed earlier.

5.2.4 Comparison of the experimental distribution behaviour with thermodynamic predictions

The distribution behaviour of minor elements in an FCS slag/copper system predicted by Yawaza *et al.* was based on the regular solutions model of a ternary slag consisting of SiO_2, CaO and metal oxide, MO as discussed in Chapter 2.7.3. The ternary models are reproduced in Figures 5.2.5(a) and 5.2.5(b), for neutral metal oxide, FeO, and basic metal oxide, PbO, respectively.

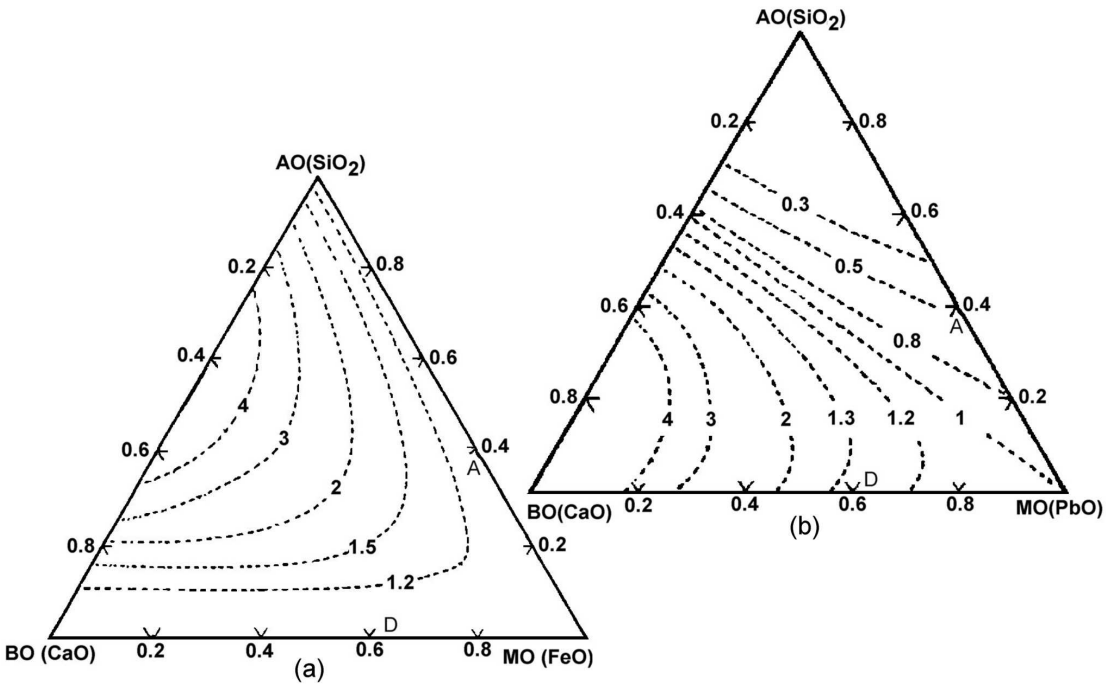

Figure 5.2.5: Isoactivity coefficients of a neutral oxide (a) and a basic oxide (b) in SiO_2-CaO-MO. (Yazawa, 1994, Reproduced, and modified)

Illustrated in Figure 5.2.5(a) is the activity coefficients for a "neutral" oxide such as Cu_2O, FeO, NiO etc. in a slag containing SiO_2 and CaO, as predicted by the model, where $\alpha_{AO\text{-}BO} = -9$, $\alpha_{BO\text{-}MO} = -1$ and $\alpha_{MO\text{-}AO} = 0$. The activity coefficients for MO in iron silicate slag 'A' and in calcium ferrite slag 'D' are very similar, but for FCS slag, which lies between the FeO and $xCaO.SiO_2$ tie-lines, where x is the CaO/SiO_2 ratio and is between 1 and 2, the activity coefficient for MO is predicted to be slightly larger. This predicted behavior is in accord with the calculated activity coefficient values given in Table 5.2.5 for all three slags.

According to Equation 5.2.3, for a fixed temperature (i.e. fixed K) and oxygen partial pressure, the distribution ratio of an element in a slag/metal system is inversely proportional to the activity coefficient of metal oxide (γ_{MOv}) in slag. In Equation 5.2.3, (n_T) and [n_T] are essentially constant when all species are expressed in their monocation format (Section 2.7.1) and when the impurities are present in small amounts γ_M will also be constant and will be the limiting activity coefficient γ^o_M. Based on this and the predicted activity coefficient behaviour of a neutral metal oxide in Figure 5.2.5(a), the distribution of elements with neutral oxides such as NiO in FCS slag can be expected to be lower than both iron silicate and calcium ferrite slag. The experimental data on the distribution of nickel in FCS slag and copper metal when compared to the distribution in iron silicate and calcium ferrite slags in Table 5.2.4 and

Figure 5.2.4 is in accord with thermodynamic predictions. As expected, nickel distributes similarly in iron silicate and calcium ferrite slag however has a slightly lower distribution ratio in FCS slag.

The distribution behavior of nickel and other elements with neutral oxides is explained in Section 2.7.3 in terms of their interactions with other species in slag. In summary, in the silicate and ferrite slags, which consist of strong acidic oxide, SiO_2 and strong basic oxide, CaO, respectively, the activity coefficient of a neutral metal oxide is unaffected by the solvent slag, as the interactions between a neutral metal oxide and SiO_2 or CaO are weak. If the two oxides are in solution together, as is the case in FCS slag, they are strongly associating, forming a stable solution of $xCaO.SiO_2$ and the addition of a neutral metal oxide such as NiO which does not have strong interactions with either CaO or SiO_2 results in even weaker interactions between NiO, CaO and SiO_2, such that the activity coefficient on NiO in the ternary slag is larger than both the silicate and ferrite slags.

Figure 5.2.5(b) shows the activity coefficients for the basic oxide PbO in a slag containing SiO_2 and CaO, where $_{\alpha AO\text{-}BO} = -9$, $\alpha_{BO\text{-}MO} = 2$ and $\alpha_{MO\text{-}AO} = -5$. The curves of $\gamma_{MObasic}$ at the composition of iron silicate slag display negative deviation from ideality with γ_{PbO} being less than one. Such behaviour suggests that there exist strong interactions between PbO and SiO_2 in the silicate slag and the distribution of lead in iron silicate slag will be high. As the slag composition shifts from the AO-MO binary slag to the BO-MO binary slag in Figure 5.2.5(b), the $\gamma_{MObasic}$ curves begin to deform, displaying less negative and a more positive deviation in the activity behaviour of MO_{basic}. Here, the activity coefficient of PbO is increasing and is a maximum in calcium ferrite slag (i.e. BO-MO binary). As seen in Figure 5.2.5(b) the activity coefficient of lead in iron silicate slag is an order of magnitude higher than in calcium ferrite slag. This behavior is in accord with the experimentally determined activity coefficient values of PbO in the silicate and ferrite slags shown in Table 5.2.5. In the FCS slag region of Figure 5.2.5(b), whilst $\gamma_{MObasic}$ curve displays positive deviation from ideality, the deviation in the curve is not as strong as in the case with calcium ferrite slag, with $\gamma_{MObasic}$ being smaller, signifying that the distribution ratio of lead and other elements with basic oxides in FCS slag will be higher than in calcium ferrite slag and in terms of removing lead from copper, FCS slag is much more effective than calcium ferrite slag. Once again the experimental data in Table 5.2.5 agrees with the thermodynamic predictions. As evident in Table 5.2.5, the activity coefficient of PbO in FCS slag is smaller than the activity coefficient of PbO in calcium ferrite slag. The experimental distribution data in Table 5.2.4 and the

thermodynamic predictions made from Figure 5.2.5(b) agree that the maximum removal of lead from copper is possible by application of iron silicate slag, where the activity coefficient of PbO is the smallest. The degree of interactions between PbO and SiO_2 in FCS slag are not as strong as those between PbO and SiO_2 in iron silicate slag, due to the presence of CaO in FCS slag, which interacts much more strongly with SiO_2 than PbO as CaO is a stronger basic oxide than PbO.

Whilst a ternary model for the AO-BO-MO system when MO is an acidic oxide is not available, if MO is an acidic oxide such as $SbO_{1.5}$, the iso-activity coefficient lines in Figure 5.2.5(b) are obtained if AO and BO are exchanged and so the activity coefficient of $SbO_{1.5}$ is lowest for calcium ferrite slag and highest for iron silicate slag, with that for FCS slag being similar to calcium ferrite slag. Although it may be expected that $\gamma_{MOacidic}$ in FCS slag should be between iron silicate and calcium ferrite slags, since adding SiO_2 to a CaO-based slag will make the slag less basic, this is not the case. The activity coefficient of an acidic oxide in FCS slag is similar to calcium ferrite slag as shown in Figure 5.2.6. Figure 5.2.6 illustrates $\gamma_{AsO1.5}$ curves in the ternary FeO_x-SiO_2-CaO system as determined experimentally be Yawaza *et al.* (1986). Although the current discussion is on antimony oxide, a similar diagram illustrating the behaviour of $\gamma_{SbO1.5}$ in the ternary system was not available in literature.

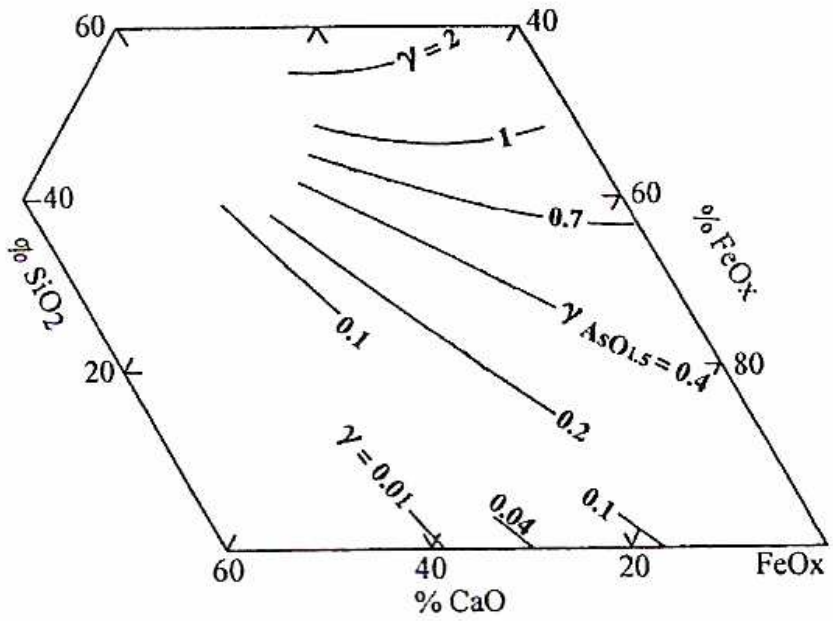

Figure 5.2.6: Activity coefficient of $AsO_{1.5}$ (solid lines) in slag (Yazawa, Takeda and Nakazawa, 1999)

However as is evident in Figure 5.2.7 at converting conditions, the distribution behaviour of both arsenic and antimony is very similar in both the ferrite and silicate slags, with the distribution lines converging at high oxygen partial pressures. In the case of iron silicate slag, arsenic and antimony distribute strongly to the metal phase and in calcium ferrite slag they distribute to the slag phase. Therefore from the relationship displayed in Figure 5.2.7 it can be assumed that the activity coefficient behaviour of antimony oxide will be similar to arsenic oxide in the ternary FeO_x-SiO_2-CaO system, thus allowing application of Figure 5.2.6 to verify the predicted distribution and activity coefficient behaviour of acidic oxide $SbO_{1.5}$ in iron silicate, FCS and calcium ferrite slag to the experimentally determined values.

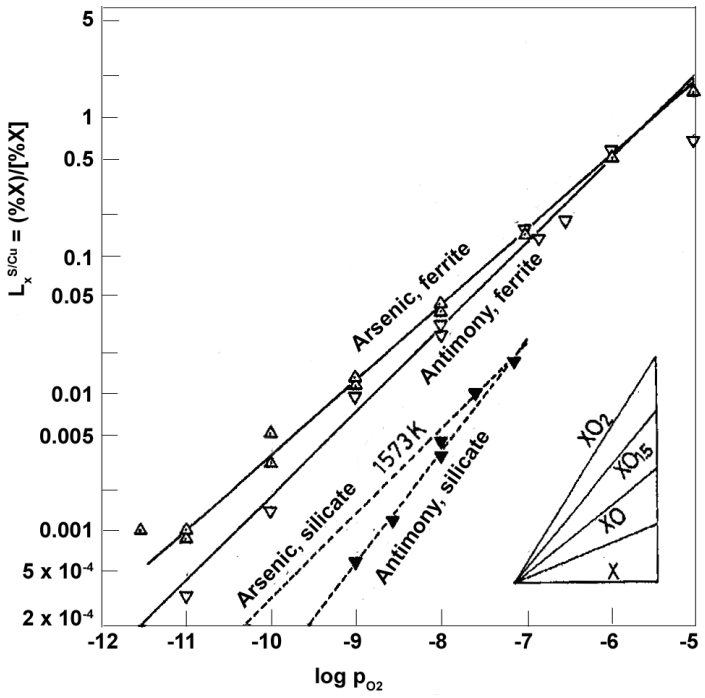

Figure 5.2.7: Distribution ratios of Sb and As between slag and liquid copper at 1250°C (Yazawa, 1984)

In the case of calcium ferrite and FCS slags, the $\gamma_{AsO1.5}$ curves in Figure 5.2.6, display negative deviation, with $\gamma_{AsO1.5}$ being less than one in both slags. As observed in Figure 5.2.6, not only is the deviation from ideality very similar in both calcium ferrite and FCS slags, as is evident by the similarity in the 'shape' of the $\gamma_{AsO1.5}$ curves, but so are the numerical values of $\gamma_{AsO1.5}$. The $\gamma_{AsO1.5}$ curves show positive deviation in activity behaviour from ideality in iron silicate slag, with $\gamma_{AsO1.5}$ being greater than one, suggesting weak interactions between $AsO_{1.5}$ and species in the silicate slag. As observed in Figure 5.2.6, the activity coefficient of arsenic oxide in iron silicate slag is higher than both calcium ferrite and FCS slags. This behavior is

also expected for the $\gamma_{SbO1.5}$ in the three slags, such that it is predicted that $\gamma_{SbO1.5}$ in the ferrite and FCS slags will be similar in value and higher in the silicate slag. The predicted behavior of $\gamma_{SbO1.5}$ in the three slags is in agreement with the experimentally calculated data in Table 5.2.5. As seen in Table 5.2.5, the activity coefficient of antimony oxide is highest in iron silicate slag and similar in calcium ferrite and FCS slags. The metal oxide $SbO_{1.5}$ is acidic and is strongly associating with basic CaO in calcium ferrite slag. Interactions between antimony oxide and silica in iron silicate slag are weak due to the acidic character of both oxides. Thus, the activity coefficient of antimony oxide is large in iron silicate slag. Whilst it is expected that due to the presence of both lime and silica in FCS slag, the degree of interactions between $SbO_{1.5}$ and CaO will be reduced as there exists strong interactions between SiO_2 and CaO, this is not the case. The activity coefficient of $SbO_{1.5}$ in FCS slag is very similar to that in calcium ferrite slag. This indicates that whilst SiO_2 and CaO interact very strongly with each other in FCS slag, CaO is also interacting as strongly in calcium ferrite slag, with $SbO_{1.5}$. The experimental distribution ratios and activity coefficient data presented in Tables 5.2.4 and 5.2.5, respectively, supports the thermodynamic predictions that, for the removal of acidic oxides such as antimony from copper, FCS slag will be equally effective as calcium ferrite slag and superior to iron silicate slag.

The current experimental data on the distribution of an acidic ($SbO_{1.5}$), basic (PbO) and neutral (NiO) oxide between FCS slag and copper metal and its comparison to the experimental data for iron silicate and calcium ferrite slags verifies the predicted behavior of such oxides in a ternary FeO_x-SiO_2-CaO system. From the current experimental data, FCS slag appears to be suitable for copper converting in terms of minor element distributions and is in fact superior to calcium ferrite slag if lead is a significant impurity and is equally economically beneficial as calcium ferrite slags if by-product metals such as cobalt and nickel are present in the copper ore in significant amounts.

5.3 COMMERCIAL ASPECTS OF FCS SLAG

It has been shown that FCS slag is superior to calcium ferrite slag in terms of refractory wear at 1300°C and an oxygen partial pressure of 10^{-6} atm. Whilst calcium ferrite slag had severely disintegrated the refractory, attack of the refractory by FCS slag was not serious. In terms of minor element distribution, it was determined that FCS slag is superior to calcium ferrite slag in the removal of elements with basic oxides, such as PbO, from copper and as effective in removing acidic oxides (i.e. $SbO_{1.5}$) and recovering valuable by-products with neutral oxides, such as NiO or CoO. However, when applying a new slag on a commerical scale, refractory wear and minor element distribution are not the only issues of concern for operators. Other factors with affect the application of a slag system include:

- the overall copper recovery,
- the mass of slag produced which needs to be recycled and
- the viscosity of the slag, which can affect the successful tapping of the slag from the converter and the copper lost to entrainment.

Although viscosity data for FCS slag is not available, it is very likely that the viscosity of FCS slag is higher than that of calcium ferrite slag. However it will be less than that of iron silicate slag so the viscosity should be low 'enough' to not impede the tapping of FCS slag from the converter. Vartiainen *et al.* (2003) found that in pilot plant tests, FCS slag was fluid enough to be easily tapped from the furnace through the 'normal' tapping holes. The slag composition used by Vartiainen *et al.* (2003) was similar to that used in the current study.

Some basic process calculations were carried out to further examine the feasibility of applying FCS slag to continuous copper converting and they are detailed in Appendix 3. The calculations were used to estimate the amount of slag produced and the percent recovery of copper when FCS slag is used. Similar calculations were also carried out for calcium ferrite slag. It was assumed that 1 tonne of matte at 70wt% Cu entered the furnace and contained only Cu2S and FeS. The slag compositions used in the calculations were those of MS-CF and MS-24. The copper oxide content of MS-24 was analysed using ICP-AES, following the minor element distribution experiments. Due to the high Fe^{3+}/Fe^{2+} ratio of both calcium ferrite and FCS slags, FeO_x was assumed to be $FeO_{1.5}$ (i.e. magnetite Fe_3O_4). The results from the calculations are given in Table 5.3.1. As evident in the table, the amount of slag produced per tonne of matte converted is higher in the case of FCS slag than calcium ferrite slag. However

the direct recovery of copper into blister is higher when FCS slag is used (98% recovery) than when calcium ferrite slag is used (96% recovery).

Table 5.3.1: Results from the basic material balance calculations *(CF= calcium ferrite slag, FCS= ferrous calcium silicate slag)*

		Flash Converting	
		CF Slag	**FCS Slag**
FeO_x in Slag	**% FeO_x**	66.8	50.3
CaO in Slag	**% CaO**	17.0	24.1
SiO_2 in Slag	**% SiO_2**	0.0	18.7
Cu_2O in Slag	**% Cu_2O**	15.1	9.1
Slag Amount	**t/t matte**	0.16	0.21
Cu in Slag	**t/t matte**	0.022	0.017
Direct recovery of Cu	**%**	96.0	98.0

Although the larger mass of FCS slag produced, which needs to be recycled to recover the copper lost to slag, will slightly decrease the capacity of the smelter for new feed compared to calcium ferrite slag, the amount of recyclable copper held "in-process" is actually smaller and this has some economical benefit. With less copper held within the process, more copper is recovered in the blister stream, which can be sold.

Thus overall, taking into account refractory wear, minor element distribution, the amount of slag produced and the direct recovery of copper, FCS slag offers a serious alternative to calcium ferrite slag in continuous copper converting.

6.0 CONCLUSIONS

The aim of this work was to evaluate the potential of FCS slag for application to continuous converting operations. The two issues which most determine whether or not a given slag system is suitable for converting are the severity of refractory attack and the ability of the slag to remove minor elements from copper. The objectives of the research were fulfilled by determining the extent and mechanism of attack of chrome-magnesia refractories by FCS slag and the distribution ratios of three minor elements between FCS slag and copper. The representative elements selected for examination were lead, nickel and antimony.

FCS slag was observed to attack the magnesia-chrome refractories much less aggressively than calcium ferrite slag under the same process conditions i.e. a temperature of 1300^{o}C and an oxygen partial pressure of 10^{-6} atm. As the contact time between slag and refractory increased, calcium ferrite slag caused severe disintegration of the refractory whilst the integrity of the refractory in contact with FCS slag was not significantly jeopardized. The microstructure of the refractory was similar to that of an 'uncontacted' refractory with some FCS slag penetration. Detailed analysis of the refractory in contact with FCS slag revealed that some changes had occurred in the refractory after exposure to FCS slag. Interdiffusion was occurring between chromium (Cr^{3+}) and aluminum (Al^{3+}) cations in the chromite spinel and iron (Fe^{3+}) cations in the slag. Interdiffusion was also taking place between magnesium (Mg^{2+}) cations in the periclase and iron (Fe^{2+}) cations in the slag. The extent of interdiffusion was very limited and it was inferred that the rate of solid-state diffusion was slow. These changes did not cause disintegration of the refractory structure; in contrast, in the refractory in contact with calcium ferrite slag, loss of bonding as a result of degradation of the secondary chromite spinel phase was so great that the brick integrity was destroyed. At 1400^{o}C FCS slag penetrated further into the refractory and there was also an increase in the rate of solid state diffusion between both Fe^{2+} and Fe^{3+} cations in FCS slag and species cations in phases within the refractory. Refractory degradation was evident with detached periclase grains in the slag. Although the wear of magnesia-chrome refractory by FCS slag at 1400^{o}C was significant, no copper converting processes operate at such high temperatures.

The slag/metal distribution ratios of nickel, lead and antimony between FCS slag and copper metal were found to be 0.98, 0.93 and 0.54 respectively. These results were compared with distribution data available from literature for calcium ferrite slag and iron silicate slag in equilibrium with copper and it was shown that the results are as predicted by a thermodynamic analysis.

The use of FCS slag in a continuous copper converter will result in a longer campaign life as the life of the refractory bricks will be prolonged due to the reduced refractory wear caused by the slag. This will result in reduced operating costs associated with refractory maintenance. In addition, FCS slag is also suitable for copper converting in terms of minor element distribution. FCS slag can remove antimony from copper as effectively as calcium ferrite slag and is also as effective as the ferrite slag, if not better, in recovering nickel from copper. FCS slag offers the additional advantage of being able to remove lead from copper more effectively than calcium ferrite slag. In summary, FCS slag is capable of producing copper of a similar quality to that currently produced by converting processes utilizing calcium ferrite slag. Although the amount of FCS slag produced is slightly higher than that of calcium ferrite slag, the copper content of FCS slag is much than that of calcium ferrite slag, so the overall recovery of copper into the blister is actually higher when using FCS slag. FCS slag is considered to be a serious alternative to calcium ferrite slag for use in continuous copper converting.

7.0 REFERENCES

- Acuna, C.; Yazawa, A., (1987), "Behaviours of Arsenic, Antimony and Lead in Phase Equilibria among Copper, Matte and Calcium or Barium Ferrite Slag", *Transactions of the Japan Institute of Metals*, Vol. 28, No. 6, pp 498-506.
- Ainsworth, J.H.; Starzacher, A., (1988), "An Overview of R & D on Basic Refractories", *Proceedings on the International Symposium on Advances in Refractories for the Metallurgical Industry*, pp 181-193.
- Ajima, S.; Hayashi, M.; Nishiyama, Y.; (1994), "The Mitsubishi Continuous Process-Present and Future", *Metallurgical Processes for Early Twenty-First Century*, pp 161-176.
- Ajima, S.; Hayashi, M.; Nishiyama, Y.; Shimizu, T., (1993), "Converting and Anode Furnace Operation of the Mitsubishi Process at Naoshima", *Converting, Fire Refining and Casting*, pp 333-348.
- Ajima, S.; Igarashi, T.; Shimizu, T.; Matsutani, T., (1995), "The Mitsubishi Process Ensures Lower Copper Content in Slag", *Quality in Non-Ferrous Pyrometallurgy*, pp 185-204.
- Allen, N.; Sun, S.; Jahanshahi, S., (1995), "Stability of MgO Refractory in contact with Iron-Rich Slags", *Proceedings of the Second Australian Melt Chemistry Symposium*, pp 55-58.
- Altman, R.; Kellogg, H.H.; (1972), "Solubility of Copper in Silica-Saturated Iron Silicate Slag", *Transactions of IMM*, Sect C, Vol. 81, pp C163-175.
- Barthel, H., (1981), "Wear of Chrome Magnesite Bricks in Copper Smelting Furnaces", *Interceram*, Vol. 30, pp 250-255.
- Biswas, A.K.; Davenport, W.G., (1980), "Extractive Metallurgy of Copper", 2nd Edition, Pergamon Press, Great Britain.
- Bodsworth, C., (2000), "The Extraction and Refining of Metals", CRC Press, USA.
- Boldt, J.R.; Queneau, P., (1967), "The Winning of Nickel: its geology, mining and extractive metallurgy", London, Methuen.
- Buchebner, G.; Molinari, G.; Rumpf, D., (2000), "Developing Basic High-Preformance Products for Furnaces in the Non-Ferrous Metals Industries", *Journal of Metals*, Vol. 52, No. 2, February 2000, pp 68-72.
- Chaubal, P.C.; Sohn, H.Y.; George, D.B.; Bailey, L.K.; (1989), "Mathematical Modeling of Minor-Element Behaviour in Flash Smelting of Copper Concentrates and Flash Converting of Copper Mattes", *Metallurgical and Materials Transactions B*, Vol. 20B, February 1989, pp 39-51.

- Chaudhuri, J.; Padhy, B.P.; Deysarkar, S.; Singh, D.K.; Kamath, C.D., (2001), "Study of Pore Dynamics- An unique approach for developing refractory materials", *UNITECR '01. Proceedings of the Unified International Technical Conference on Refractories, 7th Biennial Worldwide Congress*, Vol. 1, pp 405 – 422.
- Cherif, K.; Pandolfelli, V.; Rigaud, M., (1997), "Factors Affecting the Corrosion by Fayalite Slags and the Thermal Shock Performance of Magnesia-Chrome Bricks", *Journal of the Canadian Ceramic Society*, Vol. 66, No. 3, August 1997, pp 210-216.
- Correia, R.N.; White, J., (1988), "Phase Equilibrium Relationships Controlling the Reactions of Basic Refractories with Slags Produced during Matte-Smelting Processes: Part II. Phase Relationships in the System MgO-FeO-Fe_2O_3-Cr_2O_3-SiO_2 in Air", *British Ceramics Transactions Journal*, Vol. 87, pp 200-206.
- Crites, M.D.; Schlesinger, M.E., (1999), "Corrosion Testing of Chrome-free Refractories for Copper Production Furnaces", *Copper 99- Copre 99 International Conference*, Vol. 6, pp 187-194.
- Davies, L.J.; Hoyson, G.J., (1988), "Refractories for Nickel Extractive Metallurgy", *Extractive Metallurgy of Nickel and Cobalt*, pp 293 – 305.
- Davies, L.J.; McCollum, J.M., (1988), "Refractory Selection for Non-Ferrous Smelting Applications", *Proceedings on the International Symposium on Advances in Refractories for the Metallurgical Industry*, pp 195-214.
- Donald, J. R.; Toguri, J. M., (1997), "Interactions between calcium ferrite slag and synthetic refractory materials", *Pyrometallurgy Fundamentals and Process Deveopment, Proceedings of the Nickel-Cobalt 97 International Symposium*, Vol. 1, pp 225-226.
- Duffy, J.A.; Ingram, M.D., (1978), "Acid-Base Properties of Molten Oxides and Metallurgical Slags", *Journal of the Chemical Society*, Vol. 74, pp 1410-1419.
- Eerola, H.; Jylha, K.; Taskinen, P.; (1984), "Thermodynamics of Impurities in Calcium Ferrite Slags in Copper fire-refining", *Transactions of the Institute of Mining and Metallurgy, Section C: Mineral Processing and Extractive Metallurgy*, Vol. 93 (Dec), C193-199.
- Elliot, J.F., (1984), "Slag for Metallurgical Processes", *Metallurgical Slags and Fluxes-Proceedings from the Second International Symposium*, pp 44-61.
- Elliot, J.B.; See, J.B.; Rankin, W.J., (1978), "Effect of Slag Composition on Copper losses to Silica-saturated Iron Silicate Slag", *Transactions of IMM*, Sect C, Vol. 87, pp C204-211.

- Engel, R.; Marr, R.; Pretorius, E., (1997), "Refractory/Slag Systems for Ladles and Secondary Refining Processes", *Iron and Steelmakers*, March 1997, pp 93-94.
- Fahey, N., (2002), "Refractory Wear by Calcium Ferrite Slag in Continuous Copper Converting", *PhD Thesis*, Faculty of Engineering, Department of Chemical and Metallurgical Engineering, RMIT University.
- Fahey, N.; Swinbourne, D.R.; Yang, Y.h, (2000), "Slag containment in emerging copper converting technologies", *Minprex 2000*, Melbourne, Australia, pp 461 – 470.
- Fahey, N.P.; Swinbourne, S.; Yan, S.; Orbourne, J.M., (2004), "The Solubility of Cr_2O_3 in Calcium Ferrite Slags at 1573K", *Metallurgical and Materials Transactions B*, Vol. 35B, April 2004, pp 197 – 202.
- Fukuyama, H.; Donald, J.R.; Toguri, J.m., (1996), "Wetting behaviour and interfacial reactions between fayalite slag and MgO", *EPD Congress 1996*, pp 109 – 121.
- Geiger, G.H.; Poirier, D.R., (1973), "Transport Phenomena in Metallurgy", Addison-Wesley Publishing Company, U.SA.
- George, D.B., (2002), "Continuous Copper Converting- A Perspective and View of the Future", *Sulfide Smelting 2002, Proceedings of a Symposium held during the TMS Annual Meeting*, Feb. 17-21, pp 3-13.
- Goto, M.; Hayashi, M., (2003), "Recent Advances in Modern Continuous Converting", *Yazawa International Symposium- Metallurgical and Materials Processing: Principles and Technologies*, Vol. 2, pp 179-187.
- Goto, M.; Kanamori, K., (1979), "Converting Furnace Operation of the Mitsubishi Process", *Copper and Nickel Converters*, pp 210-224.
- Goto, S.; Ogawa, O.; Jimbo, I., (1980), "Dissolution of Copper, Arsenic, Antimony and Bismuth in Silica-Saturated Iron Silicate Slags", *Australia/Japan Extractive Metallurgy Symposium; Sydney; Australia; 16-18 July 1980.*, pp 127-132.
- Grimsey, E.; Biswas, A.; (1976), "Solubility of nickel in silica-saturated iron silicate slags at 1573K", *Transactions of the Institute of Mining and Metallurgy, Section C: Mineral Processing and Extractive Metallurgy*, Vol. 85 (Dec), C200-207.
- Hanniala, P.; Kojo, I.V.; Kyto, M., (1993), "The Kennecott-Outokumpu Flash Converting Process: Facts and Fictions", *Converting, Fire Refining and Casting*, pp 107-119.
- Hanniala, P.; Kojo, I.V.; Kyto, M., (1998), "The Kennecott-Outokumpu Flash Converting Process: Copper by Clean Technology", *Sulfide Smelting '98: Current and Future Practices*, pp 239-247.

- Hasegawa, N.; Sato, H., (2003), "Control of Magnetite Behaviour in the Mitsubishi Process at Naoshima", *Yazawa International Symposium- Metallurgical and Materials Processing: Principles and Technologies*, Vol. 2, pp 509-519.
- Henao, H.M.; and Itagaki K.; (2006), "Phase Relations and Activity of Iron Oxide in the FeO_x-CaO-SiO_2 system at 1300-1400^oC under various Partial Pressures of Oxygen", *Sohn International Symposium- Advanced Processing of Metals and Materials*, Vol. 1, pp 755-766.
- Hino, J.; Itagaki, K.; Yazawa, A., (1989), "Phase Relations in the CaO-FeO_n-Cu_2O and CaO-FeO_n-Cu_2O-SiO_2 Systems at 1200-1300^oC", *Journal of the Mining and Materials Processing Institute of Japan*, Vol. 105, No. 4, pp 315-320.
- Ikesue, A.; Yoshitomi, J.; Shikano, H.; Eguchi, T., (1992), "Formation of Precipitated-Complex Spinel in Magnesia-Chrome Refractories and its Characteristics", *Interceram*, Vol. 41, pp 406-412.
- Itagaki, K., (2003), "Distribution of Minor Elements in Sulphide Smelting", *Yazawa International Symposium- Metallurgical and Materials Processing: Principles and Technologies*, Vol. 1, pp 293-306.
- Jahanshahi, S.; Sun, S., (2003), "Some Aspects of Calcium Ferrite Slags", *Yazawa International Symposium- Metallurgical and Materials Processing: Principles and Technologies*, Vol. 1, pp 227-244.
- Jimbo, I.; Goto, S.; Ogawa, O., (1984), "Equilibria between Silica-Saturated Iron Silicate Slags and Molten Cu-As, Cu-Sb, and Cu-Bi Alloys, *Metallurgical and Materials Transactions B*, Vol. 15B, September 1984, pp 535-541.
- Kaiura, G.H.; Toguri, J.M.; Marchant, G., (1977), "Viscosity of Fayalite-Based Slags", *Canadian Metallurgical Quarterly*, Vol. 16, pp 156-160.
- Kashima, M.; Eguchi, M.; Yazawa, A., (1978), "Distribution of Impurities between Crude Copper, White Metal and Silica-Saturated Slag", *Transactions of the Japan Institute of Metals*, Vol. 19, No. 3, pp 152-158.
- Kenfack, F.; Langbein, H., (2004), "Influence of temperature and the oxygen partial pressure on the phase formation in the system Cu-Fe-O", *Crystal Research and Technology*, Vol. 39, No. 12, pp 1070 – 1079.
- Kim, H.G.; Sohn, H.Y., (1991), "Computer Analysis of Minor Element Behaviour of Copper Smelting and Converting under High Oxygen Enrichment and in Converting with Calcium Ferrite Slag", *Copper 91-Copre 91 International Conference,* Vol. 4, pp 617-635.

- Kim, H.G.; Sohn, H.Y., (1993), "Effects of slag composition on the copper solubility in slag and the behavior of minor elements", *First International Conference on Processing Materials for Properties*, pp 365 – 368
- Kim, H.G.; Sohn, H.Y., (1996), "Thermodynamic modelling of minor-element behaviour in in-bath copper smelting and converting with calcium ferrite slag", *Transactions of the Institute of Mining and Metallurgy, Section C: Mineral Processing and Extractive Metallurgy"*, Vol. 105 (Sept-Dec), C151-163.
- Kim, H.G.; Sohn, H.Y., (1998), "Effects of CaO, Al_2O_3 and MgO Additions on the Copper Solubility, Ferric/Ferrous Ratio and Minor Element Behaviour of Iron-silicate Slag", *Metallurgical and Materials Transactions B*, Vol. 29B, June 1998, pp 583-590.
- Kim, H.G.; Sohn, H.Y., (1998), "Minor-Element Behaviour in Copper Smelting and Converting with the use of tonnage oxygen", *Transactions of the Institute of Mining and Metallurgy, Section C: Mineral Processing and Extractive Metallurgy"*, Vol. 107 (May-Aug), C43-C59.
- Kofstad, P., (1966), "High Temperature Oxidation of Metals", John Wiley and Sons, Inc, USA.
- Kongoli, F., (2003), "Slags and Fluxes in Pyrometallurgical Processes", *Yazawa International Symposium- Metallurgical and Materials Processing: Principles and Technologies*, Vol. 1, pp 199-209.
- Kongoli, F.; McBow, I.; Yazawa, A., (2003), "Liquidus Surface of "Lime Ferrite" Slags at Intermediate Oxygen Potentials", *Materials Transactions*, Vol. 44, No. 10, pp 2136-2140.
- Kongoli, F.; McBow, I.; Yazawa, A., (2003), "Quantification of the Liquidus Surface of "Lime Ferrite" Slags at Several Oxygen Potentials", *Yazawa International Symposium-Metallurgical and Materials Processing: Principles and Technologies*, Vol. 2, pp 227-238.
- Kongoli, F.; McBow, I,; Yazawa, A., (2006), "Phase Relations of Ferrous Calcium Silicate Slag and its Possible Application in the Industrial Practice", *Sohn International Symposium ADVANCED PROCESSING OF METALS AND MATERIALS*, Vol. 8, pp 367-385.
- Kongoli, F.; McBow, I.; Yazawa, A.; Takeda, Y.; Yamaguchi, K.; Budd, R.; Llubani, S., (2006), "Liquidus Relations of Calcium Ferrite and Ferrous Calcium Silicate Slag in Continuous Copper Converting", *Sohn International Symposium ADVANCED PROCESSING OF METALS AND MATERIALS*, Vol. 1, pp 69-87.

- Kongoli, F.; Yazawa, A., (2000), "Phase Relations of "Ferrous Calcium Silicate Slag" with special reference to Copper Smelting and Sintering of Iron Ore", *Fundamentals of Metallurgical Processing- Proceedings of James M. Toguri Symposium*, August 20-23, pp 365-377.
- Kongoli, F.; Yazawa, A., (2001), "Liquidus Surface of FeO-Fe_2O_3-SiO_2-CaO Slag Containing Al_2O_3, MgO and Cu_2O at Intermediate Oxygen Partial Pressures", *Metallurgical and Materials Transactions B*, Vol. 32B, August 2001, pp 583-592.
- Kongoli, F.; Yazawa, A., (2003), "Liquidus Surface of FeO-Fe_2O_3-SiO_2-CaO Slags at Constant CO_2/CO ratios", *Materials Transactions*, Vol. 44, No. 10, pp 2130-2135.
- Kudo, M.; Jak, E.; Hayes, P.; Yamaguchi, K.; Takeda, Y., (2000), "Lead Solubility in FeO_x-CaO-SiO_2 Slags at Iron Saturation", *Metallurgical and Materials Transactions B*, Vol. 31B, February 2000, pp 15-24.
- Lee, J.H.; Kang, S.W.; Cho, H.Y.; Lee, J.J., (1999), "Expansion of Onsan Smelter", *Copper 99- Copre 99 International Conference*, Vol. 5, pp 255-267.
- Leonard, R. J.; Herron, R. H., (1972), "Volume Expansion and Structural Damage in Periclase-Chrome Refractories", *Ceramic Bulletin*, Vol. 51, No. 12, pp 891-895.
- Levin, E.M.; McMurdie, H.F., (1975), *Phase Diagrams for Ceramicists*, The American Ceramic Society.
- Lindkvist, G.; Zednicek, W., (1981), "Studies of Wear on Refractory Basic Bricks after Use in the Copper Kaldo Converter in Boliden", *Interceram*, Vol. 30, pp 256-264.
- Mackey, P.J., (1982), "The Physical Chemistry of Copper Smelting Slag- A Review", *Canadian Metallurgical Quarterly*, Vol. 21, No. 3, pp 221-260.
- MacRae, A.; Wallgren, M.; Wasmund, B.; Lenz, J.; Majumdar, A.; Zuliani, P.; Elvestad, P., (1998), "Converting Furnace Upgrades at the Kidd Metallurgical Division Copper Smelter", *Sulfide Smelting '98: Current and Future Practices*, pp 387-397.
- Makinen, J.K.; Jafs, G.A., (1982), "Production of Matte, White Metal and Blister Copper by Flash Furnace", *Journal of Metals*, June 1982, pp 54-58.
- Mäkipää, M.; Taskinen, P., (1992), "Fayalite Slag-Refractory Interactions in Copper Converters", *12th Scandinavian Corrosion Congress and Eurocorr '92*, pp 601-611.
- Mäkipää, M.; Taskinen, P., (1993), "Refractory wear in copper converters", *Scandinavian Journal of Metallurgy*, Vol. 22, pp 203-212.
- Martinek, C.A., (1982), "Basic Refractory Raw Materials", *Iron and Steel Metallurgy*, June 1982, pp 13 – 16.

- Masson, C.R., (1984), "The Chemistry of Slag- An Overview", *Metallurgical Slags and Fluxes- Proceedings from the Second International Symposium*, pp 3-44.
- Mikami, H.M.; Sidler, A.G., (1963), "Mechanism of Refractory Wear in Copper Converters", *Transactions of the Metallurgical Society of AIME*, Vol. 227, October 1963, pp 1229 – 1244.
- Michal, E.J.; Schuhmann, R., (1952), "Thermodynamics of Iron-Silicate Slags: Slags Saturated with Solid Silica", *Journal of Metals- Transactions of AIME*, July 1952, pp 723-728.
- Moon, N.; Hino, M.; Lee, Y.; Itagaki, K., (1997), "PbO Activity and Impurity Dissolution in PbO- FeO_x-CaO-SiO_2 Slag", *Proceedings of the 5th International Conference on Molten Slags, Fluxes and Salts '97- Jan 5-8, 1997, Sydney, Australia*, pp 753-759.
- Muan, A., (1955), "Phase Equilibria in the System FeO-Fe_2O_3-SiO_2", *Journal of Metals*, September, pp 965-976.
- Nagamori, M.; Chaubal, P.C., (1982), "Thermodynamics of Copper Matte Converting: Part III. Steady-State Volatilisation of Au, Ag, Pb, Zn, Ni, Se, Te, Bi, Sb and As from Slag, Matte and Metallic Copper", *Metallurgical and Materials Transactions B*, Vol. 13B, September 1982, pp 319-329.
- Nagano, T.; Suzuki, T., (1976), "Commercial Operation of Mitsubishi Continuous Copper Smelting and Converting Process", *Extractive Metallurgy of Copper: An International Symposium*, Ch. 22, pp 439-457.
- Newman, C.J.; MacFarlane, G.; Molnar, K.; Storey, A.G., (1991), "The Kidd Creek Smelter- an Update on Plant Performance", *Copper 91- Copre 91 International Conference*, Vol. 4, pp 65-79.
- Newman, C.J.; Probert, T.I.; Weddick, A.J., (1998), "Kennecott Utah Copper Smelter Modernization", *Sulfide Smelting '98: Current and Future Practices*, pp 205-215.
- Nikolic, S.; Hayes, P. C.; Jak, E., (2006), "Phase Equlibria in Ferrous Calcium Silicate Slags at 1250^0C and an Oxygen Partial Pressure of 10^{-6}atm", *Sohn International Symposium ADVANCED PROCESSING OF METALS AND MATERIALS*, Vol. 1, pp 791-804.
- Nikoo, A.S.; Roshanfekr, S.; Golestani-Fard, F., (2001), "Effects of slag basicity on the corrosion of refractories in copper converters", *UNITECR '01. Proceedings of the Unified International Technical Conference on Refractories, 7th Biennial Worldwide Congress*, Vol.1, pp 514-523.

- Ojima, Y., (2003), "Future of Copper Converting Process", *Yazawa International Symposium- Metallurgical and Materials Processing: Principles and Technologies*, Vol. 2, pp 255-264.
- Ojima, Y.; Kondo, Y.; Kawanaka, K.; Maeba, K.; Yamamoto, K., (2003), "Development of New Copper Continuous Converter", *Yazawa International Symposium- Metallurgical and Materials Processing: Principles and Technologies*, Vol. 1, pp 731-743.
- Oishi, T.; Kamuo, M.; Ono, K.; Moriyama, J., (1983), "A Thermodynamic Study of Silica-Saturated Iron Silicate Slags in Equilibrium with Liquid Copper", *Metallurgical and Materials Transactions B*, Vol. 14B, March 1983, pp 101-104.
- Pengfu, T.; Chuanfu, Z., (1998), "Thermodynamic analysis of copper smelting process", *Processing of Metals and Advanced Materials: Modeling, Design and Properties*, pp 109-120.
- Piatkowski, W., (1976), "SEM and Electron Microprobe Observations of some Phenomena Occurring in Magnesia-Chrome Refractories", *Ceramurgia international*, Vol. 2, No. 1, pp 38-41.
- Pressley, H.; White, J., (1981), "Chemical Requirements of Refractories for Non-Ferrous Extraction Processes", *Interceram*, Vol. 30, pp 280-287.
- Renkey, A.L.; Weaver, E.L.; Vernon, H.L., (1981), "Advances in Basic Brick Technology for the Copper Industry", *Interceram*, Vol. 30, pp 266-270.
- Richards, K.J.; George, D.B.; Bailey, L.K., (1983), "A New Continuous Copper Converting Process", *Proceedings from the Advances in Sulfide Smelting Symposium*, Vol. 2, pp 489-498.
- Richardson, F.D., (1974), "Physical Chemistry of Melts in Metallurgy", Vol. 1, Academic Press, London.
- Rigby, G.R., (1962), "A Study of Basic Brick from Various Copper Smelting Furnaces", *Transactions of the Metallurgical Society of AIME*, Vol. 224, October 1962, pp 887 – 892.
- Rigby, A.J.; Forrest, R.E., (1992), "Magnesia chrome Refractories- Quality and Performance", *Non-Ferrous Pyrometallurgy: Proceedings from the International Symposium on Trace Metals, Furnace Practice and Energy Efficient*, Vol. 1, pp 433 – 445.
- Roghani, G.; Hino, M.; Itagaki, K.; (1997), "Phase Equilibrium and Minor Element Distribution between Slag and Copper Matte under High Partial Pressure of SO_2"

Proceedings of the 5th International Conference on Molten Slags, Fluxes and Salts '97-Jan 5-8, 1997, Sydney, Australia, pp 693-703.

- Rosenqvist, T., (1974), "Principles of Extractive Metallurgy", McGraw Hill, U.S.A.
- Ruddle, R.W.; Taylor, B.; Bates, A.P.; (1966), "The Solubility of Copper in Iron Silicate Slag", *Transactions of IMM*, Sect C, Vol. 75, pp C1-12.
- Saito, N.; Hori, N.; Nakashima, K.; Mori, K., (2003), "Effects of Additives Oxides on the Viscosities of $CaO-SiO_2-Al_2O_3$ and $CaO-Fe_2O_3$ Melts", *High Temperature Materials and Processes*, Vol. 22, Nos. 3-4, pp 129-139.
- Sato, H.; Tanaka, F.; Okabe, S., (1999), "Mechanism of Refractory Wear by Calcium Ferrite Slag", *EPD Congress 1999*, pp 281-297.
- Schlesinger, M.E., (1996), "Refractories for Copper Production", *Minerals Processing and Extractive Metallurgy Review*, Vol. 16, pp 125-146.
- Schlesinger, M.E.; Crites, M.D.; Somerville, M.A.; Sun, S., (1998), "Assessment of Spinel containing Refractories for Smelting and Refining", *Journal of the Australasian Ceramic Society*, Vol. 34, No. 2, pp 39-44.
- Schuhmann, R.; and Ensio, P.J., (1951), "Thermodynamics of Iron Silicate Slags: Slags Saturated with Gamma Iron", *Journal of Metals*, May 1951, pp 401-411
- Schuhmann, M.; Powell, R.g.; Michal, E.J., (1953), "Constitution of $FeO-Fe_2O_3-SiO_2$ system at slagmaking temperatures", *Journal of Metals*, September 1953, pp 1097 – 1104.
- Sehnalek, F.; Imris, I., (1972), "Slag for Continuous Copper Production", *Advances in Extractive Metallurgy and Refining*, pp 39-62.
- Shibasaki, T.; Kanamori, K., (1989), "High Grade Matte Operation in the Mitsubishi Continuous Process at Naoshima Smelter", *Productivity and Technology in the Metallurgical Industries*, pp 365-377.
- Shiraishi, Y.; Ikeda, K.; Tamura, A.; Saito, T., (1978), "On the Viscosity and Density of the Molten $FeO-SiO_2$ System", *Transactions of the Japan Institute of Metals*, Vol. 19, pp 264-273.
- Somerville, M.; Sun, S.; Jahanshahi, S., (1995), "Effect of Silica and Oxygen Potential on the Copper Content and Iron Redox Equilibria in MgO Saturated Calcium Ferrite Slag", *Proceedings of the Second Australian Melt Chemistry Symposium.*
- Staut, R., (1972), "Effects of the lime-silica ratio on the physical properties of magnesia-chrome ore composition", *Ceramic Bulletin*, Vol. 51, No. 12, pp 901 – 907.

- Sumita, S.; Mimori, T.; Morinaga, K.; Yanagase, T., (1980), "Viscosity of Slag Melts Containing Fe_2O_3", *Journal of the Japan Institute of Metals*, Vol. 44, No. 1, pp 94 – 99.
- Sumita, S.; Morinaga, K.; Yanagase, T., (1983), "Physical Properties and Structure of Binary Ferrite Melts", *Transactions of the Japan Institute of Metals*, Vol. 24, No. 1, pp 35-41.
- Suzuki, T.; Yanagida, T.; Goto, M.; Echigoya, T.; Kikumoto, N., (1991), "Recent Operation of Mitsubishi Continuous Copper Smelting and Converting Process at Naoshima", *Copper 91- Copre 91 International Conference*, Vol. 4, pp 51-57.
- Swinbourne, D.R., (2003), "Metallurgy- Class Notes", Royal Melbourne Institute of Technology
- Takeda, Y., (1993), "Miscibility Gap in the $CaO\text{-}SiO_2\text{-}Cu_2O\text{-}Fe_2O_3$ System under Copper Saturation and Distribution of Impurities", Materials *Transactions of the Japan Institute of Metals*, Vol. 34, No. 10, pp 937-945.
- Takeda, Y., (1994), "The Effects of Basicity on Oxidic Dissolution of Copper in Slag", *Metallurgical Processes for the Twenty-First Century*, pp 453-467.
- Takeda, Y., (2001), "Copper Solubility in $SiO_2\text{-}CaO\text{-}FeO_x$ Slag Equilibrated with Matte", *High Temperature Materials and Processes*, Vol. 20, No. 3-4, pp 279-284.
- Takeda, Y.; Ishiwata, S.; Yazawa, A., (1983), "Distribution Equilibria of Minor Elements between Liquid Copper and Calcium Ferrite Slag", *Transactions of the Japan Institute of Metals*, Vol. 24, No. 7, pp 518-528.
- Takeda, Y.; Ishiwata, S.; Yazawa, A.; (1984), "Equilibrium Study on Calcium Ferrite Slags. V- Effects of Temperature and Compositions of Slag and Metal on Distribution of Minor Elements Between Slag and Copper", *Journal of the Mining and Metallurgy Institute of Japan*, Vol. 100, No. 1153, pp 259-264.
- Takeda, Y.; Ishiwata, S.; Yazawa, A.; (1984), "Equilibrium Study on Calcium Ferrite Slags. IV- Distribution of Minor Elements between Slag and Metallic Copper", *Journal of the Mining and Metallurgy Institute of Japan*, Vol. 100, No. 1152, pp 103-108.
- Takeda, Y.; Nakazawa, S.; Yazawa, A., (1980), "Thermodynamics of Calcium Ferrite Slags at 1200 and 1300^oC", *Canadian Metallurgical Quarterly*, Vol. 19, pp 297-305.
- Takeda, Y.; Yazawa, A., (1989), "Dissolution loss of Copper, Tin and Lead in $FeO_n\text{-}SiO_2\text{-}$ CaO Slag", *Productivity and Technology in the Metallurgical Industries*, pp 227 – 240.
- Tanaka, F.; Iida, O.; Takeda, Y., (2003), "Thermodynamic Fundamentals of Calcium Ferrite Slag and their Application to Mitsubishi Continuous Copper Converter", *Yazawa*

International Symposium- Metallurgical and Materials Processing: Principles and Technologies, Vol. 2, pp 495-507.

- Tanaka, F.; Sato, H.; Hasegawa, N., (1999), "Technology for decreasing refractory wear in the Mitsubishi Process: Fundamental research and its application", *Copper 99 – Copre 99 International Conference*, Vol. VI, pp 171 – 185.
- Taskinen, P.; Tikkanen, M.H., (1981), "Reactions between Magnesite-Chrome Refractories, Slag, Matte and Copper in Copper Converters", *Interceram*, Vol. 30, pp 333-336.
- Tsukihashi, F.; Kimura, H., (2003), "The Effect of MgO and Al_2O_3 Additions on the Liquidus of the CaO-SiO_2-FeO_x System at Various Partial Pressure of Oxygen", *Yazawa International Symposium- Metallurgical and Materials Processing: Principles and Technologies*, Vol. 1, pp 851-860.
- Turkdogan, E.K., (1983), "Physiochemical Properties of Molten Slag and Glasses", The Metals Society, London.
- Umakoshi, M.; Mori, K.; Kawai, Y., (1984), "Corrosion Kinetics of Refractory Materials in Molten CaO-FeO-SiO_2 Slags", *Metallurgical Slags and Fluxes-Proceedings from the Second International Symposium*.
- Vadasz, P.; Molnar, L.; (1992), "Interaction at the Periclase-Slag Melt Phase Boundary", *Ceramics-Silikaty*, Vol. 36, pp 199-204.
- Vartiainen, A., (1998), " Viscosity of Iron-Silicate Slags at Copper Smelting Conditions", *Sulfide Smelting'98: Current and Future Practices*, pp 363-370.
- Vartiainen, A.; Kojo, I.V.; Rojas, C.A., (2003), "Ferrous Calcium Silicate Slags in Direct-To-Blister Flash Smelting", *Yazawa International Symposium- Metallurgical and Materials Processing: Principles and Technologies*, Vol. 1, pp 277-290
- Vartiainen, A.; Kyto, M., (2002), "Olivine Slags: the ultimate solution to low copper slags?", *Scandinavian Journal of Metallurgy*, Vol. 31, pp 298 – 306.
- Verein Deutscher Eisenhuttenleute, (1995), *Slag Atlas*, 2nd Ed., ECSC Research, Germany.
- Wang, S.; Kurtis, A.; Toguri, J., (1973), "Distribution of copper-nickel and copper-cobalt between copper-nickel and copper-cobalt alloys and silica saturated fayalite slags", *Canadian Metallurgical Quarterly*, Vol. 12, No. 4, pp 383-390.
- Waseda, Y.; Toguri, J.M., (1998), "The Structure and Properties of Oxide Melts-Application of Basic Science to Metallurgical Processing", World Scientific Publishing, USA.

- Wright, S.; Zhang, L.; Sun, S.; Jahanshahi, S., (2001), "Viscosities of calcium ferrite slags and calcium alumino-silicate slags containing spinel particles", *Journal of Non-Crystalline Solids*, Vol. 282 (2001), pp 15-23.
- Yamaguchi, K.; Ogino, F.; Kimura, E., (1994), "Refractory Corrosion by Ferrite Slag at Elevated Temperatures", *EDP Congress 1994*, pp 803-812.
- Yamaguchi, K.; Ueda, S.; Takeda, Y., (2005), "Phase equilibrium and thermodynamic properties of SiO_2-CaO-FeO_x slags for copper smelting-research achievements of Professor Yoichi Takeda", *Scandinavian Journal of Metallurgy*, Vol. 34, 164-174.
- Yan, S; Sun, S; Jahanshahi, S., (2001), "Reactions of MgO and $MgCr_2O_4$ with calcium ferrite slags at 1300°C", *UNITECR '01. Proceedings of the Unified International Technical Conference on Refractories, 7th Biennial Worldwide Congress*, Vol.3, pp 1553 - 1562
- Yan, S.; Sun, S.; Jahanshahi, S., (2005), "Reactions of Dense MgO with Calcium Ferrite–Based Slags at 1573K", *Metallurgical and Materials Transactions B*, Vol. 36, No. 5, pp 651-656.
- Yannopoulos, J.C.; Swanson, C.E.; Hamer, E., (1983), "Copper Pyrometallurgy- The Quest for an Environmentally Acceptable Continuous Process", *Proceedings from the Advances in Sulfide Smelting Symposium*, Vol. 2.
- Yazawa, A., (1980), "Distribution of various elements between copper, matte and slag", *Erzmetall*, Vol. 33, No. 7-8, pp 377-382.
- Yazawa, A., (1984), "Slag-Metal and Slag-Matte Equilibria and their Process Implications", *Metallurgical Slags and Fluxes- Proceedings from the Second International Symposium*, pp 701-720.
- Yazawa, A.; (1994), "Thermodynamic Interpretation on Oxidic Dissolution of Metal in Slag", *Pyrometallurgy for Complex Materials and Wastes*, pp 61-72.
- Yazawa, A; Eguchi, M, (1976), "Equilibrium studies on copper slags used in continuous converting", *Extractive Metallurgy of Copper- International Symposium*, Vol. 1, pp 3-20.
    - Yazawa, A.; Hino, M., (1993), "Thermodynamics of Phase Separation between Molten Metal and Slag, Flux and their Process Implications", *ISIJ International*, Vol. 33, No. 1, pp 79-87.
    - Yazawa, A.; Hino, J.; (1995), "Dissolution Equilibria of Copper Oxide in Slag", *Copper 95 – Copre 95 International Conference*, Vol. IV, pp 489 – 498.

- Yazawa, A.; Kongoli, F., (2001), "Liquidus Surface of Newly defined "Ferrous Calcium Silicate Slag" and its Metallurgical Implications, *High Temperature Materials and Processes*, Vol. 20, No. 3-4, pp 201-207.
- Yazawa, A.; Nakazawa, S.; Takeda, Y., (1983), "Distribution Behavior of Various Elements in Copper Smelting Systems", *Advances in Sulfide Smelting*, Vol. 1, pp. 99-117.
- Yazawa, A.; Takeda, Y., (1982), "Equilibrium Relation between Liquid Copper and Calcium Ferrit Slag", *Transactions of the Japan Institute of Metals*, Vol. 23, No. 6, pp 328-333.
- Yazawa, A.; Takeda, Y., (1986), "Dissolution of Arsenic and Antimony in Slags", *Metallurgical Review of MMIJ- Symposium Proceedings,* Vol. 3, No. 2, November 1986, pp 117-130.
- Yazawa, A.; Takeda, Y.; Nakazawa, S., (1999), "Ferrous Calcium Silicate Slag to be used for Copper Smelting and Converting", *Copper 99- Copre 99 International Conference*, Vol. 6, pp 587-597.
- Yazawa, A.; Takeda, Y.; Waseda, Y.; (1981), "Thermodynamic properties and structure of ferrite slags and their process implications", *Canadian Metallurgical Quarterly*, Vol. 20, No. 2, pp 129 – 134.
- Yazdi, M.H.; Marghoussian, V.K.; Javapour, J.; Roshanfekr, S.; Khalili, N.; Akbari, M., (2001), "Effect of particle size distribution and chemical composition on the properties of magnesia-chrome bricks", *UNITECR '01. Proceedings of the Unified International Technical Conference on Refractories, 7th Biennial Worldwide Congress*, Vol. 2, pp 602 – 612.
- Yoshino, S.; Nishio, H.; Fujiwara, T., (1981), "Investigation on the Refractories used in Copper Smelting Furnaces", *Interceram*, Vol. 30, pp271-274.
- Yu, Z.; Mukai, K.; Kawasaki, K.; Furusato, I., (1993), "Relation between Corrosion Rate of Magnesia Refractories by Molten Slag and Penetration Rate of Slag into Refractories", *Journal of the Ceramic Society of Japan*, Vol. 101, No. 5, pp 533-539.
- Zhong, X. C.; Zhang, L. H., (1981), "Microstructure of Fusion-Cast Magnesite-Chrome Refractories for Use in Copper Furnaces", *Interceram*, Vol. 30, pp 337-341.
- Zotkov, O.M.; Zauzolkov, I.V.; Titarenko, A.G.; Zaitsev, A.D., (1989), "Composition of the Anode Charge and Economics of Production of Cathode Copper", *Tsvetnaya Metallurgiya*, No. 6, pp 29 – 32.

APPENDIX

APPENDIX 1: THE GAS FLOW-RATE CALCULATIONS

$$CO + \frac{1}{2}O_2 = CO_2$$

$$K = \frac{p_{CO2}}{p_{O2}^{0.5} \cdot p_{CO}}$$

$$\frac{p_{CO2}}{p_{CO}} = K \times P_{O2}^{0.5}$$

$$K_{1300^0C} = 71280$$

Assume $p_{O2} = 10^{-6}$ atm

$$\therefore \frac{p_{CO2}}{p_{CO}} = 71.28$$

$$\%CO_2 = \frac{71.28}{71.28+1} \times 100 = 98.6\%$$

$$\%CO = 100 - 98.6 = 1.4\%$$

Assume total CO_2 and CO flow = $400 cm^3/\min$

$F_{CO} = 5.53\ cm^3/\min$

$F_{CO2} = 394.47\ cm^3/\min$

In CO/N_2 mixture:

$\%CO = 5.04\%$

$\%N_2 = 94.96\%$

Thus:

$$F_{N2} = \frac{5.534 \times 0.9496}{0.0504} = 104.27\ cm^3/\min$$

$F_{CO+N2} = 109.8\ cm^3/\min$

APPENDIX 2: THE SPECIFICATIONS OF THE PROBE

The oxygen probe used was supplied by Ceramic Oxide Fabricators and was suitable for measuring oxygen concentrations over the range from pure oxygen down to 10^{-24} atmospheres at temperatures from 700°C to 1700°C. The specifications for the oxygen probe are given in Table 1.

Table 1: Specification of oxygen probe supplied by Ceramic Oxide Fabricators

Thermocouple:	R-type
Oxygen output signal:	DC millivolt, according to Nernst equation
Oxygen measurement range:	1 atm. To 10^{-24} atm.pO_2
Operating temperature:	700°C to 1700°C
Accuracy:	within 2mV of theoretical output

An EMF reading is used to calculate the oxygen partial pressure using the Nernst equation (Equation 1).

$$E = \frac{RT}{nF} \ln \frac{p_{O2}}{P_{O2'}} \qquad \textbf{Equation 1}$$

Where:

E = sensor electromotive force, (mV)

R = gas constant (8.314472 $J \cdot K^{-1} \cdot mol^{-1}$)

T = temperature, (Kelvin)

n = number of charges per reactant species

F = Faraday constant (96 485.3383 coulomb/mole)

$p_{O2'}$ = reference oxygen partial pressure (mole fraction)

p_{O2} = oxygen partial pressure to be measured (mole fraction)

Equation 1 simplifies to Equation 2 as the oxygen partial pressure was measured using a zirconia ceramic electrolyte and atmospheric air, with $p_{O2} = 0.209$, as a reference.

$$p_{O2} = 0.209 \exp\left(\frac{-46.421E}{T}\right)$$ **Equation 2**

A supply of clean reference air at a rate of 10 cm^3/min was provided to the reference air connection on the probe head using a tube coupled to a small aquarium air pump. The probe head also includes 4-pin electrical connections used for the measurements (Table 2).

Table 2: Electrical connections in the oxygen probe used to measure temperature and partial pressure

Pin 1:	Pt/Pt13%Rh leg of R-type thermocouple
Pin 2:	Pt leg of R-type thermocouple
Pin 3:	Oxygen sensor internal conductor
Pin 4:	Oxygen sensor external conductor

APPENDIX 3: MATERIAL BALANCE CALCULATIONS

Assumptions:

- 1 tonne of matte at 70wt% Cu
- Matte grade: $Cu_2S.FeS$
- Calcium ferrite slag composition: MS-CF
  - (17wt% CaO, 15.1wt% Cu_2O, 66.8wt% FeO_x)
- Ferrous calcium silicate slag composition: MS-24, following minor element distribution experiments
  - (24.1wt% CaO, 18.7wt% SiO_2, 9.1wt% Cu_2O, 50.3wt% FeO_x)
- Due to the high Fe^{3+}/Fe^{2+} ratio of both calcium ferrite and FCS slags, FeO_x is assumed to be Fe_3O_4

Calculations:

- *With 70g Cu per 100g matte ($Cu_2S.FeS$)*

$$\frac{70\,gCu}{100\,gmatte}\left|\frac{100\,g}{0.0001\,tonne}\right. = 0.7\,tonneCu/tonnematte$$

$$n(Cu) = \frac{m}{Mwt} = \frac{70}{63.55} = 1.10\,molesCu$$

$$\frac{1.10\,molesCu}{}\left|\frac{1\,moleCu_2S}{2\,molesCu}\right. = 0.55\,molesCu_2S$$

$$m(Cu_2S) = n \times Mwt = 0.55 \times 159.1 = 87.62\,gCu_2S$$

$$m(FeS) = 100 - 87.62 = 12.38\,gFeS$$

$$n(FeS) = \frac{m}{Mwt} = \frac{12.38}{88.0} = 0.14\,molesFeS/100\,gmatte$$

$$\frac{0.14\,molesFeS}{100\,gmatte}\left|\frac{1\,g}{0.000001\,tonne}\right. = 1400\,molesFeS/tonnematte$$

CALCIUM FERRITE SLAG

- *Slag produced from 1400 moles FeS/tonne matte*

$$FeS \rightarrow \frac{1}{3}Fe_3O_4$$

$$\frac{1400}{3} = 466.67 moles Fe_3O_4$$

$$m(Fe_3O_4) = n \times Mwt = 466.67 \times 231.55 = 108057\, gFe_3O_4 / tonnematte$$

$$\frac{108057\, gFe_3O_4}{tonnematte} \left| \frac{100\, gslag}{66.8\, gFe_3O_4} \right. = 161762\, gslag / tonnematte$$

$$\frac{161762\, gslag}{tonnematte} \left| \frac{0.000001 tonne}{1g} \right. = 0.16 tonneslag / tonnematte$$

- *Copper lost to slag/tonne matte*

15.1wt% Cu_2O in calcium ferrite slag

15.1g Cu_2O per 100g slag

$$\frac{15.1 gCu_2O}{100 gslag} \left| \frac{161762 gslag}{tonnematte} \right. = 24426 gCu_2O / tonnematte$$

$$n(Cu_2O) = \frac{m}{Mwt} = \frac{24426}{143.1} = 171 moles Cu_2O$$

$$\frac{171 moles Cu_2O}{1 mole Cu_2O} \left| \frac{2 moles Cu}{1 mole Cu_2O} \right. = 342 moles Cu$$

$$m(Cu) = n \times Mwt = 342 \times 63.55 = 21734\, gCu / tonnematte$$

$$= 0.022 tonne Cu / tonnematte$$

- *Direct Recovery of Copper into Blister*

$$\frac{0.022}{0.7} \times 100 = 96\%$$

FCS SLAG

- *Slag produced from 1400 moles FeS/tonne matte*

$$FeS \rightarrow \frac{1}{3}Fe_3O_4$$

$$\frac{1400}{3} = 466.67 moles Fe_3O_4$$

$$m(Fe_3O_4) = n \times Mwt = 466.67 \times 231.55 = 108057\, gFe_3O_4 / tonnematte$$

$$\frac{108057\, gFe_3O_4}{tonnematte} \left| \frac{100\, gslag}{50.3\, gFe_3O_4} \right. = 214824\, gslag / tonnematte$$

$$\frac{214824\, gslag}{tonnematte} \left| \frac{0.000001 tonne}{1g} \right. = 0.21 tonneslag / tonnematte$$

- *Copper lost to slag/tonne matte*

9.1wt% Cu_2O in FCS slag

9.1g Cu_2O per 100g slag

$$\frac{9.1 gCu_2O}{100 gslag} \left| \frac{214824\, gslag}{tonnematte} \right. = 19548\, gCu_2O / tonnematte$$

$$n(Cu_2O) = \frac{m}{Mwt} = \frac{19548}{143.1} = 136 moles Cu_2O$$

$$\frac{136 moles Cu_2O}{1 mole Cu_2O} \left| \frac{2 moles Cu}{} \right. = 272 moles Cu$$

$$m(Cu) = n \times Mwt = 272 \times 63.55 = 17285\, gCu / tonnematte$$

$$= 0.017 tonne Cu / tonnematte$$

- *Direct Recovery of Copper into Blister*

$$\frac{0.017}{0.7} \times 100 = 98\%$$

APPENDIX 4: Cu_2O IN SLAG – EQUILIBRATION STUDY FOR THE Sb, Ni AND Pb DISTRIBUTION EXPERIMENTS

Figures 1, 2 and 3 show the copper oxide content of the FCS slag in contact with copper as a function of time, together with indicative relative error bars on some data points for each distribution experiment. Figure 1 is the copper oxide in FCS slag for the lead distribution experiments, Figure 2 is for nickel distribution experiments and Figure 3 is for the antimony distribution experiments.

The accumulated percent relative error in the wt% Cu_2O in slag is given in Table 3 for each distribution experiment. As can be seen in Table 3, the relative error in the distribution experiments is the sum of the errors in each chemical analysis, in controlling temperature and in setting the oxygen partial pressure.

Table 3: Accumulated Percent Relative Error from distribution experiments of each element

Error in Distribution Measurements			
	Lead (Pb)	**Nickel (Ni)**	**Antimony (Sb)**
Temperature	± 2.66	± 3.38	± 5.15
Gas Composition	± 4.95	± 4.95	± 4.95
Analysis (Slag)	± 3.0	± 3.0	± 3.0
Analysis (Alloy)	± 3.0	± 3.0	± 3.0
Total Error	**± 13.61%**	**± 14.33%**	**± 16.10%**

As is evident from all three figures, within experimental error, equilibrium in all three distribution experiments has been reached.

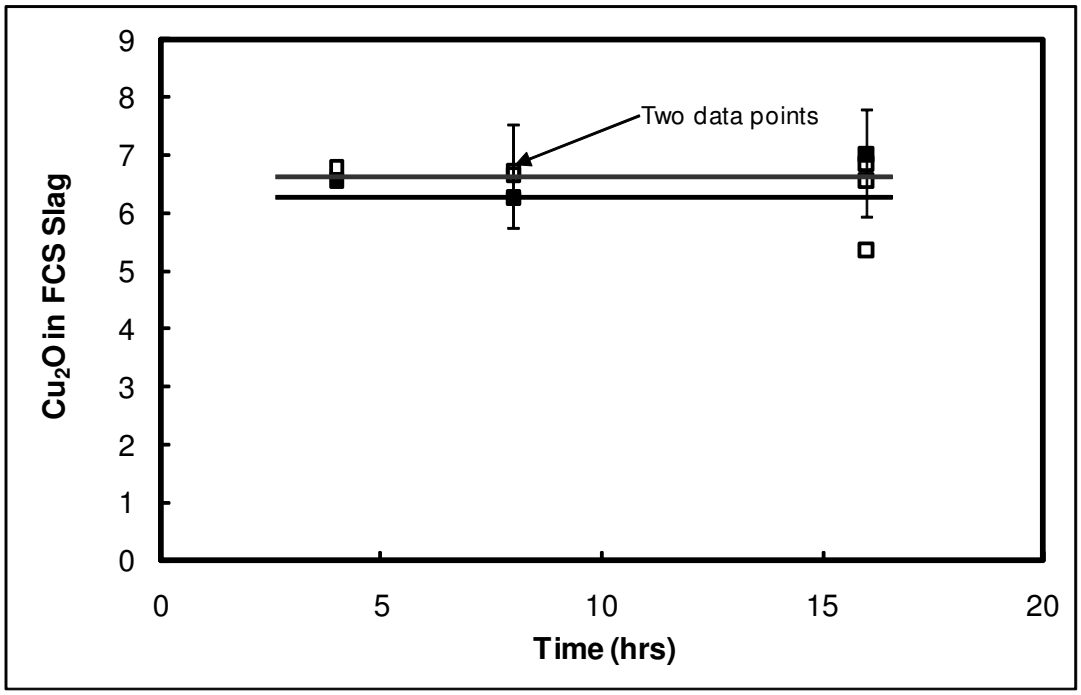

Figure 1: Copper oxide content in FCS slag in contact with copper at 1300°C and oxygen partial pressure of 10^{-6} atm., lead distribution experiments

Unfilled squares = metal oxide initially in slag, Filled squares = metal initially in copper

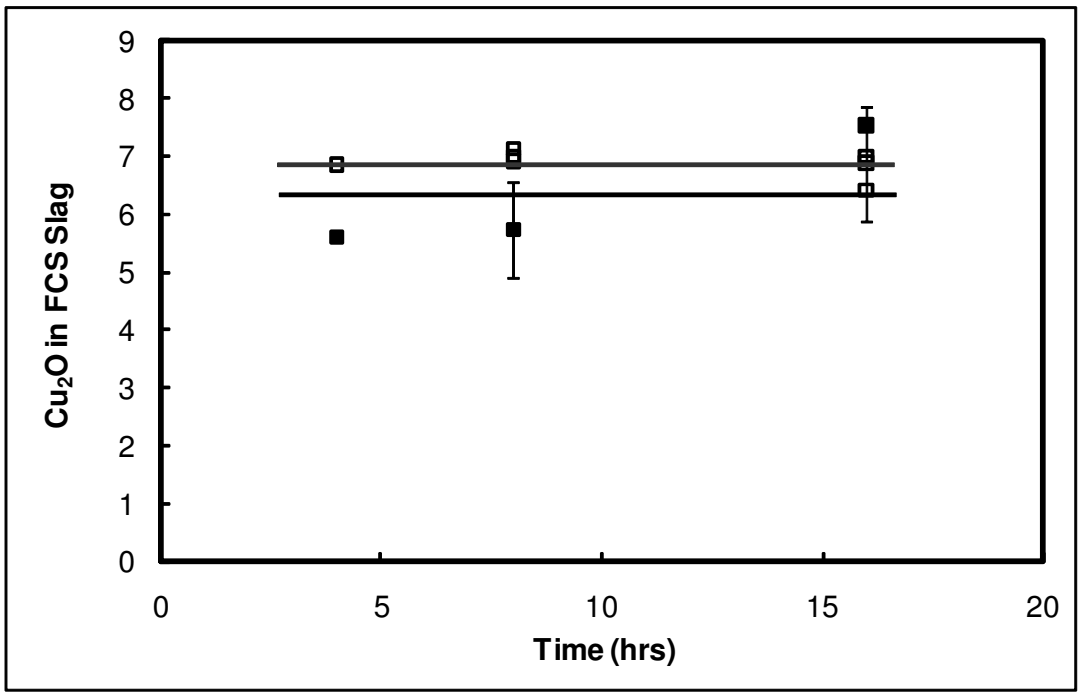

Figure 2: Copper oxide content in FCS slag in contact with copper at 1300°C and oxygen partial pressure of 10^{-6} atm., nickel distribution experiments

Unfilled squares = metal oxide initially in slag, Filled squares = metal initially in copper.

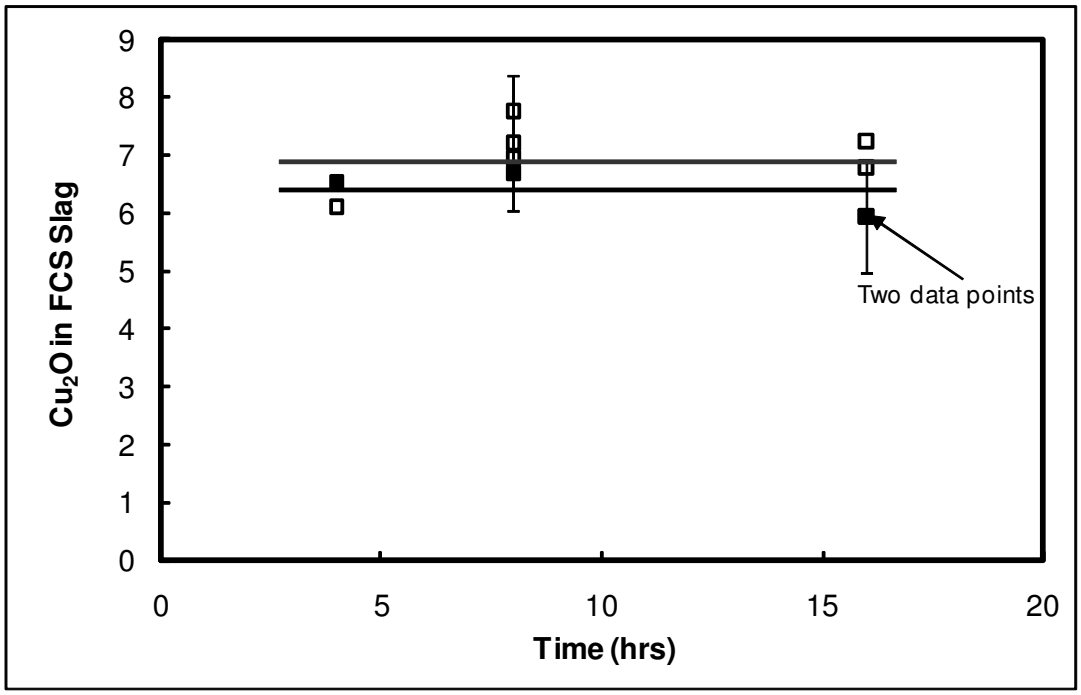

Figure 3: Copper oxide content in FCS slag in contact with copper at 1300°C and oxygen partial pressure of 10^{-6} atm., antimony distribution experiments

Unfilled squares = metal oxide initially in slag, Filled squares = metal initially in copper.